

Universitat Politècnica de València
Institute for Energy Engineering
Department of Chemical and Nuclear Engineering



*PREDICTIVE METHODS FOR
STABILITY MARGIN IN BWR*

DOCTORAL THESIS

Presented by:

José Melara San Román

Supervisors:

Dr. José Luis Muñoz-Cobo González

Dr. Alberto Escrivá

This dissertation is submitted for the degree of Doctor of Philosophy

Valencia February 2016

This dissertation is dedicated to my mother, wherever she is now, who always gave me encouragement, love and support, my father raised me with infinite patience and advised me to obtain a degree in physics, my sister Pilar, example to follow both in the study and teaching and, especially my family, because this work has been done during the time I had to spend with my wife Marina, and my children Cecilia and Jose Andrés.

I also want to thank my supervisors, Alberto Escrivá and José Luis Muñoz-Cobo without them this thesis would not have been possible.

I also thank this work to José María Izquierdo Rocha who taught me to be rigorous and convinced me of the need for a thorough knowledge of nuclear engineering.

To all my colleagues who have made me what I am today.

Thanks to all

SUMMARY

Power and flow oscillations in a BWR are very undesirable. One of the major concerns is to ensure, during power oscillations, compliance with GDC 10 and 12. GDC 10 requires that the reactor core be designed with appropriate margin to assure that specified acceptable fuel design limits will not be exceeded during any condition of normal operation, including the effects of anticipated operational occurrences. GDC 12 requires assurance that power oscillations which can result in conditions exceeding specified acceptable fuel design limits are either not possible or can be reliably and readily detected and suppressed.

If the oscillation amplitude is large, before the scram occurs the fuel rods may experience periodic dry-out and rewetting, or if the oscillation is larger enough, extended dry-out.

The Decay Ratio (DR) is the typical linear stability figure of merit. For analytical estimation of DR frequency domain codes are very useful. These types of codes are very fast and their results are very robust in comparison with time domain codes, whose results may be dependent on numeric scheme and nodalization. The only drawback of frequency domain is that you are limited to the linear domain; however, because of regulatory requirements imposed by GDC-12, reactors must remain stable and, thus, reactors always operate in the linear domain.

LAPUR is a frequency domain stability code that contains a mathematical description of the core of a boiling water reactor. It solves the steady state governing equations for the coolant and fuel, and the dynamic equations for the coolant, fuel and the neutron field in the frequency domain. Several improvements have been performed to the current version of the code, LAPUR5, in order to upgrade it for use with new fuel design types. The channel geometry has been changed from constant area to variable area. The local losses due to the spacers and contractions along the flow path have been upgraded to use industry standard correlations. This new version is LAPUR 6.

In this work, in order to check the correct implementation of these changes, a two-fold LAPUR 6 validation has been performed:

First, an exhaustive validation of the models implemented has been performed, comparing single channels LAPUR 6 outputs against SIMULATE-3 results. Cofrentes NPP SIMULATE-3 thermal-hydraulic models have been independently validated against experimental data.

Second, a Methodology for calculating Decay Ratios with LAPUR 6 has been developed, defining a validation matrix against analytical and plant measured decay ratios.

Analysis of measured data from the Cofrentes NPP has shown that decay ratios have values lower than 0.3 confirming the large stability margin of Cofrentes NPP when proper operating procedures are followed, and the comparison with LAPUR shows deviations less than ± 0.1 . Past experience suggests that the uncertainty in low decay ratio ranges is usually larger than with higher decay ratio values.

Finally a BWR noise generator has been used for estimating the uncertainty of the signal analyses methods used in this work for experimental estimation of decay ratio from the autocorrelation function of the APRM or LPRM power signals.

RESUMEN

Las oscilaciones de potencia y caudal en un BWR no son deseables. Una de las principales preocupaciones es asegurar, durante oscilaciones de potencia, el cumplimiento de la GDC 10 y 12. GDC 10 requiere que el núcleo del reactor se haya diseñado con un margen adecuado para asegurar que los límites admisibles establecidos en el diseño del combustible no se excederán en cualquier condición de operación normal, incluyendo los efectos de los sucesos operacionales anticipados. GDC 12 requiere garantías de que las oscilaciones de potencia que pueden resultar en condiciones que excedan los límites admisibles establecidos de diseño del combustible, o bien no son posibles o puedan ser detectadas y suprimidas de forma pronta y segura.

Si la amplitud de la oscilación es grande, antes de que se produzca el scram las varillas de combustible pueden experimentar secados y remojados periódicos, o si las oscilaciones son suficientemente grandes, un secado extendido.

La tasa de amortiguamiento (DR) es la típica figura de mérito de la estabilidad lineal. Para la estimación analítica de la DR los códigos en el dominio de la frecuencia son muy usados. Este tipo de códigos son muy rápidos y sus resultados son muy robustos en comparación con los códigos en el dominio temporal, cuyos resultados pueden depender del esquema numérico y la nodalización. El único inconveniente de los códigos en el dominio de la frecuencia es que está limitado al dominio lineal; sin embargo, como los requerimientos regulatorios impuestos por el GDC-12, los reactores deben permanecer estables y, por lo tanto, los reactores deben operar siempre en el dominio lineal.

LAPUR es un código de estabilidad en el dominio de la frecuencia que contiene una descripción matemática del núcleo de un reactor de agua en ebullición. Resuelve las ecuaciones de conservación en estado estacionario para el refrigerante y el combustible, las ecuaciones dinámicas para el refrigerante, el combustible y el campo neutrónico en el dominio de la frecuencia. Se han realizado varias mejoras a la versión actual del código, LAPUR 5, con el fin de actualizarlo para su uso con los nuevos tipos de diseño de combustible. La geometría del canal se ha cambiado, el área ha pasado de ser constante a poder considerar área variable. El cálculo de las pérdidas locales debido a los

espaciadores y contracciones a lo largo del camino que sigue el flujo se han actualizado, pasando a utilizar correlaciones estándar de la industria. Esta nueva versión del código se ha denominado LAPUR 6.

En este trabajo, con el fin de verificar la correcta implementación de estos cambios, se ha realizado una doble validación del código LAPUR 6:

En primer lugar se ha realizado una validación exhaustiva de los modelos implementados, comparando los valores de salida de LAPUR 6 para un canal con los resultados de SIMULATE-3. Los modelos termohidráulicos de la CN Cofrentes de SIMULATE-3 han sido validados de forma independiente con los datos experimentales.

En segundo lugar se ha desarrollado una metodología para el cálculo de la tasa de amortiguamiento con LAPUR 6, definiendo una matriz de validación de los valores de tasa de amortiguamiento analíticos con valores medidos en la planta.

Las tasas de amortiguamiento medidos en la Central Nuclear de Cofrentes tienen valores inferiores al 0.3, confirmando el gran margen de estabilidad de la Central Nuclear de Cofrentes cuando se siguen los procedimientos de operación adecuados, y la comparación con los resultados de LAPUR muestra desviaciones de menos de ± 0.1 . La experiencia acumulada sugiere que la incertidumbre para los rangos bajos de tasas de amortiguamiento es generalmente más grande que para los valores altos.

Por último se ha utilizado un generador de señales BWR para la estimación de la incertidumbre de los métodos de análisis de señales utilizados en este trabajo para la estimación experimental de la tasa de amortiguamiento, a partir de la función de autocorrelación de las señales de potencia APRM o LPRM.

RESUM

Les oscil·lacions de potència i flux en un BWR són molt poc desitjades. Una de les majors preocupacions és assegurar-se, durant les oscil·lacions de potència, del compliment de GDC 10 i 12. GDC 10 requerix que el nucli del reactor estiga dissenyat amb un marge apropiat per a assegurar que els límits admissibles establerts en el disseny del combustible no siguin superats davall cap condició d'operació normal, incloent els incidents esperats d'operació. GDC 12 requerix assegurar que les oscil·lacions de potència que poden resultar en condicions on es superen els límits admissibles establerts en el disseny del combustible no siguin possibles o puguen ser detectades de manera segura e immediata i suprimides.

Si l'amplitud de les oscil·lacions és gran, abans que el scram ocorrega les barres experimenten un assecat i remullat periòdic, o si l'oscil·lació és prou gran, un assecat estés.

La taxa d'amortiment (DR) és la típica figura de mèrit de l'estabilitat lineal. Per a l'estimació analítica de la DR són molt usats els codis en el domini de la freqüència. Este tipus de codis són molt ràpids i els seus resultats són molt robustos en comparació amb els codis en el domini temporal, els resultats del qual són molt dependents de l'esquema numèric i la nodalització. L'únic inconvenient del domini de la freqüència és que està limitat al domini lineal, no obstant això, com els requeriments reguladors imposats pel GDC-12, els reactors han de mantenir-se estables i, per tant, els reactors han d'operar sempre en el domini lineal.

LAPUR és un codi d'estabilitat en el domini de la freqüència que conté una descripció matemàtica del nucli d'un reactor d'aigua en ebullició. Resol les equacions de govern estacionàries del refrigerant i el combustible, les equacions dinàmiques del refrigerant, el combustible i el camp neutrònic en el domini de la freqüència. S'han realitzat diverses millores a la versió anterior del codi, LAPUR 5, amb l'objectiu d'actualitzar-ho per al seu ús amb nous tipus de disseny de combustibles. La geometria del canal s'ha canviat d'àrea constant a variable. Les pèrdues locals degudes als espaciadors i contraccions al llarg del camí del flux s'han actualitzat per a utilitzar correlacions estàndard de la indústria. Esta nova versió és LAPUR 6.

En este treball, amb l'objectiu de comprovar la correcta implementació d'estos canvis, s'ha realitzat una doble validació del LAPUR 6:

Primer, s'ha realitzat una validació exhaustiva dels models implementats, comparant els valors d'eixida per a un canal de LAPUR 6 amb els resultats de SIMULATE-3. Els models termohidràulics per a SIMULATE-3 de la Central Nuclear de Cofrentes s'han validat independentment amb dades experimentals.

Segon, s'ha desenrotllat una Metodologia per al càlcul de la Taxa d'Amortiment amb LAPUR 6, definint una matriu de validació amb valors de taxes d'amortiment analítics i mesurats en la planta.

Anàlisis de les dades mesurades en la Central Nuclear de Cofrentes mostren valors de les taxes d'amortiment inferiors al 0.3, confirmant el gran marge d'estabilitat de la Central Nuclear de Cofrentes quan se segueix un adequat procediment d'operació, i la comparació amb LAPUR mostra desviacions inferiors al +/- 0.1. L'experiència acumulada mostra que la incertesa en el rang de taxes d'amortiment baixes és normalment major que per a valors alts de les taxes d'amortiment.

Finalment s'ha utilitzat un generador de senyals per a estimar la incertesa dels mètodes d'anàlisi del senyal utilitzats en este treball per a l'estimació experimental de la taxa d'amortiment emprant la funció d'autocorrelació dels senyals de potència APRM o LPRM.

CONTENTS

1 INTRODUCTION	1
1.1 STABILITY IN BWR	1
2 PHYSICAL MECHANISMS LEADING TO INSTABILITIES	7
2.1 MECHANISM OF BWR POWER OSCILLATIONS	7
2.1.1 <i>Density-Wave Instability</i>	7
2.1.2 <i>Nuclear Feedback</i>	10
2.1.3 <i>Modes of BWR Instabilities</i>	11
2.2 DEPENDENCE OF STABILITY ON CHANGES IN OPERATING VARIABLES	12
2.3 ANALYSIS METHODS FOR BWR STABILITY	15
2.3.1 <i>Experimental Methods</i>	16
2.3.2 <i>Stochastic Methods</i>	17
2.3.3 <i>Analytical Methods</i>	17
2.3.3.1 <i>Frequency Domain Codes</i>	17
2.3.3.2 <i>Time Domain Codes</i>	18
2.4 NEW CHALLENGES FOR BWR STABILITY: NEW FUEL DESIGNS AND NEW OPERATION DOMAINS.	18
2.4.1 <i>New Fuel Designs</i>	18
2.4.2 <i>New Operational Domains</i>	20
2.5 CHAPTER SUMMARY	22
3 STABILITY CONTROL METHODS	23
3.1 INTRODUCTION	23
3.2 SAFETY CONCERNS OF BWR POWER OSCILLATIONS	24
3.3 APPROACHES FOR RESOLUTION OF THE BWR STABILITY ISSUE	25
3.3.1 <i>Interim Corrective Actions</i>	25
3.3.2 <i>Long Term Solutions</i>	28
3.3.3 <i>Prevention Based Methodologies: Enhanced IA (EIA)</i>	29
3.3.3.1 <i>E1A Stability Solution Description</i>	29
3.3.3.2 <i>E1A Methodology Application Process</i>	31
3.3.3.3 <i>E1A Methodology: Advantages and Drawbacks</i>	32
3.3.3.4 <i>Drawbacks</i>	33
3.3.4 <i>Option III. LPRM-Based Detect & Suppress</i>	34
3.3.4.1 <i>D&S Basis</i>	34
3.3.4.2 <i>Changes in Stability LTSs and in Designs</i>	34
3.4 CHAPTER SUMMARY	37
4 LAPUR FREQUENCY DOMAIN CODE	39
4.1 BRIEF DESCRIPTION OF THE CODE LAPUR	41
4.2 LAPURX	44
4.2.1 <i>The Coolant's Steady State</i>	44

4.2.2 Steady State Equations of Fuel	45
4.3 LAPURW	47
4.3.1 The Dynamics of the Neutron Field	47
4.3.2 The Dynamics of the Fuel	49
4.3.3 The Fluid Flow Dynamic	49
4.3.4 The Thermalhydraulic-Neutronic Interaction	51
4.4 THE TRANSFER FUNCTIONS OF LAPUR	52
4.4.1 Calculations of the Density Feedback Reactivity Coefficient in LAPUR	52
4.4.1.1 Flow to Density Reactivity Feedback Coefficient	52
4.4.2 Power to Density Reactivity Feedback Coefficients	57
4.4.3 Inlet Temperature to Density Reactivity Feedback Coefficient	58
4.4.4 Calculations of the Fuel-Temperature (Doppler) Reactivity Coefficients	59
4.4.5 One Core Density Reactivity Coefficient in LAPUR	61
4.4.5.1 The Block Diagram of LAPUR	61
4.4.5.2 The One-Core Reactivity Feedback Transfer Function	67
4.4.6 The Open-Loop and the Closed-Loop Transfer Functions in LAPUR	69
4.5 IMPLEMENTATION OF VARIABLE AREA INTO THE CODE LAPUR	70
4.6 IMPLEMENTATION OF THE NEW FRICTION MODEL INTO THE CODE LAPUR	78
4.6.1 New Friction Multiplier Model	78
4.6.2 New Friction Factor Model	79
4.7 CHAPTER SUMMARY	79

5 METHODOLOGY USED FOR DECAY RATIOS CALCULATION

WITH LAPUR	81
5.1 INTRODUCTION	81
5.2 DESCRIPTION OF CODES	82
5.2.1 LAPUR	82
5.2.2 SIMULATE	82
5.2.3 PAPU Post-Processor	83
5.2.4 LAPUR Input Pre-Processor (LIP)	84
5.3 METHODOLOGY	85
5.3.1 Calculation Procedure	85
5.3.1.1 Set Up of the Core Configuration	85
5.3.1.2 LAPURX Input Data Generation	85
5.3.1.3 SIMULATE Run to Perform Reactivity Perturbation Calculations	91
5.3.1.4 LAPURW Input Data	92
5.3.1.5 Perform the Core Stability Evaluation	94
5.3.2 Output and Results	96
5.4 PRELIMINARY VALIDATION OF LAPUR METHODOLOGY	97

5.5 CHAPTER SUMMARY	99
6 LAPUR 6.0 VALIDATION	101
6.1 GENERIC VALIDATION: COMPARISON OF PRESSURE DROP COMPONENTS FOR TYPE A AND TYPE B FUEL DESIGNS	102
6.2 CHAPTER OUTLINE	103
6.3 PRESSURE DROP BASIS.....	104
6.3.1 Friction Pressure Drop.....	104
6.3.2 Local Losses	104
6.3.3 Spacer or Grid Losses	105
6.3.4 Irreversible Losses for Expansion and Contraction.....	105
6.4 ACCELERATION PRESSURE LOSSES	106
6.5 ELEVATION PRESSURE DROP	106
6.6 GENERIC VALIDATION: COMPARISON OF PRESSURE DROP COMPONENTS FOR TYPE A AND TYPE B	107
6.7 INITIAL CONDITIONS	108
6.8 ELEVATION PRESSURE DROP	110
6.8.1 Elevation Pressure Drop for TYPE A.....	110
6.8.2 Elevation Pressure Drop for TYPE B.....	113
6.8.3 Conclusions of Elevation Results.....	115
6.9 EXPANSION AND ACCELERATION DATA	115
6.9.1 Expansion and Acceleration Data for TYPE A.....	116
6.9.2 Expansion and Acceleration Data for TYPE B.....	118
6.9.3 Conclusions of Expansion and Acceleration Results.....	121
6.10 FRICTION PRESSURE DROP	121
6.10.1 Friction Data for TYPE A.....	121
6.10.2 Friction Data for TYPE B.....	124
6.10.3 Conclusions of Friction Results.....	127
6.11 LOCAL PRESSURE DROP DATA.....	127
6.11.1 Local Pressure Drop Data for TYPE A	127
6.11.2 Local Pressure Drop Data for TYPE B	130
6.11.3 Conclusions of Local Losses in Pressure Drop Results.....	133
6.12 VOID FRACTION DATA	133
6.12.1 Void Fraction Data for TYPE A	133
6.12.2 Void Fraction Data for TYPE B	136
6.12.3 Conclusions of Void Fraction Comparison	139
6.13 COMPARISON OF LAPUR VOID FRACTION TO FRIGG LOOP DATA.	139
6.13.1 Experimental Conditions	140
6.13.2 Comparison of Void Fraction Results to FRIGG-2 Data	140
6.13.3 Conclusions of Void Fraction Results of LAPUR 6 Compared to FRIGG-2 Data.....	144
6.14 COMPARISON OF COFRENTES NUCLEAR POWER PLANT MEASURED DECAY RATIOS TO LAPUR 6 RESULTS	144
6.14.1 Cofrentes Nuclear Power Plant.....	144

6.14.2	<i>Stability Control in Cofrentes Nuclear Power Plant</i>	144
6.14.3	<i>Methodology of Calculating Decay Ratios with LAPUR 6</i>	146
6.14.4	<i>Decay Ratio and Frequency Validation: Start-up and End-of-Cycle Coastdowns</i>	147
6.14.5	<i>Generation of SIMULATE-3 Core Configuration Data</i>	149
6.14.6	<i>Time Series Analysis of Signal for Decay Ratio Estimation</i>	150
6.14.7	<i>Results of Decay Ratio and Oscillation Frequency</i>	150
6.14.7.1	<i>Analysis of Data</i>	152
6.14.7.2	<i>Comparison of SMART Frequency and Power Spectral Density Peaks</i>	154
6.15	DECAY RATIO AND FREQUENCY VALIDATION: COFRENTES CYCLE 6 INSTABILITY	156
6.15.1	<i>Event Description</i>	156
6.15.2	<i>Setup of the Core Configuration</i>	157
6.15.3	<i>LAPUR Input Data</i>	157
6.15.4	<i>LAPUR 6 Results</i>	158
6.15.5	<i>Decay Ratio Values Analysis</i>	159
6.15.6	<i>APRMs Signal Analysis</i>	159
6.16	LPRM AND APRM DECAY RATIO AND FREQUENCY VALIDATION ..	163
6.16.1	<i>New Data Acquisition System Test during Cycle 18 Sequence Exchanges (June 2010, September 2010)</i>	164
6.16.2	<i>Signal Analysis</i>	165
6.16.3	<i>Decay Ratio Results</i>	167
6.16.4	<i>LPRM Data</i>	169
6.17	STABILITY MARGIN SENSITIVITIES DURING CORE DESIGN WITH LAPUR	171
6.17.1	<i>Example 1 BOC-DF018</i>	172
6.17.2	<i>Example 2 BOC-DL056-VARIANTE</i>	174
6.17.3	<i>Example 3 BOC-DO079</i>	176
6.18	NEW BURNUP-DEPENDENT MODEL FOR URANIA FUEL PELLET THERMAL CONDUCTIVITY	178
6.18.1	<i>LAPUR 6.1 and LIP 1.2 Features</i>	178
6.18.2	<i>Update of Methodology for Calculation of Core and Channel Decay Ratios with LAPUR</i>	182
6.18.3	<i>Changes in LAPUR Methodology Due to the Introduction of a Burnup Dependent Conductivity</i>	184
6.19	CHAPTER SUMMARY	185

7	UNCERTAINTIES OF DECAY RATIO MEASUREMENTS FOR ANALYTICAL CODES QUALIFICATION PURPOSES	189
7.1	BWR SIGNAL SIMULATOR	190
7.2	REDUCED ORDER MODEL	191
7.3	TRANSFER FUNCTION ON FREQUENCY DOMAIN	191
7.4	INPUT FILE	193

7.4.1 <i>Introduction to the Model Parameters</i>	193
7.4.2 <i>Structure</i>	195
7.4.3 <i>Input File Cards</i>	196
7.5 OUTPUT PROCESSING	200
7.5.1 <i>File DR+Freq.sal</i>	201
7.5.2 <i>Signal Representation Example</i>	202
7.6 VALIDATION WITH A REDUCED ORDER SYNTHETIC SIGNAL	
GENERATOR	205
7.6.1 <i>Preliminary Checking</i>	206
7.6.2 <i>Checking</i>	206
7.6.3 <i>Results</i>	207
7.7 INFLUENCE OF THE INPUT PARAMETERS VARIATION	208
7.8 CREATION OF A DATABASE WITH THEORETICAL RESULTS OF	
DECAY RATIO AND FREQUENCY	208
7.9 VALIDATION WITH A SET OF 1000 SIGNALS.....	209
7.10 RESULTS	211
7.11 CHAPTER SUMMARY	213
8 CONCLUSIONS AND RECOMMENDATIONS FOR FUTURE	
WORK	215
8.1 RECOMMENDATIONS FOR FUTURE WORK	219
9 REFERENCES	221
APPENDIX A. PROCEDURE FOR USING PAPU	
POSTPROCESSOR	231
A.1 INPUT FILES DESCRIPTION	232
A.2 PAPU INPUT FILE MODIFICATIONS	235
A.3 PAPU OUTPUT FILES	236
A.4 LAPURX INPUT EXAMPLE	237
A.5 LAPURW INPUT EXAMPLE	242

LIST OF TABLES

Table 5.1. SIMULATE perturbation set.....	91
Table 5.2. Recirculation transfer function data for BWR-6	93
Table 5.3. Sample input of frequency point for LAPURW	94
Table 6.1. Typical pressure drop uncertainties.....	107
Table 6.2. TYPE A boundary conditions.	108
Table 6.3. TYPE B boundary conditions.....	108
Table 6.4. FRIGG-2 test conditions	140
Table 6.5. Number of channels assigned to LAPUR for channel decay ratio calculations.....	157
Table 6.6. Number of channels assigned to LAPUR for channel decay ratio calculations.....	158
Table 6.7. Number of channels assigned to LAPUR for channel decay ratio calculations.....	158
Table 6.8. SIMULATE-LAPUR pressure drops comparison.....	158
Table 6.9. Comparison of SIMULATE and LAPUR flow rate channels	158
Table 6.10. State point 290191 decay ratio values.	159
Table 6.11. Filters applied to APRM signal	161
Table 6.12. Cofrentes 290191 instability (signal analysis results)	162
Table 6.13. RTP2316-M input channels.....	164
Table 6.14. Fbias obtained for the example 1.	174
Table 6.15. Fbias obtained for the example 2.	176
Table 6.16. Fbias obtained for the example 3.	178
Table 6.17. Comparison of LAPUR 6.1 and LAPUR 6.0 results with a LAPUR 6.0 input deck.	181
Table 6.18. Effect of gap conductance increase and burnup fuel conductivity dependence in LAPUR 6.1.	182
Table 6.19. Effect of gap conductance increase, burnup fuel conductivity dependence in LAPUR 6.1 and a 1.1 multiplier in REAMUL.	184
Table 6.20. Cofrentes instability results.	186
Table 7.1. Input parameters obtained executing zeropole45.m with Matlab R2009b.	207
Table 7.2. Input parameters obtained executing zeropole45.m with Matlab R2011b.	207
Table A.2.1. Modified values in entrada input file for PAPU reactivity coefficient calculation	235

LIST OF FIGURES

Figure 1.1. Schematic representation of the dynamic processes pertaining to power generation in the core of a BWR.	3
Figure 2.1. Density wave instability mechanism. Local pressure drop variations due to inlet flow fluctuation (from [10])......	9
Figure 2.2. Variations of pressure drop components for parallel-channel type oscillations (from [11]).	10
Figure 2.3. Nuclear feedback loop in a BWR (adapted from [12]).	11
Figure 2.4. Definition of the Decay Ratio (adapted from [12])......	16
Figure 2.5. Examples of fuel designs: ATRIUM 10XP (AREVA NP) and SVEA-96 OPTIMA-2 (WESTINGHOUSE SWEDEN AB) from [32]. ...	19
Figure 2.6. Fuel design GNF2 (GNF) [33]......	20
Figure 2.7. Maximum Extended Load Line Limit Analysis (MELLLA +) domain [34].	21
Figure 3.1. Exclusion regions defined by the Interim Corrective Actions (adapted from [44]).	26
Figure 3.2. Power-flow map for a BWR-6 with E1A stability regions. Example of a typical start-up path.....	32
Figure 4.1. Schematic representation of the dynamic processes pertaining to power generation in the core of a BWR.	42
Figure 4.2. Schematic representation of a no-uniformly heated channel.	43
Figure 4.3. Schematic representation of the fuel rod composition and thermal mesh.	46
Figure 4.4. Block diagram of LAPUR transfer functions.....	62
Figure 4.5. Block diagram of LAPUR transfer functions in compact form. ...	67
Figure 5.1. Decay ratio calculation steps.....	86
Figure 5.2. Nyquist diagram for a stable channel.....	97
Figure 5.3 Wide core DR IVM comparison LAPUR 6 Vendor's code.....	98
Figure 5.4 Hot channel DR IVM comparison LAPUR 6 Vendor's code.....	98
Figure 6.1. Axial power profile used in TYPE A analyses.	109
Figure 6.2. Axial power profile used in TYPE B analyses.....	109
Figure 6.3. Elevation CASE 1 TYPE A.	110
Figure 6.4. Elevation CASE 2 TYPE A.	111
Figure 6.5. Elevation CASE 3 TYPE A.	111
Figure 6.6. Elevation CASE 4 TYPE A.	112
Figure 6.7. Elevation CASE 5 TYPE A.	112
Figure 6.8. Elevation CASE 1 TYPE B.	113

Figure 6.9. Elevation CASE 2 TYPE B.	113
Figure 6.10. Elevation CASE 3 TYPE B.	114
Figure 6.11. Elevation CASE 4 TYPE B.	114
Figure 6.12. Elevation CASE 5 TYPE B.	115
Figure 6.13. Expansion and acceleration pressure drop for CASE 1 TYPE A.	116
Figure 6.14. Expansion and acceleration pressure drop for CASE 2 TYPE A.	116
Figure 6.15. Expansion and acceleration pressure drop for CASE 3 TYPE A.	117
Figure 6.16. Expansion and acceleration pressure drop for CASE 4 TYPE A.	117
Figure 6.17. Expansion and acceleration pressure drop for CASE 5 TYPE A.	118
Figure 6.18. Expansion and acceleration pressure drop for CASE 1 TYPE B.	118
Figure 6.19. Expansion and acceleration pressure drop for CASE 2 TYPE B.	119
Figure 6.20. Expansion and acceleration pressure drop for CASE 3 TYPE B.	119
Figure 6.21. Expansion and acceleration pressure drop for CASE 4 TYPE B.	120
Figure 6.22. Expansion and acceleration pressure drop for CASE 5 TYPE B.	120
Figure 6.23. Friction CASE 1 TYPE A.	122
Figure 6.24. Friction CASE 2 TYPE A.	122
Figure 6.25. Friction CASE 3 TYPE A.	123
Figure 6.26. Friction CASE 4 TYPE A.	123
Figure 6.27. Friction CASE 5 TYPE A.	124
Figure 6.28. Friction CASE 1 TYPE B.	124
Figure 6.29. Friction CASE 2 TYPE B.	125
Figure 6.30. Friction CASE 1 TYPE B.	125
Figure 6.31. Friction CASE 4 TYPE B.	126
Figure 6.32. Friction CASE 5 TYPE B.	126
Figure 6.33. Local CASE 1 TYPE A.	128
Figure 6.34. Local CASE 2 TYPE A.	128
Figure 6.35. Local CASE 3 TYPE A.	129
Figure 6.36. Local CASE 4 TYPE A.	129
Figure 6.37. Local CASE 5 TYPE A.	130

Figure 6.38. Local CASE 1 TYPE B.....	130
Figure 6.39. Local CASE 2 TYPE B.....	131
Figure 6.40. Local CASE 3 TYPE B.....	131
Figure 6.41. Local CASE 4 TYPE B.....	132
Figure 6.42. Local CASE 5 TYPE B.....	132
Figure 6.43. Void fraction CASE 1 TYPE A.	134
Figure 6.44. Void fraction CASE 2 TYPE A.	134
Figure 6.45. Void fraction CASE 3 TYPE A.	135
Figure 6.46. Void fraction CASE 4 TYPE A.	135
Figure 6.47. Void fraction CASE 5 TYPE A.	136
Figure 6.48. Void fraction CASE 1 TYPE B.	137
Figure 6.49. Void fraction CASE 2 TYPE B.	137
Figure 6.50. Void fraction CASE 3 TYPE B.	138
Figure 6.51. Void fraction CASE 4 TYPE B.	138
Figure 6.52. Void fraction CASE 5 TYPE B.	139
Figure 6.53. Void fraction of FRIGG-2 Test 313009.....	141
Figure 6.54. Void fraction of FRIGG-2 Test 313014.....	141
Figure 6.55. Void fraction of FRIGG-2 Test 313016.....	142
Figure 6.56. Void fraction of FRIGG-2 Test 313018.....	142
Figure 6.57. Void fraction of FRIGG-2 Test 313020.....	143
Figure 6.58. Void fraction of FRIGG-2 Test 313024.....	143
Figure 6.59. Typical path during EOC coastdown (Cycle 16b).	148
Figure 6.60. Typical start-up path (Cycle 18).	149
Figure 6.61. Power history used for SIMULATE-3 simulation of C. 18 start-up.....	150
Figure 6.62. Average APRM decay ratio and frequency versus LAPUR results (EOC Cyles 16 and C17 coastdowns).	151
Figure 6.63. Average APRM decay ratio and frequency versus LAPUR results (Cycles 17 and 18 start-ups and coastdowns).	152
Figure 6.64. Decay ratio based on monitor SMART versus LAPUR.	153
Figure 6.65. Natural frequency based on monitor SMART versus LAPUR.	154
Figure 6.66. Comparison of Welch’s method periodogram and LAPUR- calculated frequency.....	155
Figure 6.67. Welch’s method periodogram at 0.1 Hz resolution.....	155
Figure 6.68 .Welch’s method periodogram at 0.05 Hz resolution (peak close to LAPUR frequency).	156
Figure 6.69. APRM A 1991/01/29 Cofrentes instability event.	160
Figure 6.70. PSD based on Welch’s method periodogram (290191 Cofrentes instability).	160

Figure 6.71. Bode diagram of applied Butterworth filters to split up fundamental and first mode.	161
Figure 6.72. Effect of type 1 and type 2 filtering in APRM A signal.	162
Figure 6.73. June 2010 control sequence exchange roadmap.	165
Figure 6.74. September 2010 control sequence exchange roadmap.	166
Figure 6.75. Histogram of APRM-C and LPRM 22-23B with and without optoisolator.	166
Figure 6.76. Decay ratio sample for June and September 2010 maneuvers. .	168
Figure 6.77. June and September 2010 maneuver—decay ratio comparison.	168
Figure 6.78. June and September 2010 maneuver—frequency comparison. .	169
Figure 6.79. LPRM and APRM-C decay ratio from autocorrelation versus LAPUR decay ratio comparison—September and June 2010 sequence exchange.	170
Figure 6.80. LPRM and APRM-C frequency autocorrelation-based versus LAPUR decay ratio comparison—September and June 2010 sequence exchange.	170
Figure 6.81. BOC-DF018-VARIANTE MAP. Distribution of TYPE B (blue) and TYPE A (red) in this example.	172
Figure 6.82. Histogram of relative peaking factors for TYPE A and TYPE B	173
Figure 6.83. BOC-DL056-VARIANTE MAP. Distribution of TYPE B (blue) and TYPE A (red) in this example.	175
Figure 6.84. Histogram of relative peaking factors for TYPE A and TYPE B.	175
Figure 6.85. BOC-DL0079. Distribution of TYPE B (blue) and TYPE A (red) in this example.	177
Figure 6.86. Relative peaking factors histogram for this example.	177
Figure 6.87. Decay ratio autocorrelation based on LAPUR calculation.	186
Figure 6.88. Frequency autocorrelation based on LAPUR calculation.	187
Figure 7.1. Blocks diagram of the system.	192
Figure 7.2. Example of input file.	195
Figure 7.3. DR+frec.SAL.	201
Figure 7.4. Neutron excess.	203
Figure 7.5. Precursors excess.	203
Figure 7.6. Temperature.	204
Figure 7.7. Void reactivity.	204
Figure 7.8. Total reactivity.	205
Figure 7.9. Data acquisition hardware.	210

Figure 7.10 Decay Ratio. Analytical vs. Theoretical values 211
Figure 7.11. Oscillation Frequency. Analytical vs. Theoretical values. 212
Figure 7.12. DR error vs. Frequency 212
Figure 7.13. Frequency error vs. DR 213

LIST OF ABBREVIATIONS AND ACRONYMS

ABA	Amplitude Based Algorithm
ACF	AutoCorrelation Function
APRM	Average Power Range Monitor
ATWS	Anticipated Transient Without Scram
BBR	Bulk-Boiling Region
BEO	Bottom Entry Orifice
BEPU	Best Estimate Plus Uncertainty
BOC	Beginning Of Cycle
BWR	Boiling Water Reactor
BWROG	Boiling Water Reactor Owners Group
CPR	Critical Power Ratio
CSAU	Code Scaling, Applicability and Uncertainty
D&S	Detect and suppress
DID	Defense-in-Depth
DR	Decay Ratio
DROP	Decay Ratio On-line Predictor
DSS-CD	Detect and Suppress Solution – Confirmation Density
E1A	Enhanced 1A
EOC	End Of Cycle
FCBB	Fraction of Core Boiling Boundary
FFWTR	Final FeedWater Temperature Reduction operation mode
FW	Feedwater
GE	General Electric Company
GRA	Growth Rate Algorithm
LHGR	Linear Heat Generation Rate
LPRM	Local Power Range Monitor
LTP	Lower Tie Plate
LTS	Long Term Solution
MCPR	Minimum Critical Power Ratio

MELLLA	Maximum Extended Load Line Limit Analysis
MIMO	Multiple-Input Multiple-Output systems
NBR	Non-Boiling Region
NMS	Neutron Monitoring System
NPP	Nuclear Power Plant
NRC	Nuclear Regulatory Commission
OLMCPR	Operating Limit Minimum Critical Power Ratios
OLTP	Original Licensed Thermal Power
OPRM	Oscillation Power Range Monitor
PBDA	Period Based Detection Algorithm
PBDS	Period Based Detection System
PCI	Pellet Clad Interaction
PCIOMR	Preconditioned Interim Operational Management Recommendations
PRBS	Pseudo Random Binary Sequence
RPF	Relative Power Fraction
RPT	Recirculation Pump Trip
SAFDL	Specified Acceptable Fuel Design Limit
SEO	Side Entry Orifice
SBR	Subcooled-Boiling Region
SLMCPR	Safety Limit Minimum Critical Power Ratio
SISO	Single-Input, Single-Output system
UPV	Valencia Polytechnic University
UTP	Upper Tie Plate
US NRC	United States Nuclear Regulatory Commission
WNP-2	Washington Nuclear Power Unit 2

SELECTED NOMENCLATURE

a_{1c}	Parameter for the void reactivity equation
a_{2c}	Parameter for the void reactivity equation
$a_q(i)$	Coolant flow to heat flux to coolant transfer function at axial level i
$a_T(i)$	Coolant flow to average fuel temperature transfer function at axial level i
A	Cross section flow area
A	Parameter related to the power generated per neutron
b_{d1}	Parameter related with the intensity of the noise added to the theoretical model (multiplicative).
b_{d2}	Parameter related with the intensity of the noise added to the theoretical model (additive).
$b_q(i)$	Power to coolant heat flux transfer function at axial level i
$b_T(i)$	Power average fuel temperature transfer function at axial level i
B	Parameter from the heat transfer model related to the heat transferred from the fuel to the coolant
B_i^2	Geometric buckling of the i -th mode
c_p	Specific heat at constant pressure
$c_q(i)$	Coolant temperature to heat flux to coolant transfer function at axial level i
$c_T(i)$	Coolant temperature to average fuel temperature transfer function at axial level i
$d_q(ix)$	Power to Doppler feedback reactivity transfer function for a channel ix
$d_T(ix)$	Coolant temperature to Doppler feedback reactivity transfer function for a channel ix
$d_y(ix)$	Flow to Doppler feedback reactivity transfer function at channel ix
D	Diffusion coefficient
D_f	Doppler Coefficient
D_H	Hydraulic diameter
e_a	Accumulative energy
e_{ix}	Flow to feedback reactivity at channels belonging to type ix

f	Moody friction multiplier
f_{ix}	Power to reactivity feedback coefficient at channel ix
f_p	Adjustable factor of the fraction of energy invested in the formation of steam
F_s	Fraction of energy invested in the formation of steam
g	Gravity
g_{ix}	Fraction of the total flow which goes through the channel ix
G	Mass flux
G	Total reactivity to total power transfer function
G_1	Upstream mass flux
G_2	Downstream mass flux
h	Specific enthalpy
h_{fg}	Vaporization enthalpy
h_{ix}	Inlet temperature to reactivity feedback coefficient at channel ix
h_0	Specific stagnation enthalpy
H	Normalized degree of subcooling
H	Power to reactivity feedback transfer function
H_D	Power to Doppler feedback reactivity transfer function
H_ρ	Power to density reactivity transfer function
k	Heat conductivity
K	Parameter related with the feedback of the model
K_{exp}	Single phase irreversible expansion loss
K_{con}	Single phase irreversible contraction loss
K_F	Crud-deposition friction multiplier
K_0	Contraction coefficient at inlet of the channels
K_{LTP}	Contraction coefficient at the lower tie plate
l^*	Neutron generation time
L	Channel length
$N_{ch}(ix)$	Number of channels of the ix type
N_f	Number of fuel-rods per channel
NN	Total number of axial nodes in the channel
P	Pressure
P_i	Interfacial perimeter

P_i	Power at node i
P_{lw}	Liquid region wet perimeter
P_{sw}	Steam region wet perimeter
Q'	Energy supply by the fuel per unit length
Q	Power to feedback reactivity transfer function
Q_D	Doppler feedback reactivity transfer function
Q_ρ	Power to density feedback reactivity transfer function
q''_{li}	Heat flux to the liquid region thought the interface
q''_{lw}	Heat flux to the liquid region thought the wall
q''_{si}	Heat flux to the steam region thought the interface
q''_{sw}	Heat flux to the steam region thought the wall
q'''	Heat generation rate per unit volume
R	Total flow to feedback reactivity transfer function.
R_{clp}	Normalized differential pressure to inlet flow transfer function, due to the presence of the recirculation loop
R_D	Core flow to Doppler feedback reactivity transfer function
R_r	Relative roughness
Re_l	Liquid Reynolds number
R_ρ	Core total flow to density feedback reactivity transfer function
S	Inlet temperature to feedback reactivity transfer function
S_D	Coolant temperature to Doppler feedback reactivity transfer function
S_ρ	Inlet temperature to feedback reactivity transfer function
t	Time
T	Temperature
u	Velocity
w	Mass flow rate
w_i	Square power reactivity weighting factor
W_o	Inlet flow rate
W_{act}	Active flow
W_{LTP}	Flow through LTP
X	Flow quality

X_f	Flow quality
$\langle x \rangle$	Cross section averaged flow quality
y	Normalized mass flow rate
z_1	Inception point for subcooled boiling
α	Void fraction
$\langle \alpha \rangle$	Cross section averaged void fraction
β_i	Fraction of delay neutron precursors of group i
Γ	Mass generation rate per volume unit
γ	Slip ratio
$\delta \bar{n}$	Neutronic density perturbation
$\delta \bar{q}$	Driving perturbation of power generation in the fuel
$\delta \bar{T}_{in}$	Driving perturbation of inlet temperature
$\langle \delta \bar{T}_F \rangle_i$	Average fuel temperature perturbation at axial level i
$\delta \bar{y}_{in}$	Driving perturbation of inlet flow rate
$\delta \bar{y}_1(ix)$	Inlet flow perturbation to the first node
$\delta \bar{Y}$	Perturbation in total core flow rate
$\delta \bar{\Pi}_{z_1}$	Flow perturbation at the boiling inception boundary
$\delta \Delta \bar{k}_\rho$	Density reactivity change
$\delta \Delta \bar{k}_D$	Doppler reactivity change
$\delta \bar{\rho}$	Reactivity perturbation
ΔP_{acc}	Acceleration pressure drop
ΔP_{elev}	Elevation (gravitational) pressure drop
ΔP_{fric}	Frictional pressure losses
Δz	Node length
η	Relative density decrement in the evaporation process
θ	Angle
λ	Semidesintegration period of the precursors
λ_i	Eigenvalue of the i -th neutronic mode
λ_s	Bubble decay rate

Λ	Mean generation time (Prompt Lifetime)
μ	Viscosity
$\nu\Sigma_f$	Fission neutron yield times fission cross section
ρ	Density
ρ_F	Liquid density at saturated conditions
ρ_{per}	Core averaged density of perturbed case
ρ_{ref}	Core averaged density of reference case
Σ_a	Absorption cross section.
τ_i	Interfacial shear stress
τ_w	Wall shear stress
Π	Normalized pressure
ϕ_{MN}^2	Martinelli-Nelson two-phase friction multiplier
$\phi_{2-phase\ friction}^2$	Two-phase friction multiplier.
Ω	Jones flow rate corrector

Subscripts

a	Node average
BB	Bulk boiling region
F	Saturated conditions
g	Steam
i	Interface
j	Node or face
l	Liquid
li	Liquid interface
NB	Non-boiling region
SB	Subcooled boiling region
s	Steam
si	Steam interface
w	Wall
0	Reference value or steady state

1 INTRODUCTION

1.1 STABILITY IN BWR

The general design of a nuclear power plant is always based in the same patterns [1] & [2], in the sense that a fluid is caused to flow through a volume inside which heat is generated by nuclear fission. In some nuclear reactors, the fluid acts as a heat remover only, having small or no effect on the heat generating process, whereas in other reactors the fluid plays the dual role of coolant and neutron moderator. In these latter reactors, two distinct interacting dynamic loops can be considered: a neutronic loop which controls the way in which the heat is produced, and a thermal-hydraulic loop whose flow characteristics determine the heat transfer rates, coolant density and flow rate distributions inside the reactor core volume. The coupling of these two dynamic loops is through the density dependence of the neutron moderation characteristics of the cooling fluid. Changes in coolant density alter the neutron population balance in the core, thus causing power generation variations which in turn affect the coolant density.

The interrelation of the physical mechanisms governing the dynamic response of a BWR core is schematically represented in figure 1.1. As depicted in this figure, a disturbance of reactivity can enter the core via either control

rod actuation or changes in coolant parameters such as inlet subcooling, flow rate or pressure. Any of these disturbances results in a change in the neutron population that varies the void content in the core which in turn affects the neutron population. If there were no time delays in the physical processes involved in the system response to a disturbance, the possibility for dynamic instability or oscillations about the new equilibrium value, would not exist. However, the combination of the heat transfer time delay in the fuel (~5 to 7 seconds) and the finite sweeping time of void perturbations in the core, can cause self-sustained oscillations of power. The magnitude of the void reactivity coefficients, length of the boiling region in the core, void sweep speed and fuel time constant, are the most important parameters affecting the dynamic stability of the BWR core.

Another mechanism that adds negative reactivity feedback to the core is the Doppler effect. This effect is due to the temperature dependence of the parasitic absorption of neutrons of the U-238 in the fuel. The magnitude of the Doppler reactivity feedback is small compared with the void reactivity, but its immediacy makes it (i) an extremely important factor during large transients, and (ii) a stabilizing agent, even if secondary, for small perturbation transients.

The chained dependences of (i) coolant flow rate on driving pressure, (ii) void fraction on coolant flow rate, and (iii) friction losses on void fraction, can cause the occurrence of void-flow hydrodynamic oscillations in the fuel assemblies. These oscillations could impair effective heat removal from the fuel and could cause thermal fatigue in the fuel clad, as well as drive the core into power oscillations. The core oscillations could be localized in the area surrounding the driving channels, or could extend to the whole core, depending on the number of channels with flow oscillations, the responsiveness of the core reactivity perturbations at the driving oscillation frequency, and the degree of neutronic coupling across the core volume. The most important parameters affecting the hydrodynamic stability of the flow channels are: inlet orifice diameter, channel length and void axial distribution.

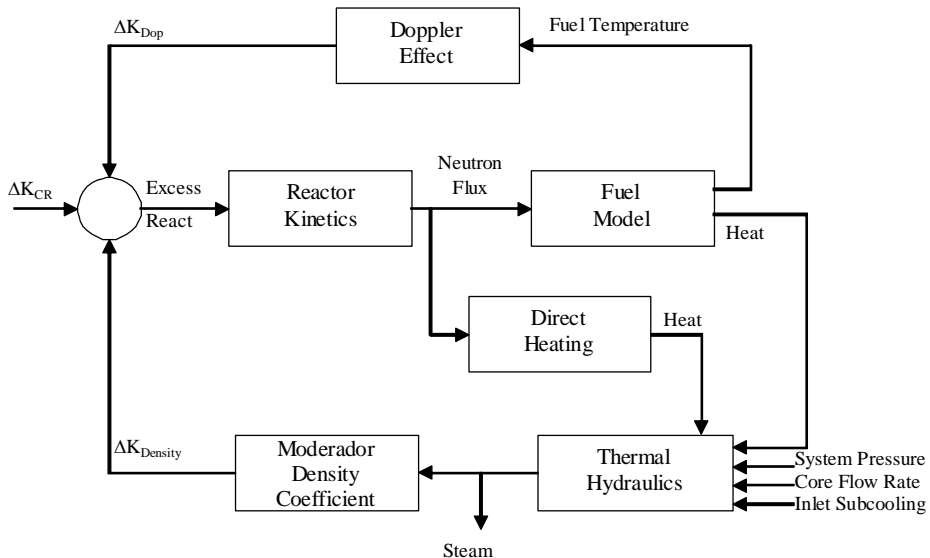


Figure 1.1. Schematic representation of the dynamic processes pertaining to power generation in the core of a BWR.

Although all system components (viz., neutronics, heat transfer, hydraulics, pressure regulator, recirculation flow controller, feedwater level controller, and turbine controller) may be dynamically stable when analyzed individually, their interaction may result in oscillatory behavior of system variables such as pressure, water level, core flow, etc. To eliminate this possibility, the control settings are adjusted in conjunction with the desired smooth and stable dynamic performance of the system during all phases of operation (i.e., startup, at power, shutdown, manual and automatic).

A wide variety of codes exists that may be used to analyze the stability of a Boiling Water Reactor [3]. These codes are classified in two classes: frequency domain codes (LAPUR, NUFREQ, ODYSY, STAIF), whose purpose is the linear stability analysis of BWRs; they are based on linearization and Laplace transform of the governing equations, and time domain codes (ATHLET, RAMONA, RELAP, RETRAN, SIMULATE-3K, TRAC, TRACE), which include analysis tools specifically developed to simulate the transient behaviour of plant systems.

Before the core refueling with fresh fuel is necessary to confirm that the BWR behaviour, in the start-up, will be stable. Furthermore, we can use these

codes to prevent the instability. In this last case, the frequency domain codes are more suitable because they obtain the stability margin in a few seconds.

In this work we present the improvements performed in the frequency domain code LAPUR, in order to upgrade it for the new fuel design types, the extensive qualification performed of the new implemented models and of LAPUR 6 results against experimental data and finally, the application of this code for stability licensing and core design.

Chapter 2 provides a more in-depth discussion of the physical mechanisms leading to instabilities, with emphasis on density-wave oscillations and coupled neutronic-TH oscillations and the main features of the newest fuel designs are presented under stability control standpoint.

Chapter 3 shows the main methodologies for BWR stability control and an overview of their advantages under technical and economical point of views.

Chapter 4 gives an introduction to the LAPUR 6 code and the numerical methods and the upgrade performed. Model development and important numerical considerations for LAPUR 6 stability analysis are also discussed.

Chapter 5 describes the methodology used for decay ratios calculation with LAPUR. LAPUR is able to calculate wide core decay ratio and hot channel decay ratio with is a very useful combination to know the stability margin of the reactor.

Chapter 6 presents the results of two-fold validation performed, First, a complete validation of implemented new models is presented. Second, Cofrentes NPP decay ratio and natural frequency values, obtained from APRM and LPRM applying noise analyses techniques, are compared with LAPUR 6 analytical results. In addition, a real LAPUR 6 application to support core design is described. Three different examples of the sensitivity to LAPUR 6 to power radial distribution and fuel design type are shown with the aim to confirm the good accuracy of LAPUR 6. Finally, the last upgrade of LAPUR is presented, the implementation of a burnup dependent Urania conductivity model in LAPUR 6. This latest LAPUR 6 version is called LAPUR 6.1.

One of the main important features in the qualification of analytical methods for decay ratio calculation is the estimation of the uncertainty of the

method used for the estimation of decay ratio through power signal analysis. Chapter 7 describes the method used to obtain the uncertainty of the noise techniques used to estimate experimentally the decay ratio and natural frequency. A noise simulator generates signals with a known decay ratio and applying noise techniques, we will obtain the estimated decay ratio. We have generated one thousand signals and the deviations between the real and estimated decay ratio allows us to get the standard deviation of the estimation method.

Finally, Chapter 8 gives an overview of the conclusions gained from this thesis and a series of recommendations for future work on these topics.

2 PHYSICAL MECHANISMS LEADING TO INSTABILITIES

2.1 MECHANISM OF BWR POWER OSCILLATIONS

The basic mechanism of BWR power oscillations has been identified as nuclear-coupled density-wave oscillations [4]. Two types of power oscillations have been observed: core-wide (or in phase) and regional (or out of phase) oscillations.

2.1.1 Density-Wave Instability

A BWR core contains a two-phase coolant and is susceptible to two-phase flow instabilities. Various types of two-phase flow instabilities have been

studied. At reasonably high pressures, the density-wave instability is the most commonly encountered type [5], [6], [7].

Density-wave oscillations are usually observed in systems with a two-phase mixture. It may also occur in a system with a single-phase fluid if the density change is large enough. The essential ingredients to produce density-wave oscillations are [8]:

1. A density distribution throughout the system which depends on the flow rate of the system.
2. A time delay between the flow rate changes and the density responses.
3. A cause/effect relationship between flow rate and density changes, and pressure loss/buoyancy changes.

Density-wave instabilities can be explained by the phenomenon of kinematic wave propagation. They are caused by the finite time necessary for the enthalpy and void fraction waves to propagate in the channel. These finite propagation times induce time-lag effects and phase-angle shifts between the channel pressure drop and flow rate, which under certain conditions can result in self-sustained oscillations [5].

Consider a heated channel containing a two-phase fluid initially at steady-state. An incremental decrease in the inlet flow rate produces an increase of the void fraction along the channel. This void fraction perturbation (or density wave) travels in a speed near the vapor velocity, and produces a channel pressure drop fluctuation with a time delay with respect to the initial flow rate change. If the flow rate and pressure drop fluctuations satisfy certain relations, self-sustained oscillations may occur. The period of density-wave oscillations is usually close to twice that of the vapor transit time through the channel and is on the order of seconds [7].

Two types of density-wave instabilities have been observed: loop instabilities and parallel-channel instabilities [9]. For loop instabilities, the boundary conditions of the channel are determined by the flow rate versus pressure drop characteristics of the external loop. Figure 2.1 shows the variations of the local pressure gradients of a boiling channel with sinusoidal inlet flow rate fluctuations [10]. The time delay of local pressure

drops introduced by the traveling density wave is shown. The resulting total channel pressure drop variation, is sinusoidal but with a phase lag with respect to the inlet flow rate. If this phase lag reaches 180 degrees, then the effective channel pressure drop versus flow rate characteristic curve will have a negative slope, and loop instabilities may occur. This stability type is call “density wave instability”.

The total pressure drop is broken down into frictional, elevation (gravity), spatial acceleration, and temporal acceleration (inertia) terms. Each term has a different dependency on velocity and void fraction profiles and, thus, has different phase shift with respect to the inlet mass velocity variation. Under certain conditions, the phase relationships between pressure drop components may result in a total cancellation on the pressure drop variation. Then the flow oscillations can be sustained.

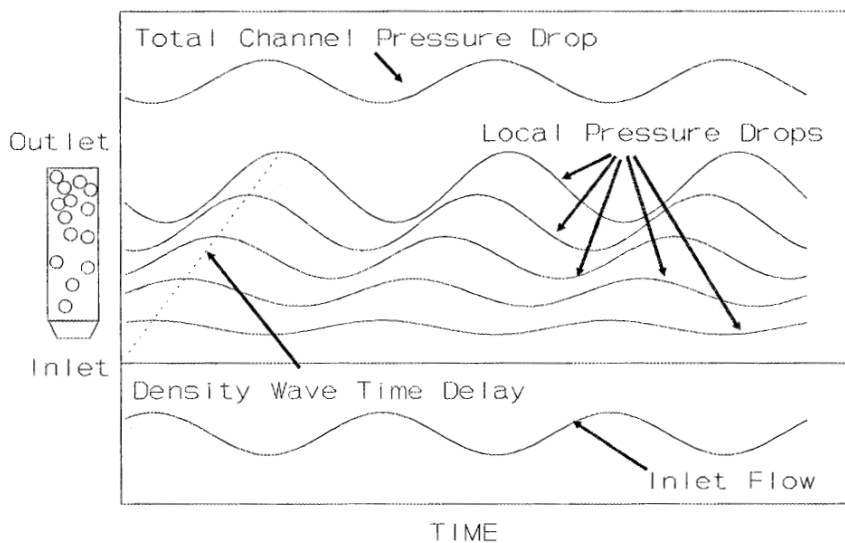


Figure 2.1. Density wave instability mechanism. Local pressure drop variations due to inlet flow fluctuation (from [10]).

Several modes of parallel-channel oscillations can occur [10]. It can be that only the flow of one channel is oscillating, while the flow of the rest of the channels stays nearly constant; or it can be that the flow of half of the channels oscillates out of phase with the flow of the other half of the channels; or it can

be three groups of channels oscillate 120 degrees out of phase with respect to each other.

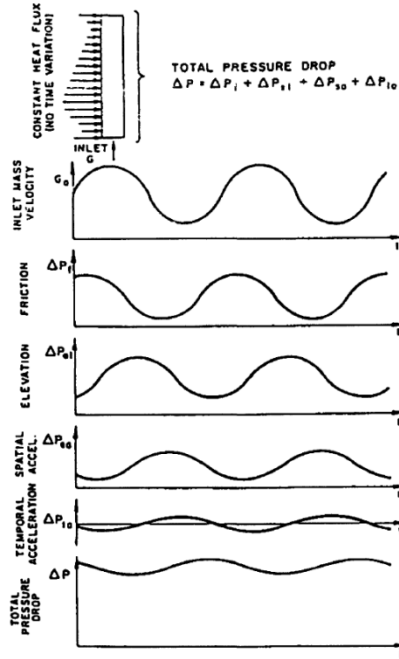


Figure 2.2. Variations of pressure drop components for parallel-channel type oscillations (from [11]).

2.1.2 Nuclear Feedback

The power generation from a BWR core is coupled to the coolant thermal-hydraulic conditions through a reactivity feedback mechanism. The water in a BWR acts both as a coolant and a neutron moderator. The density of the water affects the efficiency of neutron moderation. A BWR usually has a negative void reactivity feedback coefficient. If the void fraction in a BWR core increases, it produces a negative reactivity change and the power decreases. This coupling between the void fraction and power, combined with the dynamics of fuel rods, forms a feedback loop that can lead to power oscillations. Figure 2.3 illustrates the nuclear feedback loop in a BWR [12]. Starting from the upper left corner of figure 2.3, an increase in voids in the core reduces reactivity and the power. The heat transfer from the fuel rods to the coolant is reduced, but with a time delay due to the thermal inertia of the fuel

rods. With less heat transferred to the coolant, the void in the core is reduced, and the power is increased through the void reactivity feedback. Then, after the time delay due to fuel rod dynamics, the void is increased again. This completes a cycle of power oscillations. This mechanism when acting alone is also called reactivity instability [10].

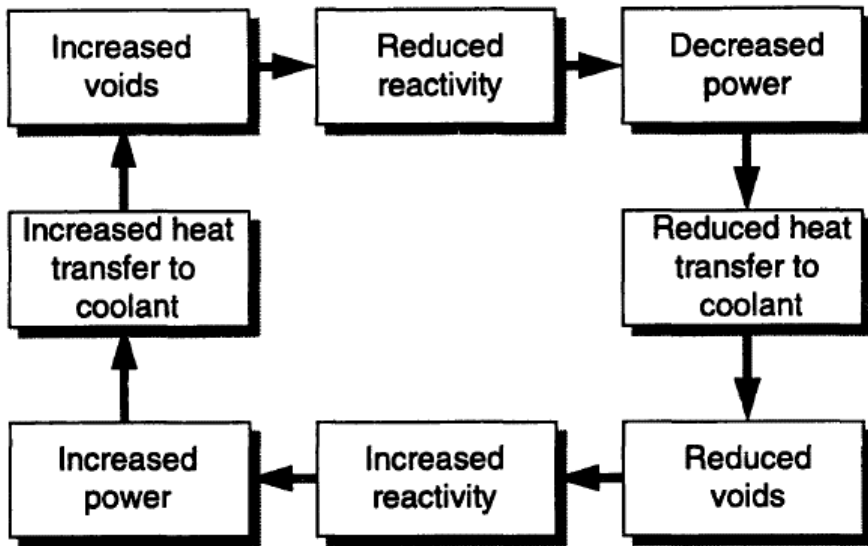


Figure 2.3. Nuclear feedback loop in a BWR (adapted from [12]).

2.1.3 Modes of BWR Instabilities

Three spatial modes of BWR instabilities have been observed: single channel, core-wide (in phase), and regional (out of phase) oscillations [10] [13].

Single channel oscillations were observed during special tests when a coolant channel was partially blocked by a failed flowmeter. The flow of this channel then oscillated following the density-wave mechanism while all other channels remained stable. This type of instability has been reported only once, but it can be very dangerous because it is hard to detect [10].

Core-wide oscillations are caused by loop type density-wave instabilities coupled with reactivity instabilities. In this type of instability, all the channels in the core oscillate in phase with each other. The spatial power shape during

oscillations corresponds to the fundamental mode of neutron flux shape (steady-state distribution). Axial power shape changes have also been observed during core-wide power oscillations. Because the whole core responds in phase, this type of oscillation can be detected by Average Power Range Monitors (APRMs).

Regional oscillations are parallel-channel type density-wave instabilities coupled with neutronic oscillations. During regional oscillations, part of the channels oscillates out of phase with the other channels: the power or flow of the channels in one region increases while that of the channels in the other region decreases. The power shape in regional oscillations relates to a higher harmonic mode of the neutron flux shape (subcritical modes). Normally, these subcritical modes would be damped out because the eigenvalues of these modes are less than one. However, when these subcritical flux modes are coupled with parallel-channel oscillations, sustained power oscillations can be realized [14] [15].

The variations in the total power and flow rate during regional power oscillations are smaller than the local variations due to spatial cancellations. Multiple Local Power Range Monitors (LPRMs) are needed for early detection of out of phase oscillations.

2.2 DEPENDENCE OF STABILITY ON CHANGES IN OPERATING VARIABLES

Many parameters affect the stability of a BWR. Because BWR power oscillations involve complex processes, the effect of a physical parameter on BWR stability some-times depends on other parameters. So it is not always possible to find a set of system parameters that can ensure stability.

In general, the following changes of individual parameter decrease stability [6], [7], [10], [12], [16], [17], [18], [19], [20]:

1. Increasing power: This increases the void content of the core, which increases feedback from the density-wave mechanism. It also increases reactivity feedback because the magnitude of the void reactivity coefficient is increased [10].
2. Decreasing core flow: This also increases the core void content.

3. Increasing two-phase pressure drop in the core: This enhances the density-wave mechanism.
4. Decreasing single-phase pressure drop in the core: This also enhances the density-wave mechanism.
5. Increasing void reactivity feedback: This enhances the reactivity feedback mechanism.
6. Reducing the fuel rod thermal time constant: This increases the variation of heat flux on the fuel surface during power oscillations, which then increases the void fraction variations and enhances power and flow oscillations. Decreasing the fuel rod thermal time constant also reduces the phase shift between the flow rate and power responses which trends to stabilize the system. For the current BWR fuel designs, the stabilizing effect is usually out-weighed by the destabilizing effect [10], [17], [20].
7. Increasing radial peaking factor: The channel with the highest power usually has more voids and has a higher weighting for reactivity feedback. This hot channel is less stable. The stability of high power channels dominates over lower power channels. So a high radial peaking factor is destabilizing.

The effects of system pressure, axial power shape and inlet subcooling on stability are more complex:

8. System pressure: Decreasing system pressure increases the density difference between water and steam, which is destabilizing. However, Blakeman and March-Leuba observed the opposite effect for extremely bottom-peaked power shapes [16].
9. Axial power shape: Bottom-peaked power shapes have a longer two-phase region and larger voids, so they are more unstable. However, extremely bottom-peaked shapes have been shown to be more stable than intermediate shapes because the reactivity weighting in the upper part is reduced [16].
10. Core inlet subcooling: For the density-wave mechanism, the effect of changing inlet subcooling depends on the original inlet subcooling level [6]. At medium or high subcoolings, an increase in subcooling increases non-boiling length and stabilizes the flow. However, at small subcoolings, the non-boiling length is very short. An increase in

subcooling reduces voids near the inlet region, so the pressure drop that is in phase with the inlet flow rate is reduced, and the flow is destabilized. For nuclear feedback, increasing the core inlet subcooling reduces the void contents in the core and increases core power. The net effect of increasing inlet subcooling, maintaining the power constant, is stabilizing when at high subcoolings and destabilizing when at low subcoolings.

Core-wide and regional oscillations have different sensitivities to system parameters. Regional oscillations have a large gain from parallel-channel instabilities because they do not have damping of the external loop, but they have a damped feedback from subcritical neutronic modes. The damping of subcritical neutronic modes depends on the eigenvalue of each mode, and a larger eigenvalue corresponds to a less damped mode. From the one-group diffusion theory, the eigenvalue of a harmonic mode can be expressed as [21]

$$\lambda_i = \frac{\nu \Sigma_f}{DB_i^2 + \Sigma_a} \quad (2.1)$$

where

λ_i is the eigenvalue of the i -th neutronic mode,

$\nu \Sigma_f$ is the fission neutron yield times fission cross section,

D is the diffusion coefficient,

B_i^2 is the geometric buckling of the i -th mode, and

Σ_a is the absorption cross section.

These eigenvalues are less than one except for the fundamental mode which is equal to one for steady-state conditions. The reactivity separation between fundamental and subcritical modes can be expressed as [14]

$$\Delta_{\rho_{subcritical},i} = \frac{1}{\lambda_i} - \frac{1}{\lambda_0} = \frac{D \Delta B_i^2}{\nu \Sigma_f} \quad (2.2)$$

where $\Delta B_i^2 = B_i^2 - B_0^2$. A small subcritical reactivity means less damping of the subcritical mode. In that case, the reactor is more prone to the out of phase type instability.

So, the conditions that favour out of phase oscillations over the core wide type are [10]:

1. low geometric buckling,
2. high fission cross section,
3. high pressure drop across the core,
4. high core flow rate,
5. high pressure loss in the external loop,
6. highly bottom-peaked axial power shapes, and
7. low single-phase friction.

Another important factor that greatly affects stability is the uniformity of channel hydrodynamics characteristics. If a core contains two or more types of channels with different pressure drop characteristics (mixed cores), then this core will be less stable than the cores with channels of only one type [22], [23]. Therefore, when doing reload designs, the compatibility between different fuel designs must be examined.

2.3 ANALYSIS METHODS FOR BWR STABILITY

Various methods have been used to analyze BWR stability. These methods have different applications, and they are complimentary to each other in understanding and controlling BWR stability.

BWR stability is traditionally described in terms of Decay Ratios (DRs). The decay ratio is defined as the ratio of the peak amplitude of an oscillation to that of the previous oscillation following an impulse disturbance (see figure 2.4, [12]). A system is stable with a DR less than one, and unstable with a DR greater than one. The DR relates to the poles of a system's closed loop transfer function [24]. For a second order linear dynamic system, the DR is the same for any two consecutive oscillation peaks. For higher order system, the DR is not a constant, and the appropriate stability indicator is the asymptotic DR corresponding to the least stable poles of the system.

The decay ratio is the stability indicator for single-input, single-output systems (SISO). BWRs, however, are multiple-input, multiple-output systems (MIMO). A single DR cannot be expected to represent the whole picture of the stability of a BWR [25].

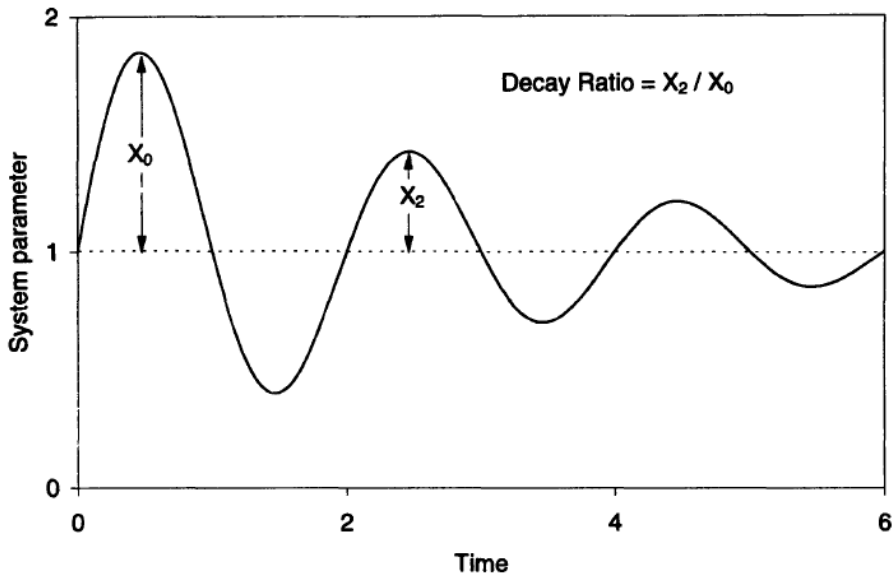


Figure 2.4. Definition of the Decay Ratio (adapted from [12]).

2.3.1 Experimental Methods

Several BWRs have performed special stability tests [26], [27]. These tests not only determined the stability of the particular plant but also formed a data base for the qualification of analytical methods.

These tests were done by perturbing one input parameter and measuring the output responses of reactor power. The two input parameters that have been used are pressure and reactivity. Control rod oscillations were used to generate reactivity perturbations. Pressure perturbations were produced by disturbing the system pressure controller.

Two time variations have been used for input perturbations. The first type is sinusoidal oscillations. Several frequencies of sinusoidal signals were used to cover the frequency range of interest. The other type of perturbation is Pseudo Random Binary Sequence (PRBS), which simulate white noise.

Collected test data were reduced by frequency domain analysis. A transfer function was fitted to the test data, and the decay ratio was calculated from this transfer function.

2.3.2 Stochastic Methods

Stochastic methods are based on neutron noise analysis to deduce stability information. Random processes such as the collapse of a steam bubble in the core produce noise in neutron flux signals. This noise contains information about the system.

The stability of BWR can be estimated by methods such as an autocorrelation function, autoregressive modeling, or a power spectral density fit [24]. To have an accurate estimation, a long history of neutron noise data is needed. The required data length also depends on the system conditions: the more stable the system is, the longer data length is needed.

On-line stability monitors based on neutron noise analysis have been developed [28]. This type of stability monitor can only provide the current status. It cannot predict stability that would result from changes in conditions.

2.3.3 Analytical Methods

Analytical calculations of BWR stability are very complex and require computer simulations. Many computer codes have been used to study BWR stability. They fall in two categories: frequency domain and time domain codes [4].

2.3.3.1 Frequency Domain Codes

Frequency domain codes are developed particularly for BWR stability analysis. The procedure of stability analysis in the frequency domain is:

1. Select a set of governing equations and constitutive relations,
2. Linearize these equations by using a first order perturbation approximation,
3. Laplace transform the linearized equations into frequency domain, and
4. Determine the stability by using linear control theories.

The advantages of using frequency domain codes are less computer time and fewer numerical problems [23]. Some examples of frequency domain codes are FABLE, LAPUR and NUFREQ [4]. Note, however, that non-linear phenomena such as limit-cycle oscillations cannot be modeled.

2.3.3.2 Time Domain Codes

Time domain codes integrate the system governing equations directly, and calculate the state variables at each time step. These codes are usually general purpose codes, not developed specifically for stability analysis. They are useful in calculating system parameters, such as the peak clad temperature and MCPR during power oscillations. They can also predict the peak amplitude of non-linear limit cycle oscillations.

When using time domain codes to study BWR stability, special caution should be paid to the numerical damping problem [29], [30], [31]. Many time domain codes incorporate special numerical methods for avoiding numerical instability and reducing computer time. Numerical schemes such as up-wind differencing and multi-step methods will produce a numerical damping effect that may mask the oscillatory behavior.

Examples of time domain codes used for BWR stability analysis are RAMONA-3B, TRAC-BF1, TRACG, TRACE, RETRAN, BNL EPA, SABRE, TRAB, TOSDYN-2, STANDY, and SPDA [4].

2.4 NEW CHALLENGES FOR BWR STABILITY: NEW FUEL DESIGNS AND NEW OPERATION DOMAINS.

2.4.1 New Fuel Designs

One determining parameter for BWR fuel assemblies' operational and safety margins is the linear heat generation rate (LHGR). The LHGR is calculated as the thermal power of a reactor divided by the accumulated (active) length of all fuel rods. The LHGR decreases as the fuel rod arrays increase. The introduction of a 10x10 or 11x11 array with a slightly reduced rod diameter (smaller fuel time constant) and a larger rod surface area (higher pressure loss due to friction) has an adverse effect on the thermal-hydraulic/nuclear stability of the core. These effects must be compensated by the increased number of the part-length rods and a careful balance of their arrangement supported by a low pressure drop spacer grid design and upper tie plate. Thermal-hydraulic models must reproduce each effect separately, applying the best two-phase flow friction models to be able to account for accurately each contribution.

On the other hand, it is worth noting that there are other circumstances that unintentionally introduced stabilizing factors in new fuel designs. It is known that the major cause of failure of fuel is debris fretting and the implementation of anti-debris filters introduced additional local losses in the lower support piece which has a stabilizing effect.

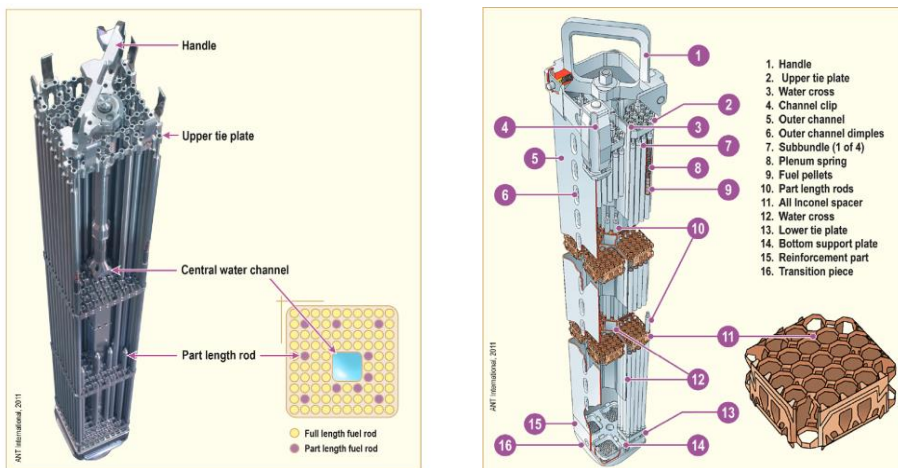


Figure 2.5. Examples of fuel designs: ATRIUM 10XP (AREVA NP) and SVEA-96 OPTIMA-2 (WESTINGHOUSE SWEDEN AB) from [32].

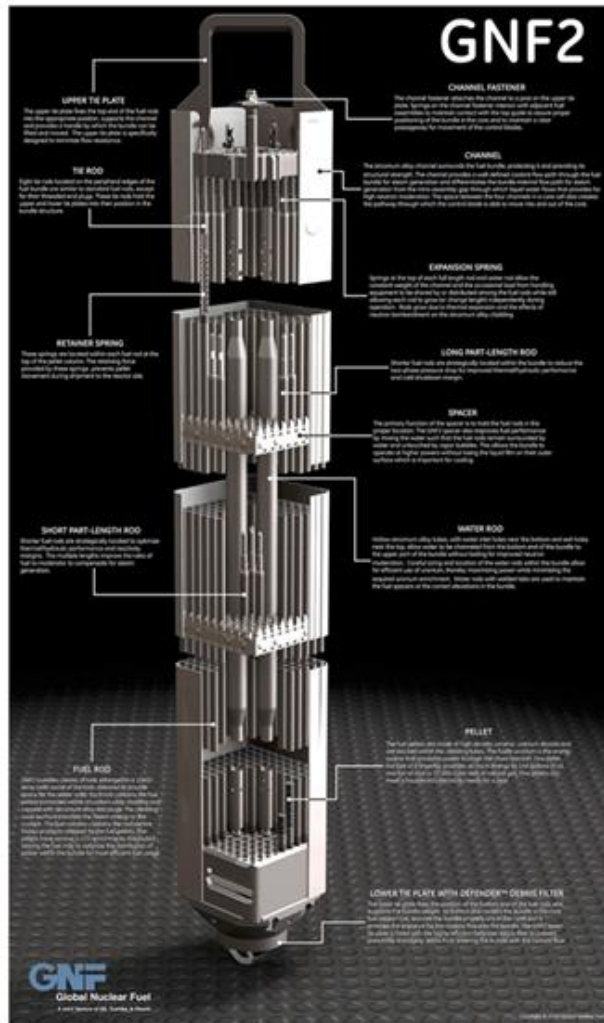


Figure 2.6. Fuel design GNF2 (GNF) [33].

2.4.2 New Operational Domains

In general, boiling water reactors (BWRs) have a characteristic relation between core flow and power generation. For a fixed amount of control rod withdrawal from the core, constant rod lines (also called flow control lines and load lines, e.g., Maximum Extended Load Line Limit Analysis (MELLLA) and MELLLA+) can be established. Increasing the core flow slowly will increase the power along these constant rod lines by reducing voids in the moderator

and its associated void reactivity feedback. Load line limits are established to satisfy various safety limits including fuel thermal limits.

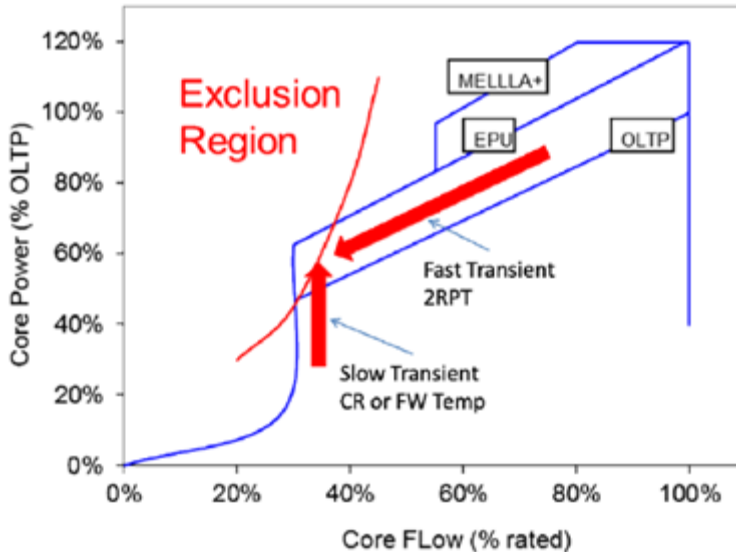


Figure 2.7. Maximum Extended Load Line Limit Analysis (MELLLA +) domain [34].

As power uprates (e.g., up to 120% of the original licensed power) are implemented, load line limits are raised to realize increased power generation at a design (maximum) core flow limit. However, core thermal hydraulic stability is aggravated by power uprates and changes the power/flow operating map in a direction that causes a tendency to encounter instability at the upper left corner of the power/flow map (that is, high power/low core flow conditions), as shown in figure 2.7. The unstable operation of the reactor core can result in diverging neutron flux (and heat flux) generation due to resonance occurring between void reactivity feedback and heat flux generation which effects void creation. Diverging power oscillations can give rise to alternate dry-out and re-wetting of fuel cladding and eventually cause cladding failures. It is therefore highly desirable to avoid core operation in this region of the power/flow map (upper left corner).

Two different types of transients (See figure 2.7) are limiting in terms of stability:

1. Slow transients associated with start-up procedures, where the instability region is entered slowly and slightly because of control rod motion. These transients have been observed in the fleet and result in small amplitude oscillations that could be handled manually by the operator, but the LTS (Long Term Solution) are designed to provide protection. Using figure 2.7 as a reference, this type of event would start at low flow-low power, and slowly increase power by either withdrawing control rods or from an unexpected feedwater (FW) heating transient.
2. Fast transients associated with loss of recirculation flow. These transients occur when one or two recirculation pumps are tripped. The instability region may be entered fully and rapidly, resulting in large amplitude oscillations that would be hard to manage manually by the operator. For this event, the initial operating conditions would be a full power and the flow reduction (e.g., a recirculation pump trip) would force a trajectory parallel to the blue lines in figure 2.7, which would enter into the exclusion region.

2.5 CHAPTER SUMMARY

The leading mechanism to produce a 180° phase delay to become a BWR reactor unstable has been reviewed. The importance of the two phase pressure drop role and the neutronic feedback is also described. The stability of a BWR depends on many factors such as the reactor power, core flow, pressure, power shape, reactivity feedback coefficients, and the core inlet subcooling. The effects of changing these variables on the system stability may be counter intuitive. Wide core or in phase and regional or out of phase oscillations fundamentals and the difficulty of detecting out of phase limit cycle with the conventional Average Power Range Monitor (APRM) have been also compiled in this chapter. Finally, the challenges of the new operational domains increasing the slope of the Maximum Extended Load Limit Line in order to gain spectral shift margin at the uprated power and main concerns under stability standpoint have been pointed out.

3 STABILITY CONTROL METHODS

3.1 INTRODUCTION

The potential for Boiling Water Reactor (BWR) instabilities has been recognized since the beginning of BWR development. In US NRC regulations require that a nuclear reactor be designed such that power oscillations "are not possible or can be reliably and readily detected and suppressed" [35]. For BWRs, analyses in the design stage were used to show compliance with the regulations in the past.

BWR power oscillation experience outside the United States include the Coarso NPP in Italy [36], the Ringhals-1 in Sweden [37], and the Cofrentes NPP in Spain [38]. In the United States, several significant BWR power oscillation events occurred. First, on March 9, 1988, a power oscillation event occurred at LaSalle NPP Unit 2 (LaSalle-2) reactor [39]. This event raised

concerns about the adequacy of the past analyses and the impact on plant safety; research was initiated to resolve this issue. On August 15, 1992, another power oscillation event was experienced by Washington Nuclear Power Unit 2 (WNP-2) [22]. This event again confirms the need for new approaches to ensure BWR stability. On July 24, 2003, a core wide mode instability event occurred at Nine Mile Point 2. The instability event lasted for about 40 seconds and terminated by the PBDA in a reactor scram [40]. Recently, on March 19, 2015, the reactor protection system at Fermi 2 initiated an automatic reactor scram on Oscillation Power Range Monitor (OPRM) Upscale following the manual trip of the north reactor recirculation pump due to a cooling water leak [41].

This chapter reviews the issue of BWR stability. First, the safety concerns of BWR power oscillation are described. Then, the oscillation mechanism and the sensitivity of stability to system parameters are discussed. Next, the methods to study BWR stability are summarized. Finally, the approaches to resolve this issue are presented.

3.2 SAFETY CONCERNS OF BWR POWER OSCILLATIONS

Power and flow oscillations in a nuclear reactor are very undesirable. One of the major concerns is the fuel integrity during power oscillations. If the oscillation amplitude is large, the fuel rods may experience periodic dry-out and rewetting [42], if the scram is not initiated on time. The safety limit of the Minimum Critical Power Ratio (MCPR) may be violated during an extended period of dry-out.

Another safety concern is the consequences of an Anticipated Transient Without Scram (ATWS) event. By procedure, if an ATWS event occurs the recirculation flow is reduced to reduce the reactor power. For most ATWS events, extraction steam from the turbine will not be available, which will result in a large subcooling event that will increase the power significantly. If the reactor is operating in the highest power minimum flow state-point (MELLL), the reactor will be driven into a high power, low flow condition which is most susceptible to power oscillations. If an ATWS event is followed by power oscillations, the heat capacity of the suppression pool may not be

large enough to accommodate the possible heat load. Several analyses have shown that the mean fission power increases as the amplitude of power oscillation increases [29], [43]. The steam that is discharged into the suppression pool during the ATWS and power oscillation event may cause the temperature of the suppression pool to exceed its limit.

Because of these safety concerns, it is necessary to demonstrate the stability margin of a BWR in the design stage and identify the stability boundary in the operation stage. If a power oscillation event occurs, it has to be suppressed immediately.

3.3 APPROACHES FOR RESOLUTION OF THE BWR STABILITY ISSUE

On March 9, 1988, LaSalle Unit 2 experienced an instability event. The LaSalle event is described in NRC Information Notice 88-39, "LaSalle Unit 2 Loss of Recirculation Pumps With Power Oscillation Event," dated June 15, 1988. NRC Bulletin 88-07, also dated June 15, 1988, highlighted the generic concerns identified in light of the LaSalle event and requested all BWR licensees, regardless of BWR type or analytical core stability margin, to review the adequacy of procedures and instrumentation to respond to power oscillations, and requested review of operator training programs with regard to power oscillations. In response to these concerns, the BWR Owners' Group (BWROG) initiated a project to investigate actions that should be taken to resolve the BWR stability issue.

3.3.1 Interim Corrective Actions

On October 28, 1988, the General Electric Company (GE) notified the NRC under 10 CFR Part 21 that thermal margins might not be sufficient to prevent violation of the minimum critical power ratio safety limit for some BWR plants if a 10-percent average power range monitor (APRM) oscillation was used as a procedural action point for manual scram of the plant. Based on this possibility, GE recommended stability "interim corrective actions" in a November 1988 letter to BWR utilities. On December 30, 1988, the NRC issued Bulletin 88-07, Supplement 1, [44] approving the proposed BWROG/GE interim operating recommendations and stating additional

conditions. One of these conditions addressed the applicability of the experience-based stability exclusion boundaries defined in the interim operating recommendations, and noted the need to re-evaluate and justify these boundaries for cores that include new fuel designs. This bulletin also discussed long-term corrective actions. Such corrective actions might include hardware modifications or additions to facilitate manual or automatic protective response to avoid neutron flux oscillations or to suppress oscillations should they occur. Since it is possible for some oscillations to grow to levels exceeding NRC safety limits in the order of a minute, automatic protection action is generally indicated. The detailed design specifications for the automatic protection are being defined by an expanded post-LaSalle BWROG study to develop a generic resolution to the stability issue.

The Interim Corrective Actions define exclusion regions on the power-flow map (see figure 3.1).

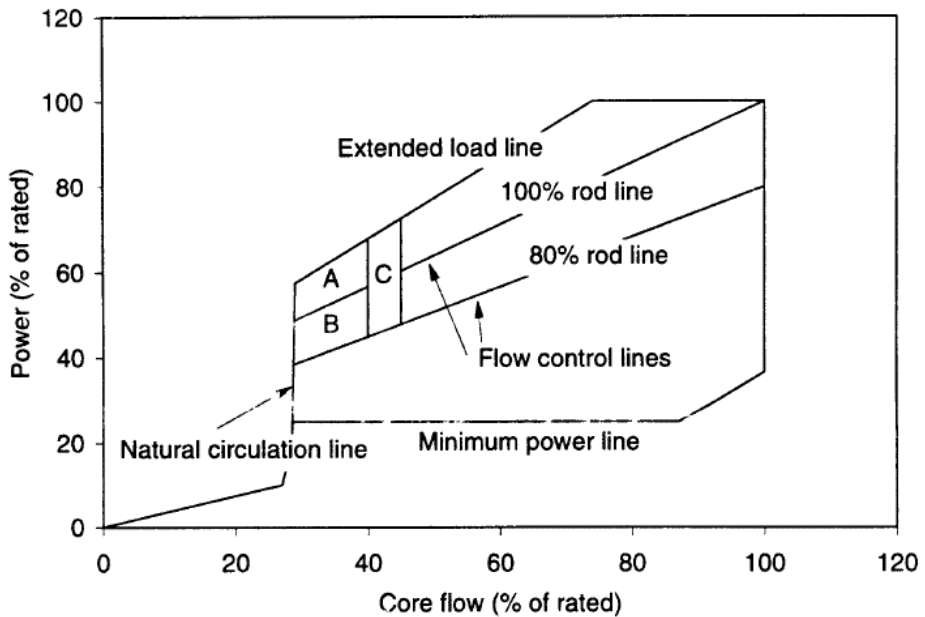


Figure 3.1. Exclusion regions defined by the Interim Corrective Actions (adapted from [44]).

These high powers, low flow regions are most susceptible to instability. In these regions, the natural circulation flow contributes to a large portion of the

total core flow. So the core flow is very sensitive to the void contents in the core. This situation enhances the density-wave instability.

Region A in figure 3.1 is the area above 100% rod line and on the left of the 40% flow line; Region B is the area between 100% and 80% rod lines, and on the left of the 40% flow line; Region C is the area above 80% rod line and on the left of the 45% flow line. Operation within Regions A and B are prohibited, and if entered, the operators should bring the reactor out of these regions immediately by inserting control rods or scram. Operation in Region C is allowed only for control rod withdrawals during startup requiring Preconditioned Interim Operational Management Recommendations (PCIOMR). Operators are also required to scram the reactor if power oscillations occur, or if all the recirculation pumps are tripped.

In June 1991, the BWROG issued NEDO-31960, which documented proposed long-term solutions to the stability issue as well as methodologies that have been developed to support the design of these long-term solutions. Supplement 1 to NEDO-31960 was issued in March 1992 and contained final methodology details and additional information requested by the NRC.

On August 15, 1992, Washington Nuclear Power Unit 2 (WNP-2) experienced power oscillations during startup. The WNP-2 operators recognized the oscillations and responded promptly, consistent with their procedures and training, to initiate a manual scram. The NRC evaluated this event, concluding that the primary cause of the oscillations was very skewed radial and bottom peaked axial power distributions due to insufficient procedural control of control rod removal patterns during power ascension. It was concluded from discussions with other licensees that similar procedural practices were not unusual for some other BWRs. The skewed power distributions make the core tend towards the "harder to detect" out-of-phase oscillation mode. The WNP-2 power distribution was inconsistent with the more normal operating conditions that have been associated with the experience-based stability exclusion boundaries, and was also inconsistent with the power distribution assumptions employed in the methodology for development of long-term solution exclusion region boundaries based only on power and flow parameters. The WNP-2 core design, consisting of a mixture of 9x9 and 8x8 fuel types which caused unbalanced flow and pressure drop

characteristics, was also a contributor to uncertainty in its stability exclusion boundary. The WNP-2 event is described in [45].

The operating point of the WNP-2 when power oscillations occurred is outside the exclusion regions and it was attributed to an aggressive control rod pattern during startup that resulted in an extreme radial power peaking. This event proves again that the approaches used in the past are insufficient in dealing with BWR stability problem. It also shows that these exclusion regions do not cover all the unstable conditions.

3.3.2 Long Term Solutions

NRC issued a new Generic Letter [46], requiring:

1. All licensees of BWRs, except for Big Rock Point which does not have the capability for operation under variable flow conditions, are requested to review their current procedures and training programs and modify them as appropriate to strengthen the administrative provisions intended to avoid power oscillations or to detect and suppress them if they occur prior to implementation of the long-term solutions.
2. All licensees of BWRs, except for Big Rock Point, are requested to develop and submit to the NRC a plan for long-term stability corrective actions, including design specifications for any hardware modifications or additions to facilitate manual or automatic protective response needed to ensure that the plant is in compliance with General Design Criteria 10 and 12.

The BWROG submitted and the NRC staff approved three different stability LTS options [47], [48]. These options can be summarized as follows:

- Option I. Based on Exclusion Region definition: A region outside which instabilities are very unlikely is calculated for each representative plant type using well-defined procedures. If the reactor is operated inside this exclusion region, an automatic protective action is initiated to exit the region. This action is based exclusively on power and flow measurements, and the presence of oscillations is not required for its initiation.

Two concepts of Solution I were submitted by the BWROG and approved by the NRC staff:

- Option I-A. Immediate protection action (either scram or select rod insert) upon entrance to the exclusion region.
- Option I-D. Some small-core plants with tight inlet orifices have a reduced likelihood of out of phase instabilities. For these plants, the existing flow-biased high APRM scram provides a Detect and Suppress (D&S) function to avoid safety limits being exceeded for the expected instability mode. In addition, administrative controls are proposed to maintain the reactor outside the exclusion region.
- Option II. Quadrant-Based APRM scram. In a BWR/2, the quadrant-based APRM is capable of detecting both in phase and out of phase oscillations with sufficient sensitivity to initiate automatic protective action to suppress the oscillations before safety margins are compromised.
- Option III. LPRM-Based D&S. Local Power Range Monitor (LPRM) signals or combinations of a small number of LPRMs are analyzed on-line by using three diverse algorithms. If any of the algorithms detects instability, automatic protective action is taken to suppress the oscillations before safety margins are compromised. The licensing algorithm is the PBDA, whereas the Amplitude Based Algorithm (ABA) and the Growth Rate Algorithm (GRA) have a Defense-in-Depth (DID) function.

3.3.3 Prevention Based Methodologies: Enhanced 1A (E1A)

3.3.3.1 E1A Stability Solution Description

The E1A stability solution [49], developed by General Electric Company (GE) and BWR Owners Group, complies with General Design Criterion 12 of 10CFR50.55 Appendix A through the use of licensing features that prevent reactor instabilities from occurring considering reasonably limiting anticipated operating conditions. Defense-in-depth (DID) features are incorporated into the solution to improve overall reactor safety. In addition to providing diverse methods and systems to prevent the onset of reactor instability, defense in

depth features provide protection against unanticipated and hypothetical events that can result in an unstable condition.

Reactor instability is a continuous function of power and flow in the operating domain. In general, there is a gradual increase in the likelihood for instabilities to occur as core power is raised and core flow is lowered. The E1A solution design addresses the implications of these characteristics by affording progressively more restrictive operating requirements as susceptibility to reactor instability increases. Automatic prevention is warranted where susceptibility to instabilities is anticipated during normal operations and a result of moderate frequency events. Protection from instabilities under conditions that are not anticipated or are beyond the existing design basis of the reactor systems should come from combined automatic and manual actions. This approach provides assurance that the degree of protection against instabilities is commensurate with the likelihood of occurrence.

The design philosophy of progressive protection is coupled with conservative stability regions boundaries and mandated operator actions. These stability regions boundaries as well as the associated automatic or manual actions with each area can be summarized as follow:

1. Areas of existing operating domain anticipated to be susceptible to reactor instabilities such that Exclusion region and Restricted region. The E1A solution introduces combination of automatic protection and operating limits to enforce these stability licensing regions.
 - i) The Exclusion Region is analytically defined to be that area of the licensed core power and flow operating domain where the reactor is susceptible to coupled neutronic/thermal-hydraulic instability. The reactor is automatically prevented from operating in this excluded region by the APRM flow-biased reactor trip function of the Neutron Monitoring System (NMS).
 - ii) The Restricted Region of E1A is defined to be that area of the licensed core power and flow operating domain where the reactor is susceptible to coupled neutronic/thermal-hydraulic instability without regard to core void distributions. Automatic controls such that E1A APRM control rod block setpoints, as well as administrative

controls (boiling boundary) [50], are implemented to prevent entry into Restricted Region during deliberate reactor operation. Anticipated transients that initiate outside the Restricted Region and terminate inside the Restricted Region are also not expected to result in reactor instability. However, continued operation inside Restricted Region is not permitted without placing specified administrative controls.

- iii) Monitored Region, which is defined to be that area of the core power and flow operating domain where the reactor may be susceptible to reactor instabilities under conditions exceeding the licensing basis of the current reactor system. This defense-in-depth (DID) feature is provided to preclude reactor instability even under unanticipated conditions. Continued operation within the Monitored Region boundary requires the presence of an automatic stability detection system.

3.3.3.2 E1A Methodology Application Process

The E1A application process can be divided into two steps:

1. Initial application process. The initial application process of E1A encompasses:
 - i) the generation of stability region boundaries,
 - ii) the analysis to validate the region boundaries,
 - iii) the generation of E1A APRM trips reference setpoints, and specification of performance requirements for stability methods utilized in the process.

The initial application process is used for all plant applications.

2. Reload review process. Reload review process for E1A establishes the continued applicability of existing stability region boundaries for each new cycle. Changes to reactor, core, and fuel designs are assessed to establish the scope of any required stability reload analysis. If the continued applicability of the existing region boundaries cannot be demonstrated, the appropriate reload analysis has to be performed,

including, if necessary, the generation of new region boundaries and trip reference setpoints.

This process is designed to ensure that the E1A stability methodology can be implemented in any GE design BWR using qualified stability analytical tools. Decay ratio calculations form the framework for the generation and validation of the stability region boundaries.

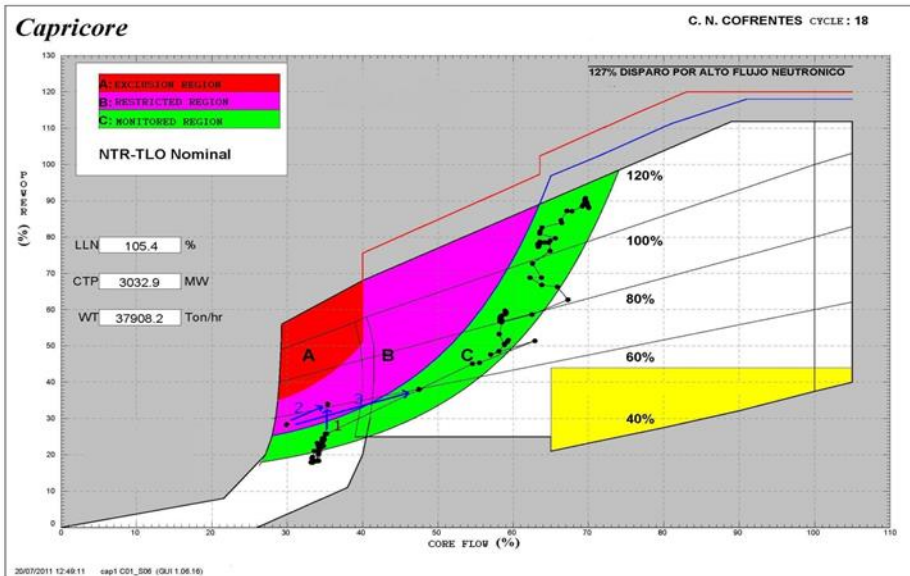


Figure 3.2. Power-flow map for a BWR-6 with E1A stability regions. Example of a typical start-up path.

3.3.3.3 E1A Methodology: Advantages and Drawbacks

3.3.3.3.1 Advantages

E1A could be implemented with a minimum hardware upgrade. Automatic stability detection system associated with Monitored Region requires only connecting a sample of LPRM to an analogic to digital converter. The algorithm is based on period named Period Based Detection System (PBDS), filters the signal to detect a period close to two seconds (frequency of 0.5 Hz) to determine the onset of an instability above an amplitude threshold. The economic cost is very low in comparison with other methodologies which require the upgrade of the nuclear analogic nuclear instrumentation to digital.

Decay ratio based prevention philosophy precludes supporting the automatic protection in thermal limits explicit calculation (Critical Power Ratio, CPR). This option does not affect to plant thermal limits.

3.3.3.4 Drawbacks

Decay ratio calculations are based on end of cycle (EOC) Haling depletions [51]. Haling's principle is based on fuel depletion with a constant flat power profile. Axial power distributions used in decay ratio calculation leads to more bottom peaked axial profiles. The use of real burnup distribution at EOC in a BWR produces less conservative results.

For power ascension during the startup, operation in restricted region requires boiling boundary control. After upshift recirculation pumps to high speed is required to withdraw shallow rods used for boiling boundary control. From this state-point the startup is not compatible with boiling boundary control and the power increase must be carried out of restricted region (figure 3.2). This is not desirable under a pellet clad interaction PCI stress control.

During rapid power increases above previous operating levels, thermal expansion of the fuel pellets can produce Pellet Clad Interaction (PCI) [52] that causes high localized stress in the cladding. When these stresses occur in the presence of fission products, the PCI may cause failure of the cladding. The PCI "envelope", estimated value of linear power versus burnup at models consider "closed" the rod gap for the limiting fuel (typically 80%) is reached at higher core flow rate because is not possible to penetrate into restricted region. At this power and core flow levels, withdrawing control rods makes impossible the power increase without violating PCI limits. Once this envelope is reached slow controlled power ramp is required, typically 20 MWe per hour, in order to maintain a controlled stress on the fuel clad.

Even though the fuel clad incorporates an internal layer of an alloy of Zirconium and Fe ("barrier fuel") [53] defects in the pellets could increase stress to reach the failure level threshold and some Preconditioning Interim Operating Management Recommendation (PCIOMR), with some differences in implementation depending on vendor suppliers, are still in use.

3.3.4 Option III. LPRM-Based Detect & Suppress

3.3.4.1 D&S Basis

The existing “detect and suppress” algorithms of Long-Term Solution Option III, [47], [48], [54] and [55], are based on a common approach. An Oscillation Power Range Monitor (OPRM) cell signal oscillation, consistent with that characteristic of the reactor T-H oscillation frequencies, is identified. The presence of these characteristic power oscillations is then confirmed by various methods. The Period Based Detection Algorithm (PBDA) monitors successive oscillation periods and provides an oscillation amplitude trigger to generate a reactor trip signal. The Growth Rate Algorithm (GRA) consists of an oscillation growth rate limit, which if exceeded, generates a reactor trip. Finally, the Amplitude Based Algorithm (ABA) consists of an oscillation amplitude limit, which if exceeded, generates a reactor trip. The Option III licensing basis [54] and [56] relies on the PBDA, with setpoints based on a combination of power oscillation period successive confirmation counts (SCCs) and oscillation amplitude. These setpoints are designed to ensure that the Safety Limit MCPR (SLMCPR) is not exceeded by the presence of growing power oscillations resulting from anticipated instability events. In addition to these, several other stability solutions have been developed and adopted for other BWRs worldwide.

3.3.4.2 Changes in Stability LTSs and in Designs

Options I-D, II and III are all based on a D&S approach and have been implemented as stability LTS in most of the commercial BWR Nuclear Power Plants (NPPs) in the United States (US). Nevertheless there are three significant areas of consideration, which merit a revisit of these three Long Term Solutions (LTS). These areas are: (a) deficiencies identified in the Critical Power Ratio (CPR) versus oscillation amplitude correlation used for D&S solutions (i.e., the DIVOM correlation), which resulted in a 10 CFR Part 21 notification, (b) proposed increases in power density, and (c) advanced fuel bundles designs with increased array size and changes in core design/fuel cycle length.

Options I-D, II and III are currently based on a DIVOM methodology [55], [56], [57] and [58] to determine/confirm acceptable OPRM/APRM setpoints

and corresponding Operating Limit Minimum Critical Power Ratios (OLMCPRs) required to ensure that SLMCPRs are not exceeded as a result of anticipated stability events in BWRs. The DIVOM methodology is based on a correlation that is used to estimate the Δ CPR as a function of oscillation amplitude, and it is required to select the scram setpoint for D&S solutions. The generic DIVOM correlation was approved on the basis that it would be bounding for all reasonable circumstances; however, later analysis demonstrated that some plant-specific calculations result in larger loss of CPR margin than the DIVOM prediction. Therefore, the generic DIVOM curve may be non-conservative for some plant applications. A non-conservative DIVOM curve would then result in stability-related setpoints that would not guarantee that Specified Acceptable Fuel Design Limits (SAFDLs) would be maintained if a limiting instability event were to occur. This potential for a nonconservative generic DIVOM curve introduced the use of plant and cycle-specific DIVOM correlations, which is the approach used by most plants today. The Option I-D, II and III are all based on this plant and cycle-specific DIVOM methodology. In recent years, the industry has been moving to reactor operation at higher and higher power densities and power-to-flow ratios. This operation is, in principle, detrimental to the stability characteristics of the reactor and results in two consequences: (a) it may increase the probability of instability events, and (b) it may increase the severity of the event should it occur (e.g., larger amplitude oscillations). Indeed, simulations of Two Recirculation Pump Trip (2RPT) transients initiated at minimum flow conditions and 120% Original Licensed Thermal Power (OLTP) indicate that instabilities of sufficiently large amplitude to compromise the SLMCPR are possible. In addition to power uprates and flow domain expansions in recent years, advanced BWR fuel designs have been introduced in many plants along with much longer fuel burn-ups. Several US plants now have fuel cycles running on a 24-month schedule with fuel reload performed approximately every two years. As a result, core design strategies have also changed and become more sophisticated. These extended flow and power domains, along with fuel and core design changes, have introduced additional elements of complexity that required more sophisticated tools and analyses of plant conditions under normal operation, anticipated transients, or accident scenarios. These changes require the validation of models and the development of methodologies capable of providing proper predictions of the underlying physical phenomena that are relevant under these new conditions. All of these

changes have introduced challenges to the use of conservative, and, in some instances, excessively conservative methodologies such as DIVOM to determine cycle-specific stability based setpoints and OLMCPRs used for reload licensing and plant operation. The results of the excessive conservatism in DIVOM methodology have caused a significant increase in the stability-based OLMCPRs (for any given setpoint), making stability the limiting event setting the OLMCPR for several units operating cycles.

This circumstance has led to develop new methodologies based on a BEPU methodology, in which the uncertainty is quantified by applying the Code Scaling, Applicability and Uncertainty (CSAU) process.

The Detect and Suppress Solution – Confirmation Density (DSS-CD) is an evolutionary stability LTS approved by the NRC [54] and [55]. DSS-CD is based on the same hardware design as Option III. However, it introduces an enhanced detection algorithm that detects the inception of power oscillations and generates an early power suppression trip signal based on successive period confirmation recognition and an amplitude component. DSS-CD is designed to provide adequate automatic SLMCPR protection for anticipated reactor instability events. The existing Option III algorithms are retained (with generic setpoints) to provide Defense-in-Depth protection for unanticipated reactor instability events. Confirmation Density (DSS-CD) is an evolutionary stability LTS approved by the NRC [54] and [55] which is applicable to MELLLA+ domain.

GS3 [34] is the newest BEPU methodology to demonstrate the validity of stability-related scram setpoints. GS3 is only a methodology to demonstrate the validity of stability-related scram setpoints. It does not also require any hardware and/or software change for plants already implementing Options I-D, II, III. The DIVOM methodology is conservative by design. In the past, industry determined that these conservatisms were a good trade off when best-estimate calculations were very difficult and expensive to perform. However, experience over many years of implementation has shown that the scram setpoints developed using the DIVOM methodology were conservative and satisfied SAFDL requirements with large margins. The results of these conservatisms in the DIVOM methodology have caused a significant increase in the stability-related OLMCPRs (for any given setpoint), making stability the limiting event setting the OLMCPR for several units operating cycles. The

proposed GS3 methodology is essentially a BEPU pre-calculation of the required OLMCPR. In essence, the plant chooses to move to GS3 to prevent spurious scrams, and GS3 specifies the minimum OLMCPR which the plant must use. GS3 is not applicable in the MELLLA+ domain.

3.4 CHAPTER SUMMARY

In this chapter, a review of the main instability events and the regulatory historical and present perspectives and control approaches of BWR stabilities have been outlined. Two main long term approaches for stability control solutions, based on prevention and detection philosophies have been discussed and the advantages and drawbacks for each methodology has been exposed. The computational capabilities the CSAU statistical approaches and the knowledge in depth BWR stability mechanism has led to apply at present full statistical approach in detection based methodologies, increasing significantly operational margins.

E1A is the simplest option: minimum hardware upgrade and a maximum independence of vendors, which lead to a significant cost saving. On the other hand, the D&S option, based on the latest CSAU approaches, minimizes the risk of scram introducing a more flexibility and margin on the operation domain.

4 LAPUR FREQUENCY DOMAIN CODE

LAPUR is a computer code developed at Oak Ridge National Laboratory for the calculation of BWR core stability parameters. It uses a multinodal description of the neutron dynamics together with a distributed parameter model of the core thermal hydrodynamics to produce a space-dependent representation of the dynamics of a BWR in the frequency domain for small perturbations around a steady state condition. The LAPUR program consists of two autonomous modules, LAPURX and LAPURW, which are linked by means of an intermediate storage routine. The first module, LAPURX, solves the governing equations for the coolant and the fuel steady state. Maps of the core steady state are generated and stored in data files for subsequent utilization by LAPURW. The second module, LAPURW, solves the dynamic equations for the coolant, fuel, and neutron field in the frequency domain. A set of open-loop transfer functions are generated and the stability indices are estimated from the closed loop reactivity to power transfer function.

The fuel equations in LAPUR assume no axial heat flow in the fuel rods, use a radial mesh within the fuel pellet to account for the radial dependence of the UO_2 fuel heat conductivity, and include the effect of the nonconductive transfer of heat to the coolant by γ -ray absorption and neutron moderation processes. Coolant dynamics include three flow regions in a flow channel: a no-boiling region, a subcooled-boiling region, and a bulk-boiling region. The conservation equations and the two-phase fluid mechanical equations, in conjunction with the fuel equations, yield a set of transfer functions relating perturbations of the nodal coolant density and pressure drop to nodal perturbations of coolant temperature, flow rate, and power generation. The integration of these functions, along the length of the channel, results a fuel-and-coolant matrix equation of transfer function.

To obtain the reactivity feedback transfer functions matrices, the fuel temperature and coolant density nodal transfer functions are weighted by both the local power and the local density reactivity coefficients and integrated over the volume of the neutronic core.

The overall space-dependent transfer function matrix representation of the BWR core dynamics with feedback is obtained by consideration of the hydraulic coupling through the inlet and outlet plena and the recirculation loop, in conjunction with the neutronic matrix equation. In order to calculate the stability indices (decay ratio and natural frequency), the position of the most unstable pole of the core closed-loop transfer function is determined.

Several improvements have been performed in the code in order to upgrade it for the new fuel design types. The previous LAPUR 5 release 1 code does not consider channel with variable area and does not distinguish specifically local pressure drop due to spacers in a bundle. The only way to take into account local pressure losses and gains due to spacers and area changes is by means of a friction multiplier given by input. This deficiency leads to adjusting by input friction multiplier in order to account for accurately local and variable area effect on the pressure drop.

The new version is LAPUR 6. This version includes new correlations for computing friction and local losses and capabilities for modelling bundles with variable cross-area. As additional improvements, LAPUR 6 allows to use up to 200 thermalhydraulic channel to represent the core and calculates transfer

functions with up to 100 frequency points instead of 25 points for LAPUR 5.1 release 1.

In the next sections we present these improvements, being organized as follows: In section 4.1 we present a LAPUR code overview, the two modules LAPURX and LAPURW are outlined in section 4.2 and 4.3 respectively. The fundamental equations have been described in detail, in section 4.2 the steady state equations for LAPURX, as well as the dynamic equations and the frequency domain formulation in section 4.3 for LAPURW. In section 4.4 the LAPUR transfer function and their topology are explained as well as the numerical method used. Finally the upgrades performed in LAPUR 6, new conservation equations obtained with variable area and a new friction model have been summarized in the sections 4.5 and 4.6 respectively.

4.1 BRIEF DESCRIPTION OF THE CODE LAPUR

In a BWR two distinct interacting dynamic loops are present: a neutronic loop and a thermal-hydraulic loop. The coupling of these two dynamic loops is through the density dependence of the neutron moderation characteristics of the cooling fluid.

The interrelation of the physical mechanisms governing the dynamic response of a BWR core is schematically represented in figure 4.1. As depicted in this figure, a disturbance of reactivity can enter the core via either control rod actuation or changes in coolant parameters such as inlet subcooling, flow rate or pressure. Any of these disturbances results in a change in the neutron population that varies the void content in the core, which in turn affects the neutron population. The magnitude of the void reactivity coefficients, length of the boiling region in the core, void sweep speed and fuel time constant are the most important parameters affecting the dynamic stability of the BWR core.

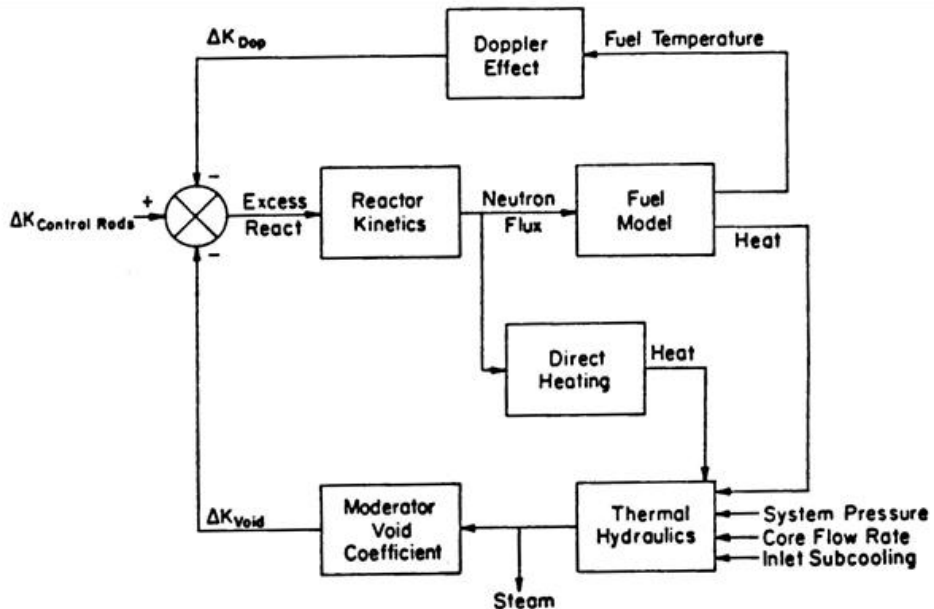


Figure 4.1. Schematic representation of the dynamic processes pertaining to power generation in the core of a BWR.

Another mechanism that adds negative reactivity feedback to the core is the Doppler effect. This effect is due to the temperature dependence of the parasitic absorption of neutrons of the U-238 in the fuel. The magnitude of the Doppler reactivity feedback is small compared with the void reactivity but its immediacy makes it an extremely important factor during large transients, and a stabilizing agent, even if secondary, for small perturbation transients.

In LAPUR, the fuel bundles that form the BWR core are grouped in channels. This core, for LAPUR, is viewed as a group of parallel channels through which water flows and cools numerous heat sources in the form of fuel rods.

The upper and lower plena are common to all of the channels and provide for the hydrodynamic coupling of the channels.

Three distinct regions exist along the direction of flow in a BWR channel: a non-boiling region, a subcooled-boiling region, and a bulk-boiling region. The non-boiling region (NBR) is characterized by the flow of a single liquid phase.

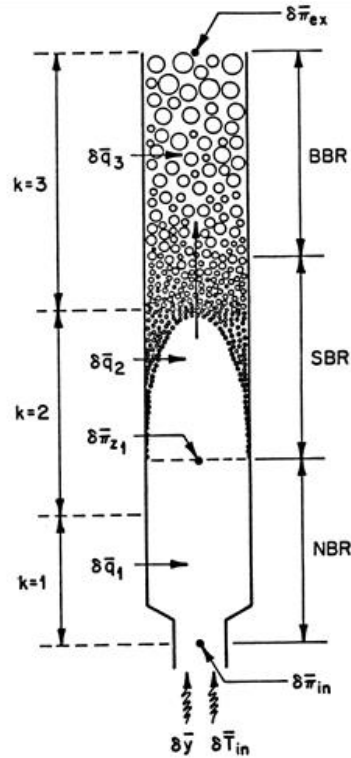


Figure 4.2. Schematic representation of a no-uniformly heated channel.

The subcooled-boiling region (SBR) is characterized by the existence of steam bubbles in thermodynamic non-equilibrium with the surrounding medium. The fluid layers closer to the heating surface are hotter than the ones in the center of the stream. At a certain point, these layers reach saturation temperature, become super-heated and start generating steam bubbles. These bubbles at first move in a thin layer close to the heating surface. This layer continues to grow and the bubbles move to the subcooled main stream. Recondensation of the bubbles is present over the whole subcooling range. Thus, in this region part of the heat communicated by the fuel is used to generate steam bubbles and part to increase the sensible heat of the liquid. So, in order to determine the steam quality at a certain position along the channel, the knowledge of the integrated heat generation from the channel entrance to this position or the flow enthalpy will not suffice. Also, since the steam bubbles moving in a subcooled medium have a probability of collapsing, a destruction rate must be considered.

The bulk-boiling region (BBR) is characterized by the thermodynamic equilibrium of the two phases. The temperature gradient across the flow area is vanishingly small and since the liquid is at saturation temperature, nucleation takes place in the bulk of the flow. In this region, all the heat transferred to the coolant is invested in steam production; therefore, the steam quality can be calculated directly from the flow enthalpy.

To obtain the stability of each channel in the reactor we need to know the response of the pressure drop along the channels to the driving perturbations of:

- inlet flow rate $\delta \bar{y}_{in}$,
- inlet temperature $\delta \bar{T}_{in}$, and
- power generation in the fuel $\delta \bar{q}$.

The knowledge of this response allows the determination of the feedback reactivity transfer functions, by means of the appropriate density reactivity coefficients.

4.2 LAPURX

The first module, LAPURX, solves the governing equations for the coolant and the fuel steady state.

4.2.1 The Coolant's Steady State

The purpose of this steady state calculation is the determination of the mass flow rate of coolant entering each channel and the distribution of densities, temperatures and velocities of the coolant along each channel.

Based on the system's design characteristics and its operating conditions, the steady state is determined as follows:

1. Estimate the mass flow rate entering each channel.
2. Determine the enthalpy distribution along the channel length.
3. Determine the boiling boundaries.
4. Solve the mass and energy balance equations for the liquid and vapor phases in the subcooled boiling region.
5. Solve the mass and energy equations in the bulk boiling region.

6. Solve the momentum equation to produce a map of the pressure field along the channel flow. This calculational step produces the total flow pressure drop between inlet and outlet of the channel.
7. Repeat steps 2 through 6 for each channel type.
8. Check if the equal pressure differential between inlet and outlet plena is the same through all the channels. If this boundary condition is not satisfied, the sensitivity of each channel to flow variations is calculated by repetition of steps 2 through 6 with the mass flow rate increased by a small percentage.
9. When the pressure boundary condition is satisfied, the steady state characteristics of the coolant have been determined, and as a result the calculation of the fuel steady state can be performed.

4.2.2 Steady State Equations of Fuel

The thermal analysis of a fuel element consists of the calculation of the steady state distribution of temperature.

The general heat conduction equation for an element of volume is

$$\rho c_p \frac{\partial T}{\partial t} = \nabla \cdot k \nabla T + q''' \quad (4.1)$$

where

- $t \equiv$ time,
- $\rho \equiv$ density of the medium,
- $c_p \equiv$ specific heat at constant pressure,
- $k \equiv$ heat conductivity,
- $T \equiv$ temperature, and
- $q''' \equiv$ volumetric heat source (J/sm^3).

Four distinct regions are present in the path of the heat flow from the fuel to the coolant, see figure 4.3. In counterflow order, they are:

1. Film of coolant attached to the outer surface of the clad;
2. Clad of Zircaloy which provides structural support, corrosion resistant heating surface, and fission product barrier;

3. Helium gap which acts as inert thermal bond between the clad and the fuel pellets and provides room for the fission gases released by the fuel pellets as burnup progresses; and
4. Uranium oxide fuel pellet within which heat is generated by the fission process.

In the LAPUR code only radial heat transfer is considered.

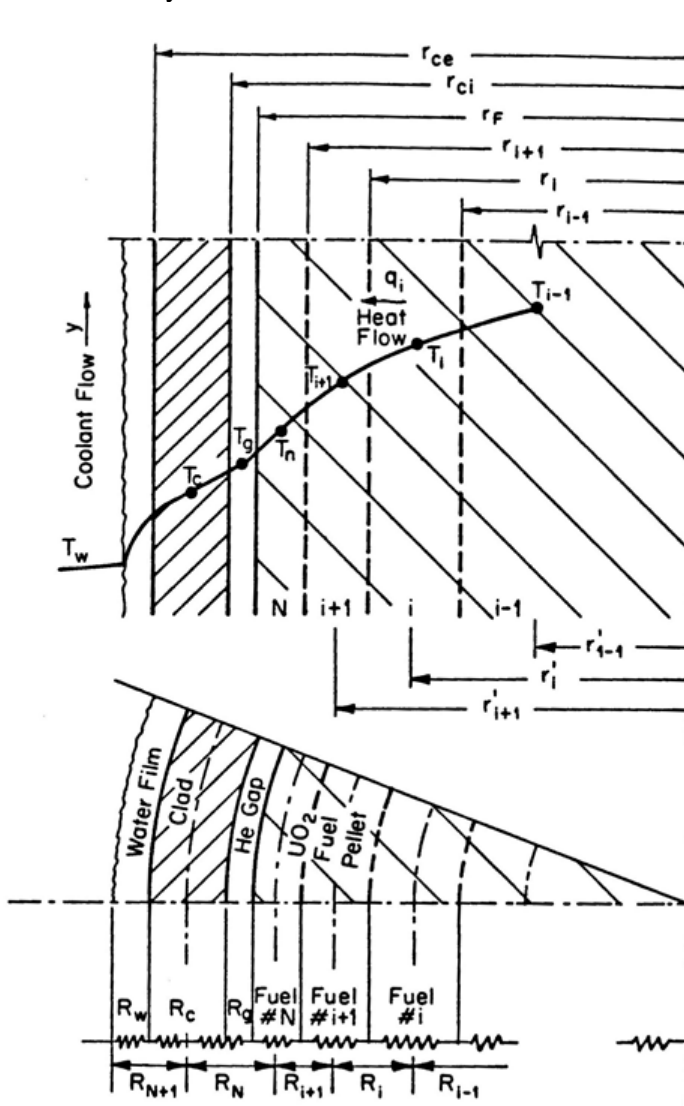


Figure 4.3. Schematic representation of the fuel rod composition and thermal mesh.

Because of the non-uniform heat generation inside the fuel caused by the neutronic shelf-shielding effects and the strong temperature dependence of the thermal conductivity of the UO_2 , it is necessary divide the fuel pellet into concentric annuli along its radius. These annuli constitute the nodes of the finite element calculations. These nodes are defined so that they have equal volume per unit length of rod and the node center is defined by the radius that separates the annulus into two equal areas.

From the mesh created and considering the boundary conditions, the steady calculation of fuel temperatures is performed.

4.3 LAPURW

The second module, LAPURW, solves the dynamic equations for the coolant, fuel, and neutron field in the frequency domain. A set of open-loop transfer functions are generated and the stability indices are estimated from the closed loop reactivity to power transfer function.

The procedure followed is: to analyze the dynamics of the core neutron field; then the dynamics of the heat transferred to the coolant is studied. Thereafter the dynamics of coolant flow is analyzed and finally the connection between the thermalhydraulic and neutronic due to the dual role of water as a coolant and neutron moderator, using feedback transfer functions.

4.3.1 The Dynamics of the Neutron Field

The reactor core dynamic analysis is concerned with the temporal behavior of the heat sources in the reactor medium. The fundamental heat sources in the reactor core are fission and capture events due to the interaction of the neutron field and the nuclei of the fuel.

The dynamics of the neutron field are governed by the Boltzmann equation which is a statement of the balance of the neutron population in an infinitesimal element of volume. Since the characteristics of the neutron population are determined by the properties of the medium in which it exists, and in a BWR this medium's properties depend on the heat source distribution, feedback effects need to be considered.

The rigorous solution of the Boltzmann equation, even when feedback effects are neglected, is a formidable task. However, this equation provides the basis for simpler descriptions which can be tailored to specific needs and can be treated analytically, giving good results.

In the approximation used by the code, the reactor core is divided in a relatively small number of regions or subcores. A subcore is regarded as a separate subcritical core coupled to its adjacent subcores by neutron exchange through the common surface boundaries. The dynamics of the reactor core are thus investigated in a nodal average sense, without concern to the particulars within the node.

To obtain the multinodal neutron kinetic equations, the variational principles will be used. The variational principles can be used in two distinct manners. First, they can be used to obtain accurate estimates of particular characteristics of a system, such as interaction rates, eigenvalues of a homogeneous equation, or weighted integral solutions to inhomogeneous equations. Second, the functional can be viewed as a Lagrangian function for the system, so that the demand that its first variation vanishes for arbitrary independent variations of the variables is equivalent to stating the equations describing the system. LAPUR uses this second manner as variational principle. The objective is the derivation of the multinodal neutron kinetic equations using a variational functional for spatially discontinuous trial functions.

Upon linearization and Laplace transformation a small perturbation frequency domain nodal representation of the neutron dynamics in the core is obtained. Next, the P1-1-speed approximation is used to yield a nodal matrix representation of the neutronics, with analytic formulation of the coupling coefficients. Summarizing, a set of equations is derived which describes the dynamics of the power generation process in the nuclear fuel, in terms of driving reactivity perturbations in the reactor core. It can be expressed mathematically as:

$$\delta\bar{n} = G \delta\bar{\rho} \quad (4.2)$$

where $\delta\bar{n}$ is the neutronic density perturbation and $\delta\bar{\rho}$ is the reactivity perturbation. The bar over the symbol indicates vector and capital letter indicates matrix.

4.3.2 The Dynamics of the Fuel

The analysis consists in the calculation of the heat flux and fuel temperature dynamics for driving perturbations of coolant flow rate, coolant temperature and power generation. From the heat flux equation in a time dependent case, and considering small perturbations about the steady state conditions we can obtain the equations that describes the perturbation in heat flux transfer to the coolant in terms of perturbations in heat generation, coolant flow rate, coolant temperature and clad temperature. From these equations, the fuel transfer functions corresponding to these perturbations are calculated, thus the total perturbation of the heat flux from the fuel to the coolant, and of the average temperature of the UO₂ fuel, can be expressed, for a generic node, by:

$$\delta\bar{Q}' = A_0 \delta\bar{q} + B_0 \delta\bar{T}_{in} + C_0 \delta\bar{y}_{in} \quad (4.3)$$

$$\delta\langle\bar{T}_F\rangle = A_1 \delta\bar{q} + B_1 \delta\bar{T}_{in} + C_1 \delta\bar{y}_{in} \quad (4.4)$$

where $\delta\bar{q}$, $\delta\bar{T}_{in}$ and $\delta\bar{y}_{in}$ are the driving perturbation of power generation in the fuel, inlet temperature, and inlet flow rate.

These two equations link the fuel dynamics to (a) the coolant flow dynamics through the conservation of energy equation, and (b) the neutron dynamics through the Doppler reactivity coefficients, respectively.

4.3.3 The Fluid Flow Dynamic

To describe the dynamics of the two-phase flow along a heated channel three conservation equations: mass, energy and momentum; and four mechanical equations which relate the steam velocity slip ratio, heat flux, sub-cooled boiling, and frictional forces to the core's physical parameters, and coolant properties, are needed.

The conservation equations are stated by writing a balance over a thin element of fluid or control volume. This approach requires the following assumptions:

1. zero radial pressure gradient, so that at any channel cross-section a unique velocity can be assigned to each fluid phase;
2. uniform temperature of the liquid phase across the flow area; and

3. negligible contribution of the kinetic and potential (gravitational) energy terms to the energy equations.

The mass, energy and momentum equation are solved at each mesh-node. Moreover, to calculate the fluid flow dynamics is necessary to consider the pressure drop that occurs at the channel flow discontinuities, such as area changes, orifices, spacers, fittings, etc. These equations, in conjunction with the fuel equation, form a group of thermalhydraulic equations that allow us to determine, in the frequency domain, of: (a) the response of the coolant average density distribution along the channel to driving perturbations of inlet flow rate, inlet temperature and power generation in the fuel; and (b) the response of the pressure drop along the channel to these same driving perturbations.

The knowledge of the spatially dependent response of the density of the coolant-moderator allows the determination of feedback reactivity transfer functions, by means of appropriate density reactivity coefficients, to be used in the neutronic model to calculate the response of the power generation to the above driving perturbations. With the response of the pressure drop along the channels to the driving perturbations: (a) the flow stability of each channel in the reactor can be determined; and (b) the dynamic redistribution of the flow of coolant among the different channels can be calculated.

The integration of the nodal response along the boiling length of a channel yields the inlet coolant flow rate-to-driving pressure differential, an inlet coolant temperature-to-driving-pressure differential transfer function. And the integration along the channel section pertaining to a neutronic subcore yields the power-to-driving pressure differential transfer function. These transfer functions, in conjunction with the lower plenum equations, determine the dynamics of the core coolant flow.

Summarizing, we obtain an expression that links the perturbation of mass flow rate entering in each channel with the perturbations in total core flow rate $\delta\bar{Y}$, power generation $\delta\bar{q}$, and coolant lower plenum temperature $\delta\bar{T}_{in}$:

$$\delta \bar{y}_{in} = L \delta\bar{Y} + M \delta\bar{q} + N \delta\bar{T}_{in} \quad (4.5)$$

4.3.4 The Thermalhydraulic-Neutronic Interaction

To establishing the link between the thermalhydraulics and neutronics, the dual role of the core water as coolant and neutron moderator, and the neutronic Doppler effect of the fuel temperature are considered.

The nodal coolant density response to the local driving perturbations of inlet coolant temperature, inlet coolant flow rate, and power are weighted by the corresponding reactivity coefficients, to yield the following feedback transfer functions:

- inlet coolant temperature-to-subcore moderator-density and Doppler reactivity,
- total core inlet coolant flow rate-to-subcore moderator density and Doppler reactivity, and
- subcore power-to-subcore moderator density and Doppler reactivity.

Using these transfer functions, the can obtain the moderator density feedback as:

$$\delta \Delta \bar{k}_\rho = A_2 \delta \bar{q} + B_2 \delta \bar{T}_{in} + C_2 \delta \bar{y}_{in} \quad (4.6)$$

Changes in temperature in a nuclear fuel affect the nuclear resonant interactions between the fuel materials and the neutron field. In BWR's the parasitic interactions change more than those leading to fission. Hence a perturbation in the fuel temperature causes a perturbation of reactivity in the opposite direction.

Taking into consideration the heat flow dynamics of the fuel, and using the Doppler reactivity coefficient, the following transfer functions are obtained:

- Doppler reactivity transfer function for liquid coolant temperature,
- Doppler reactivity transfer function for coolant mass flow rate,
- Doppler reactivity transfer function for power generation.

In terms of these transfer functions, the reactivity contribution of the fuel's Doppler effect is

$$\delta \Delta \bar{k}_D = A_3 \delta \bar{q} + B_3 \delta \bar{T}_{in} + C_3 \delta \bar{y}_{in} \quad (4.7)$$

The section 4.4 contains a detailed derivation of the equations of this section.

4.4 THE TRANSFER FUNCTIONS OF LAPUR

In this section, the overall space-dependent transfer function matrix representation of the BWR core dynamics with feedback is obtained. In order to calculate the stability indices (decay ratio and natural frequency), the core closed-loop transfer function is determined.

4.4.1 Calculations of the Density Feedback Reactivity Coefficient in LAPUR

4.4.1.1 Flow to Density Reactivity Feedback Coefficient

The calculation of the flow to density reactivity feedback coefficients at a specific channel type ix is performed in the TRANS subroutine. In this subroutine we calculate first:

$$e_{ix} = \left(\frac{\partial \Delta k_{\rho}}{\partial y} \right)_{ix} = \left[\delta \overline{\Delta k}_{\rho} \right]_{\substack{\delta \bar{y}_{in}=1+0j \\ \delta \bar{q}=0 \\ \delta \bar{T}_{in}=0}} \equiv CEX(ix) \quad (4.8)$$

e_{ix} is the flow to feedback reactivity at channels belonging to type ix .

To obtain e_{ix} , the code performs a unitary perturbation in the inlet mass flow to this channel type as follows:

$$\begin{aligned} \delta \bar{q} &= (0., 0.) \equiv CDRAMB \\ \delta \bar{y}_{in} &= (1., 0.) \equiv CDYPB \\ \delta \bar{T}_{in} &= (0., 0.) \equiv CDTIN \end{aligned} \quad (4.9)$$

From TRANS, the program calls to the FREQ subroutine. In this subroutine it solves the linearized mass, energy and momentum equations for this particular type of perturbation and this particular type of channel.

The inlet flow perturbation is the inlet flow perturbation to the first node given by:

$$\delta \bar{y}_1(ix) = \delta \bar{y}_{in}(ix) = 1 + 0j \quad (4.10)$$

This perturbation is the only independent one, the rest are dependent and can be found by solving the conservation equations, for instance, in the subcooled boiling region we must solve the set of linearized conservation equations, for the i -th node of the channel:

$$\delta \bar{y}_{a,i} + D_{1,i} \delta \bar{\alpha}_{a,i} = E_{1,i} \quad (\text{mass}) \quad (4.11)$$

$$D_{2,i} \delta \bar{y}_{a,i} + D_{3,i} \delta \bar{\alpha}_{a,i} + D_{4,i} \delta \bar{H}_{a,i} = E_{2,i} \quad (\text{steam energy}) \quad (4.12)$$

$$D_{5,i} \delta \bar{y}_{a,i} + D_{6,i} \delta \bar{\alpha}_{a,i} + D_{7,i} \delta \bar{H}_{a,i} = E_{3,i} \quad (\text{total energy}) \quad (4.13)$$

where $E_{1,i}$, $E_{2,i}$, and $E_{3,i}$ depend on the node inlet perturbation and are given by:

$$E_{1,i} = \delta \bar{y}_i \quad (4.14)$$

$$E_{2,i} = D_{11,i} \delta \bar{y}_i + D_{12,i} \delta \bar{\alpha}_i + D_{13,i} \delta \bar{H}_i + D_{17,i} \delta \bar{q} \quad (4.15)$$

$$E_{3,i} = D_{14,i} \delta \bar{y}_i + D_{15,i} \delta \bar{\alpha}_i + D_{16,i} \delta \bar{H}_i + D_{18,i} \delta \bar{q} \quad (4.16)$$

and the subscript a,i indicate average value at node i .

We note that for inlet flow perturbation $\delta \bar{q} = 0$.

This linear system of equations is easily solved by the Kramer's method, with determinant:

$$\Delta = \begin{vmatrix} 1 & D_1 & 0 \\ D_2 & D_3 & D_4 \\ D_5 & D_6 & D_7 \end{vmatrix}_i = \left\{ (D_3 D_7 - D_4 D_6) - D_1 (D_2 D_7 - D_4 D_5) \right\}_i \quad (4.17)$$

The average values of the mass flow, void fraction and liquid enthalpy perturbations at the i -th node are given by:

$$\delta \bar{y}_{a,i} = \frac{\begin{vmatrix} E_1 & D_1 & 0 \\ E_2 & D_3 & D_4 \\ E_3 & D_6 & D_7 \end{vmatrix}_i}{\Delta} = \left\{ \frac{E_1 (D_3 D_7 - D_4 D_6) - D_1 (E_2 D_7 - E_3 D_4)}{\Delta} \right\}_i \quad (4.18)$$

$$\delta \bar{\alpha}_{a,i} = \frac{\begin{vmatrix} 1 & E_1 & 0 \\ D_2 & E_2 & D_4 \\ D_5 & E_3 & D_7 \end{vmatrix}_i}{\Delta} = \left\{ \frac{(E_2 D_7 - E_3 D_4) - E_1 (D_2 D_7 - D_4 D_5)}{\Delta} \right\}_i \quad (4.19)$$

$$\delta \bar{H}_{a,i} = \frac{\begin{vmatrix} 1 & D_1 & E_1 \\ D_2 & D_3 & E_2 \\ D_5 & D_6 & E_3 \end{vmatrix}_i}{\Delta} = \left\{ \frac{E_1(D_2 D_6 - D_3 D_5) - E_2(D_6 - D_1 D_5) + E_3(D_3 - D_1 D_2)}{\Delta} \right\}_i \quad (4.20)$$

The values of the flow, void fraction and enthalpy perturbations at the exit of the i -th node of the SBR region, are obtained from the following set of equations:

$$\delta \bar{y}_{i+1} = (2\delta \bar{y}_{a,j} - \delta \bar{y}_j) \equiv CDY(I+1) \quad (4.21)$$

$$\delta \bar{\alpha}_{i+1} = (2\delta \bar{\alpha}_{a,i} - \delta \bar{\alpha}_i) \equiv CDB(I+1) \quad (4.22)$$

$$\delta \bar{H}_{i+1} = (2\delta \bar{H}_{a,i} - \delta \bar{H}_i) \equiv CDH(I+1) \quad (4.23)$$

Once we know the values of all the perturbations $\delta \bar{y}_{a,i}$, $\delta \bar{\alpha}_{a,i}$, $\delta \bar{H}_{a,i}$ along the channel, we integrate the momentum conservation equation, in order to get the response $\delta \bar{\pi}_i$ of the pressure field along the channel.

Then, the program computes the coolant density perturbations along the channel. To perform this step, we start from the average density at node i , given by:

$$\rho_{a,i} = (1 - \alpha_{a,i}) \rho_{l,a,i} + \alpha_{a,i} \rho_s \quad (4.24)$$

Therefore, the perturbation in the average density is given in the subcooled boiling region (SBR) by:

$$\delta \bar{\rho}_{a,i} = (1 - \alpha_{a,i}) \delta \bar{\rho}_{l,a,i} - (\rho_{l,a,i} - \rho_s) \delta \bar{\alpha}_{a,i} \quad (4.25)$$

Now we note that in the subcooled region we can express the perturbation in the liquid density as follows:

$$\delta \bar{\rho}_{l,a,i} = \left(\frac{\partial \rho}{\partial h} \right)_i \delta \bar{h}_{l,a,i} = \left(\frac{\partial \rho}{\partial H} \right)_i \delta \bar{H}_{a,i} \quad (4.26)$$

where

$$\bar{H}_{a,i} = \frac{h_f - \bar{h}_{l,a,i}}{h_{fg}} \quad (4.27)$$

Therefore, equation (4.25) can be rewritten, on account of expression (4.26), in the form:

$$\delta\bar{\rho}_{a,i} = \left(\frac{\partial\rho}{\partial H} \right)_i (\delta\bar{H} - \alpha \delta\bar{H})_{a,i} + (\rho_s - \rho_{l,a,i}) \delta\bar{\alpha}_{a,i} \quad (4.28)$$

In the bulk boiling region, $\delta\bar{H}_{a,i} = 0$, and the density perturbations are given by:

$$\delta\bar{\rho}_{a,i} = (\rho_s - \rho_{l,a,i}) \delta\bar{\alpha}_{a,i} \quad (4.29)$$

The calculation of expression (4.8) is performed in subroutine `FREQ`, by means of the following expression

$$e_{ix} = \left[\delta\bar{\Delta k}_{\rho} \right]_{\substack{\delta\bar{y}_{in}=1+0j \\ \delta\bar{q}_L=0 \\ \delta\bar{T}_{in}=0}} = \left[\delta\bar{\Delta K}_{\rho,NB} + \delta\bar{\Delta K}_{\rho,SB} + \delta\bar{\Delta K}_{\rho,BB} \right]_{\substack{\delta\bar{y}_{in}=1+0j \\ \delta\bar{q}_L=0 \\ \delta\bar{T}_{in}=0}} \quad (4.30)$$

where $\delta\bar{\Delta K}_{\rho,NB}$, $\delta\bar{\Delta K}_{\rho,SB}$, and $\delta\bar{\Delta K}_{\rho,BB}$, are the reactivity variations due to the unit inlet flow perturbation, in the non-boiling region, subcooled boiling region, and bulk boiling region, respectively.

To obtain these afore mentioned reactivity perturbations, the following calculations are performed at subroutine `FREQ`:

- *Non Boiling Region (NBR)*

In this region the reactivity variations due to the unit inlet flow perturbation is given by:

$$\left[\delta\Delta k_{\rho,NB} \right]_{\substack{\delta\bar{y}_{in}=1+0j \\ \delta\bar{q}_L=0 \\ \delta\bar{T}_{in}=0}} = \sum_{i=1}^{NNB} \left(\frac{\partial\Delta k}{\partial\rho} \right)_i w_i \left[\delta\bar{\rho}_{a,i} \right]_{\substack{\delta\bar{y}_{in}=1+0j \\ \delta\bar{q}_L=0 \\ \delta\bar{T}_{in}=0}} \quad (4.31)$$

In this equation w_i is the reactivity weighting factor that depends on the square of the power distribution, and is given by:

$$w_i = \frac{P_i^2}{\sum_i P_i^2} \quad (4.32)$$

where P_i is the power at node i , and the summation in equation (4.32) runs over all the nodes.

$\left(\frac{\partial \Delta k}{\partial \rho}\right)_i$ is the density reactivity coefficient for the node i of the channel.

This coefficient is obtained, at each node, from a set of tabulated density reactivity coefficients as a function of the average relative water density $\left(\frac{\rho}{\rho_f}\right)_{a,i}$ at the i -th node.

The density variation at the i -th node of the non-boiling region due to one unit flow perturbation is obtained from the expression:

$$\left[\delta \bar{\rho}_{a,i}\right]_{\substack{\delta \bar{y}_{in}=1+0j \\ \delta \bar{q}=0 \\ \delta \bar{T}_{in}=0}} = \left(\frac{\partial \rho}{\partial S}\right)_{a,i} \left[\delta \bar{S}_{a,i}\right]_{\substack{\delta \bar{y}_{in}=1+0j \\ \delta \bar{q}=0 \\ \delta \bar{T}_{in}=0}} \quad (4.33)$$

where $S = \frac{h_l}{(h_{z_1} - h_0)} = \frac{h_l}{\Delta h_0}$, and $\delta \bar{S}_{a,i}$ is obtained solving the perturbed energy equation in the NB region.

Finally $\left(\frac{\partial \rho}{\partial S}\right)_{a,i}$ is given by:

$$\left(\frac{\partial \rho}{\partial S}\right)_{a,i} = \left(\frac{\partial \rho}{\partial h_l}\right)_{a,i} \Delta h_0 \quad (4.34)$$

we note that z_l is the inception point for subcooled boiling.

- Subcooled Boiling Region (SBR)

In this region, the reactivity variation due to the unit inlet flow perturbation is given by:

$$\left[\delta \overline{\Delta k}_{\rho,SB}\right]_{\substack{\delta \bar{y}_{in}=1+0j \\ \delta \bar{q}=0 \\ \delta \bar{T}_{in}=0}} = \sum_{i=NNB+1}^{NNB+NSB} \left(\frac{\partial \Delta k}{\partial \rho}\right)_i w_i \left[\delta \bar{\rho}_{a,i}\right]_{\substack{\delta \bar{y}_{in}=1+0j \\ \delta \bar{q}=0 \\ \delta \bar{T}_{in}=0}} \quad (4.35)$$

The summation in equation (4.35) runs over all the nodes of the subcooled boiling region. The density perturbation in equation (4.35) is obtained from equation (4.28), and therefore we can write:

$$\left[\delta \bar{\rho}_{a,i} \right]_{\substack{\delta \bar{y}_{in}=1+0j \\ \delta \bar{q}=0 \\ \delta \bar{T}_{in}=0}} = \left[\left(\frac{\partial \rho}{\partial H} \right)_i (\delta \bar{H} - \alpha \delta \bar{H})_{a,i} + (\rho_s - \rho_{l,a,i}) \delta \bar{\alpha}_{a,i} \right]_{\substack{\delta \bar{y}_{in}=1+0j \\ \delta \bar{q}=0 \\ \delta \bar{T}_{in}=0}} \quad (4.36)$$

- Bulk Boiling Region (BBR)

In this region, the reactivity variation due to the unit inlet flow perturbation is given by:

$$\left[\delta \bar{\Delta k}_{\rho, BB} \right]_{\substack{\delta \bar{y}_{in}=1+0j \\ \delta \bar{q}=0 \\ \delta \bar{T}_{in}=0}} = \sum_{i=NNB+NSB+1}^{NNB+NSB+NSB} \left(\frac{\partial \Delta k}{\partial \rho} \right)_i w_i \left[\delta \bar{\rho}_{a,i} \right]_{\substack{\delta \bar{y}_{in}=1+0j \\ \delta \bar{q}=0 \\ \delta \bar{T}_{in}=0}} \quad (4.37)$$

Where the density variation due to the inlet flow perturbation in the bulk boiling region is given by:

$$\left[\delta \bar{\rho}_{a,i} \right]_{\substack{\delta \bar{y}_{in}=1+0j \\ \delta \bar{q}=0 \\ \delta \bar{T}_{in}=0}} = \left[(\rho_s - \rho_f)_{a,i} \delta \bar{\alpha}_{a,i} \right]_{\substack{\delta \bar{y}_{in}=1+0j \\ \delta \bar{q}=0 \\ \delta \bar{T}_{in}=0}} \quad (4.38)$$

4.4.2 Power to Density Reactivity Feedback Coefficients

The calculation of the power to reactivity feedback coefficient f_{ix} , at a specified channel type ix , is performed in the TRANS subroutine. In this subroutine we calculate

$$f_{ix} = \left(\frac{\partial \Delta k_{\rho}}{\partial q} \right)_{ix} = \left[\delta \bar{\Delta k}_{\rho} \right]_{\substack{\delta \bar{y}_{in}=0 \\ \delta \bar{q}=1+0j \\ \delta \bar{T}_{in}=0}} \equiv CFX(ix) \quad (4.39)$$

To obtain f_{ix} , the code performs a unitary perturbation in the power as follows:

$$\begin{aligned} \delta \bar{q} &= (1., 0.) \equiv CDRAMB \\ \delta \bar{y}_{in} &= (0., 0.) \equiv CDYPB \\ \delta \bar{T}_{in} &= (0., 0.) \equiv CDTIN \end{aligned} \quad (4.40)$$

Then, the program calls to the FREQ subroutine, and it solves the linearized Laplace transformed mass, energy and momentum equations for this particular type of perturbation and this particular type of channel. For instance, in the SBR region, we solve equations (4.11), (4.12), and (4.13) with $\delta \bar{q} = 1$. We observe that the coefficients $D_{17,i}$ and $D_{18,i}$ convert the unit power perturbations

in energy perturbations for the energy transferred to the steam and the two phase mixture at a particular node i .

We remind that these coefficients, $D_{17,i}$ and $D_{18,i}$, are defined by the following expressions:

$$D_{17,i} = \frac{\eta \bar{F}_{s,i} Q'_{F0,i} \Delta z}{(1-\eta) w_0 h_{fg}} \left(\frac{\partial q'_F}{\partial q} \right)_i \quad (4.41)$$

$$D_{18,i} = \frac{\eta Q'_{F0,i} \Delta z}{(1-\eta) w_0 h_{fg}} \left(\frac{\partial q'_F}{\partial q} \right)_i \quad (4.42)$$

These coefficients are computed at subroutine COEFIW, where

$$Q'_{F0,i} \Delta z = Q''_{F0,i} P_w \Delta z = \dot{Q}_{F0,i} \quad (4.43)$$

is the heat transfer rate to the fluid of channel node i , at steady state conditions.

Once we solve the linearized conservation equations, we get at each node $\delta \bar{y}_{a,i}$, $\delta \bar{\alpha}_{a,i}$, and $\delta \bar{H}_{a,i}$, and therefore we can compute the density perturbation $\delta \bar{\rho}_{a,i}$, at each channel node. Finally, the power to reactivity feedback coefficient will be given by:

$$f_{ix} = \sum_{i=1}^{NNB+NSB+NBB} \left(\frac{\partial \Delta k}{\partial \rho} \right)_i w_i \left[\delta \bar{\rho}_{a,i} \right]_{\substack{\delta \bar{y}_{in}=0 \\ \delta \bar{q}=1+0j \\ \delta \bar{T}_{in}=0}} \equiv CFX(ix) \quad (4.44)$$

4.4.3 Inlet Temperature to Density Reactivity Feedback Coefficient

The calculation of the inlet temperature to reactivity feedback coefficient h_{ix} , at a specified channel type ix , is performed in the TRANS subroutine. In this subroutine we calculate:

$$h_{ix} = \left(\frac{\partial \Delta k_\rho}{\partial T_{in}} \right)_{ix} = \left[\delta \bar{\Delta k}_\rho \right]_{\substack{\delta \bar{y}_{in}=0 \\ \delta \bar{q}=0 \\ \delta \bar{T}_{in}=1+0j}} \equiv CHX(ix) \quad (4.45)$$

To obtain h_{ix} , we perform a unitary perturbation in the inlet temperature to the channel, denoted by $\delta \bar{T}_{in}$, as follows:

$$\begin{aligned}
 \delta \bar{q} &= (0., 0.) \equiv CDRAMB \\
 \delta \bar{y}_{in} &= (0., 0.) \equiv CDYPB \\
 \delta \bar{T}_{in} &= (1., 0.) \equiv CDTIN
 \end{aligned} \tag{4.46}$$

Then, we call to the `FREQ` subroutine, and we solve in the frequency domain the linearized conservation equations of mass, energy of the steam, and total energy, for this particular type of perturbation and this particular type of channel. Once we solve this system of equations, we get at each node $\delta \bar{y}_{a,i}$, $\delta \bar{\alpha}_{a,i}$, $\delta \bar{H}_{a,i}$, and therefore we can compute the density perturbation $\delta \bar{\rho}_{a,i}$, at each channel node. Finally, the inlet temperature to reactivity feedback coefficient is computed in subroutine `FREQ`, by means of the expression:

$$h_{ix} = \sum_{i=1}^{NNB+NSB+NB} \left(\frac{\partial \Delta k}{\partial \rho} \right)_i w_i \left[\delta \bar{\rho}_{a,i} \right]_{\substack{\delta \bar{y}_{in}=0 \\ \delta \bar{q}=0 \\ \delta \bar{T}_{in}=1+0j}} \equiv CHX(ix) \tag{4.47}$$

where w_i is the square power reactivity weighting factor.

4.4.4 Calculations of the Fuel-Temperature (Doppler) Reactivity Coefficients

The calculation of the Doppler reactivity feedback coefficients at a specific channel type ix is performed in the `TRANS` subroutine. In this subroutine we obtain first the flow to Doppler feedback reactivity transfer function $d_y(ix)$:

$$d_y(ix) \equiv CDYX(ix) \tag{4.48}$$

After we obtain the power to Doppler feedback reactivity transfer function $d_q(ix)$ for a given channel:

$$d_q(ix) \equiv CDQX(ix) \tag{4.49}$$

And, finally, the coolant temperature to Doppler feedback reactivity transfer function:

$$d_T(ix) \equiv CDTX(ix) \tag{4.50}$$

To obtain these coefficients, subroutine `TRANS` calls to subroutine `FUELW`. In this subroutine the program solves the Laplace transformed fuel

nodal equations, and computes the average fuel temperature perturbation $\langle \delta \bar{T}_F \rangle_i$ at each axial level i of channel ix , for each type of perturbation:

$$a_T(i) = \frac{\partial \langle T_F \rangle_i}{\partial y} = \left[\langle \delta \bar{T}_F \rangle_i \right]_{\substack{\delta \bar{y}=1+0j \\ \delta \bar{q}=0 \\ \delta T_i=0}} \equiv CAT(i) \quad (4.51)$$

at the same time the program computes the change in the heat flux $\delta \bar{q}''_{F,N+1}$, produced by one unitary perturbation in the coolant

$$a_q(i) = \frac{\partial q''_{F,N+1}(i)}{\partial y} = \left[\delta \bar{q}''_{F,N+1}(i) \right]_{\substack{\delta \bar{y}=1+0j \\ \delta \bar{q}=0 \\ \delta T_i=0}} \equiv CAQ(i) \quad (4.52)$$

where:

$a_T(i) \equiv$ is the coolant flow to average fuel temperature transfer function at axial level i ,

$a_q(i) \equiv$ is the coolant flow to heat flux to coolant transfer function at axial level i -th.

Then in FUELW, the program performs unitary perturbations in the power and solves the Laplace transformed fuel nodal equations, for unitary power perturbations, computing the average temperature perturbation $\langle \delta \bar{T}_F \rangle_i$ at each axial level

$$b_T(i) = \frac{\partial \langle T_F \rangle_i}{\partial q} = \left[\langle \delta \bar{T}_F \rangle_i \right]_{\substack{\delta \bar{y}=0 \\ \delta \bar{q}=1+0j \\ \delta T_i=0}} \equiv CBT(i) \quad (4.53)$$

at the same time the program computes the change in the heat flux to the coolant:

$$b_q(i) = \frac{\partial q''_{F,N+1}(i)}{\partial q} = \left[\delta \bar{q}''_{F,N+1}(i) \right]_{\substack{\delta \bar{y}=0 \\ \delta \bar{q}=1+0j \\ \delta T_i=0}} \equiv CBQ(i) \quad (4.54)$$

where:

$b_T(i) \equiv$ is the power average fuel temperature transfer function at axial level i ,

$b_q(i) \equiv$ is the power to coolant heat flux transfer function at axial level i .

The last step in FUELW is to perform unitary perturbations in the coolant temperature, and to compute at each axial level i :

$$c_T(i) = \frac{\partial \langle T_F \rangle_i}{\partial T_l} = \left[\langle \delta \bar{T}_F \rangle_i \right]_{\substack{\delta \bar{y}=0 \\ \delta \bar{q}=0 \\ \delta T_l=1+0j}} \equiv CCT(i) \quad (4.55)$$

$$c_q(i) = \frac{\partial q''_{F,N+1}(i)}{\partial T_l} = \left[\partial \bar{q}''_{F,N+1}(i) \right]_{\substack{\delta \bar{y}=0 \\ \delta \bar{q}=0 \\ \delta T_l=1+0j}} \equiv CCQ(i) \quad (4.56)$$

Then, in the `FREQ` subroutine we compute the power to Doppler feedback reactivity transfer function $d_q(ix)$ for a given channel:

$$d_q(ix) = N_f \sum_{i=1}^{NN} \left[\frac{\partial \Delta k}{\partial \langle T_F \rangle} \right]_i \left[\frac{\partial \langle T_F \rangle}{\partial q} \right]_i = N_f \sum_{i=1}^{NN} \left[\frac{\partial \Delta k}{\partial \langle T_F \rangle} \right]_i b_T(i) \quad (4.57)$$

where N_f is the number of fuel-rods per channel, and NN is the total number of axial nodes in the channel.

The flow to Doppler feedback reactivity transfer function $d_y(ix)$, for a channel ix , is given by

$$d_y(ix) = N_f \sum_{i=1}^{NN} \left[\frac{\partial \Delta k}{\partial \langle T_F \rangle} \right]_i \left[\frac{\partial \langle T_F \rangle}{\partial y} \right]_i = N_f \sum_{i=1}^{NN} \left[\frac{\partial \Delta k}{\partial \langle T_F \rangle} \right]_i a_T(i) \quad (4.58)$$

Finally, the coolant temperature to Doppler feedback reactivity transfer function at a given channel ix , will be given by:

$$d_T(ix) = N_f \sum_{i=1}^{NN} \left[\frac{\partial \Delta k}{\partial \langle T_F \rangle} \right]_i \left[\frac{\partial \langle T_F \rangle}{\partial T_l} \right]_i = N_f \sum_{i=1}^{NN} \left[\frac{\partial \Delta k}{\partial \langle T_F \rangle} \right]_i c_T(i) \quad (4.59)$$

4.4.5 One Core Density Reactivity Coefficient in LAPUR

4.4.5.1 The Block Diagram of LAPUR

The interrelation of the physical mechanisms governing the dynamic response of a BWR core are modeled in the code LAPUR using feedback equations for reactivity and Doppler.

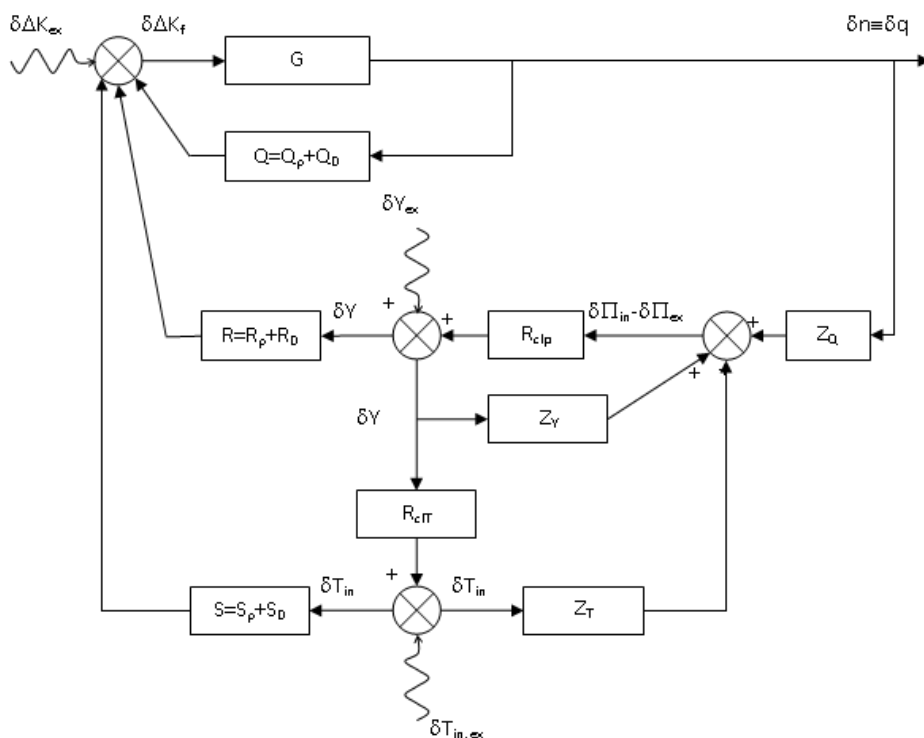


Figure 4.4. Block diagram of LAPUR transfer functions.

G is the neutron kinetics open loop transfer function. $R_{c,lp}$ is the core differential pressure to inlet flow transfer function. Q is the power to feedback reactivity transfer function. R is the total flow to feedback reactivity transfer function. S is the inlet temperature to feedback reactivity transfer function.

The block diagram displayed at figure 4.4 is formed by the following blocks:

i) The open loop transfer function G

The open loop transfer function G , for neutron kinetics in LAPUR is given by:

$$G = CG = \frac{0.01}{s \left(l^* + \sum_i \frac{\beta_i}{s + \lambda_i} \right)} = \frac{\delta \bar{n}}{\delta \Delta k} \quad (4.60)$$

where

- $G \equiv$ total reactivity to total power transfer function
- $l^* \equiv$ neutron generation time
- $\beta_i \equiv$ fraction of delay neutron precursors of group i
- $\lambda_i \equiv$ decay constant of precursors or group i .

ii) The thermalhydraulic to reactivity transfer functions

ii-1 The feedback reactivity by density transfer functions

The density reactivity change $\delta \overline{\Delta k}_\rho$ due to inlet perturbations $\delta \overline{y}_{in}$, $\delta \overline{q}$ and $\delta \overline{T}_{in}$, is obviously given by:

$$\delta \overline{\Delta k}_\rho = \sum_{ix} \left(\frac{\partial \Delta k}{\partial y} \right)^{ix} \delta \overline{y}_{in}(ix) N_{ch}(ix) + \sum_{ix} \left(\frac{\partial \Delta k}{\partial q} \right)^{ix} \delta \overline{q} N_{ch}(ix) + \sum_{ix} \left(\frac{\partial \Delta k}{\partial T_{in}} \right)^{ix} \delta \overline{T}_{in}(ix) N_{ch}(ix) \quad (4.61)$$

where $N_{ch}(ix)$ is the number of channels of the ix type.

Expression (4.61) can be recasted in terms of the coefficients e_{ix} , f_{ix} and h_{ix} , to give:

$$\delta \overline{\Delta k}_\rho = \sum_{ix} e_{ix} N_{ch}(ix) \delta \overline{y}_{in}(ix) + \sum_{ix} f_{ix} N_{ch}(ix) \delta \overline{q} + \sum_{ix} h_{ix} N_{ch}(ix) \delta \overline{T}_{in}(ix) \quad (4.62)$$

From the linearized momentum conservation equation we can relate the momentum perturbations at the lower and upper plena with the total core flow perturbation $\delta \overline{Y}$, the coolant inlet temperature perturbation $\delta \overline{T}_{in}$, and the power perturbation $\delta \overline{q}$

$$\delta \overline{\Pi}_{in} - \delta \overline{\Pi}_{ex} = Z_Y \delta \overline{Y} + Z_Q \delta \overline{q} + Z_T \delta \overline{T}_{in} \quad (4.63)$$

where Z_Y , Z_Q , and Z_T , are the flow, power and temperature impedances, respectively. Next we relate the total flow perturbation with the total flow perturbation to the channels:

$$\delta \overline{Y} = \sum_{ix} g_{ix} N_{ch}(ix) \delta \overline{y}_{in}(ix) \quad (4.64)$$

where g_{ix} is the fraction of the total flow which goes through one particular channel.

If R_{clp} is the normalized differential pressure to inlet flow transfer function, due to the presence of the recirculation loop, then we can write:

$$\delta\bar{Y} = R_{clp} (\delta\bar{\Pi}_{in} - \delta\bar{\Pi}_{ex}) + \delta\bar{Y}_{ex} \quad (4.65)$$

Combining equations (4.64) and (4.65) we obtain:

$$\delta\bar{\Pi}_{in} - \delta\bar{\Pi}_{ex} = \frac{\delta\bar{Y}}{R_{clp}} - \frac{\delta\bar{Y}_{ex}}{R_{clp}} = Z_Y \delta\bar{Y} + Z_Q \delta\bar{q} + Z_T \delta\bar{T}_{in} \quad (4.66)$$

Therefore

$$Z_Q \delta\bar{q} + Z_T \delta\bar{T}_{in} = \frac{(1 - Z_Y R_{clp})}{R_{clp}} \delta\bar{Y} - \frac{\delta\bar{Y}_{ex}}{R_{clp}} \quad (4.67)$$

From this last equation we get that $\delta\bar{Y}$ is given by:

$$\delta\bar{Y} = \frac{R_{clp} Z_Q}{1 - Z_Y R_{clp}} \delta\bar{q} + \frac{R_{clp} Z_T}{1 - Z_Y R_{clp}} \delta\bar{T}_{in} + \frac{1}{1 - Z_Y R_{clp}} \delta\bar{Y}_{ex} \quad (4.68)$$

Because the flow perturbations $\delta\bar{\Pi}_{in}$, to one channel are related to the flow perturbation $\delta\bar{y}_{in}(ix)$ by the linearized momentum equation in the non-boiling region:

$$\delta\bar{y}_{in}(ix) = a(ix) \delta\bar{\Pi}_{in} - a(ix) \delta\bar{\Pi}_{z1}(ix) \quad (4.69)$$

where $\delta\bar{\Pi}_{z1}$ is the flow perturbation at the boiling inception boundary that is obtained by solving the momentum equations, and going back from the exit to the non-boiling region. This calculation yields:

$$\delta\bar{\Pi}_{z1}(ix) = b(ix) \delta\bar{y}_{in}(ix) + c(ix) \delta\bar{q} + d(ix) \delta\bar{T}_{in} \quad (4.70)$$

Then, from equations (4.63), (4.64), (4.69) and (4.70) we obtain the following expression relating the inlet flow perturbation to one channel with the total flow perturbation, the power perturbation, and the inlet temperature perturbation:

$$\delta\bar{y}_{in}(ix) = L(ix) \delta\bar{Y} + M(ix) \delta\bar{q} + N(ix) \delta\bar{T}_{in} \quad (4.71)$$

where the channel dependent coefficients $L(ix)$, $M(ix)$, and $N(ix)$ are given by:

$$L(ix) = \frac{a(ix)}{1 + a(ix)b(ix)} Z_Y \quad (4.72)$$

$$M(ix) = \frac{a(ix)}{1 + a(ix)b(ix)} (Z_Q - c(ix)) \quad (4.73)$$

$$N(ix) = \frac{a(ix)}{1 + a(ix)b(ix)} (Z_T - d(ix)) \quad (4.74)$$

Now we can compute the density feedback reactivity from (4.62) and (4.71), and we can write down:

$$\begin{aligned} \delta \bar{\Delta k}_\rho = & \left\{ \sum_{ix} e_{ix} N_{ch}(ix) L(ix) \right\} \delta \bar{Y} + \left\{ \sum_{ix} N_{ch}(ix) (e_{ix} M(ix) + f_{ix}) \right\} \delta \bar{q} \\ & + \left\{ \sum_{ix} N_{ch}(ix) (e_{ix} N(ix) + h_{ix}) \right\} \delta \bar{T}_{in} \end{aligned} \quad (4.75)$$

Therefore we can write:

$$\delta \bar{\Delta k}_\rho = Q_\rho \delta \bar{q} + R_\rho \delta \bar{Y} + S_\rho \delta \bar{T}_{in} \quad (4.76)$$

Therefore the power to density feedback reactivity transfer function Q_ρ , is given by:

$$Q_\rho = \frac{\delta \bar{\Delta k}_\rho}{\delta \bar{q}} = \sum_{ix} N_{ch}(ix) (e_{ix} M(ix) + f_{ix}) \quad (4.77)$$

this transfer function gives the change in the density reactivity induced by a unitary power perturbation.

Also we have defined the core total flow to density feedback reactivity transfer function R_ρ , that is given by

$$R_\rho = \frac{\delta \bar{\Delta k}_\rho}{\delta \bar{Y}} = \sum_{ix} N_{ch}(ix) e_{ix} L(ix) \quad (4.78)$$

this transfer function gives the change in the density reactivity induced by a unitary flow perturbation.

Finally we have defined the inlet temperature to feedback reactivity transfer function S_ρ , that is given by:

$$S_\rho = \frac{\delta \overline{\Delta k}_\rho}{\delta \overline{T}_{in}} = \sum_{ix} N_{ch}(ix) (e_{ix} N(ix) + h_{ix}) \quad (4.79)$$

this transfer function gives the change in the density reactivity induced by a unitary inlet temperature perturbation.

ii-2 The temperature feedback reactivity transfer functions

The Doppler reactivity change $\delta \overline{\Delta k}_D$, due to flow, power and temperature perturbations, in all the channels will be given by:

$$\begin{aligned} \delta \overline{\Delta k}_D = \sum_{ix} N_{ch}(ix) d_y(ix) \delta \overline{y}_{in}(ix) + \sum_{ix} N_{ch}(ix) d_q(ix) \delta \overline{q} \\ + \sum_{ix} N_{ch}(ix) d_T(ix) \delta \overline{T}_{in}(ix) \end{aligned} \quad (4.80)$$

on account of expression (4.71), that relates $\delta \overline{y}_{in}(ix)$ with $\delta \overline{Y}$, $\delta \overline{q}$, and $\delta \overline{T}_{in}$, we may write:

$$\begin{aligned} \delta \Delta k_D = \left\{ \sum_{ix} N_{ch}(ix) d_y(ix) L(ix) \right\} \delta \overline{Y} \\ + \left\{ \sum_{ix} N_{ch}(ix) (d_y(ix) M(ix) + d_q(ix)) \right\} \delta \overline{q} \\ + \left\{ \sum_{ix} N_{ch}(ix) (d_y(ix) N(ix) + d_T(ix)) \right\} \delta \overline{T}_{in} \end{aligned} \quad (4.81)$$

Expression (4.84) can be expressed as follows:

$$\delta \Delta k_D = Q_D \delta \overline{q} + R_D \delta \overline{Y} + S_D \delta \overline{T}_{in} \quad (4.82)$$

where we have defined the power to Doppler feedback reactivity transfer function, as follows:

$$Q_D = \frac{\partial \Delta K_D}{\partial q} = \sum_{ix} N_{ch}(ix) (d_y(ix) M(ix) + d_q(ix)) \quad (4.83)$$

The core flow to Doppler feedback reactivity transfer function R_D , given by

$$R_D = \frac{\partial \Delta K_D}{\partial Y} = \sum_{ix} N_{ch}(ix) d_y(ix) L(ix) \quad (4.84)$$

The coolant temperature to Doppler feedback reactivity transfer function, S_D , given by:

$$S_D = \frac{\partial \Delta K_D}{\partial T_{in}} = \sum_{ix} N_{ch}(ix) (d_y(ix) N(ix) + d_T(ix)) \quad (4.85)$$

These transfer functions are computed in the ONECOR subroutine, where are denoted by:

$$\begin{aligned} CAD &\equiv R_D \\ CBD &\equiv Q_D \\ CCD &\equiv S_D \end{aligned} \quad (4.86)$$

4.4.5.2 The One-Core Reactivity Feedback Transfer Function

The block diagram of figure 4.4 can be drawn in compact form as displayed in figure 4.5.

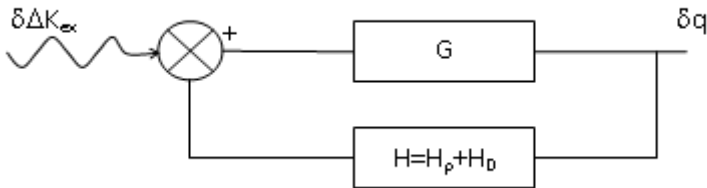


Figure 4.5. Block diagram of LAPUR transfer functions in compact form.

In figure 4.5, G is the open loop transfer function and H is the power to reactivity feedback transfer function. This transfer functions has two contributions, the density feedback reactivity and the Doppler feedback reactivity. So we write:

$$H = H_\rho + H_D \equiv CHR + CHD \quad (4.87)$$

To compute feedback transfer function by density H_ρ , we compute from equation (4.76), that gives the reactivity change due to flow power and inlet temperature perturbations:

$$\delta \bar{\Delta k}_\rho = R_\rho \delta \bar{Y} + Q_\rho \delta \bar{q} + S_\rho \delta \bar{T}_{in} \quad (4.88)$$

Then, from equation (4.66), we can obtain $\delta \bar{Y}$

$$\delta \bar{Y} = \frac{R_{clp} Z_Q}{1 - Z_Y R_{clp}} \delta \bar{q} + \frac{R_{clp} Z_T}{1 - Z_Y R_{clp}} \delta \bar{T}_{in} + \frac{1}{1 - Z_Y R_{clp}} \delta \bar{Y}_{ex} \quad (4.89)$$

Direct substitution of equation (4.89) into equation (4.88) gives:

$$\begin{aligned} \delta \bar{\Delta k}_\rho = & \left(Q_\rho + \frac{R_\rho R_{clp}}{1 - Z_Y R_{clp}} Z_Q \right) \delta \bar{q} + \left(S_\rho + \frac{R_\rho R_{clp}}{1 - Z_Y R_{clp}} Z_T \right) \delta \bar{T}_{in} \\ & + \left(\frac{R_\rho}{1 - Z_Y R_{clp}} \right) \delta \bar{Y}_{ex} \end{aligned} \quad (4.90)$$

From equation (4.90), it is obtained the power to density reactivity transfer function H_ρ , that is given by:

$$H_\rho = Q_\rho + \frac{R_\rho R_{clp}}{1 - Z_Y R_{clp}} Z_Q = \left(\frac{\partial \Delta k_\rho}{\partial q} \right) + \left(\frac{\partial \Delta k_\rho}{\partial Y} \right) \left(\frac{\partial Y}{\partial q} \right) \quad (4.91)$$

The notation employed by LAPUR is:

$$\begin{aligned} CHR &\equiv H_\rho \\ CAR &\equiv R_\rho \\ CBR &\equiv Q_\rho \\ CCR &\equiv S_\rho \\ CQY &\equiv \frac{\partial Y}{\partial q} = \frac{R_{clp} Z_Q}{1 - Z_Y R_{clp}} \end{aligned} \quad (4.92)$$

The Doppler feedback reactivity transfer function H_D is computed on account of equation (4.88), that gives the Doppler reactivity change due to flow, power and inlet temperature perturbations

$$\delta \bar{\Delta k}_D = Q_D \delta \bar{q} + R_D \delta \bar{Y} + S_D \delta \bar{T}_{in} \quad (4.93)$$

Direct substitution of equation (4.89) into equation (4.93) yields

$$\begin{aligned} \delta \bar{\Delta k}_D = & \left(Q_D + \frac{R_D R_{clp}}{1 - Z_Y R_{clp}} Z_Q \right) \delta \bar{q} \\ & + \left(S_D + \frac{R_D R_{clp}}{1 - Z_Y R_{clp}} Z_T \right) \delta \bar{T}_{in} + \left(\frac{R_D}{1 - Z_Y R_{clp}} \right) \delta \bar{Y}_{ex} \end{aligned} \quad (4.94)$$

From equation (4.94), it is obtained the power to Doppler reactivity transfer function H_D , that is given by:

$$H_D = Q_D + \frac{R_D R_{clp}}{1 - Z_Y R_{clp}} Z_Q = \left(\frac{\partial \Delta k_D}{\partial q} \right) + \left(\frac{\partial \Delta k_D}{\partial Y} \right) \left(\frac{\partial Y}{\partial q} \right) \quad (4.95)$$

The notation employed by LAPUR, in the subroutine ONECOR, is:

$$\begin{aligned} CHD &\equiv H_D \\ CAD &\equiv R_D \\ CBD &\equiv Q_D \\ CCD &\equiv S_D \end{aligned} \quad (4.96)$$

4.4.6 The Open-Loop and the Closed-Loop Transfer Functions in LAPUR

From figure 4.5, it is obtained that the open-loop transfer function GH , is given by:

$$GH = G * H \quad (4.97)$$

where G is the reactivity to power one core transfer function, and H is the power to reactivity feedback transfer function. These transfer functions are denoted in LAPUR by:

$$\begin{aligned} GH &\equiv CGH \\ G &\equiv CG \\ H &\equiv CH \end{aligned} \quad (4.98)$$

The closed-loop transfer function is obtained on account of figure 4.5, and is given by the expression:

$$CG1GH = \frac{G}{1 - GH} \quad (4.99)$$

4.5 IMPLEMENTATION OF VARIABLE AREA INTO THE CODE LAPUR

The geometry of the channels simulated by the code has been changed from constant area to variable area, in order that the code can manage the new fuel designs with partial length rods. This change has been performed in both the steady state and the frequency domain modules.

In the previous version, the existence of a variable area in the element is not allowed. Hence reversible losses or gaining pressures and irreversible losses have to be modeled by a frictional multiplier.

The new conservation equations of mass, energy, and momentum used to describe the two-phase flow dynamics along the heated channel are, for steam phase:

$$\frac{\partial}{\partial t}(\rho_s(z)A_s(z)) = -\frac{\partial}{\partial z}(\rho_s(z)u_s A_s(z)) + \Gamma_s A(z) \quad (4.100)$$

$$\begin{aligned} \frac{\partial}{\partial t}(\alpha \rho_s e_{a,s} A(z)) = & \left[-\frac{\partial}{\partial z}(\alpha \rho_s h_{0,s} u_s A(z)) \right] + [P_{sw} q''_{sw}] + [P_{si} q''_{si}] \\ & - \left[P \frac{\partial \alpha}{\partial t} A(z) \right] + [\Gamma_s h_{0,si} A(z)] + [\alpha q''_s A(z)] \end{aligned} \quad (4.101)$$

$$\begin{aligned} \frac{\partial}{\partial t}(\alpha \rho_s u_s A(z)) = & \left[-\tau_{sw} P_{sw} - \tau_{si} P_{si} - \rho_s g \alpha A(z) \cos \theta - \alpha \frac{\partial P}{\partial z} A(z) \right] \\ & - \left[\frac{\partial}{\partial z}(\alpha \rho_s u_s^2 A(z)) \right] + [\Gamma u_i A(z) \Delta z \hat{e}_z] \end{aligned} \quad (4.102)$$

For the liquid phase:

$$\frac{\partial}{\partial t}(\rho_l(z)A_l(z)) = -\frac{\partial}{\partial z}(\rho_l(z)u_l A_l(z)) + \Gamma_l A(z) \quad (4.103)$$

$$\begin{aligned} \frac{\partial}{\partial t}((1-\alpha)\rho_l e_{a,l} A(z)) = & \left[-\frac{\partial}{\partial z}((1-\alpha)\rho_l h_{0,l} u_l A(z)) \right] + [P_{lw} q''_{lw}] + [P_{li} q''_{li}] \\ & - \left[P \frac{\partial(1-\alpha)}{\partial t} A(z) \right] + [\Gamma_l h_{0,li} A(z)] + [(1-\alpha)q''_l A(z)] \end{aligned} \quad (4.104)$$

$$\begin{aligned} & \frac{\partial}{\partial t} \left((1-\alpha) \rho_l u_l A(z) \right) = \\ & \left[-\tau_{lw} P_{lw} + \tau_{li} P_{li} - \rho_l g (1-\alpha) A(z) \cos \theta - (1-\alpha) \frac{\partial P}{\partial z} A(z) \right] \\ & - \left[\frac{\partial}{\partial z} \left((1-\alpha) \rho_l u_l^2 A(z) \right) \right] - [\Gamma u_l A(z) \Delta z \hat{e}_z] \end{aligned} \quad (4.105)$$

From these equations and using the following normalized values of the mass flow rate:

$$y = \frac{w}{w_0} \quad (4.106)$$

the degree of subcooling:

$$H = \frac{h - h_l}{h_{fg}} \quad (4.107)$$

and the pressure:

$$\Pi = \frac{P}{g \rho_F L} \quad (4.108)$$

we can obtain, after the combination of the conservation equations (4.100) to (4.105), the following expressions:

i) Mass conservation of the two phase mixture:

$$\frac{A_0}{A(z)} \frac{\partial y}{\partial z} = \frac{\eta}{u_0} \frac{\partial \alpha}{\partial t} \quad (4.109)$$

ii) Energy conservation of the mixture:

$$\frac{\eta}{(1-\eta) h_{fg} w_0} Q' = \frac{\partial}{\partial z} \left[y \left\{ \sigma - H \left(\frac{1}{1-\eta} - \sigma \right) \right\} \right] - \frac{\eta}{(1-\eta) u_0} \frac{1}{\partial t} \left[H (1-\alpha) \frac{A(z)}{A_0} \right] \quad (4.110)$$

iii) Energy conservation of the steam:

$$\frac{\eta F_s}{(1-\eta) h_{fg} w_0} Q' = \lambda_s \frac{\eta}{u_0} \alpha \frac{A(z)}{A_0} + \frac{\partial y \sigma}{\partial z} \quad (4.111)$$

iv) Momentum conservation of the mixture:

$$\begin{aligned}
 -L \frac{\partial \Pi}{\partial z} \frac{A(z)}{A_0} &= \frac{u_0}{g} \frac{\partial y}{\partial t} + \frac{u_0^2}{g} \frac{\partial}{\partial z} \left(B y^2 \frac{A_0}{A(z)} \right) \\
 &+ F(z) y^{(2-a_2)} \phi_{MN}^2 \Omega \left(\frac{A_0}{A(z)} \right) + (1 - \alpha \eta) \cos \theta \frac{A(z)}{A_0}
 \end{aligned} \tag{4.112}$$

where η is the relative density decrement in the evaporation process $\left(\eta = \frac{\rho_F - \rho_s}{\rho_F} \right)$, Q' is the energy supply by the fuel per unit length ($Q' = P_{sw} q_{sw}'' + P_{lw} q_{lw}''$), F_s is the fraction of energy invested in the formation of steam, λ_s is the bubble decay ratio, ϕ_{MN}^2 is the Martinelli-Nelson two-phase friction multiplier, σ is given by:

$$\sigma = 1 + \frac{\eta}{1 - \eta} X \tag{4.113}$$

the parameter B is given by the expression:

$$B = \frac{[1 - \alpha(1 - \gamma^2(z)(1 - \eta))]}{[1 - \alpha(1 - \gamma(z)(1 - \eta))]^2} \tag{4.114}$$

and $\gamma(z)$ is the slip ratio, $F(z)$ is given by:

$$F(z) = \frac{u_0^2}{2g D_H(z)} f_0(z) \tag{4.115}$$

where $f_0(z)$ is the Moody friction factor at the steady state.

Equations (4.109) to (4.112) constitute a system of equations with a dependent variable, Q ; three independent variables, y , α and H ; and three functionals, ϕ^2 , λ_s and F_s , of these variables.

The next step involves the formulation and solution of the thermal-hydraulic conservation equations in the frequency domain, with the objective of determine:

1. The response of the coolant average density distribution along the channel to driving perturbations of:
 - Inlet flow rate, $\delta \bar{y}$,
 - Inlet sub-cooling temperature, δT_{in}^* , and

- Power generation in the fuel, $\delta\bar{q}$.

2. The response of the pressure drop along the channel to these same driving perturbations.

The knowledge of the spatially dependent response of the coolant-moderator density allows, by means of appropriate density reactivity coefficients, the determination of feedback reactivity transfer functions to be used in the neutronic model to calculate the response of the power generation to the above driving perturbations.

Starting from the response of the pressure drop along the channels to the driving perturbations, we can determine:

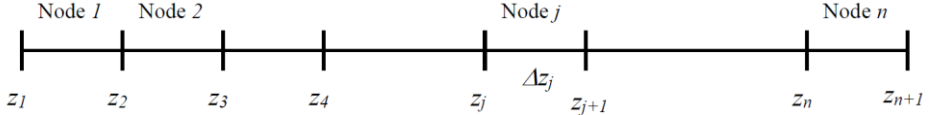
1. The flow stability of each channel in the reactor, and
2. The dynamic redistribution of the flow of coolant among the different channels.

To perform the linearization of the mass, energy and momentum equations we perform the following substitution in the mass, energy and momentum equations:

$$\begin{aligned}
 H &= H_0 + \delta H \\
 \alpha &= \alpha_0 + \delta\alpha \\
 y &= y_0 + \delta y \\
 Q' &= Q'_0 + \delta Q' \quad . \quad (4.116) \\
 F_s &= F_{s0} + \left(\frac{\partial F_s}{\partial H} \right)_0 \delta H \\
 \lambda_s &= \lambda_{s0} + \left(\frac{\partial \lambda_s}{\partial H} \right)_0 \delta H + \left(\frac{\partial \lambda_s}{\partial y} \right)_0 \delta y \\
 X &= X_0 + \left(\frac{\partial X}{\partial H} \right)_0 \delta H + \left(\frac{\partial X}{\partial \alpha} \right)_0 \delta \alpha
 \end{aligned}$$

We neglect the terms that contains products of perturbations, retaining only first order perturbation terms. Then we subtract from the resulting equations the steady state equations, obtaining in this way the linearized equation in the perturbations.

Linearization of the mass conservation equation around the steady state equation, followed by Laplace transformation, and integration over the j -th node yields:



$$\delta\bar{y}_{a,j} = \delta\bar{y}_j + \frac{1}{\left[\frac{A_0}{A_{j+1}} + \frac{A_0}{A_j} \right]} \frac{\eta}{u_0} s \Delta z_j \delta\bar{\alpha}_{a,j} \quad (4.17)$$

where $A_j = A(z_j)$.

For the energy conservation we use that the total perturbation of the heat flux from the fuel to the coolant, that it can be expressed, for a generic node i along the channel length, in terms of transfer functions, by:

$$\delta\bar{Q}'_i = Q'_{0,i} \left(CB_{q,i} \delta\bar{q}'_i + CC_{q,i} \delta\bar{T}'_{l,i} + CA_{q,i} \delta\bar{y}'_i \right) \quad (4.117)$$

Then, the integration of the energy conservation equation for the two-phase mixture between the limits of the node j yields:

$$\begin{aligned}
 & \left\{ 2 \left[\sigma - H \left(\frac{1}{1-\eta} - \sigma \right) \right]_{0,j+1} - \left[\frac{\eta}{(1-\eta)w_0 h_{fg}} \right] \Delta z_j \mathcal{Q}'_{0,j} C A_{q,j} \right\} \delta \bar{y}_{a,j} \\
 & + \left\{ \frac{\eta}{1-\eta} 2(1+H)_{0,j+1} \left(\frac{\partial X}{\partial \alpha} \right)_{0,j+1} + \frac{\eta}{1-\eta} \frac{1}{u_0} s \frac{A_{a,j}}{A_0} H_{0,a,j} \Delta z_j \right\} \delta \bar{\alpha}_{a,j} \\
 & + \left\{ -2 \left[\frac{1}{1-\eta} - \sigma \right]_{0,j+1} - \frac{\eta}{1-\eta} \frac{1}{u_0} s \frac{A_{a,j}}{A_0} (1-\alpha_0)_{a,j} \Delta z_j \right. \\
 & \left. + \frac{\eta}{1-\eta} 2(1+H)_{0,j+1} \left(\frac{\partial X}{\partial H} \right)_{0,j+1} + \left[\frac{\eta}{(1-\eta)w_0 h_{fg}} \right] \Delta z_j \mathcal{Q}'_{0,j} C C_{q,j} \frac{h_{fg}}{c_p} \right\} \delta \bar{H}_{a,j} = \\
 & \left\{ \left[\sigma - H \left(\frac{1}{1-\eta} - \sigma \right) \right]_{0,j+1} + \left[\sigma - H \left(\frac{1}{1-\eta} - \sigma \right) \right]_{0,j} \right\} \delta \bar{y}_j \\
 & + \left\{ \frac{\eta}{1-\eta} (1+H)_{0,j+1} \left(\frac{\partial X}{\partial \alpha} \right)_{0,j+1} + \frac{\eta}{1-\eta} (1+H)_{0,j} \left(\frac{\partial X}{\partial \alpha} \right)_{0,j} + \frac{\eta}{1-\eta} \frac{s}{u_0} \frac{A_{a,j}}{A_0} \frac{(H_{0,j+1} - H_{0,j})}{2} \Delta z_j \right\} \delta \bar{\alpha}_j \\
 & + \left\{ - \left[\frac{1}{1-\eta} - \sigma \right]_{0,j+1} - \left[\frac{1}{1-\eta} - \sigma \right]_{0,j} + \frac{\eta}{1-\eta} \frac{s}{u_0} \frac{A_{a,j}}{A_0} \frac{(\alpha_{0,j+1} - \alpha_{0,j})}{2} \Delta z_j \right. \\
 & \left. + \frac{\eta}{1-\eta} \left[(1+H)_{0,j+1} \left(\frac{\partial X}{\partial H} \right)_{0,j+1} + (1+H)_{0,j} \left(\frac{\partial X}{\partial H} \right)_{0,j} \right] \right\} \delta \bar{H}_j \\
 & \left\{ \left[\frac{\eta}{(1-\eta)w_0 h_{fg}} \right] \mathcal{Q}'_{0,j} C B_{q,j} \Delta z_j \right\} \delta \bar{q}_{a,j}
 \end{aligned} \tag{4.118}$$

The integration of the energy conservation equation for the steam phase gives:

$$\begin{aligned}
 & \left\{ - \left(\frac{\eta}{1-\eta} \right) \left(\frac{Q'_0}{w_0 h_{fg}} \right) CA_{q,a,j} \Delta z_j \frac{2F_s(j+1)+F_s(j)}{3} + \frac{A_{a,j}}{A_0} \frac{\eta}{u_0} \Delta z_j \alpha_{j+1} 1.6 \lambda_{s,j+1} + 2\sigma_{0,j+1} \right\} \delta \bar{y}_{a,j} \\
 & \left\{ \frac{A_{a,j}}{A_0} \frac{\eta}{u_0} \Delta z_j \lambda_{s,j+1} + 2 \left(\frac{\eta}{1-\eta} \right) \left(\frac{\partial X}{\partial \alpha} \right)_{0,j+1} \right\} \delta \bar{\alpha}_{a,j} \\
 & \left\{ \left(\frac{\eta}{1-\eta} \right) \left(\frac{Q'_0}{w_0 h_{fg}} \right) \frac{h_{fg}}{c_p} CC_{q,a,j} \Delta z_j \frac{2F_s(j+1)+F_s(j)}{3} + \frac{A_{a,j}}{A_0} \frac{\eta}{u_0} \Delta z_j \alpha_{j+1} 2 \frac{\lambda_{s,j+1}}{H_{j+1}} \right. \\
 & \left. + \left(\frac{\eta}{1-\eta} \right) \left(\frac{Q'_0}{w_0 h_{fg}} \right) \Delta z_j \frac{f_{p,j+1}}{(1-\eta)} F_{s,j+1}^2 + 2 \left(\frac{\eta}{1-\eta} \right) \left(\frac{\partial X}{\partial H} \right)_{0,j+1} \right\} \delta \bar{H}_{a,j} = \\
 & \left\{ \frac{A_{a,j}}{A_0} \frac{\eta}{u_0} \frac{\Delta z_j}{2} [\alpha_{j+1} 1.6 \lambda_{s,j+1} - \alpha_j 1.6 \lambda_{s,j}] + (\sigma_{0,j+1} + \sigma_{0,j}) \right. \\
 & \left. - \left(\frac{\eta}{1-\eta} \right) \left(\frac{Q'_0}{w_0 h_{fg}} \right) CA_{q,a,j} \Delta z_j \frac{F_s(j+1) - F_s(j)}{6} \right\} \delta \bar{y}_j \\
 & + \left\{ \frac{A_{a,j}}{A_0} \frac{\eta}{u_0} \frac{\Delta z_j}{2} [\lambda_{s,j} - \lambda_{s,j+1}] + \left(\frac{\eta}{1-\eta} \right) \left[\left(\frac{\partial X}{\partial \alpha} \right)_{0,j+1} + \left(\frac{\partial X}{\partial \alpha} \right)_{0,j} \right] \right\} \delta \bar{\alpha}_j \\
 & + \left\{ \frac{A_{a,j}}{A_0} \frac{\eta}{u_0} \Delta z_j \left[\alpha_{j+1} \frac{\lambda_{s,j+1}}{H_{j+1}} - \alpha_j \frac{\lambda_{s,j}}{H_j} \right] - \left(\frac{\eta}{1-\eta} \right) \left(\frac{Q'_0}{w_0 h_{fg}} \right) \frac{\Delta z_j}{2} \left[\frac{f_{p,j} F_{s,j}^2 - f_{p,j+1} F_{s,j+1}^2}{1-\eta} \right] \right. \\
 & \left. + \left(\frac{\eta}{1-\eta} \right) \left[\left(\frac{\partial X}{\partial H} \right)_{0,j+1} + \left(\frac{\partial X}{\partial H} \right)_{0,j} \right] + \left(\frac{\eta}{1-\eta} \right) \left(\frac{Q'_0}{w_0 h_{fg}} \right) \frac{h_{fg}}{c_p} CC_{q,a,j} \Delta z_j \left[\frac{F_s(j+1) - F_s(j)}{6} \right] \right\} \delta \bar{H}_j \\
 & + \left\{ \left(\frac{\eta}{1-\eta} \right) \left(\frac{Q'_0}{w_0 h_{fg}} \right) [F_{s,a,j} CB_{q,a,j} \Delta z_j] \right\} \delta \bar{q}_{a,j}
 \end{aligned} \tag{4.119}$$

The integration of the momentum equation over the node j of the channel gives:

$$\begin{aligned}
 & -(\delta\bar{\Pi}_{j+1} - \delta\bar{\Pi}_j) = \\
 & \left\{ \frac{u_0}{gL} \Delta z_j \frac{A_0}{A_{a,j}} s + 4 \frac{u_0^2}{gL} B_{j+1} \frac{A_0}{A_{j+1}} \frac{A_0}{A_{a,j}} + \right. \\
 & \quad \left. + K_F f_{0,j} \frac{u_0^2}{2gL} \left((2-a_2)_j \Omega_j + \left(\frac{\partial \Omega}{\partial y} \right)_j \right) \phi_{MN,j+1}^2 \Delta z_j \frac{1}{D_{H,j+1}} \frac{A_0}{A_{j+1}} \frac{A_0}{A_{a,j}} \right\} \delta\bar{y}_{a,j} \\
 & + \left\{ 2 \frac{u_0^2}{gL} \left(\frac{\partial B}{\partial \alpha} \right)_{j+1} \frac{A_0}{A_{j+1}} \frac{A_0}{A_{a,j}} - \eta \frac{\Delta z_j}{L} \cos \theta \right. \\
 & \quad \left. + K_F f_{0,j} \frac{u_0^2}{2gL} \Omega_j \left(\frac{\partial \phi_{MN}^2}{\partial \alpha} \right)_{j+1} \Delta z_j \frac{1}{D_{H,j+1}} \frac{A_0}{A_{j+1}} \frac{A_0}{A_{a,j}} \right\} \delta\bar{\alpha}_{a,j} \\
 & + \left\{ K_F f_{0,j} \frac{u_0^2}{2gL} \left(\frac{\partial \Omega}{\partial H} \right)_{j+1} \phi_{MN,j+1}^2 \Delta z_j \frac{1}{D_{H,j+1}} \frac{A_0}{A_{j+1}} \frac{A_0}{A_{a,j}} \right. \\
 & \quad \left. + 2 \frac{u_0^2}{gL} \left(\frac{\partial B}{\partial H} \right)_{j+1} \frac{A_0}{A_{j+1}} \frac{A_0}{A_{a,j}} \right\} \delta\bar{H}_{a,j} \\
 & - \left\{ 2 \frac{u_0^2}{gL} \frac{A_0 (1^s)}{A_{a,j}} \left[\frac{A_0}{A_{j+1}} B_{j+1} + \frac{A_0}{A_j} B_j \right] \right. \\
 & \quad \left. + K_F f_{0,j} \frac{u_0^2}{2gL} \left((2-a_2)_j \Omega_j + \left(\frac{\partial \Omega}{\partial y} \right)_j \right) \frac{\Delta z_j}{2} \frac{A_0}{A_{a,j}} \left[\frac{A_0}{A_{j+1} D_{H,j+1}} \phi_{MN,j+1}^2 - \frac{A_0}{A_j D_{H,j}} \phi_{MN,j}^2 \right] \right\} \delta\bar{y}_j \\
 & - \left\{ \frac{u_0^2}{gL} \frac{A_0}{A_{a,j}} \left[\frac{A_0}{A_{j+1}} \left(\frac{\partial B}{\partial \alpha} \right)_{j+1} + \frac{A_0}{A_j} \left(\frac{\partial B}{\partial \alpha} \right)_j \right] \right. \\
 & \quad \left. + K_F f_{0,j} \frac{u_0^2}{2gL} \Omega_j \frac{\Delta z_j}{2} \frac{A_0}{A_{a,j}} \left[- \frac{A_0}{A_j D_{H,j}} \left(\frac{\partial \phi_{MN}^2}{\partial \alpha} \right)_j + \frac{A_0}{A_{j+1} D_{H,j+1}} \left(\frac{\partial \phi_{MN}^2}{\partial \alpha} \right)_{j+1} \right] \right\} \delta\bar{\alpha}_j \\
 & - \left\{ K_F f_{0,j} \frac{u_0^2}{2gL} \frac{\Delta z_j}{2} \frac{A_0}{A_{a,j}} \left[- \frac{A_0}{A_j D_{H,j}} \left(\frac{\partial \Omega}{\partial H} \right)_j \phi_{MN,j}^2 + \frac{A_0}{A_{j+1} D_{H,j+1}} \left(\frac{\partial \Omega}{\partial H} \right)_{j+1} \phi_{MN,j+1}^2 \right] \right. \\
 & \quad \left. + \frac{u_0^2}{gL} \frac{A_0}{A_{a,j}} \left[\frac{A_0}{A_{j+1}} \left(\frac{\partial B}{\partial H} \right)_{j+1} + \frac{A_0}{A_j} \left(\frac{\partial B}{\partial H} \right)_j \right] \right\} \delta\bar{H}_j
 \end{aligned} \tag{4.120}$$

4.6 IMPLEMENTATION OF THE NEW FRICTION MODEL INTO THE CODE LAPUR

The version 5 of the code LAPUR has various deficiencies in the friction model implemented in the code. These are:

1. There is no model that evaluates local or secondary losses in the cell of the element. Only friction losses are modelled. Therefore, it is necessary to include the local losses through a multiplier, so that it corrects frictional losses obtaining at the same time the equivalent to the local losses.
2. Two-phase friction multipliers are estimated by using the Martinelli-Nelson multiplier, which uses the Jones correction factor. This multiplier overestimates friction pressure drop for steam qualities greater than 0.6, so it must be modified in order to reproduce the experimental data that are available.

The new version of LAPUR includes new correlations for computing friction and local losses.

4.6.1 New Friction Multiplier Model

The original version of LAPUR uses the Martinelli-Nelson two-phase multiplier, with the Jones correction for the flow. It is well known that for the operating conditions of a BWR, this multiplier over-estimate the two phase friction mainly for high qualities of the mixture. To correct this situation, we have included the possibility to use the Chisholm-Barocky correlation to compute the friction multiplier.

This model uses the following equations:

$$GMSQ = \left[\left(\frac{\mu_s}{\mu_F} \right)^{0.2} \left(\frac{\rho_l}{\rho_s} \right) \right] \quad (4.121)$$

$$BGM = \sqrt{GMSQ} \quad (4.122)$$

$$B = \frac{55.0}{[G]^{0.5}} \quad BGM \leq 9.5 \quad (4.123)$$

$$B = \frac{520.0}{BGM \cdot [G]^{0.5}} \quad 9.5 < BGM < 28, \quad (4.124)$$

$$B = \frac{15000.0}{GMSQ \cdot [G]^{0.5}} \quad 28 \leq BGM, \quad (4.125)$$

$$\phi_{CB}^2 = \left\{ 1.0 + (GMSQ - 1.0) \cdot \left[B \cdot X^{0.9} \cdot (1.0 - X)^{0.9} + X^{1.8} \right] \right\}, \quad (4.126)$$

where μ_s is the steam viscosity, μ_F is the saturated liquid viscosity, ρ_l is the liquid density, ρ_s is the steam density, G is the mass flux ($\text{kg/m}^2 \text{ s}$), X is the flow quality.

4.6.2 New Friction Factor Model

We have included the option to use of new friction factor model. This new model uses the equations:

$$FF_{LAM} = \frac{64.0}{Re_l} \quad (4.127)$$

$$FF = AN \cdot \left[1 + (BN \cdot R_r) + \frac{CN}{Re_l} \right]^{DN} \quad (4.128)$$

$$FF = MAX(FF, FF_{LAM}) \quad (4.129)$$

where AN , BN , CN , DN are input-user data; R_r is the relative roughness (input-user data) and Re_l is the liquid Reynolds number

4.7 CHAPTER SUMMARY

LAPUR is a computer code developed at Oak Ridge National Laboratory for the calculation of BWR core stability parameters. It uses a multinodal description of the neutron dynamics, together with a distributed parameter model of the core thermal hydrodynamics to produce a space-dependent representation of the dynamics of a BWR in the frequency domain for small perturbations around a steady state condition. The LAPUR program consists of two autonomous modules, LAPURX and LAPURW, which are linked by means of an intermediate storage routine. The first module, LAPURX, solves the governing equations for the coolant and the fuel steady state. Map of the core steady state are generated and stored in data files for subsequent utilization

by LAPURW. The second module, LAPURW, solves the dynamic equations for the coolant, fuel, and neutron field in the frequency domain. A set of open-loop transfer functions are generated and the stability index (decay ratio), is estimated from the closed loop reactivity to power transfer function.

The previous LAPUR 5 release 1 code does not consider channel with variable area and does not distinguish specifically local pressure drop due to spacers in a bundle. The only way to take into account local pressure losses and gains due to spacers and area changes is by means of a friction multiplier given by input. This deficiency leads to adjusting by input friction multiplier in order to account for accurately local and variable area effect on the pressure drop.

The new LAPUR 6 [52] is the current implementation of the LAPUR model and this version will be used in this methodology. This version includes new correlations for computing friction and local losses and capabilities for modelling bundles with variable cross-area. As additional improvements, LAPUR 6 allows to use up to 200 thermalhydraulic channel to represent the core and calculates transfer functions with up to 100 frequency points instead of 25 points for LAPUR 5.1 release 1.

5 METHODOLOGY USED FOR DECAY RATIOS CALCULATION WITH LAPUR

5.1 INTRODUCTION

This chapter describes a methodology to use LAPUR code for thermal hydraulic stability analysis. The method includes the generation the LAPUR input data that are dependent on the specific core conditions. Several codes are required in this methodology, for steady state evaluation, kinetic parameter computation, and frequency domain evaluation.

SIMULATE computer code [59] is the 3D core simulator used to calculate the core detailed hydraulic and neutronic configuration of the different state points to analyze.

PAPU [60] is a post-processor used to obtain Doppler and reactivity density coefficient from the perturbation calculations performed by SIMULATE around the base case.

LIP [61] postprocessor extracts from SIMULATE summary and output file a database for all core assemblies classified for types in different output files and generates the complete input data for LAPUR.

The figure of merit used to evaluate the stability margin is the Decay Ratio (DR). LAPUR code [67] calculates thermal-hydraulic channel and core wide decay ratios. An evaluation of the out of phase decay ratios is also performed.

Calculation steps and a detailed specification of the necessary input data to perform channel hydrodynamic and reactor core stability calculations will be provided. The possibility of performing additional out of phase decay ratio calculations is also contemplated. Besides, validation test against real plant data as well as a comparison to vendor's calculation results will be also enclosed.

5.2 DESCRIPTION OF CODES

A brief description of the computer tools involved in this method is included below.

5.2.1 LAPUR

A detailed description of LAPUR 6 code and calculation process can be seen in chapter 4. Details from previous LAPUR versions can be found in [1], [2] and [67]. LAPUR 5 release 1 improvements with respect to older versions can be found in references [69]. Specifically, LAPUR 6 improvements with respect to LAPUR 5 release 1 version can be found in [68].

5.2.2 SIMULATE.

SIMULATE, [59] and [70], is a three-dimensional two-group (steady-state) reactor analysis code which is being used by utilities to perform incore

fuel management studies, core design calculations, and calculation of safety parameters. The main three-dimensional neutron physics models which are used in SIMULATE are:

- Two-group nodal diffusion model.
- Assembly homogenization model.
- Baffle reflector model.
- Cross section/ depletion model.
- Pin power reconstruction model.

SIMULATE code is used, in this methodology, to:

1. Calculate the core detailed hydraulic and neutronic conditions for the different state-points to analyze.
2. Perform a series of reactivity perturbations to obtain nuclear dynamic parameters. Using the perturbation calculation option, SIMULATE generates the KINETIC output file. This file contains planar average edits (1-D and 0-D edits) of nuclear and thermal-hydraulic data.

5.2.3 PAPU Post-Processor

PAPU [60] is a computer code developed at The Chemical and Nuclear Engineering Department of Valencia Polytechnic University (UPV). This code uses KINETIC output file of SIMULATE, generated in the perturbation calculation option, as input. Three types of perturbations are required: Doppler (DOP), pressure (PRE) and moderator temperature (MTC). From fuel temperature perturbations PAPU obtains Doppler coefficient. From pressure and moderator temperature perturbations, PAPU obtains reactivity density coefficients. The code extracts nuclear and thermal-hydraulics data from KINETIC output file (1-D edits) to obtain reactivity values respect to fuel temperature and void fraction variations for each axial node. Additionally, the code calculates the density change associated with each nodal void fraction variation. From the reactivity changes, by means of a least square approximation, the code calculates Doppler and density reactivity coefficients. PAPU code generates PAPUSAL output file, which directly contains the reactivity coefficients. Information about the least square approximation errors can be optionally saved in another file.

A detailed description about models and methods used by PAPU to obtain point kinetic Doppler and Density coefficients can be found in [60]. Appendix A describes the procedure to obtain point kinetic coefficients and parameters of PAPU inputs files.

5.2.4 LAPUR Input Pre-Processor (LIP)

LAPURX module allows a maximum of 200 average channels to represent the totality of core channels. In order to obtain average LAPUR channel data a postprocessor has been developed. LIP postprocessor [61] extracts from SIMULATE SUMMARY and OUTPUT files geometric fuel data and generate a database for all core assemblies classified for types in different output files. Geometric fuel data and gap conductances not available from SIMULATE-3 SUMMARY and OUTPUT files are supplied by means of a configuration file. Assembly relative power fractions, axial power distributions, inlet, active and water rod flows are extracted in different output files for each type considering decreasing relative power fraction as ordination criteria.

Averaged data are calculated from this database for each LAPURX channel:

- Channel average relative power fractions and axial power distributions. These values are required as LAPURX input.
- Channel average active flow in order to check the LAPURX thermal-hydraulic model consistency.
- Averaged inlet, active and water rods flow to appropriately correct channel inlet contraction coefficients from loss coefficient vendors data for lower tie plate and side entry orifice (SEO) and bottom entry orifice (BEO).

LIP automatically generates the full input data for LAPURX and LAPURW modules, managing the necessary data for auxiliary code PAPU.

LIP performs consistency checks of flow distribution, pressure drop and reactivity, and LIP generates a report with the results of the checks and decays ratios for documentation and quality assurance purposes.

5.3 METHODOLOGY

5.3.1 Calculation Procedure

Figure 5.1 shows the basic five steps to carry out decay ratio state points calculation. The necessary data and procedure for performing these steps can be summarized in the following sections:

5.3.1.1 Set Up of the Core Configuration

The starting point of a calculation is a SIMULATE restart file with the nuclear and thermal-hydraulics conditions of the state-point to analyze.

SIMULATE calculations will be performed with:

- Explicit calculation of assembly dependent leakage and water rod flows as well as core support plate leakage paths to the bypass region.
- Internal heat balance option is activated to calculate core inlet temperature. Coherent feedwater temperature data and reactor pressure for each statepoint have been used to calculate this balance.
- Different fission product options (fission product free or pre-existing concentrations) were used depending on the case.
- Specified control rod configuration.

5.3.1.2 LAPURX Input Data Generation

LIP will generate LAPURX input according to the following criteria:

LAPURX input data can be divided into four main groups:

5.3.1.2.1 Data Dependent on Power Map. Channel Grouping Criteria

Channel grouping criteria will be different in wide core and channel decay ratio calculations.

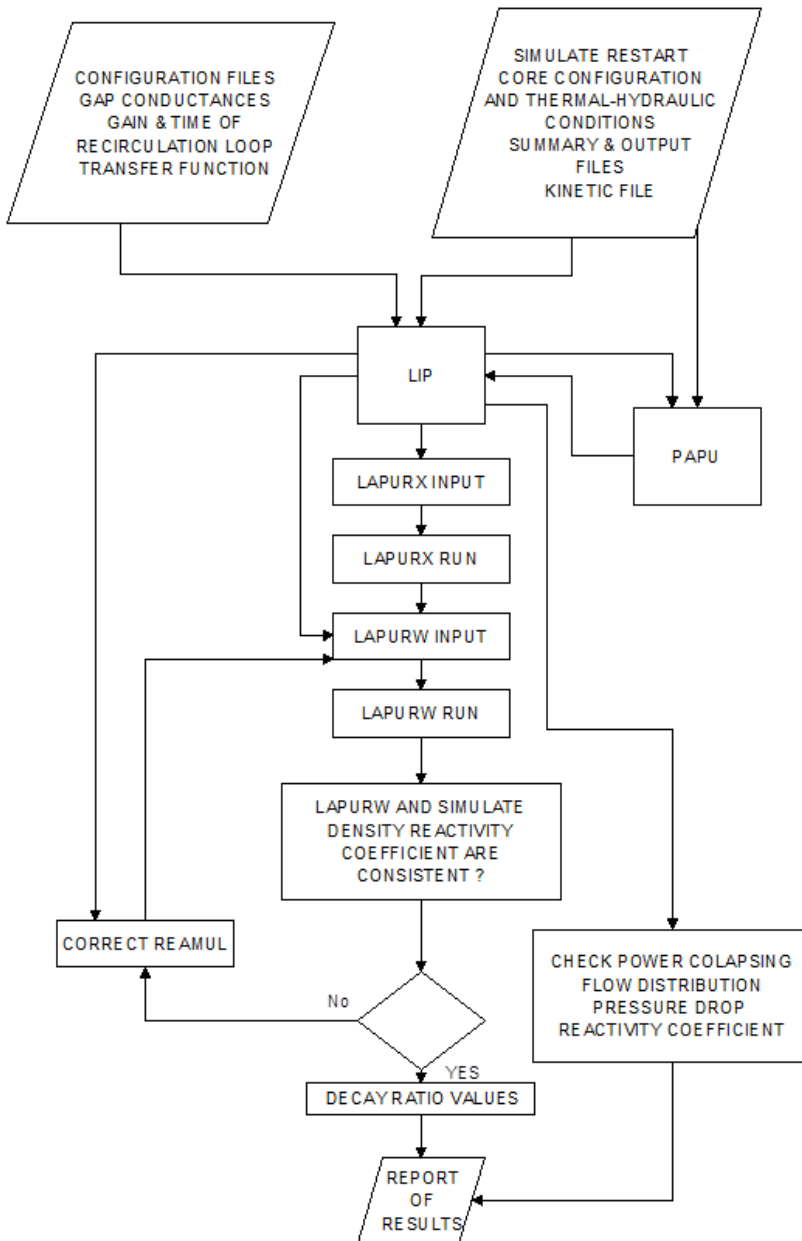


Figure 5.1. Decay ratio calculation steps.

5.3.1.2.1.1 Wide Core Decay Ratio Calculations

Core channels will be grouped in the number of regions necessary to take into account the core radial power distribution.

The grouping criteria will be based on:

- Relative power fraction.
- Different fuel designs mixed in the core.
- Peripheral or no peripheral channel. Peripheral channels have bottom entry orifice (BEO) instead of side entry orifice (SEO). Peripheral channel will be placed all together in a LAPUR averaged channel for each type.
- No more of the 20 percent of the total power will be allowed for each averaged channel. This requirement guarantees a good description of the radial power shape, especially for the high power channels.

5.3.1.2.1.2 Channel Decay Ratio Calculations

Two independent LAPUR runs, i) one hot channel including the bundle with the highest relative power fraction (RPF) and ii) with the four (4) bundles with the highest relative power fraction (RPF) will be included at least for each significant bundle type with the actual conditions of the hot channel. These hot channels will be assigned to a LAPUR thermal-hydraulic channel with its own axial power shape.

The rest of assemblies will be distributed maintaining a power less than the 20% into the others LAPURX thermal-hydraulic channels or regions.

The most conservative decay ratio result will be considered the hot channel decay ratio.

5.3.1.2.2 Thermalhydraulics and Core Power Distribution Data

5.3.1.2.2.1 Core Power Data

- Relative power fraction per region.

The relative power fraction per region is calculated from the Relative Power Fraction (RPF) 2-D map from SIMULATE SUMMARY output file.

- Power axial profile per region.

The power axial average profile for each region is calculated from the Relative Power Fraction (RPF) 2-D and 3-D maps from SIMULATE SUMMARY output file.

Relative power fraction and axial average power profile are obtained by using LIP postprocessor.

- The channel is divided into 27 axial nodes. 25 nodes corresponds to the active length of the channel according to SIMULATE axial nodalization.

5.3.1.2.2.2 *Reactor Thermalhydraulics Data*

System pressure. By using core exit and core drop pressures from SIMULATE OUTPUT SUMMARY. LAPUR system pressure is calculated as:

$$\text{System pressure} = (\text{Exit core pressure} + \text{inlet core pressure})/2$$

- Reactor power, core inlet water enthalpy, core total flow rate, fraction of total flow through bypass are directly extracted from SIMULATE.

5.3.1.2.3 *Hydraulics and Design Data*

This data set is based on fuel bundle (LAPUR channel) hydraulic and geometric data furnished by the fuel Vendor

- Contraction coefficient at the inlet of the channels. This coefficient includes the pressure drop through the bottom orifice (side entry (SEO) or bottom entry orifice (BEO)) at the channel inlet and the pressure drop due to the lower tie plate (LTP). LIP postprocessor performs a correction of this values accounting for averaged flow rates for each LAPUR channel:

First, inlet coefficient is weighted considering inlet flow and active flow

$$K_0^{LAPUR} = K_0 \cdot \frac{W_o^2}{W_{act}^2} \quad (5.1)$$

Lower tie plate (LTP) coefficient is weighted taking into account the ratio between the squares of total flow through LTP and active flow:

$$K_{LTP}^{LAPUR} = K_{LTP} \cdot \frac{W_{LTP}^2}{W_{act}^2} \quad (5.2)$$

Finally, LAPUR inlet coefficient (EKCPM) can be stated as:

$$EKCPM = K_0^{LAPUR} + K_{LTP}^{LAPUR} \quad (5.3)$$

where

W_o = inlet flow rate

W_{LTP} = flow through LTP

W_{act} = active flow

- Expansion coefficient at the exit of the channels. This coefficient takes into account the pressure gain when the flow is expanded in upper plenum. This coefficient may be negative.
- Spacers and upper tie plate (UTP) pressure drop will be calculated by LAPUR 6 according to the implemented specific model.
- Specific channel flow area at each axial location.
- Number of channel rods for each region considered.
- Total channel length .
- Heat transfer area per unit axial length of the channel.
- Fuel pellet diameter, cladding heat capacity, cladding thermal conductivity, and cladding thickness.
- Gap heat transfer coefficient.

For mixed cores:

This coefficient will be obtained from vendor calculations at channel specific burnup point and Linear Heat Generation Rate (LHGR) for each assembly type at 50% and 100% of rated power. From these data:

Constant averaged core 50% power value from vendor's data will be used to perform calculations for state-points with power values less than 50% of rated power.

Interpolated core averaged values from vendor's data between 100% and 50% of power will be used to perform calculations for state points with power values between 100% and 50% of rated power.

In case of core with no different types of fuel, the following values will be used:

Constant averaged core 50% power value from vendor's data will be used to perform calculations for state-points with power values less than 50% of rated power

Interpolated core averaged values from vendor's data between 100% and 50% of power will be used to perform calculations for state points with power values between 100% and 50% of rated power.

This approach has been considered in qualification results shown in the chapter 6.

- Friction multipliers. In LAPUR 6 the use of friction multiplier is not required due to the new correlations for computing friction and local losses and capabilities for modelling bundles with variable cross-area. Friction multiplier are set to 1.0.
- Length of the i -th axial interval within which the friction multiplier is uniform. Only one interval will be considered equal to the total length of the fuel channel because are not considered specific friction multiplier along the LAPUR 6 channels.

5.3.1.2.4 Adjustable Parameters and User Options

The following parameters are selected as default and/or recommended values in [1].

- Parameter for the calculation of Jones two-phase correction factor (0.1).
- Parameter for the calculation of slip ratio (0.1).
- Adjustable parameter to correlate the calculated and measured void fraction distribution in the subcooled boiling region. It is inversely related to the fraction of energy used to generate voids in the subcooled boiling region (1.3).

- Adjustable parameter to correlate the calculated and measured void fraction distribution in the subcooled boiling region. This one is directly related to the mean lifetime of the voids in the subcooled boiling region (0.125).

These parameters have been fixed for all calculations.

User's options.

- Allowed errors in the iterative process and convergence criteria. The values are never less than recommended values specified in [1].
- Number of nodes in the channel boiling region. 45 nodes will be considered enough for calculations.

5.3.1.3 SIMULATE Run to Perform Reactivity Perturbation Calculations

From the SIMULATE restart with the state-points conditions, a SIMULATE run is necessary to perform a set of reactivity perturbation of Doppler, pressure and moderator temperature. KINETIC output file of SIMULATE will be used as PAPU code input to obtain nuclear dynamic parameters to LAPURW module as can be seen below. The perturbation set which will be used is shown in the table below:

Table 5.1. SIMULATE perturbation set

DOPPLER:	'DDP' 20.° F 'DDP' 40 ° F. 'DDP' -20 ° F.
PRESSURE:	'PRE' 50.psia 'PRE' 75 psia.'PRE' 100 psia . 'PRE' -50 psia.
MODERATOR TEMP: COEFF	'MTC' -20 ° F. 'MTC' -10°F. 'MTC' -5°F. 'MTC' +5°F.

MTC perturbation of '+10° F' has not been used, because a more dispersed trend has been observed on density reactivity coefficients [71]. Reactivity coefficients obtained for low densities experiment higher deviations to non-conservative side in comparison with the other perturbations. For this reason, the use of 'MTC +10' leads to less conservative values in the PAPU fit of density reactivity coefficient and to a higher standard deviation of the fit.

Moderator temperature perturbation values have been chosen small enough to reproduce inlet temperature perturbations for instability events but not too much small to produce calculation perturbation errors.

Pressure perturbation ranges have been chosen to give a similar core averaged density variations as moderator inlet temperature perturbations.

5.3.1.4 LAPURW Input Data

5.3.1.4.1 *Dynamic Nuclear Parameters*

- Number of core subregions. Only one region has been considered.
- Number of delayed neutron data set considered. Only one data set has been considered.
- Number of delayed neutron groups, lambdas, betas for each group of delayed neutrons and prompt neutrons life time will be extracted from KINETIC output file.
- Reactivity initial values. The initial reactivity values have been considered zero.
- Doppler coefficient is directly extracted from PAPUSAL file (PAPU output file).
- Table of density reactivity coefficients: reactivity density coefficient versus water relative densities.

PAPU obtains density reactivity from reactivity changes respect to void fraction in each axial nodes. For this reason, axial nodes with no net void generation (i.e. non boiling and subcooled boiling regions) are not considered. Eliminating these axial nodes, which improves the approximation, the least square method error must not be higher than 7.5% [60]. Doppler and density reactivity coefficients obtained from PAPU can be directly used as LAPURW input.

- Density reactivity coefficient multiplier.

This coefficient, called REAMUL, will be used to correct density reactivity coefficients.

5.3.1.4.2 Recirculation Gain and Time Constant

In decay ratio calculations of BWR stability analyses, the effects of core inlet flow dynamics become more important as the pumping head is reduced either controlling the flow or operating at low speed recirculation pumps. Natural circulation is also a situation when the external recirculation loop may strongly contribute adding an additional delay that, coupled with the core, could become unstable the system.

The effect of the excore loop in the frequency domain may be taken into account by means of a first order lag transfer function.

The integration of the linear momentum equation for the recirculation loop allows us to obtain a lumped equation for the gain and the lag for the recirculation loop transfer function [74].

Taking specific core flow and recirculation loop characteristic and losses for Cofrentes NPP [71] a set of best estimated values for recirculation can be obtained (see table 5.2).

Table 5.2. Recirculation transfer function data for BWR-6

Wcore	gainpy	taupy
100	0.08	0.16
92	0.09	0.17
86.2	0.10	0.18
82	0.11	0.18
79.1	0.12	0.19
73.5	0.14	0.21
64.1	0.19	0.24
49.5	0.32	0.31
40.2	0.70	0.54
35	0.80	0.55
31	1.66	0.96
30	1.66	0.96

Natural circulation gain and time constant values have been calculated for a reference core flow rate of 30%. These values will be fixed for core flows less than this value and up to 31% of core flow.

Interpolated values will be used for core flow conditions with not specific values.

5.3.1.4.3 Adjustable Parameters and User Options

- Number of frequency points at which the dynamic response is to be calculated.

In general, the following table of 100 frequency points will be adequate:

Table 5.3. Sample input of frequency point for LAPURW

0.010	0.100	0.120	0.140	0.160	0.180	0.200
0.210	0.220	0.230	0.240	0.250	0.260	0.270
0.280	0.290	0.300	0.310	0.320	0.330	0.340
0.350	0.360	0.370	0.380	0.390	0.400	0.410
0.420	0.430	0.440	0.450	0.460	0.470	0.480
0.490	0.500	0.510	0.520	0.530	0.540	0.550
0.560	0.570	0.580	0.590	0.600	0.610	0.620
0.630	0.640	0.650	0.660	0.670	0.680	0.690
0.700	0.710	0.720	0.730	0.740	0.750	0.760
0.770	0.780	0.790	0.800	0.810	0.820	0.830
0.840	0.850	0.860	0.870	0.880	0.890	0.900
1.000	1.100	1.200	1.300	1.400	1.500	1.600
1.700	1.800	1.900	2.000	3.000	4.000	5.000
6.000	7.000	8.000	9.000	10.000	20.000	50.000
		100.000	200.000			

Calculation options. Core wide and channel decay ratio calculation is the selected option.

- Array of values of the reactivity of the first subcritical neutronic mode. If these values are introduced, LAPUR will estimate the stability of the first subcritical neutronic mode with a parallel channel thermal-hydraulic feedback.
- Number of iterations in the full LAPLACE domain.

5.3.1.5 Perform the Core Stability Evaluation

5.3.1.5.1 Verification of Pressure Drop

SIMULATE steady-state thermal-hydraulic data have been validated against plant and vendor's data [72]. For this reason, SIMULATE core pressure drop and flow distribution is taken as reference.

LAPURX and SIMULATE pressure drop must be very similar because both codes have basically the same thermal-hydraulic models. In the next chapter, an exhaustive validation of each component of pressure drop for single channel models indicates a very good agreement between codes.

An error less than the 2% is expected. It is not required any adjust for obtaining pressure drop in LAPURX consistent with SIMULATE-3. If higher differences than 2% to the non-conservative side in LAPURX were found (less pressure drop than SIMULATE-3) the deviation should be justified.

Additionally, averaged flow distribution in each region is calculated by LIP from planar averaged flow distribution map (2-FLO) from SIMULATE. An error less than a 10% between these data and LAPURX output data is accepted.

5.3.1.5.2 *Correct REAMUL to Make Equal LAPURW and SIMULATE Density Reactivity Coefficients*

LAPURW gives in the output a core-averaged density reactivity coefficient.

A similar coefficient can be calculated from core-averaged reactivity and density data obtained in the Moderator Temperature Coefficient and Pressure perturbation set from KINETIC output file (0-D data) by using the following equation:

$$\text{Density Reactivity Coefficient} \left(\frac{\Delta K}{K} (\%) \right) / \left(\frac{gr}{cm^3} \right) = \frac{(K_{ref} - K_{per}) \cdot 100}{K_{ref} \cdot K_{per} \cdot (\rho_{ref} - \rho_{per})} \quad (5.4)$$

where:

K_{ref} = K_{eff} of reference case

K_{per} = K_{per} of perturbed case

ρ_{ref} = core averaged density of reference case

ρ_{per} = core averaged density of perturbed case

Calculated SIMULATE coefficients in analyzed cases result to be higher than LAPURW output coefficient directly evaluated from PAPU reactivity

coefficient [71]. For this reason, and due to the least square method error generates an uncertain in these values (see above), correcting LAPURW output coefficient has been considered a conservative criterion.

There is a multiplier called REAMUL (LAPURW input card 28) that allows us to correct density reactivity coefficients. By means of REAMUL coefficient (see above), core averaged density reactivity coefficient from LAPURW output file will be corrected up to be equal to the average value obtained from all of the Moderator Temperature Coefficient and Pressure perturbation serie in SIMULATE. This average density coefficient is considered the best estimated value to make consistent with the density coefficient of LAPURW OUTPUT. An error less than 1% is accepted.

5.3.2 Output and Results

From the output of LAPURW, the following results are obtained:

Global core Decay Ratio: the calculated value is directly obtained from LAPURW output file along with the associated frequency.

Out of phase core Decay Ratio: LAPUR evaluates this DR as a function of the separation of the first subcritical mode, which is typically in the range of 0,8\$ to 1.2 \$. The highest value computed by LAPURW in this range, is selected as a bounding guess.

A more accurate determination of the out of phase core Decay Ratio will require a specific calculation of the eigenvalue separation of the subcritical modes.

Channel decay ratio: it is also obtained from LAPURW output file. A thermal-hydraulic channel decay ratio per region is calculated. However, some regions shows a so stable behaviour (i.e. decay ratios are close to zero) that abnormal decay ratios can be obtained [60]. A stability analysis on the Nyquist diagram in these cases is enough to verify the stability of such a channel. Decay ratio is evaluated as a function of the distance from the (-1,0) point to the closest value of the Nyquist diagram (more distance, more stable). If the Nyquist plot is placed on the right side of the real axis, the decay ratio has to be close to zero. Figure 5.2 shows an example of this situation.

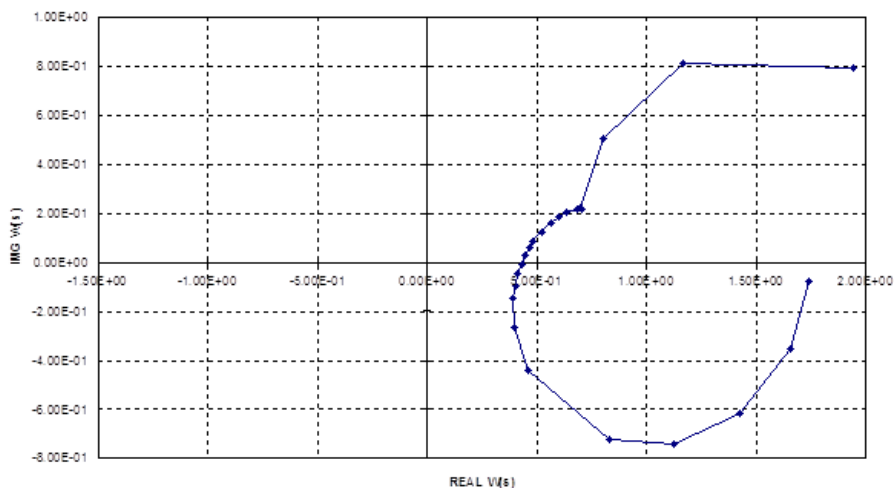


Figure 5.2. Nyquist diagram for a stable channel

5.4 PRELIMINARY VALIDATION OF LAPUR METHODOLOGY

This section presents a comparison between decay ratios obtained by vendor's code [62] and calculated decay ratios using this methodology. The state points analyzed correspond to the Initial Validation Matrix (IVM) from the analysis performed to validate the stability region boundaries for Cofrentes Cycle 10 [63] based on the E1A initial application methodology [49]. The IVM is a subset of the Demonstration Validation Matrix (DVM) created for the demonstration plant which excludes state points demonstrated to be less severe in terms of stability performance. DVM statepoints are based on E1A prescribed definitions of flow control lines (FCLs), the natural circulation line (NCL) core power and core flow [49].

Calculations were performed following step by step the general methodology described in this chapter. This preliminary validation allow us to get an insight of the results of the methodology for a set of power flow map state-points against analytical results for wide core decay ratio and specifically for hot channel decay ratio.

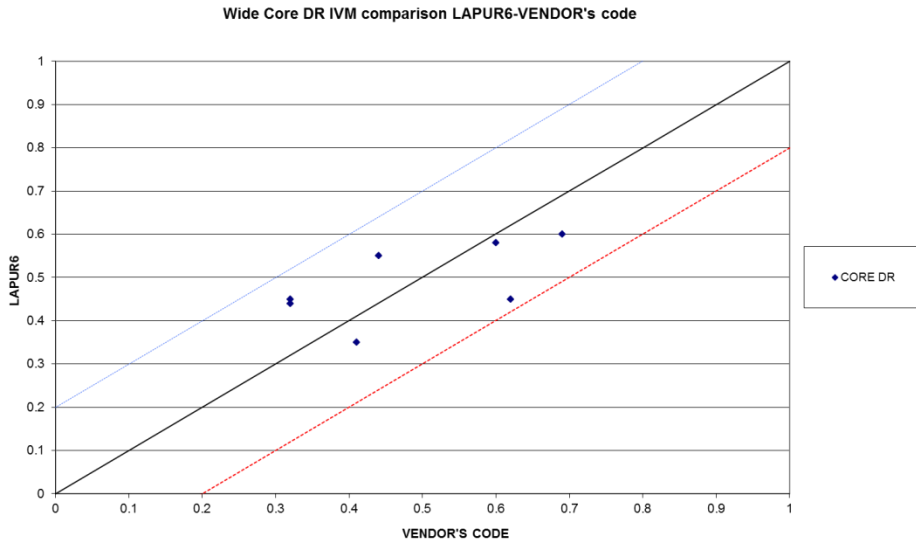


Figure 5.3 Wide core DR IVM comparison LAPUR 6 Vendor's code

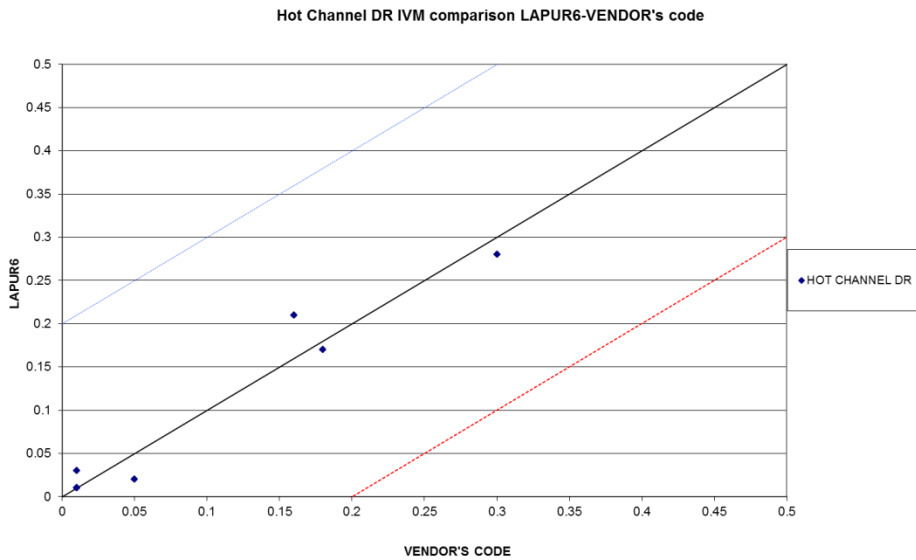


Figure 5.4 Hot channel DR IVM comparison LAPUR 6 Vendor's code

Results are very relevant for hot channel decay ratio because this decay ratio is not possible to validate against plant experimental data, a thermal-hydraulic loop is required and these data are not accessible to the author. This

validation is particularly useful to determine the accuracy of the thermal-hydraulic models and the consistency of hot channel decay ratio.

Details of the calculation can be found in [64].

Global decay ratio and channel decay ratio are directly obtained from LAPURW output file.

The core wide and the highest value of the individual thermal-hydraulic channel decay ratios (in general, the channel model with the one hottest channel) are presented in Figures 5.3 and 5.4 with vendor's decay ratios.

As can be seen, the comparison of DR is inside the generic uncertainty accepted for EIA of +/-0.2.

5.5 CHAPTER SUMMARY

A methodology for calculating Decay Ratios with LAPUR 6 [64] has been developed based on an automatic procedure, defining a validation matrix against analytical and plant-measured decay ratios.

The SIMULATE-3 computer code is a 3D core simulator which is used to calculate the core detailed hydraulic and neutronic configuration of the different state points to analyze. A preliminary validation against analytical vendor's data has been also performed. This validation is particularly useful to determine the accuracy of the thermal-hydraulic models and the consistency of hot channel decay ratio.

A good agreement of hot channels means a good selection and adjustment of thermal-hydraulic models.

6 LAPUR 6.0 VALIDATION

This chapter shows the validation of the new thermal-hydraulic model implemented in LAPUR 6 r.0 [66]. The LAPUR 6 upgrade incorporated new correlations for computing friction and local losses and capabilities for modelling bundles with variable cross areas. Additional information regarding this implementation is available in [68]. Implementation of these correlations is provided in this document. The friction and local models selected are generic and do not use any proprietary information of fuel vendors.

A comparison of pressure drop components was performed for bundles with constant (TYPE A) and variable (TYPE B) areas. LAPUR 6 results were compared to results of the well-known SIMULATE-3 code [59], a reactor analysis code being used by IBERDROLA and other utilities to perform in-core fuel management studies, core design, and calculation of safety parameters. Single-channel models for each bundle design were used. Flow and power conditions for the bundles were selected to be representatives of hot channels covering real conditions on a BWR/6 power flow map. A generic

single-phase friction factor was selected in order to validate exclusively the implementation of changes made to LAPUR 6.

Comparisons of LAPUR-calculated void fractions to FRIGG loop data for both LAPUR 5 and LAPUR 6 were performed. Indirectly, this exercise showed that the LAPUR 6 modifications did not affect relevant variables in LAPUR calculation process. The results of these comparisons showed that flow qualities and slip ratio are not affected by the changes in pressure drop calculation models in LAPUR 6.

An extensive validation comparing measured against calculated core wide decay ratios was also conducted. A set of average power range monitor (APRM) signals was recorded in steady state for the final coastdowns for Cycles 16b and 17 and start-up for Cycles 17 and 18 in Cofrentes NPP. A detailed simulation of the power, flow, and control rod sequences was carried out with SIMULATE-3 using cycle-specific CASMO-4 cross sections and the recorded operating data. Selected quasi-steady-state points were analyzed using noise techniques, and decay ratio values were compared with LAPUR 6 results. Finally, Cycle 6 Cofrentes OOP instability was reproduced using LAPUR 6, and the resulting LAPUR 6.0 decay ratios showed excellent agreement with the measured data.

6.1 GENERIC VALIDATION: COMPARISON OF PRESSURE DROP COMPONENTS FOR TYPE A AND TYPE B FUEL DESIGNS

LAPUR5 release 1 code does not consider channels with variable areas and does not distinguish specifically local pressure drop due to spacers in a bundle. The only way to take into account local pressure losses and gains due to spacers and area changes is by means of a friction multiplier, which is input. This deficiency requires adjustment by input friction multipliers in order to accurately account for local and variable-area pressure effects.

In this section, validation of computing friction, local losses, and variable cross area results obtained using LAPUR 6 is shown. The selection of basic models for implementation in LAPUR 6 is discussed in [75], RETRAN-3D-A Program for Transient and Thermal-Hydraulic Analysis for Complex Fluid

Systems [76], and by Chisholm [77]. This validation was conducted by benchmarking LAPUR 6 results against SIMULATE-3 single-channel results. For this comparison, the default single friction factor of SIMULATE-3 was used in both codes.

6.2 CHAPTER OUTLINE

This chapter documents the validation of the new thermal-hydraulic model implemented in LAPUR 6 r.0 [73]. The LAPUR 6 upgrade incorporated new correlations for computing friction and local losses and capabilities for modelling bundles with variable cross areas. Additional information regarding this implementation is available in *Improvements Made in LAPUR 5 to Obtain LAPUR 6.0.r.0* [68]. Validation of these correlations is provided in this document. The friction and local models selected are generic and do not use any proprietary information of fuel vendors.

A comparison of pressure drop components was performed for bundles with constant (TYPE A) and variable (TYPE B) areas. LAPUR 6 results were compared to results of the well-known SIMULATE-3 code [59], a reactor analysis code being used by IBERDROLA and other utilities to perform in-core fuel management studies, core design, and calculation of safety parameters. Single-channel models for each bundle design were used. Flow and power conditions for the bundles were selected to be representatives of hot channels covering real conditions on a BWR/6 power flow map. A generic single-phase friction factor was selected in order to validate exclusively the implementation of changes made to LAPUR 6.

Comparisons of LAPUR-calculated void fractions to FRIGG loop data for both LAPUR5 and LAPUR 6 were performed. Indirectly, this exercise showed that the LAPUR 6 modifications did not affect relevant variables in LAPUR calculation process. The results of these comparisons showed that flow qualities and slip ratio are not affected by the changes in pressure drop calculation models in LAPUR 6.

An extensive validation comparing measured against calculated core wide decay ratios was also conducted. A set of average power range monitor (APRM) signals was recorded in steady state for the final coastdowns for Cycles 16b and 17 and start-up for Cycles 17 and 18 in Cofrentes NPP. A

detailed simulation of the power, flow, and control rod sequences was carried out with SIMULATE-3 using cycle-specific CASMO-4 cross sections and the recorded operating data. Selected quasi-steady-state points were analyzed using noise techniques, and decay ratio values were compared with LAPUR 6 results. Finally, Cycle 6 Cofrentes out of phase instability was reproduced using LAPUR 6, and the resulting LAPUR 6.0 decay ratios showed excellent agreement with the measured data.

6.3 PRESSURE DROP BASIS

The total pressure drop for each channel is calculated as the sum of the individual pressure drop components: friction, local (form) loss, acceleration (momentum change), and elevation. Acceleration and elevation can be evaluated once the flow quality and void fraction have been determined. The friction and local loss terms require input coefficients and models to account for two-phase effects.

6.3.1 Friction Pressure Drop

The frictional pressure losses are correlated in terms of single-phase velocity head,

$$\Delta p_{fric} = f \frac{\Delta z}{D_h} \frac{G^2}{2 \cdot \rho_l} \phi_{2-phase\ friction}^2 \quad (6.1)$$

where

f = single-phase friction factor,

G = mass flux,

ρ_l = liquid density, and

$\phi_{2-phase\ friction}^2$ = the multiplier to account for the two-phase effect. The relationship selected is the Chisholm model, [75], [77], which depends on flow quality, mass flux, and viscosity.

6.3.2 Local Losses

The local pressure drop is defined as the irreversible pressure loss associated with an area change, such as an orifice, tie plate, or grid spacer. The general local pressure drop equation is similar to that for friction pressure drop.

6.3.3 Spacer or Grid Losses

Considering K to be the single-phase irreversible loss for the grid or spacer, the pressure drop equation is

$$\sum_{l=1}^L \Phi_{local\ two-phase} K \frac{G^2}{2 \cdot \rho_l} \quad (6.2)$$

and

$$\Phi_{local\ two-phase} = \left[1 + \left(\frac{\rho_l}{\rho_g} - 1 \right) \cdot X_f \right] (\text{HEM multiplier}) \quad (6.3)$$

where:

X_f = flow quality,

ρ_l = liquid densities, and

ρ_g = vapor densities.

6.3.4 Irreversible Losses for Expansion and Contraction

Irreversible losses for expansion have been calculated by means of the following equations:

$$DPEXP = \sum_{i=1}^L \left[1 + \left(\frac{\rho_l}{\rho_g} - 1 \right) \cdot X_f \right] k_{exp} \cdot \frac{G1^2}{2 \cdot \rho_l} \quad (6.4)$$

where

$G1$ = upstream mass flux, and

K_{exp} = single phase irreversible expansion loss.

Analogously,

$$DPCON = \sum_{i=1}^L \left[1 + \left(\frac{\rho_l}{\rho_g} - 1 \right) \cdot X_f \right] k_{con} \cdot \frac{G1^2}{2 \cdot \rho_l} \quad (6.5)$$

where

K_{con} = single phase irreversible contraction loss

6.4 ACCELERATION PRESSURE LOSSES

The acceleration pressure drop includes the reversible pressure change experienced from contractions or expansions, or resulting from the acceleration of the fluid during the boiling process (density change). When two phases are present,

$$\Delta P_{acc} = \frac{2}{A_1 + A_2} \left[\frac{1}{\rho M_2} G_2^2 - \frac{1}{\rho M_1} G_1^2 \right] \quad (6.6)$$

where

$$\frac{1}{\rho M} = \frac{\langle x \rangle^2}{\rho_g \langle \alpha \rangle} + \frac{(1 - \langle x \rangle)^2}{\rho_l (1 - \langle \alpha \rangle)} \quad (6.7)$$

where

$\langle \alpha \rangle$ = cross section averaged void fraction,

$\langle x \rangle$ = cross section averaged flow quality,

$G_{1,2}$ = mass flux upstream and downstream, respectively, and

$A_{1,2}$ = area upstream and downstream, respectively.

6.5 ELEVATION PRESSURE DROP

The elevation (gravitational) pressure drop is evaluated as follows:

$$\Delta P_{elev} = \bar{\rho} \Delta z \quad (6.8)$$

where

$$\bar{\rho} = \rho_l \cdot (1 - \langle \alpha \rangle) + \rho_g \cdot \langle \alpha \rangle \quad (6.9)$$

Note the dependence of acceleration and elevation pressure drop on void fraction.

6.6 GENERIC VALIDATION: COMPARISON OF PRESSURE DROP COMPONENTS FOR TYPE A AND TYPE B

LAPUR5 release 1 code does not consider channels with variable areas and does not distinguish specifically local pressure drop due to spacers in a bundle. The only way to take into account local pressure losses and gains due to spacers and area changes is by means of a friction multiplier, which is input. This deficiency requires adjustment by input friction multipliers in order to accurately account for local and variable-area pressure effects.

In this section, validation of computing friction, local losses, and variable cross area results obtained using LAPUR 6 is shown. The selection of basic models for implementation in LAPUR 6 is discussed in [75], [76], and by Chisholm [77]. This validation was conducted by benchmarking LAPUR 6 results against SIMULATE-3 single-channel results. For this comparison, the default single friction factor of SIMULATE-3 was used in both codes.

The applicability of SIMULATE-3 thermal-hydraulic models has been verified against vendor's analytical and experimental data, using exactly the same models used in LAPUR 6.

Table 6.1. Typical pressure drop uncertainties

Experimental data average relative error. Total pressure drop	0.33%
Experimental data average relative error. Bundle upper half	0.15%
Experimental data average relative error. Bundle lower half	0.34%
Sample Standard deviation. Total pressure drop..	4.28%
Sample Standard deviation. Bundle lower half.	5.63%
Sample Standard deviation. Bundle upper half.	3.9%

Results obtained are typical of thermalhydraulic codes used for steady state calculations.

6.7 INITIAL CONDITIONS

Comparison of pressure drop components will be performed for bundles with constant (TYPE A) and variable area (TYPE B). Tables 6.2 and 6.3 show the conditions used.

Table 6.2. TYPE A boundary conditions.

State point	Pressure (psi)	Inlet enthalpy (Btu/lb)	Active power (MW)	Active flow (lb/h)
1	1058.10	522.21	6.624	84366
2	1064.50	529.06	6.629	116351
3	973.50	507.62	1.908	38413
4	1005.78	500.71	4.319	42699
5	978.16	524.76	1.909	78731

Table 6.3. TYPE B boundary conditions

State point	Pressure (psi)	Inlet enthalpy (Btu/lb)	Active power (MW)	Active flow (lb/h)
1	1090.75	525.63	6.643	87039
2	998.40	513.27	3.189	58830
3	1031.36	508.85	4.779	56270
4	1038.24	523.46	4.784	89859
5	1097.94	531.51	6.647	110299

The power axial profiles used in verification analyses are shown in figures 6.1 and 6.2.

Note that the axial power profile used when performing TYPE A pressure drop comparisons is bottom peaked. However, the profile used in TYPE B is similar to a skewed cosine, with the peak at medium core height. This profile leads to elevating the boundary between bulk and subcooled boiling. The TYPE A and TYPE B corresponds with different vendor's criteria and the use of different power profiles does not affect to the comparison results.

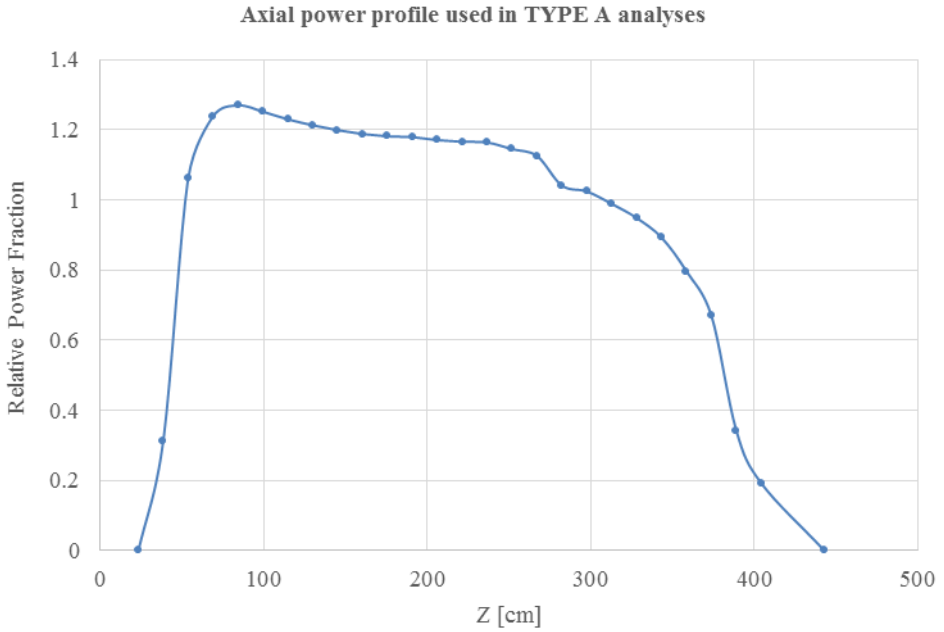


Figure 6.1. Axial power profile used in TYPE A analyses.

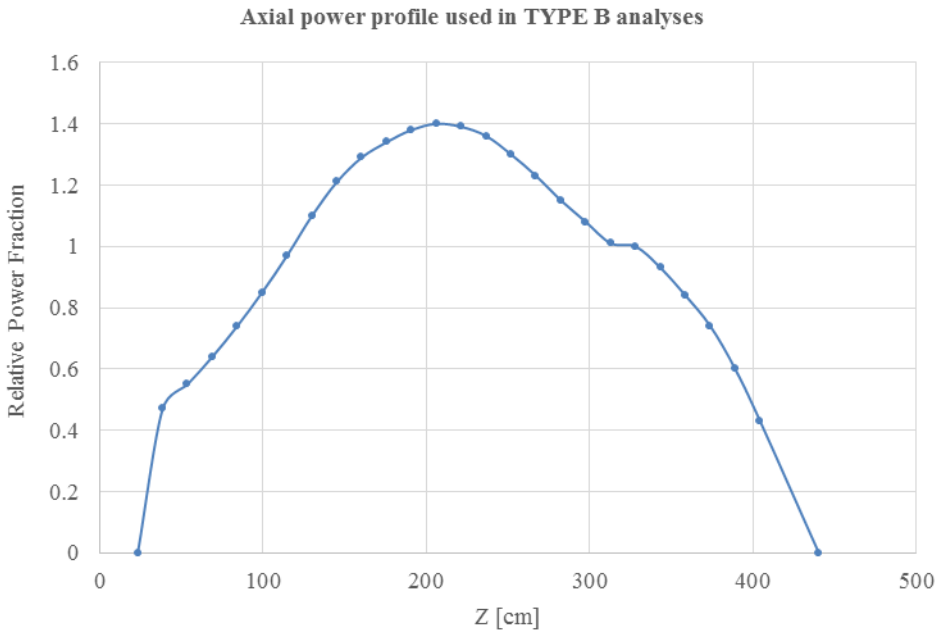


Figure 6.2. Axial power profile used in TYPE B analyses.

6.8 ELEVATION PRESSURE DROP

In this section, a comparison of elevation pressure drop in LAPURX (LX) and SIMULATE-3 (S3) is provided.

6.8.1 Elevation Pressure Drop for TYPE A

Comparisons of elevation pressure drop for TYPE A are shown in figures 6.3 to 6.7.

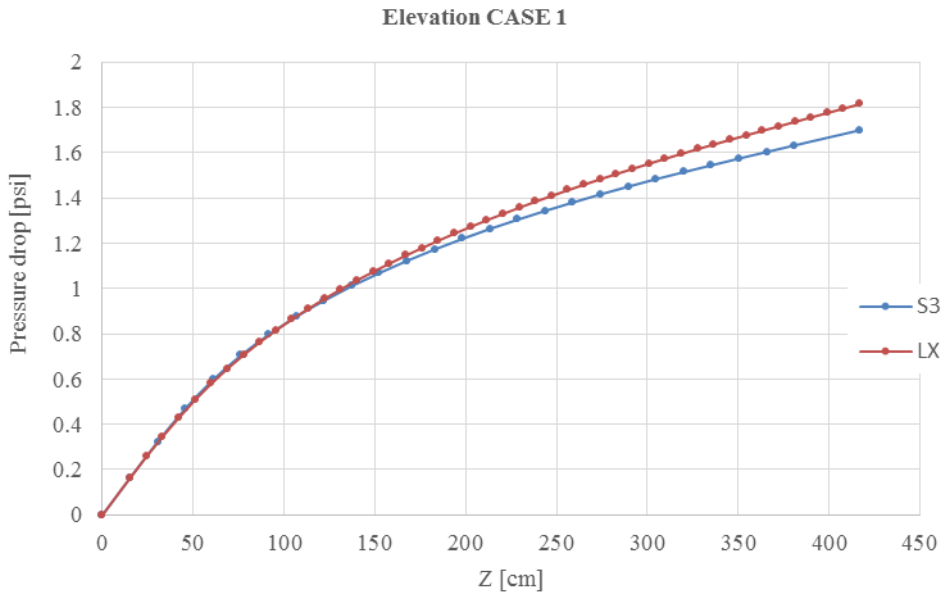


Figure 6.3. Elevation CASE 1 TYPE A.

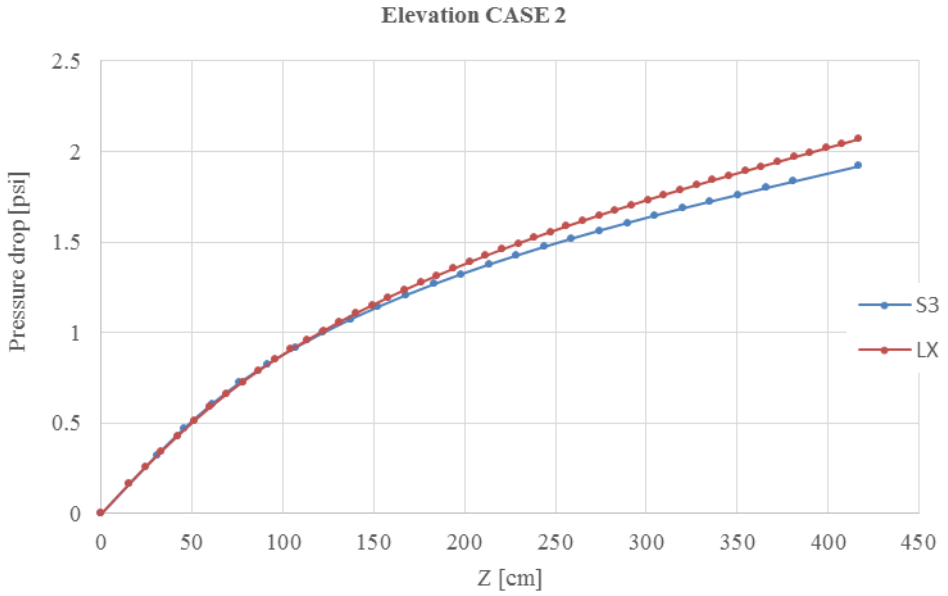


Figure 6.4. Elevation CASE 2 TYPE A.

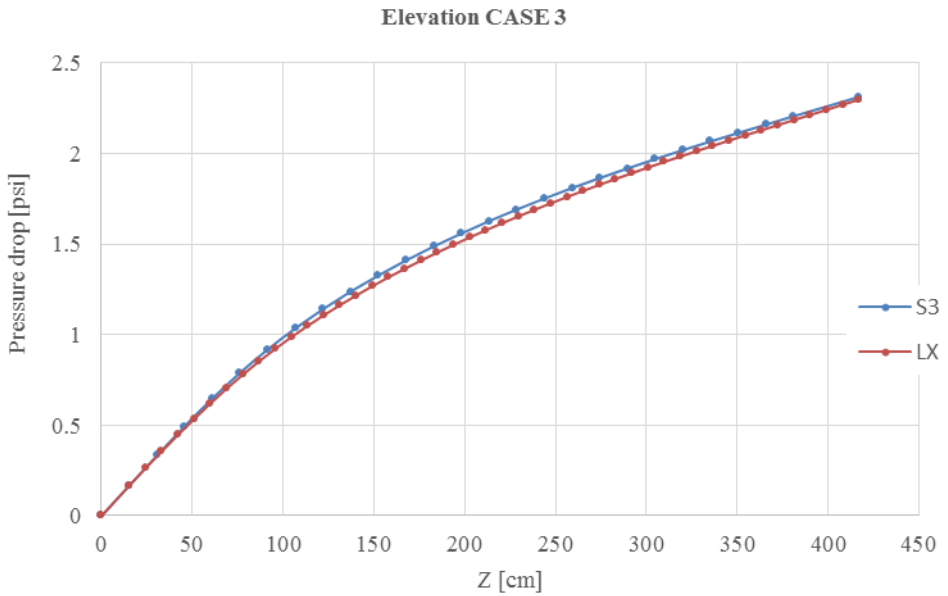


Figure 6.5. Elevation CASE 3 TYPE A.

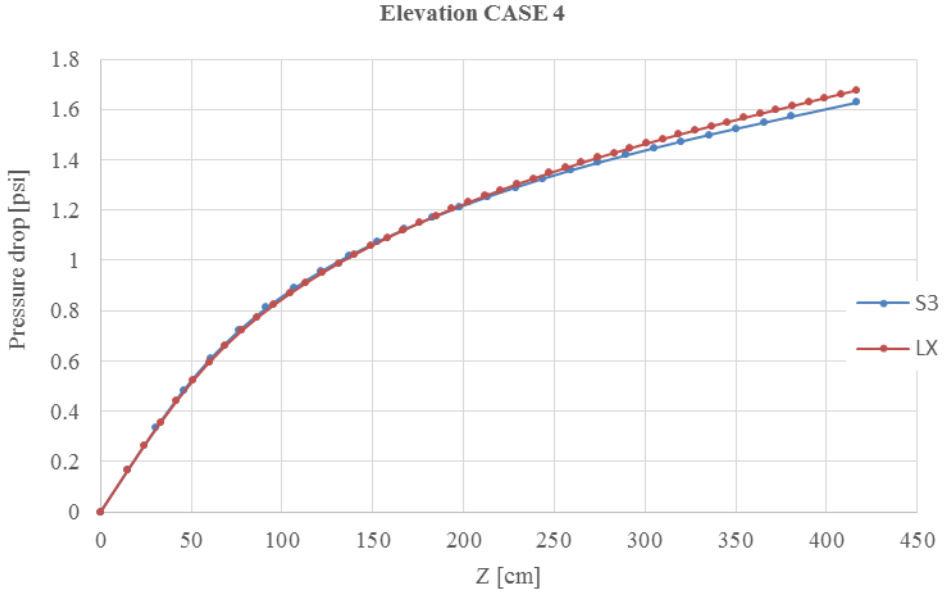


Figure 6.6. Elevation CASE 4 TYPE A.

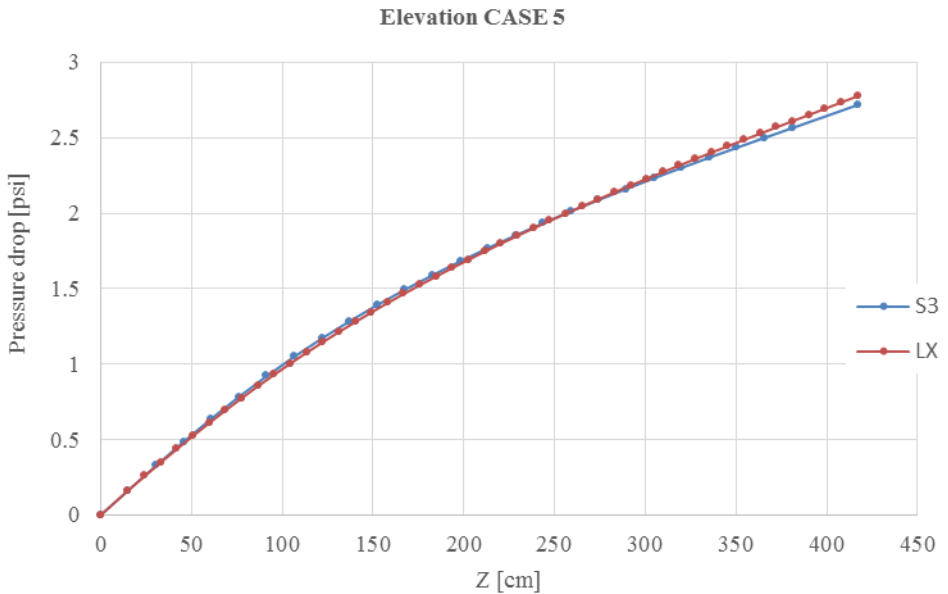


Figure 6.7. Elevation CASE 5 TYPE A.

6.8.2 Elevation Pressure Drop for TYPE B

Comparisons of elevation pressure drop for TYPE B are shown in figures 6.8 to 6.12.

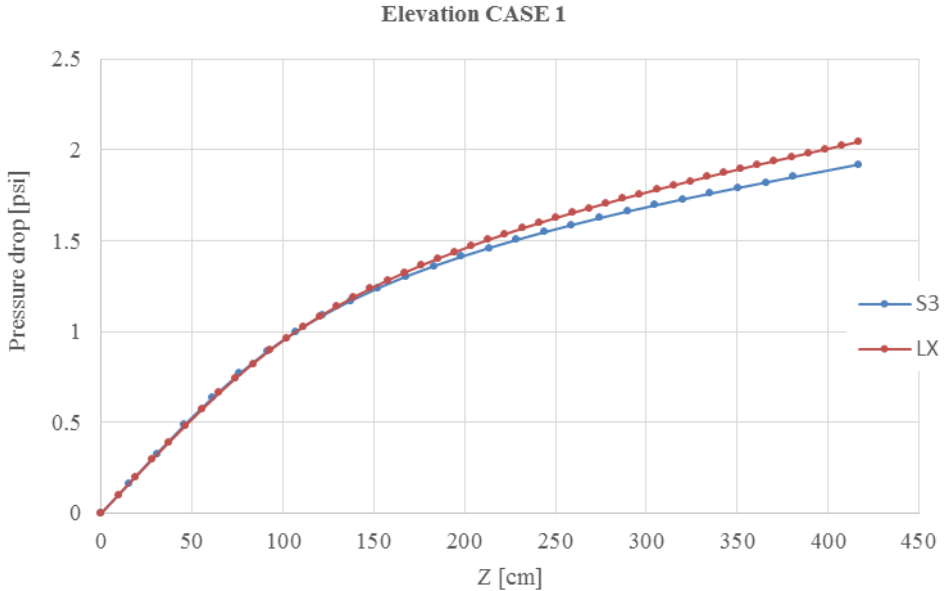


Figure 6.8. Elevation CASE 1 TYPE B.

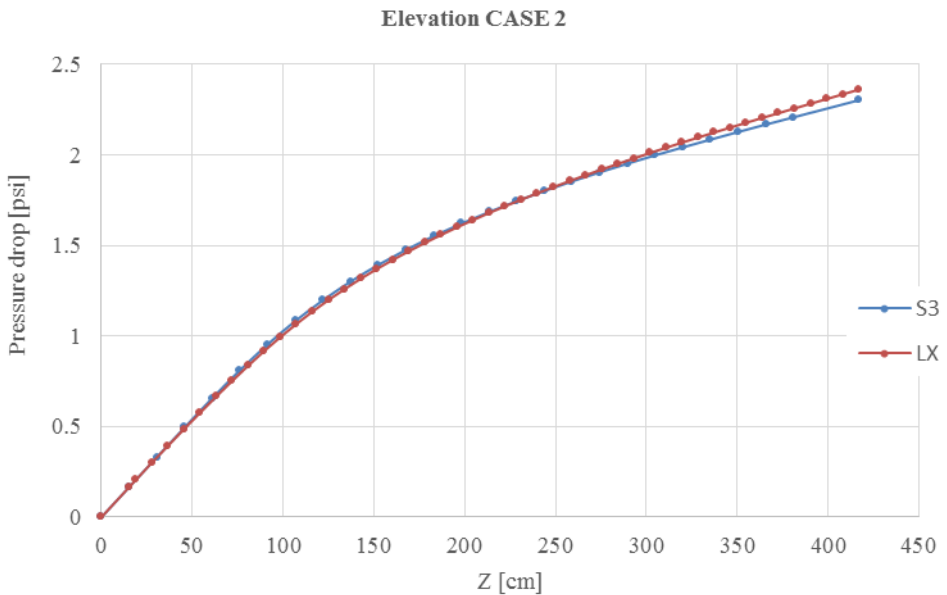


Figure 6.9. Elevation CASE 2 TYPE B.

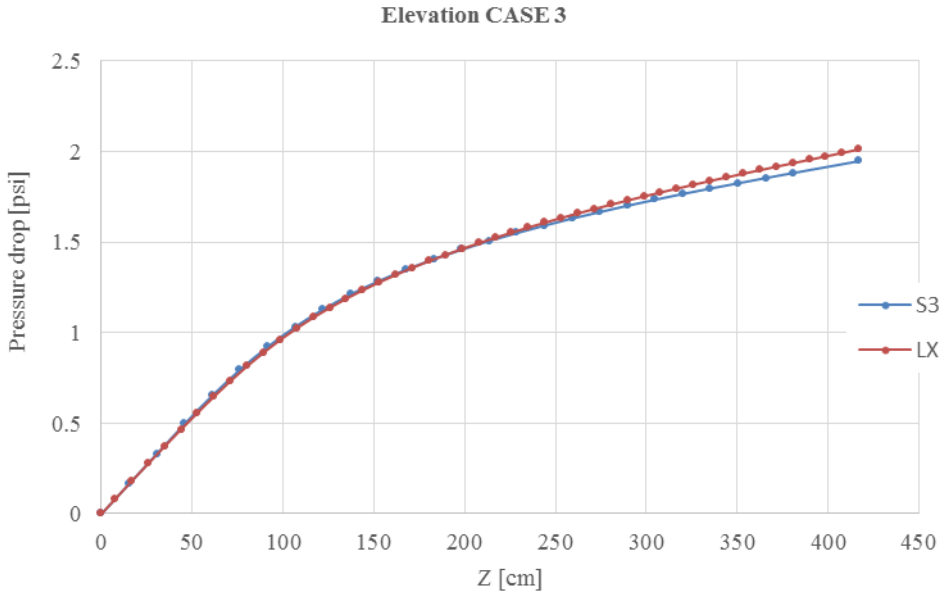


Figure 6.10. Elevation CASE 3 TYPE B.

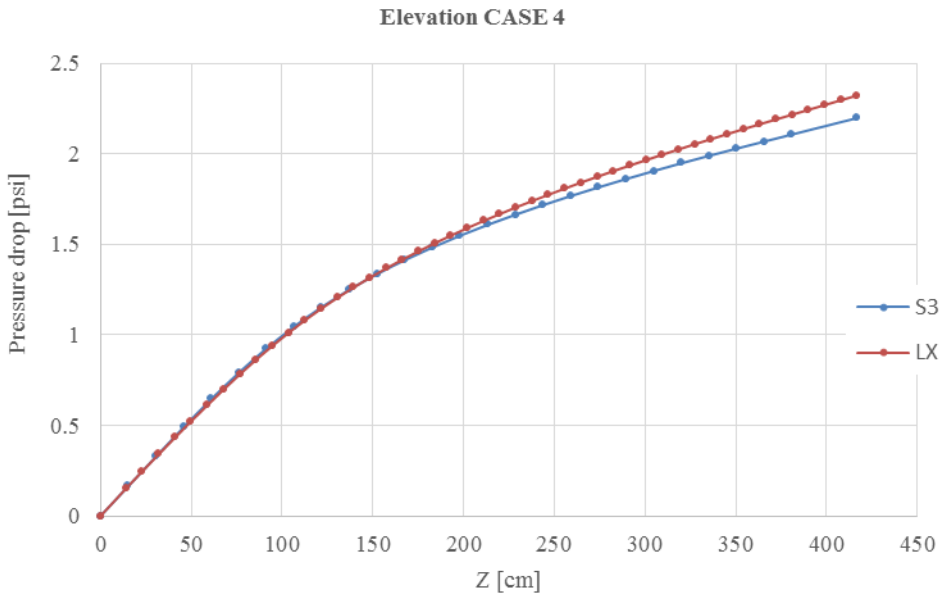


Figure 6.11. Elevation CASE 4 TYPE B.

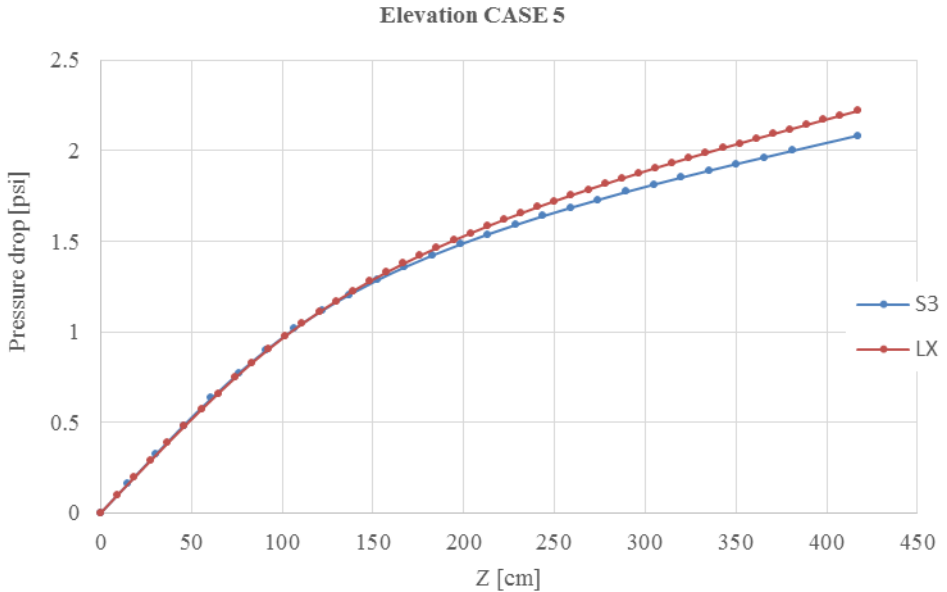


Figure 6.12. Elevation CASE 5 TYPE B.

6.8.3 Conclusions of Elevation Results

LAPURX results are in good agreement with SIMULATE-3 results. However, LAPURX systematically gives an elevation pressure drop that is slightly higher than that of SIMULATE-3. This difference is the result of void fraction axial distribution discrepancies between both codes, since slip velocity correlation, subcooled flow quality model, and therefore void fraction-quality relationships are different.

The impact of total pressure drop is evident from the magnitude of its contribution. Differences are negligible.

6.9 EXPANSION AND ACCELERATION DATA

In this section, a comparison of expansion and acceleration pressure drop in LAPUR and SIMULATE-3 is provided.

6.9.1 Expansion and Acceleration Data for TYPE A

Comparisons of expansion and acceleration pressure drop for TYPE A are shown in figures 6.13 to 6.17.

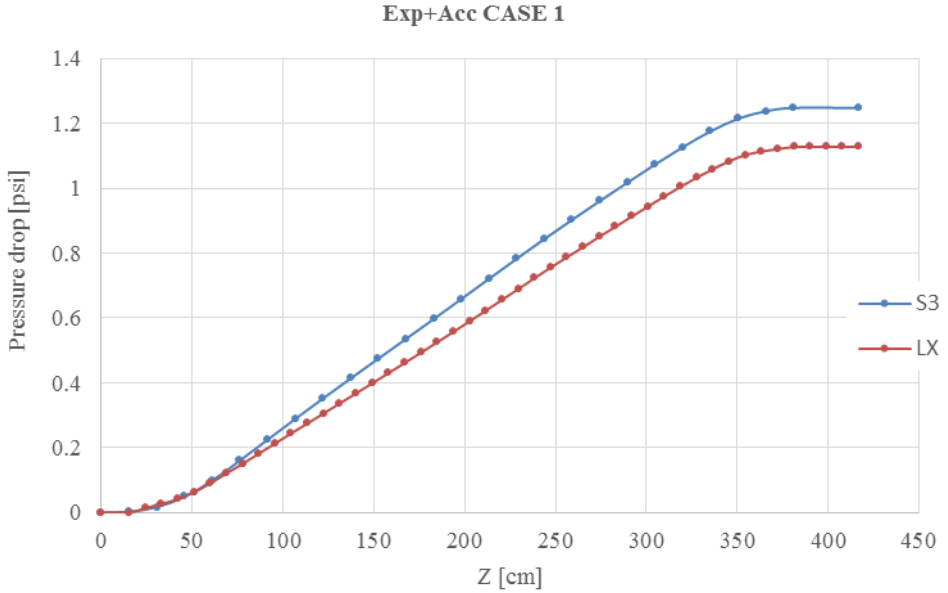


Figure 6.13. Expansion and acceleration pressure drop for CASE 1 TYPE A.

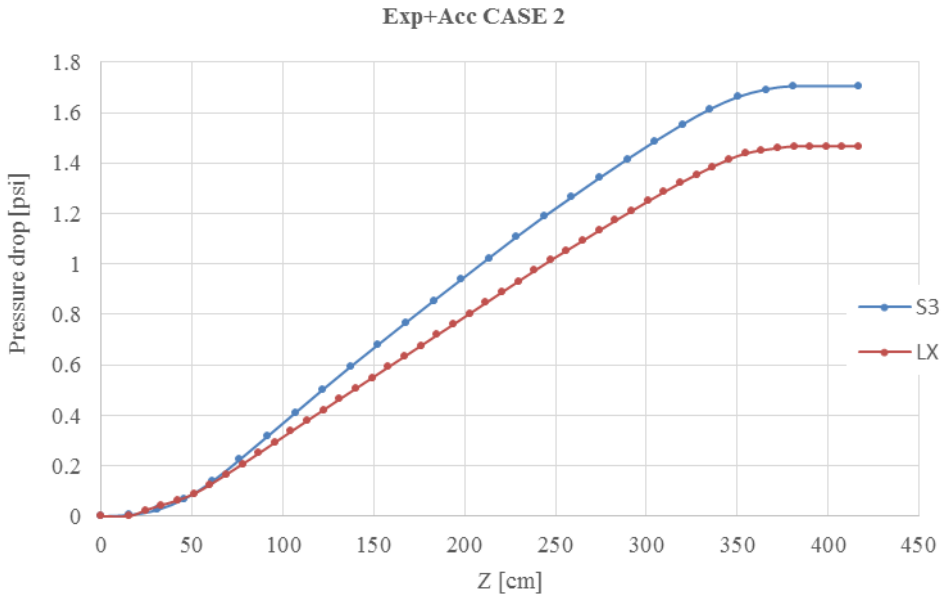


Figure 6.14. Expansion and acceleration pressure drop for CASE 2 TYPE A.

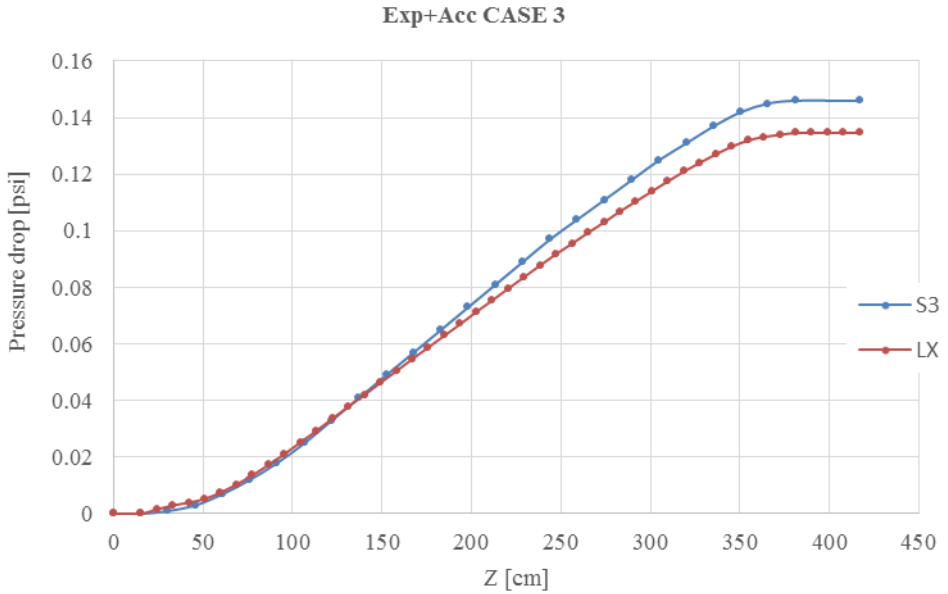


Figure 6.15. Expansion and acceleration pressure drop for CASE 3 TYPE A.

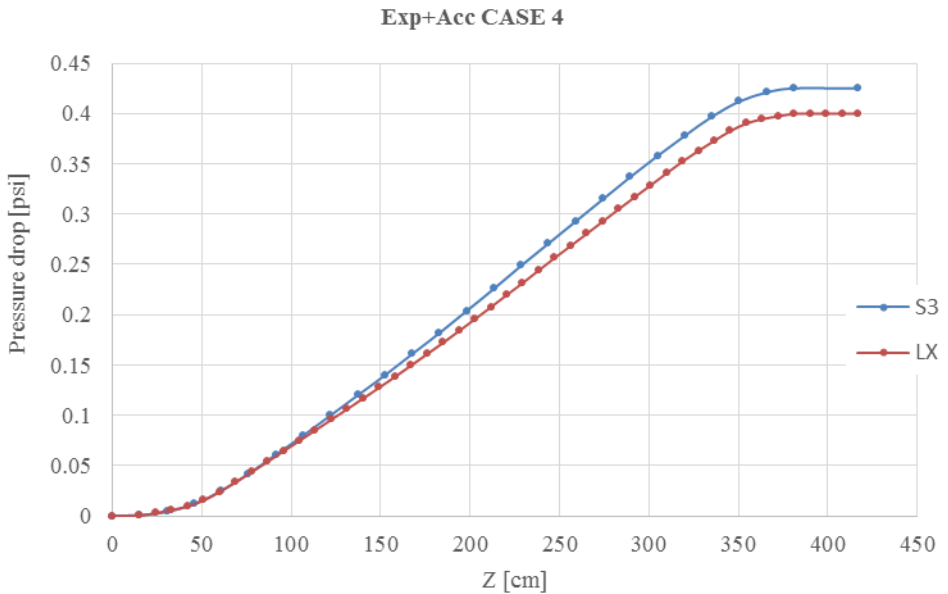


Figure 6.16. Expansion and acceleration pressure drop for CASE 4 TYPE A.

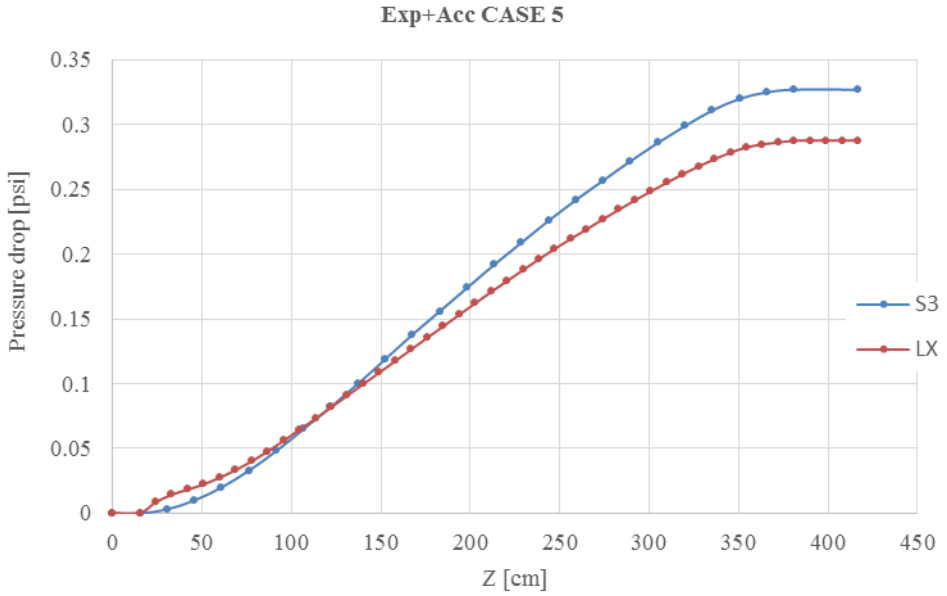


Figure 6.17. Expansion and acceleration pressure drop for CASE 5 TYPE A.

6.9.2 Expansion and Acceleration Data for TYPE B

Comparisons of expansion and acceleration pressure drop for TYPE B are shown in figures 6.18 to 6.22.

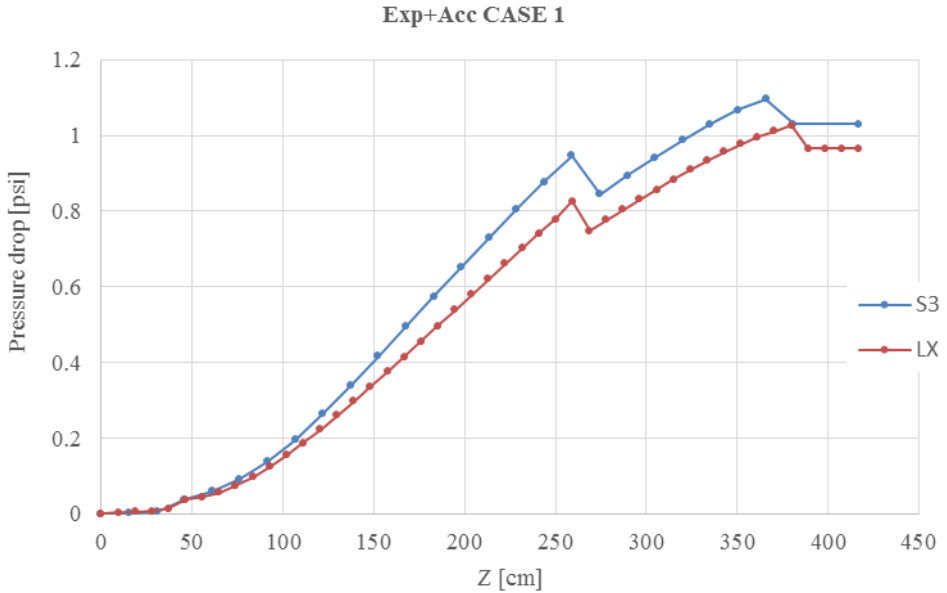


Figure 6.18. Expansion and acceleration pressure drop for CASE 1 TYPE B.

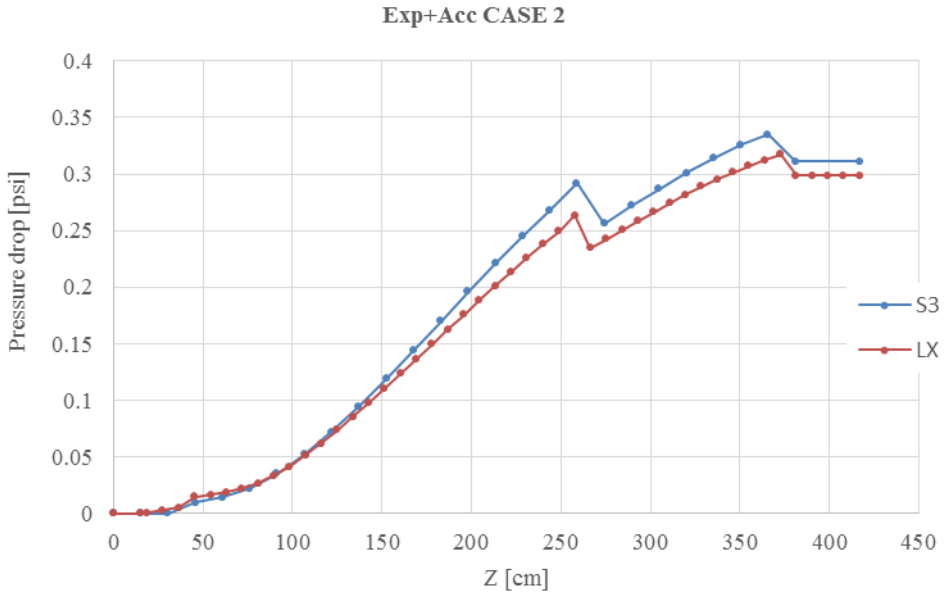


Figure 6.19. Expansion and acceleration pressure drop for CASE 2 TYPE B.

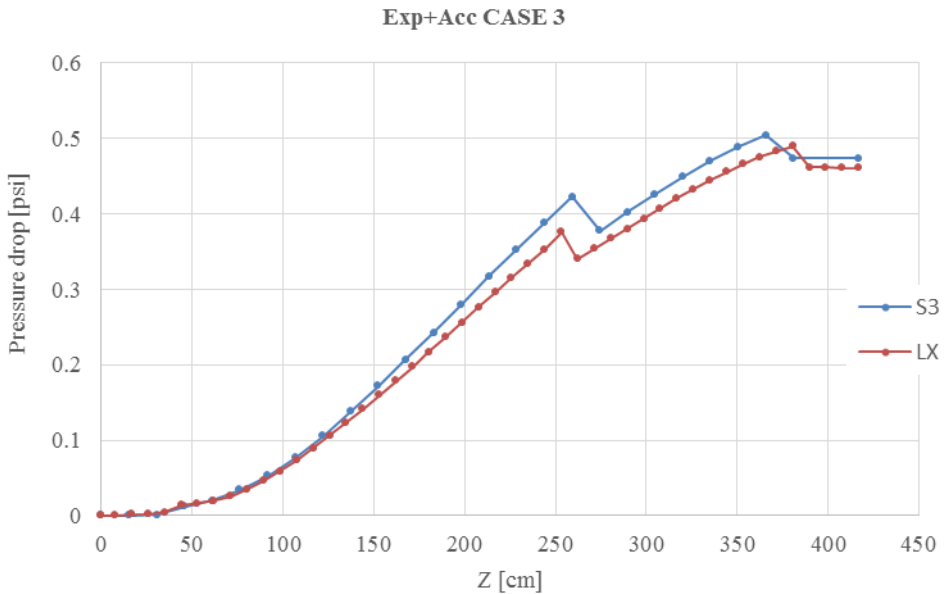


Figure 6.20. Expansion and acceleration pressure drop for CASE 3 TYPE B.

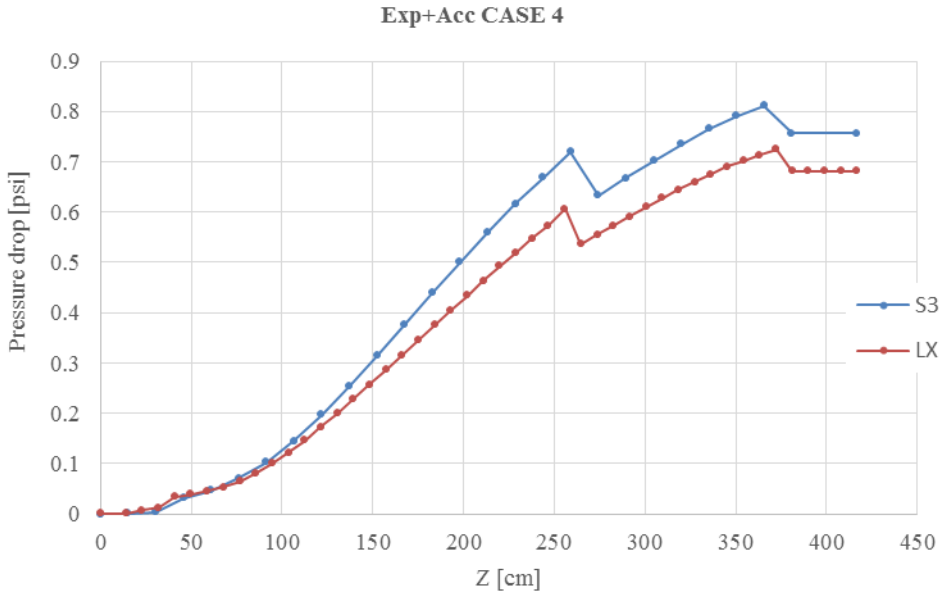


Figure 6.21. Expansion and acceleration pressure drop for CASE 4 TYPE B.

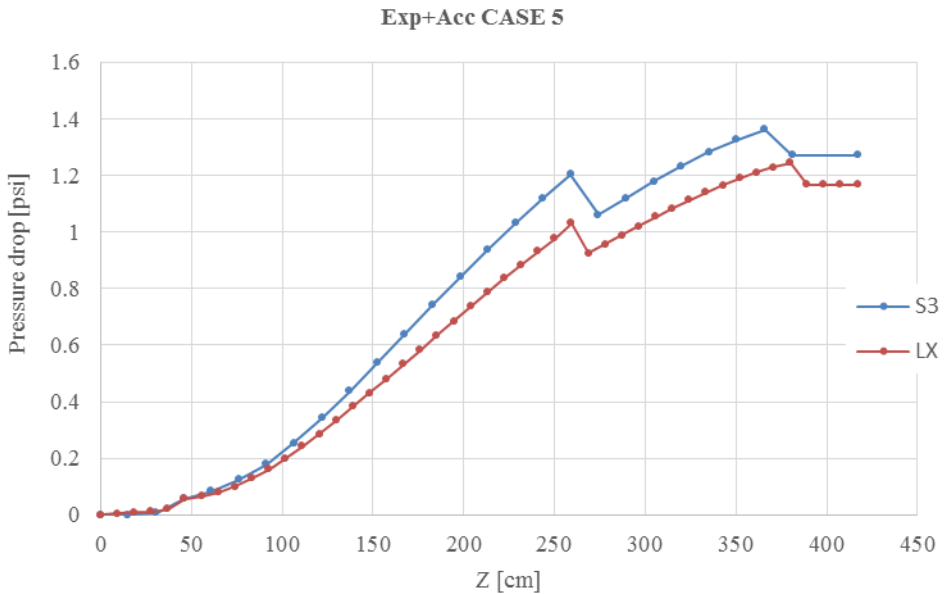


Figure 6.22. Expansion and acceleration pressure drop for CASE 5 TYPE B.

6.9.3 Conclusions of Expansion and Acceleration Results

Again, the observed differences are related to the void fractions values obtained with the models of SIMULATE-3 and LAPUR. As can be seen in the figures, changes in flow area along the channel in TYPE B fuel design lead to abrupt pressure gains. The expansions are located in channel elevations with considerable void fractions (partial length rods and changes due to water rod diameter). For this reason, the comparison reveals higher values for SIMULATE-3 for this pressure drop component. A contraction occurs due to a change in water rod diameter close to lower tie plate. However, due to the low void fractions at this part of the channel, the effect in pressure is negligible and the agreement between codes is good. On the other hand, TYPE A is a fuel design with a constant flow area and no contraction and expansion exist along the channel length. Pressure drop due to acceleration shows the same discrepancies as in TYPE B due to void fraction differences in both codes.

The impact in the total pressure drop is evident from the magnitude of its contribution. Differences are negligible.

6.10 FRICTION PRESSURE DROP

In this section, a comparison of one of the dominant contributors to the pressure drop between LAPUR and SIMULATE-3 is provided.

6.10.1 Friction Data for TYPE A

Comparisons of the friction component of pressure drop for TYPE A are shown in figures 6.23 to 6.27.

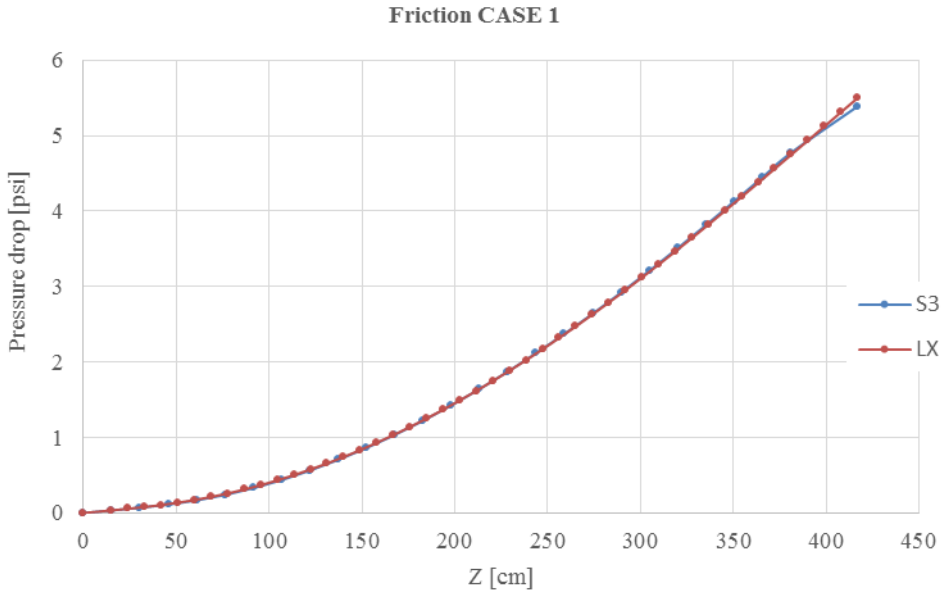


Figure 6.23. Friction CASE 1 TYPE A.

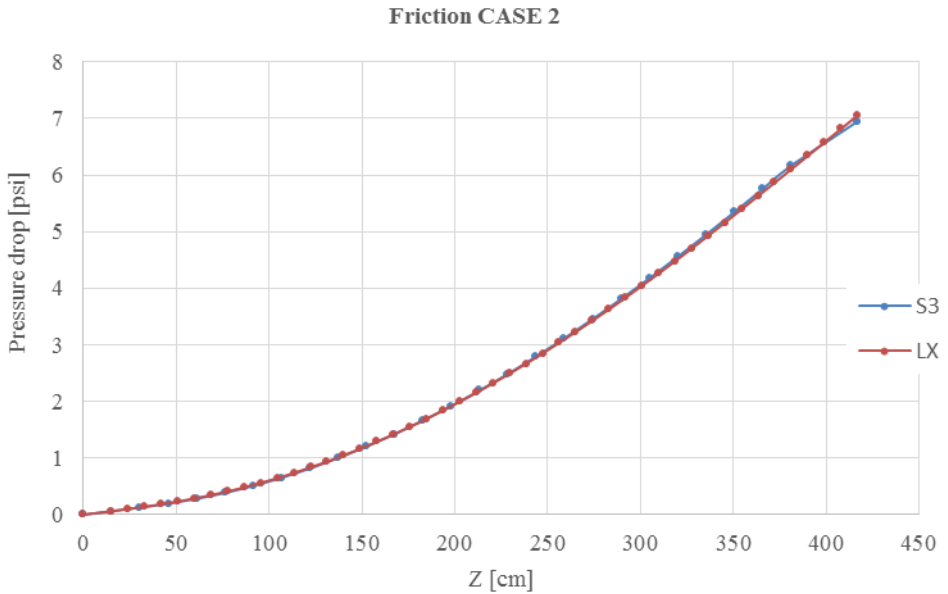


Figure 6.24. Friction CASE 2 TYPE A.

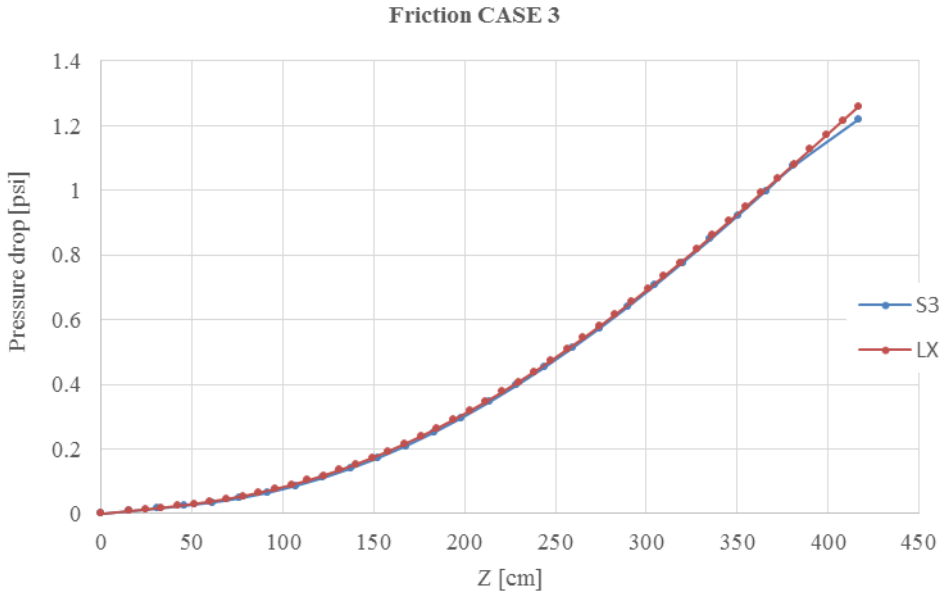


Figure 6.25. Friction CASE 3 TYPE A.

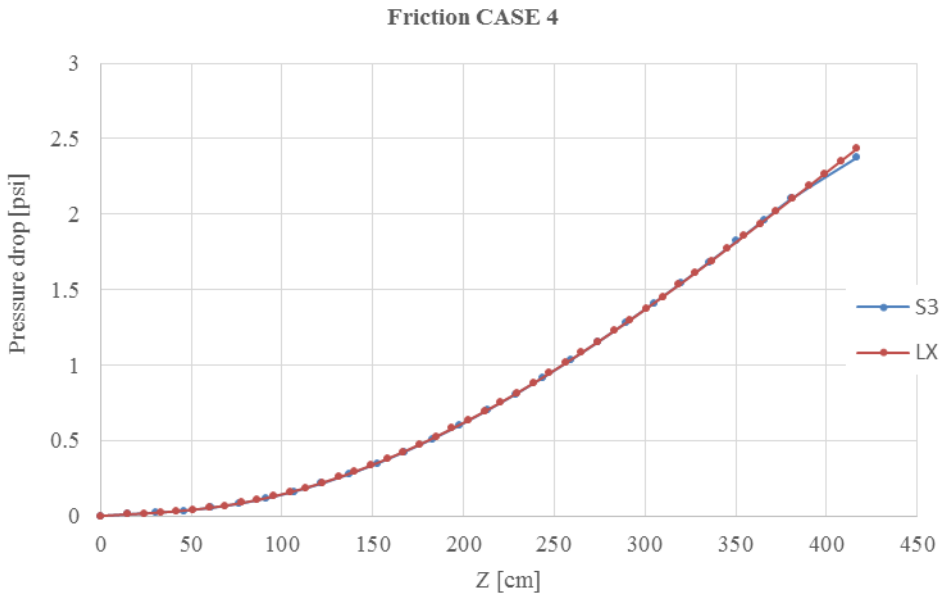


Figure 6.26. Friction CASE 4 TYPE A.

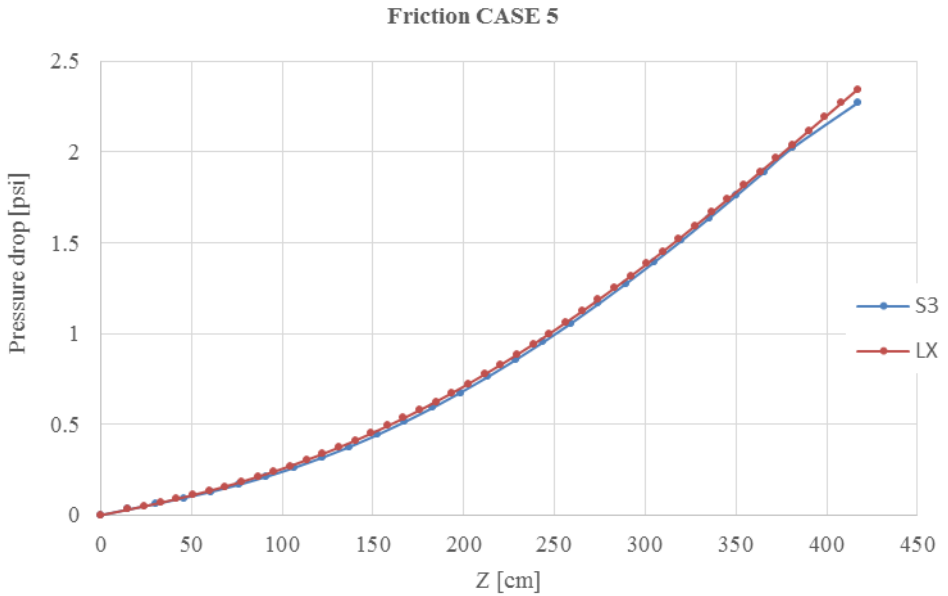


Figure 6.27. Friction CASE 5 TYPE A.

6.10.2 Friction Data for TYPE B

Comparisons of the friction component of pressure drop for TYPE B are shown in figures 6.28 to 6.32.

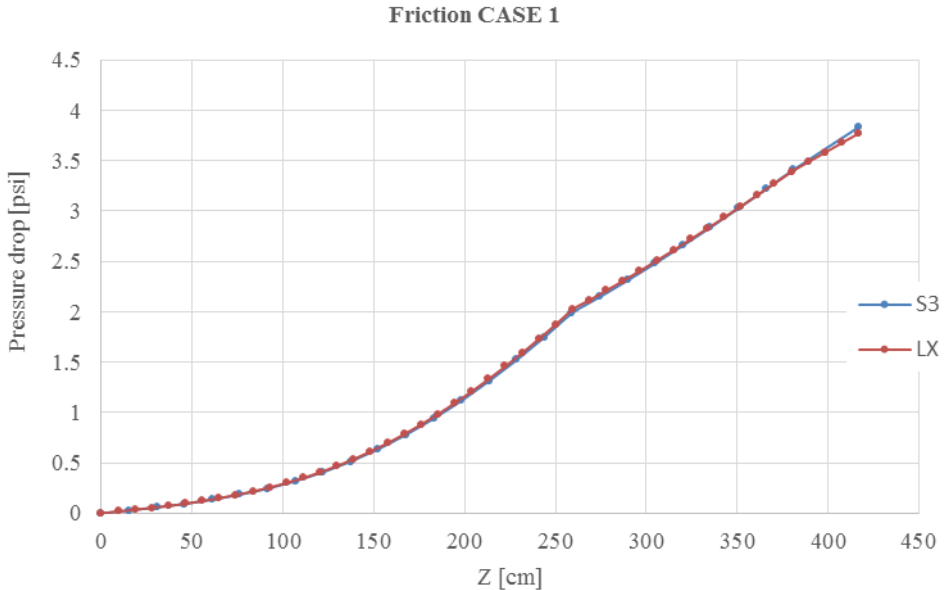


Figure 6.28. Friction CASE 1 TYPE B.

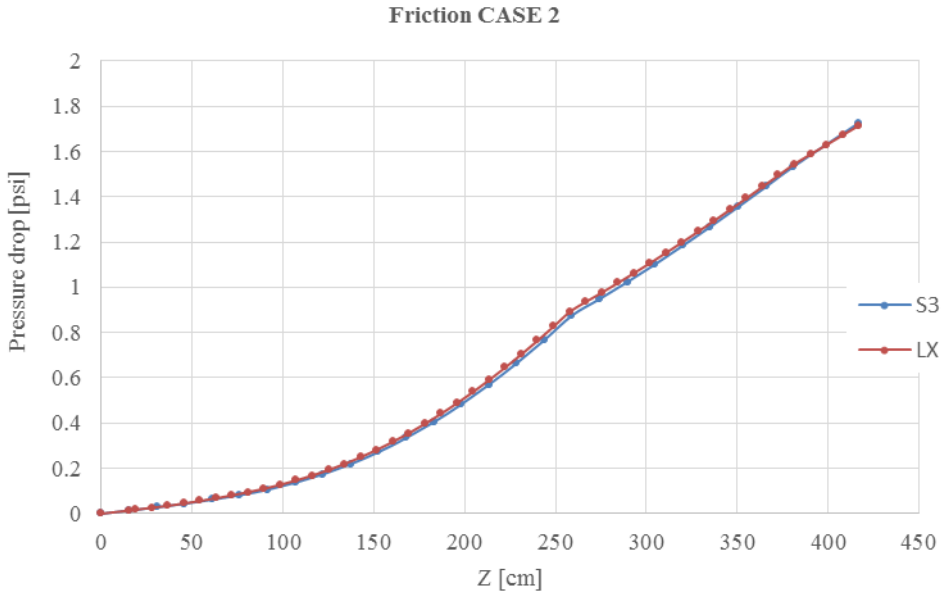


Figure 6.29. Friction CASE 2 TYPE B.

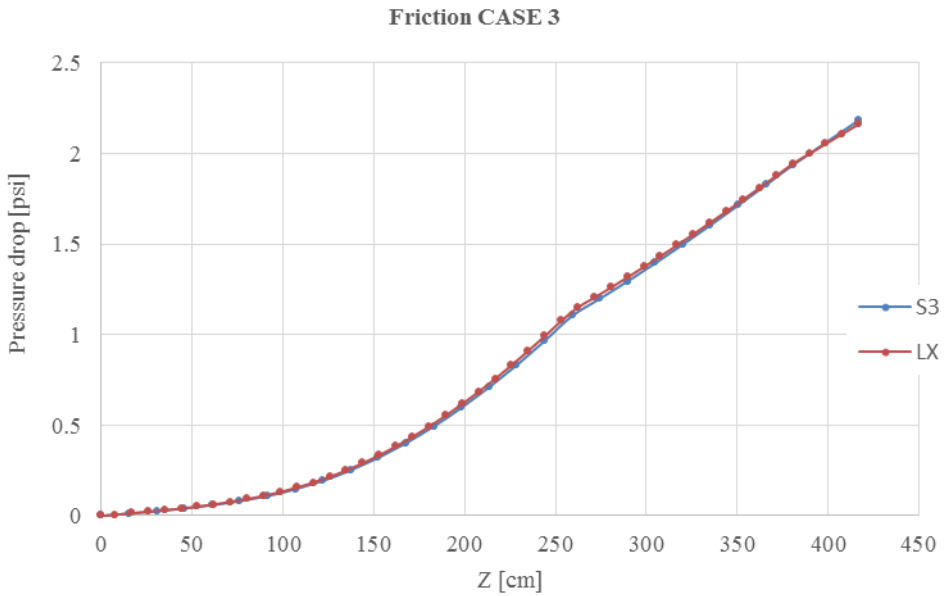


Figure 6.30. Friction CASE 1 TYPE B.

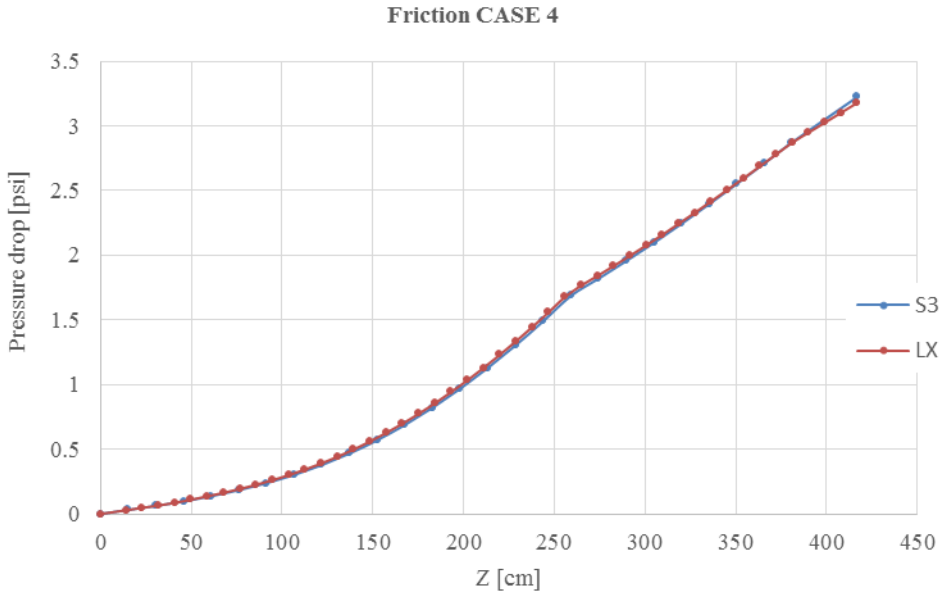


Figure 6.31. Friction CASE 4 TYPE B.

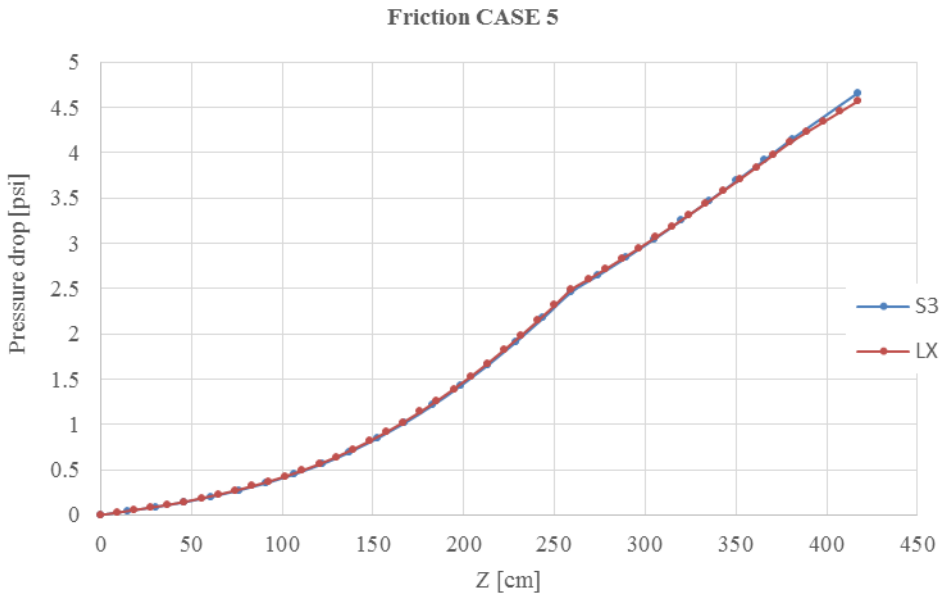


Figure 6.32. Friction CASE 5 TYPE B.

6.10.3 Conclusions of Friction Results

According to Section 6.3, two-phase friction is accounted for by means of a two-phase multiplier, which depends on flow quality. Friction pressure drop results for both codes are in very good agreement. Differences occur only in values corresponding to last node of SIMULATE-3. These differences can be attributed to (1) friction in SIMULATE taking into account exit water rod flow rate mixing and (2) friction between upper tie plate and channel exit considering only unrodded channel flow area. Changes in area in the channel length from the top of active fuel to the upper tie plate are not considered in computing friction pressure drop in this node.

It can be shown that flow quality is equivalent to flow thermodynamic quality in the bulk boiling region. However, in the subcooled boiling region, a correlation is used to obtain the “real” flow quality in this region, due to equal temperature assumption of the conservation equations. Correlations for computing real flow quality are different in LAPUR and SIMULATE-3, and flow quality results are slightly different between the two codes. The integral effect in friction is negligible, as shown in the figures.

6.11 LOCAL PRESSURE DROP DATA

In this section, a comparison of other dominant contributors to the pressure drop in LAPUR and SIMULATE-3 is provided.

6.11.1 Local Pressure Drop Data for TYPE A

Comparisons of the component of pressure drop due to local obstructions (spacers and tie plates) for TYPE A are shown in figures 6.33 to 6.37.

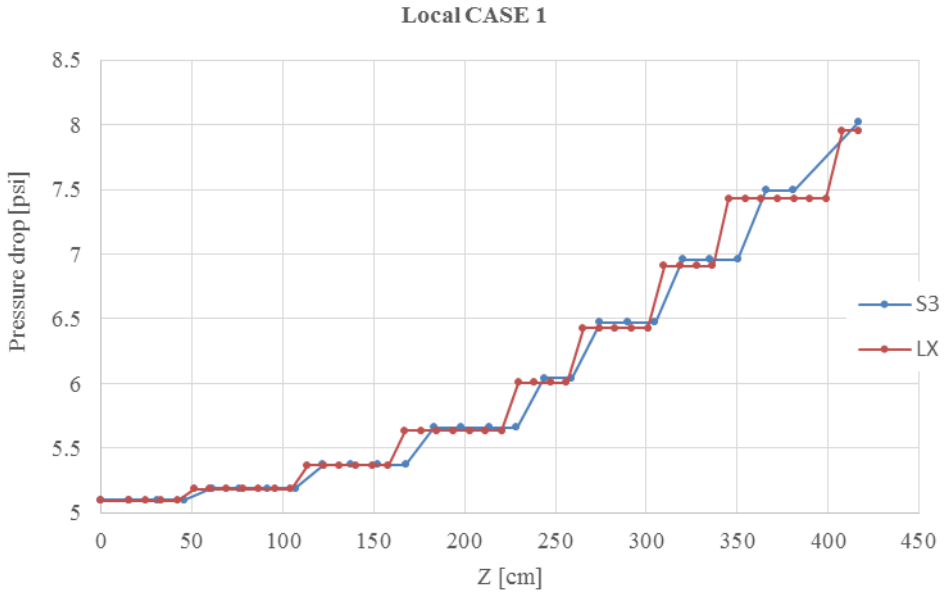


Figure 6.33. Local CASE 1 TYPE A.

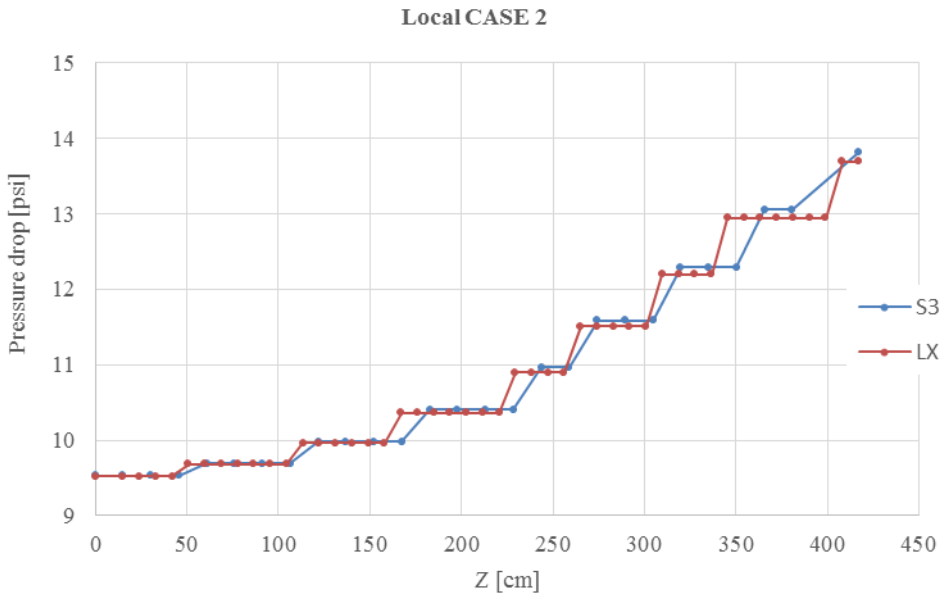


Figure 6.34. Local CASE 2 TYPE A.

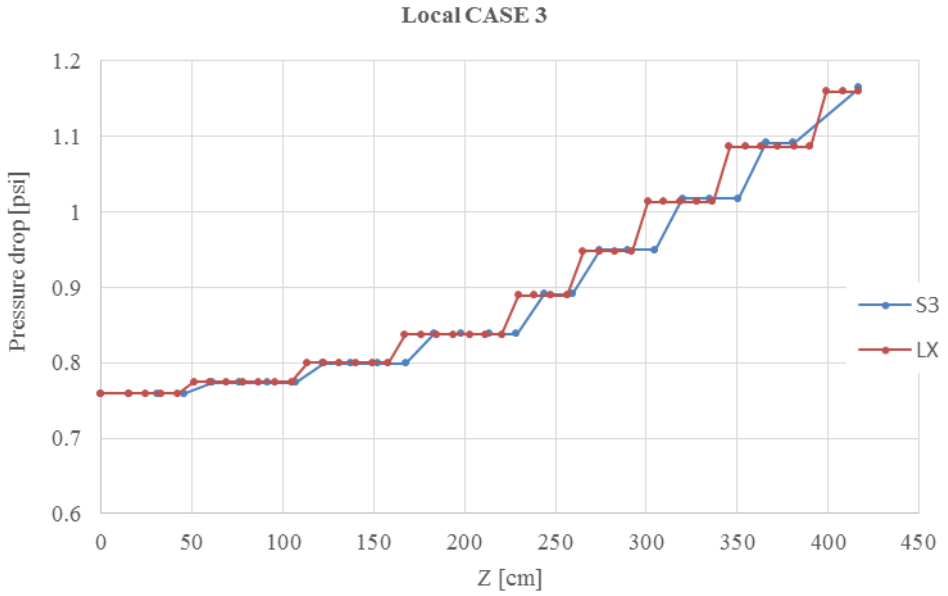


Figure 6.35. Local CASE 3 TYPE A.

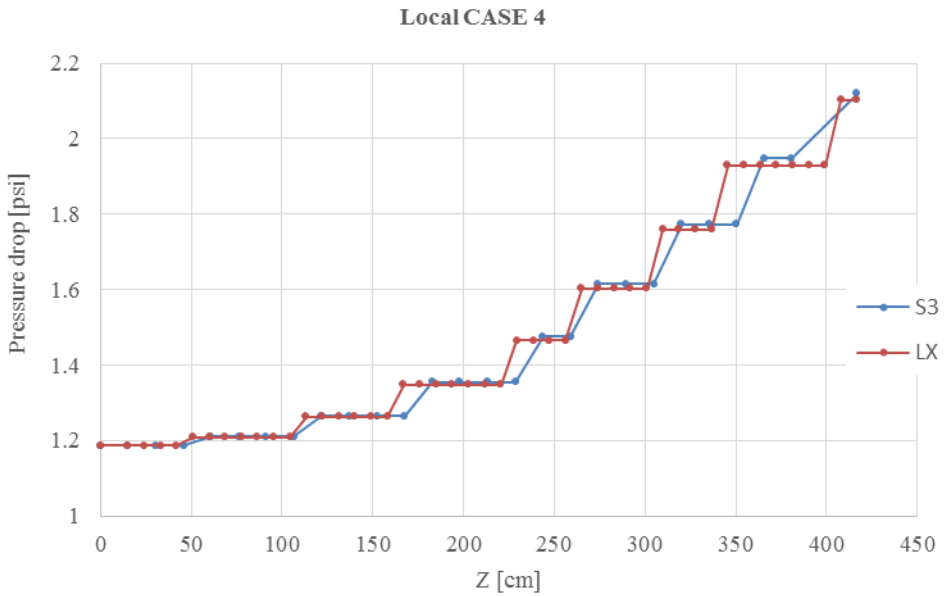


Figure 6.36. Local CASE 4 TYPE A.

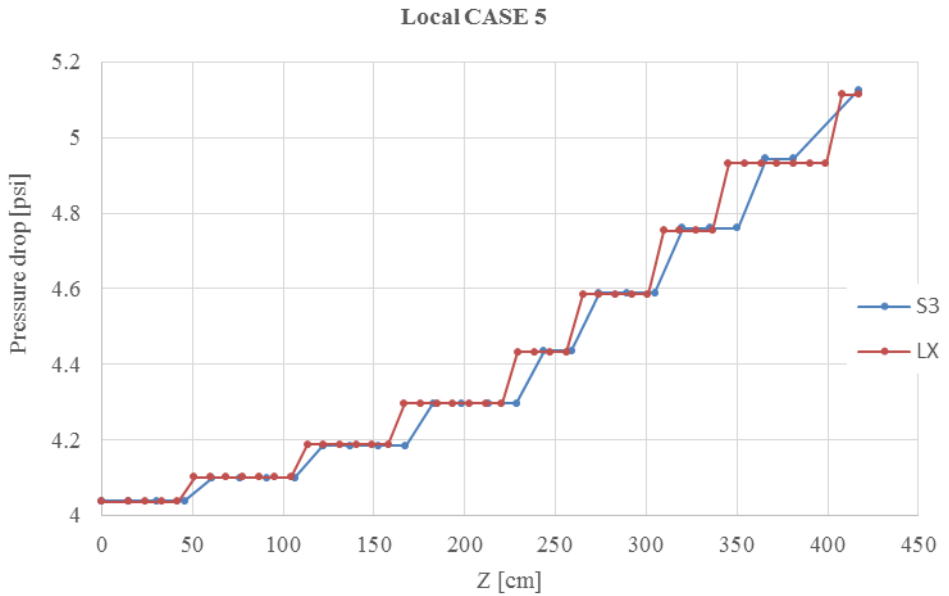


Figure 6.37. Local CASE 5 TYPE A.

6.11.2 Local Pressure Drop Data for TYPE B

Comparisons of the component of pressure drop due to local obstructions (spacers and tie plates) for TYPE B are shown in figures 6.38 to 6.42.

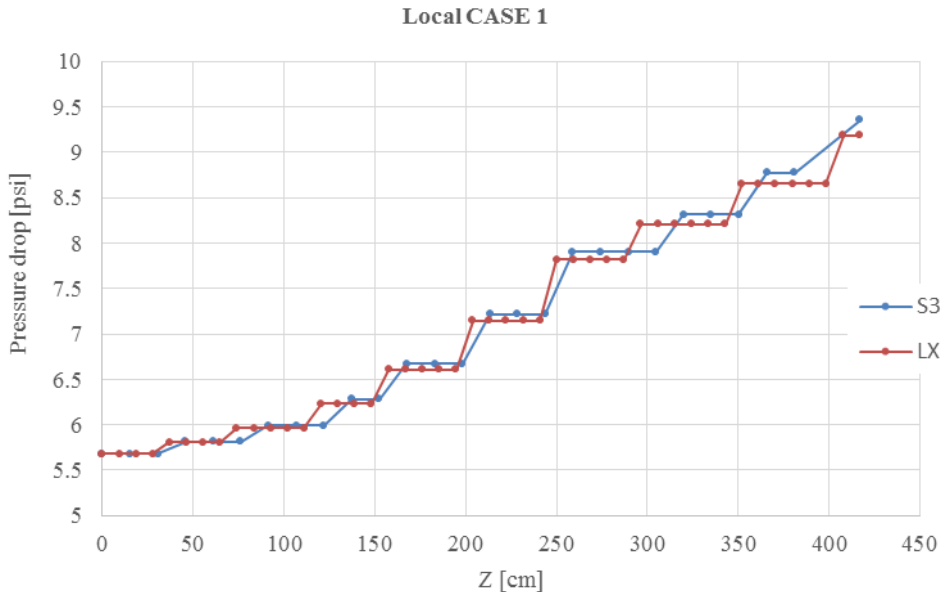


Figure 6.38. Local CASE 1 TYPE B.

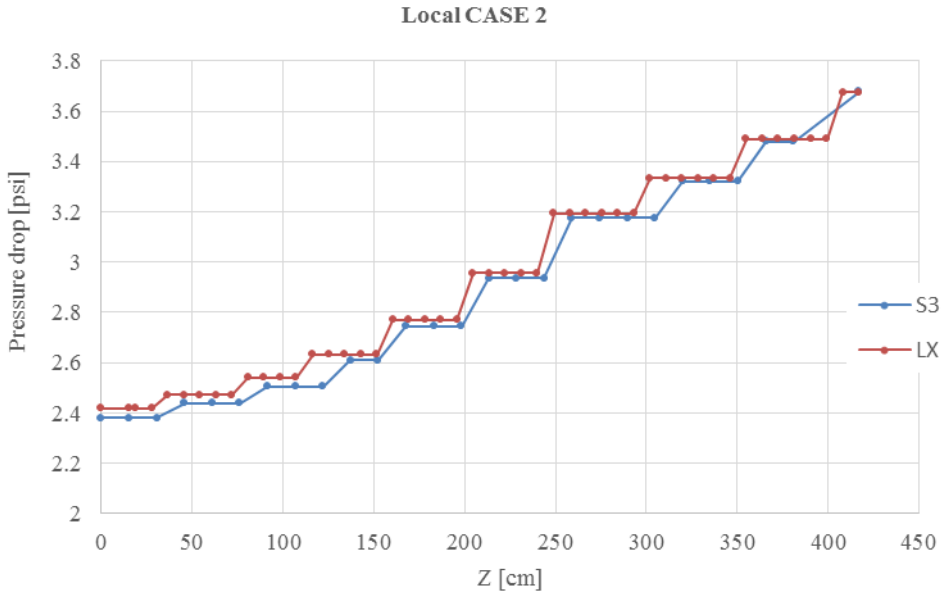


Figure 6.39. Local CASE 2 TYPE B.

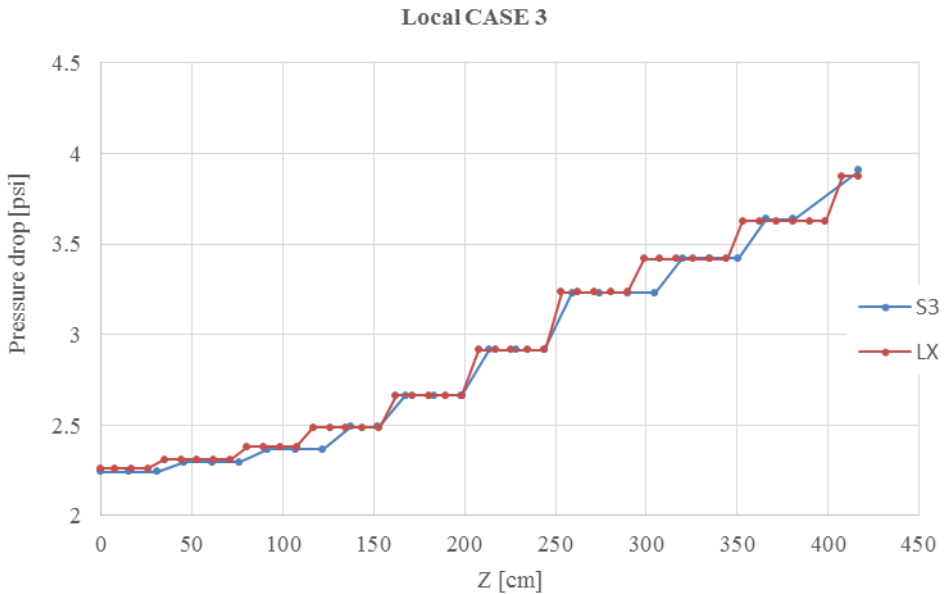


Figure 6.40. Local CASE 3 TYPE B.

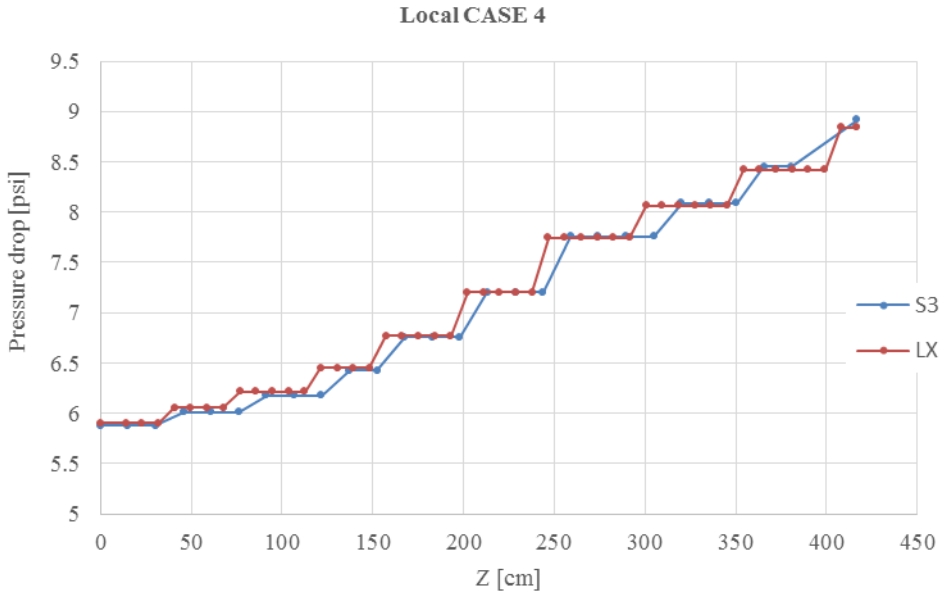


Figure 6.41. Local CASE 4 TYPE B.

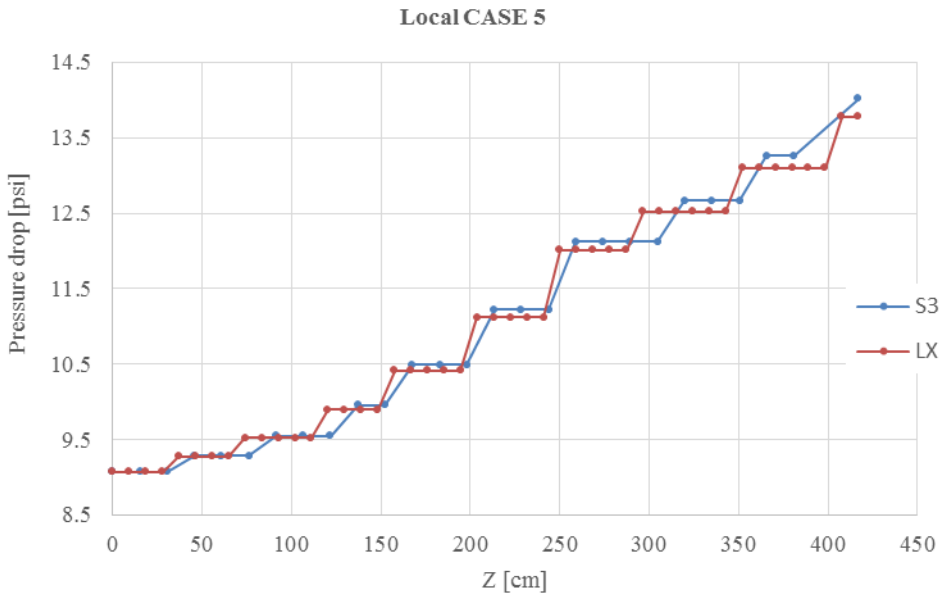


Figure 6.42. Local CASE 5 TYPE B.

6.11.3 Conclusions of Local Losses in Pressure Drop Results

The two-phase effect is accounted for by calculating local pressure drop by means of a homogeneous multiplier, as shown in Section 6.3. Due to the different number of nodes used in the LAPUR and SIMULATE-3 applications (45 nodes in boiling region for LAPUR and 25 fixed nodes for SIMULATE-3), the flow quality used in the calculation for local pressure drop is slightly different. As shown in the figures, the discrepancies are small and less than a 2% of the total local losses in pressure drop for TYPE B. Results for TYPE A type fuel are in better agreement possibly caused by compensation of errors in the pressure drops, spacer by spacer. The quality profile for both cases is different because the power profile used for TYPE B and TYPE A are different. However, overall the results show excellent agreement.

6.12 VOID FRACTION DATA

In this section, a comparison of the void fraction predicted for LAPUR and SIMULATE-3 is provided.

6.12.1 Void Fraction Data for TYPE A

Void fraction data for TYPE A test cases are shown in figures 6.43 to 6.47.

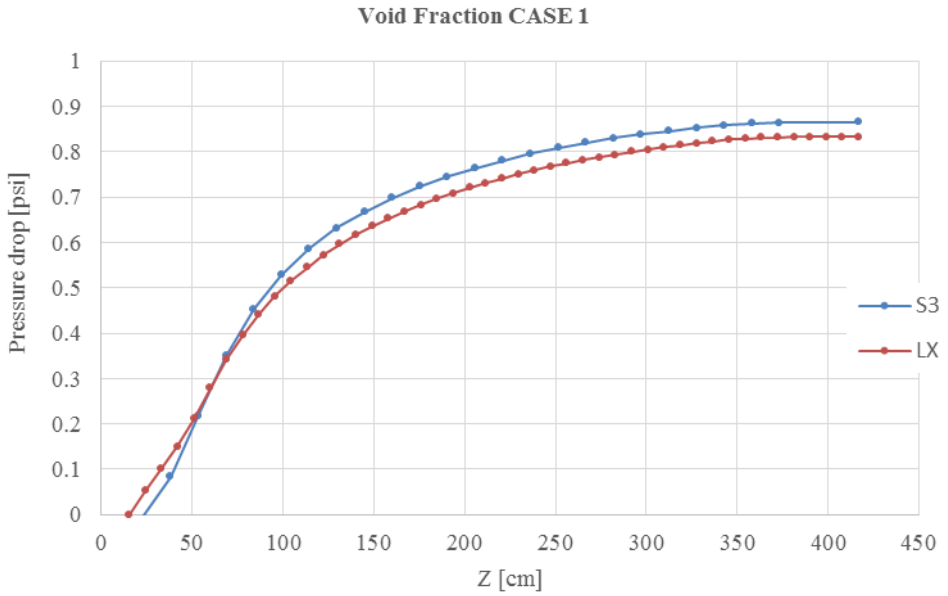


Figure 6.43. Void fraction CASE 1 TYPE A.

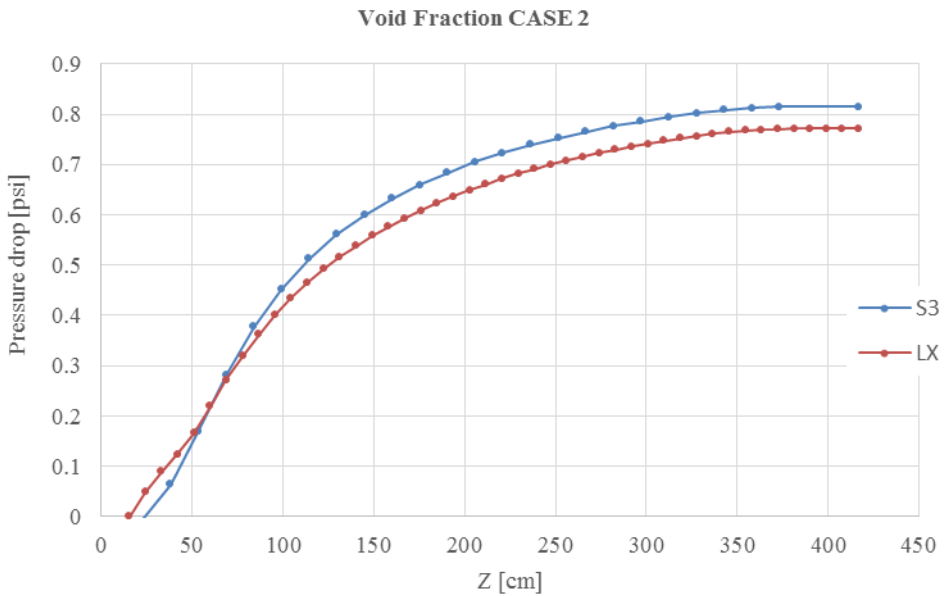


Figure 6.44. Void fraction CASE 2 TYPE A.

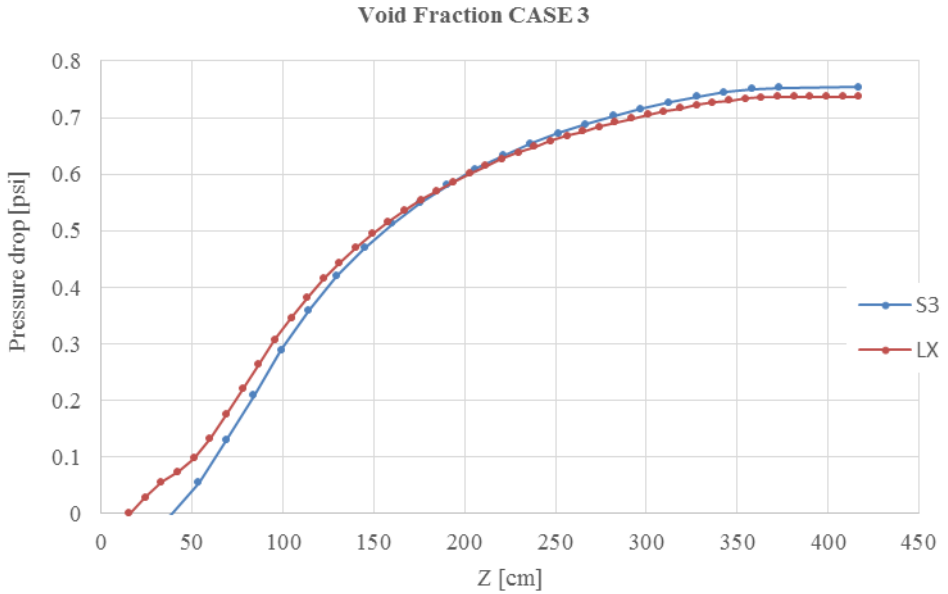


Figure 6.45. Void fraction CASE 3 TYPE A.

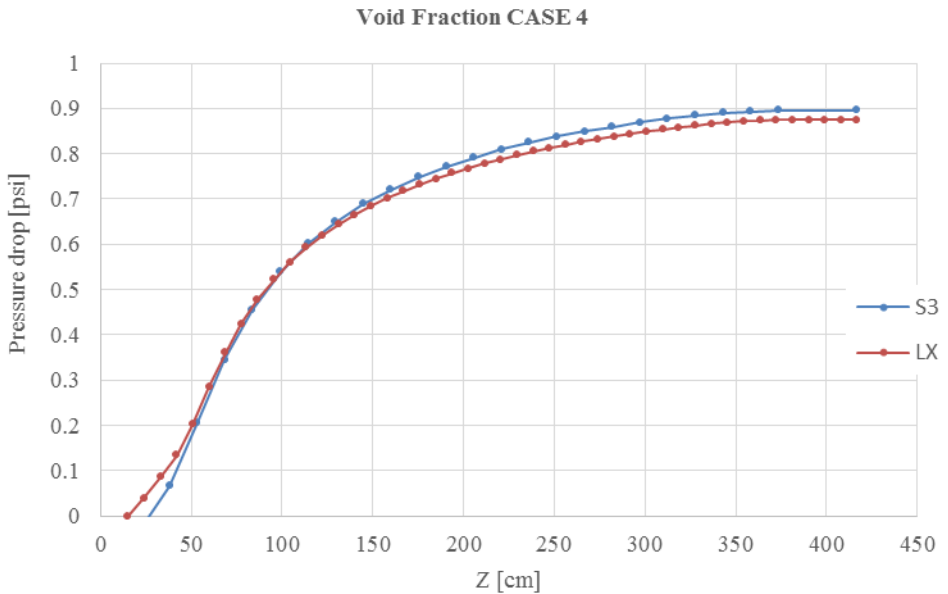


Figure 6.46. Void fraction CASE 4 TYPE A.

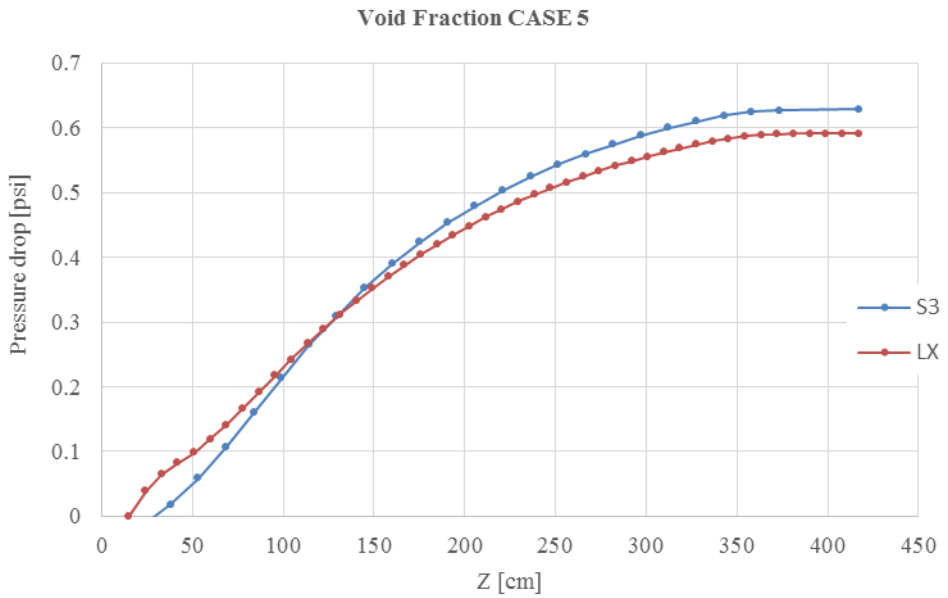


Figure 6.47. Void fraction CASE 5 TYPE A.

6.12.2 Void Fraction Data for TYPE B

Void fraction data for TYPE B test cases are shown in figures 6.48 to 6.52.

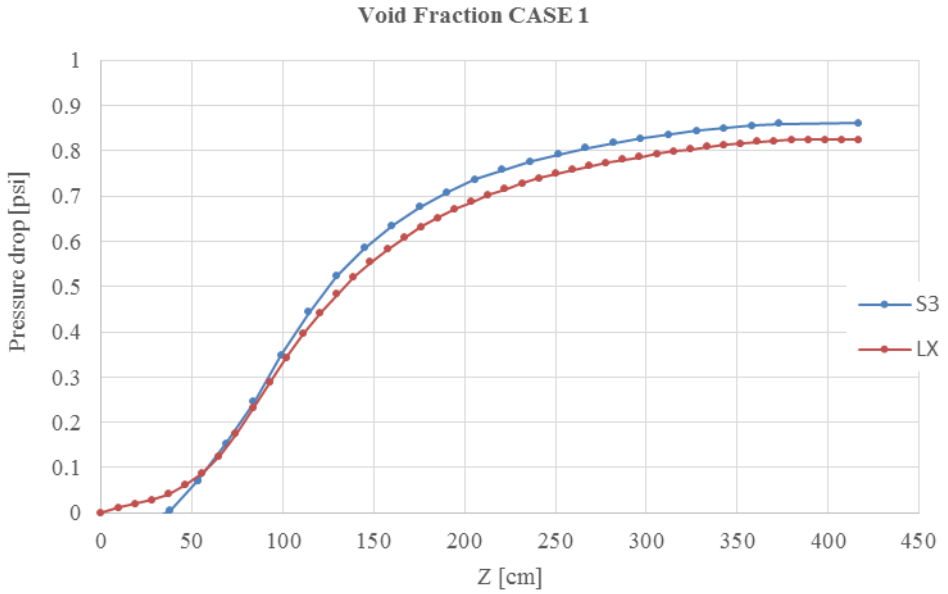


Figure 6.48. Void fraction CASE 1 TYPE B.

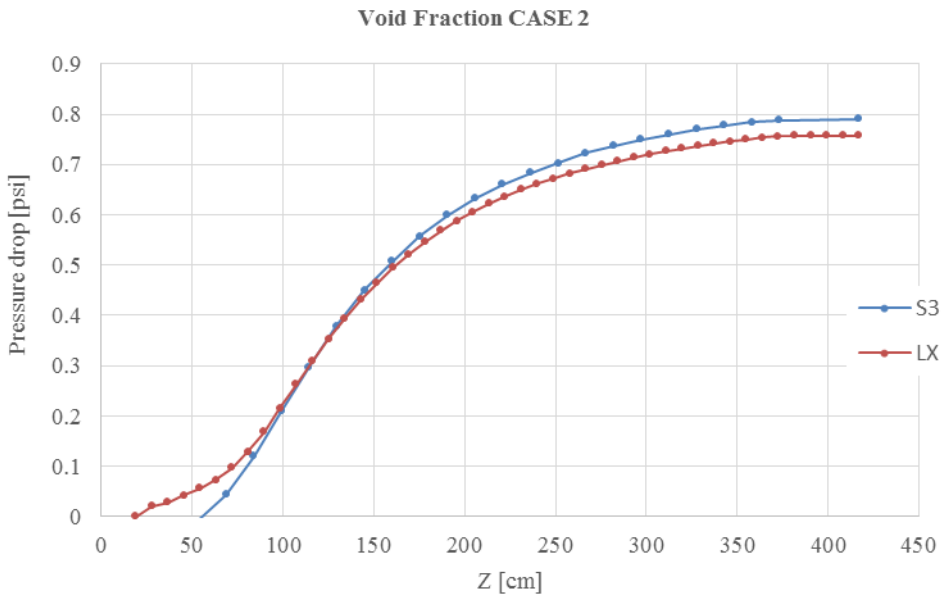


Figure 6.49. Void fraction CASE 2 TYPE B.

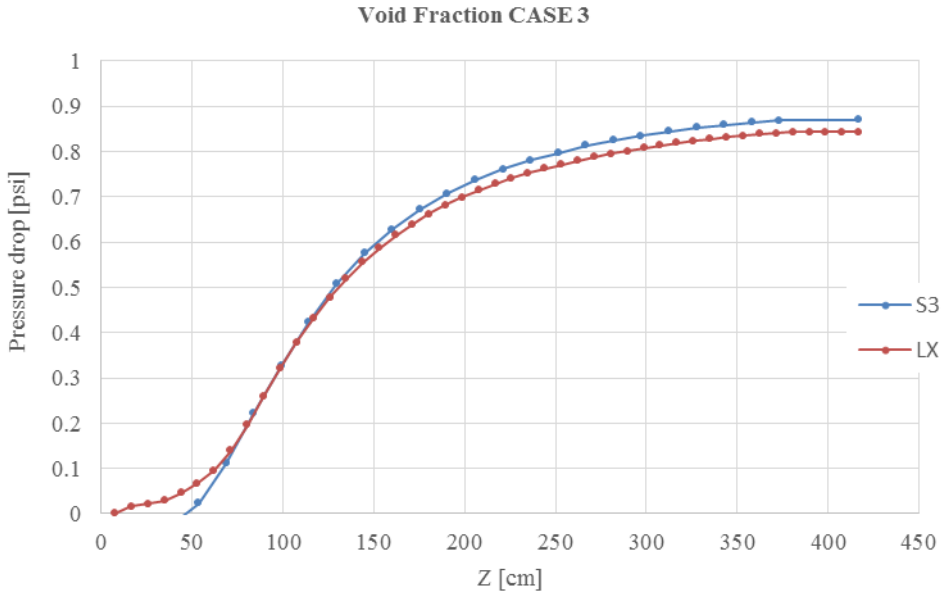


Figure 6.50. Void fraction CASE 3 TYPE B.

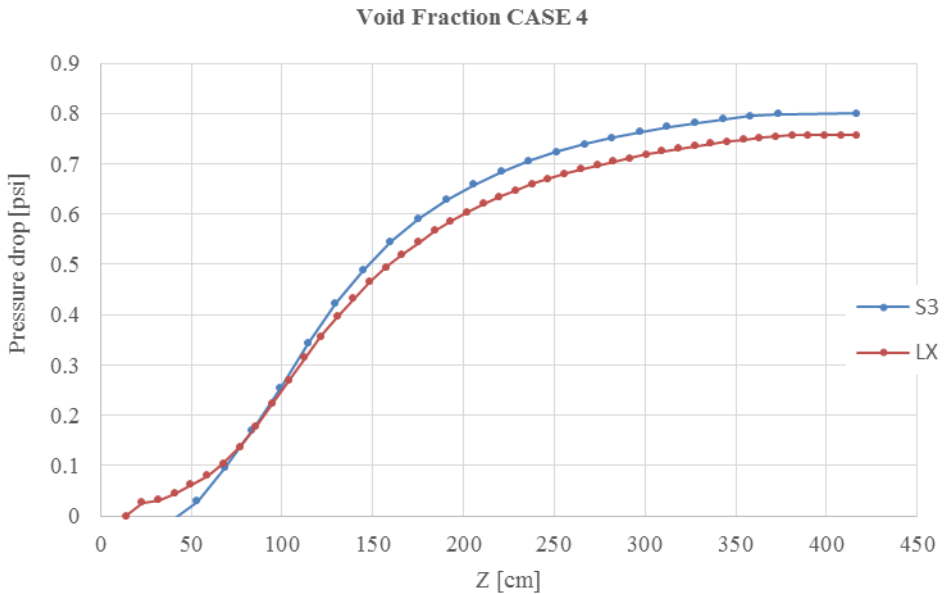


Figure 6.51. Void fraction CASE 4 TYPE B.

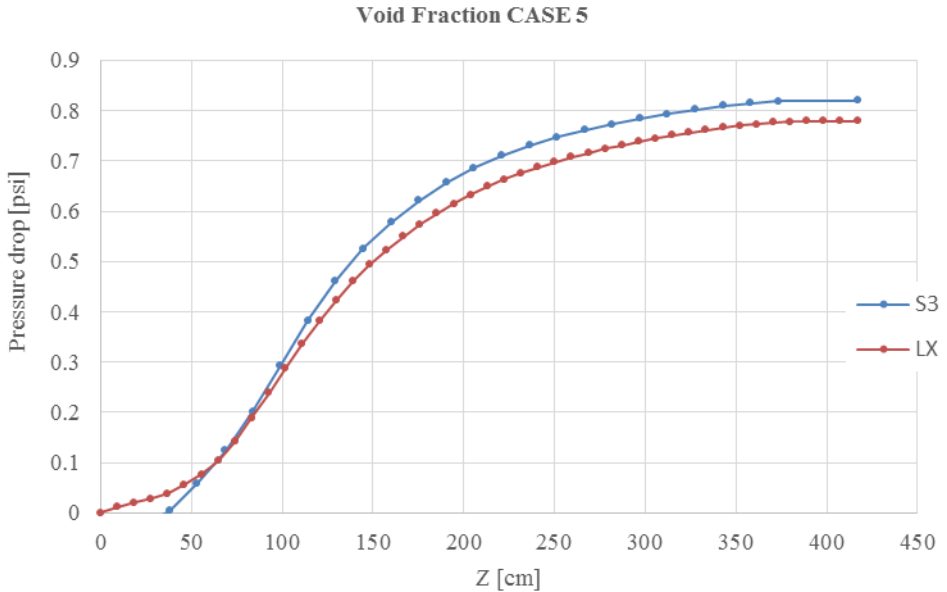


Figure 6.52. Void fraction CASE 5 TYPE B.

6.12.3 Conclusions of Void Fraction Comparison

Slight differences in the void fraction calculated by SIMULATE and LAPUR were identified. The impact on the total pressure drop was negligible; however, comparisons of void fraction calculated with LAPUR to experimental data are not readily available. The following section compares void fractions to FRIGG loop data.

6.13 COMPARISON OF LAPUR VOID FRACTION TO FRIGG LOOP DATA

Void fraction results of LAPUR 6 and LAPUR 5.1 release 1 are provided in this section. Indirectly, this study demonstrated that the modifications made did not affect the independent void fraction calculation process in LAPUR. These results show that flow qualities and slip ratio are not affected by changes in pressure drop calculation models. Runs were performed with LAPUR 5.1 and LAPUR 6, and the void fractions were practically the same (1% of maximum differences). The results of LAPUR 6 are represented as LAPURX in the figures 6.53 to 6.54.

6.13.1 Experimental Conditions

The FRIGG-2 experiments that were analyzed involved a steady-state flow test in 36-rod, electrically heated rod bundles. Subcooled liquid was introduced at the bundle inlet, and both axial and radial void fractions were obtained. Data from other experiments included mass flow rate, wall heat flux, and exit pressure values. The average bundle void fraction data were compared with LAPUR-calculated results. Table 6.4 shows input data selected from FRIGG loop [76].

Table 6.4. FRIGG-2 test conditions

Test	Pressure (psia)	Inlet enthalpy (Btu/lb)	Power (MW)	Flow rate (lb/s)
313009	725.00	487.05	2.978	34.856
313014	720.65	472.07	2.930	36.619
313016	719.20	454.55	2.909	38.036
313018	720.65	487.53	4.392	35.391
313020	720.65	448.44	4.412	34.493
313024	720.65	486.46	1.475	27.016

6.13.2 Comparison of Void Fraction Results to FRIGG-2 Data

Average bundle void fraction data are compared with LAPUR 6 calculated results in figures 6.53 to 6.58.

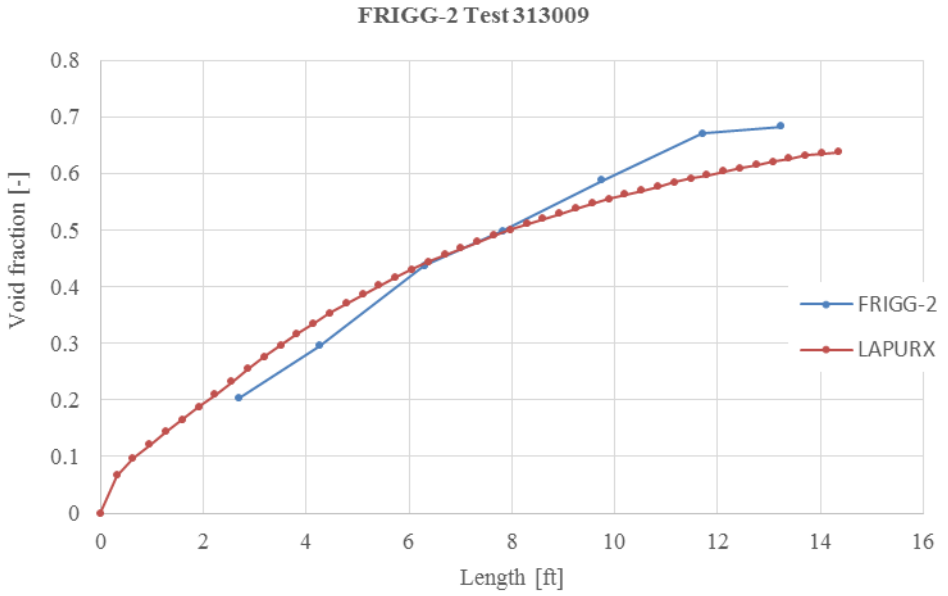


Figure 6.53. Void fraction of FRIGG-2 Test 313009.

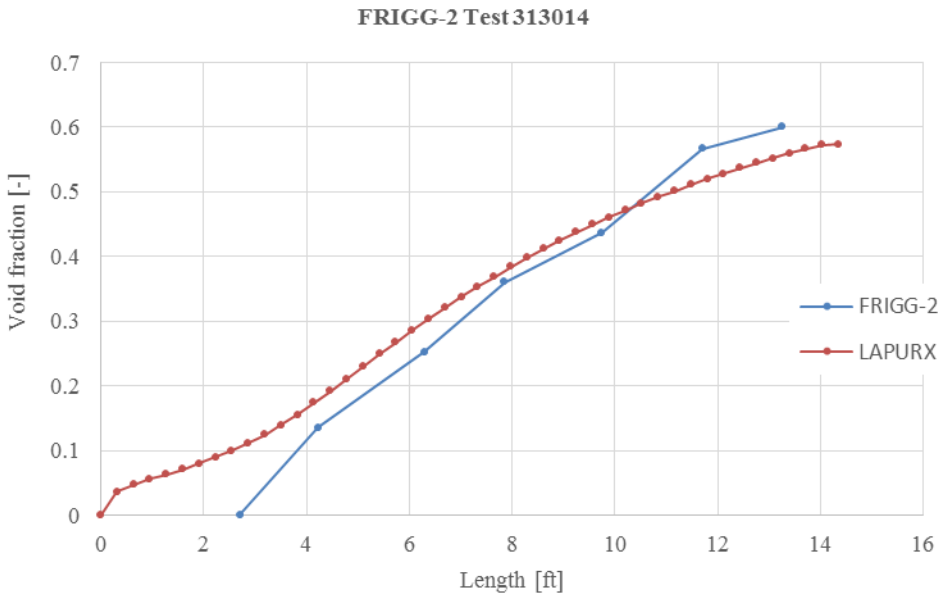


Figure 6.54. Void fraction of FRIGG-2 Test 313014.

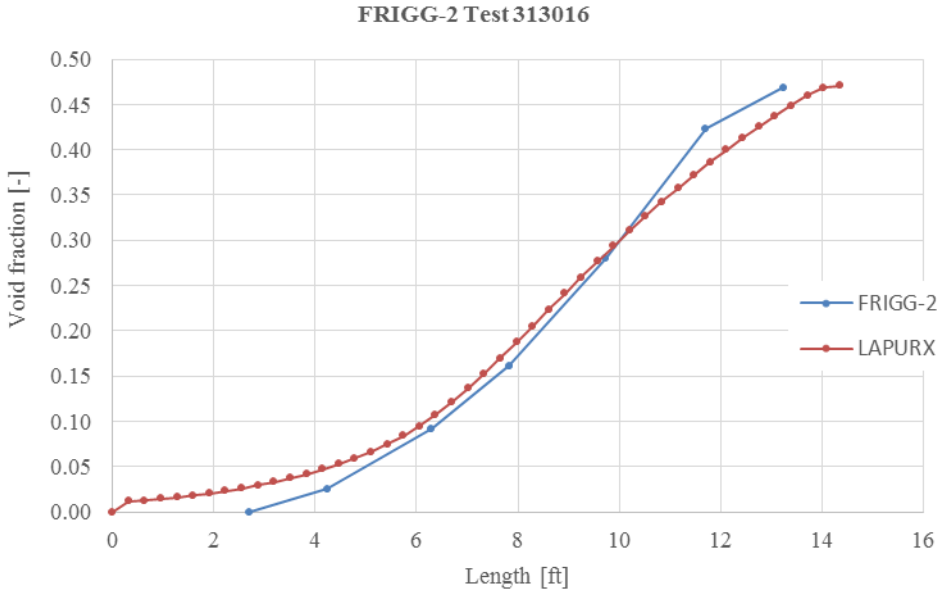


Figure 6.55. Void fraction of FRIGG-2 Test 313016.

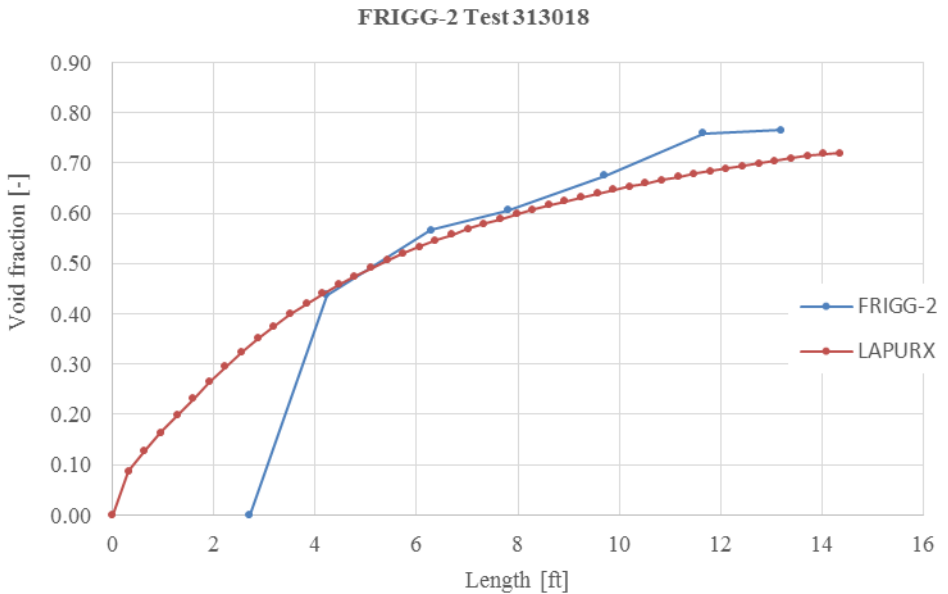


Figure 6.56. Void fraction of FRIGG-2 Test 313018.

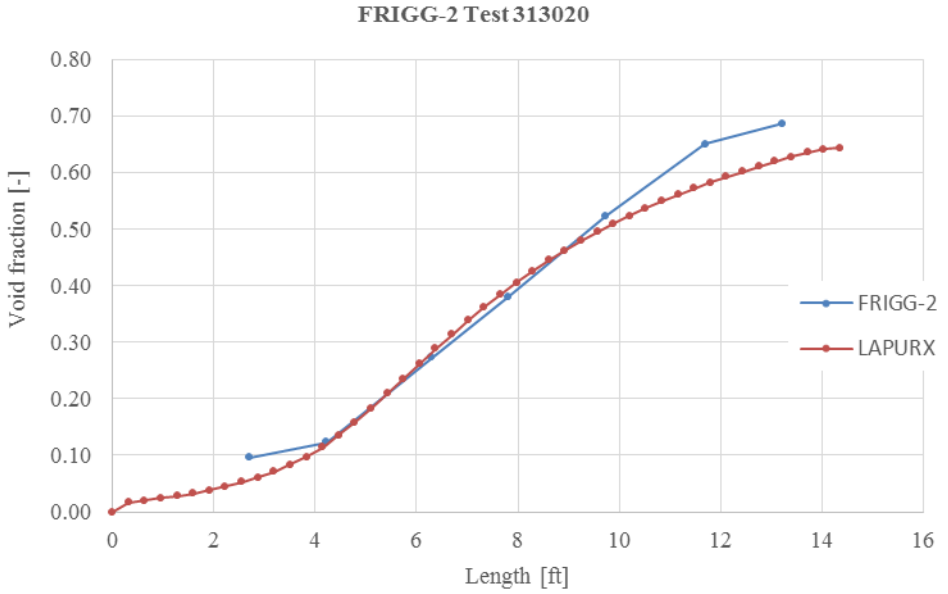


Figure 6.57. Void fraction of FRIGG-2 Test 313020.

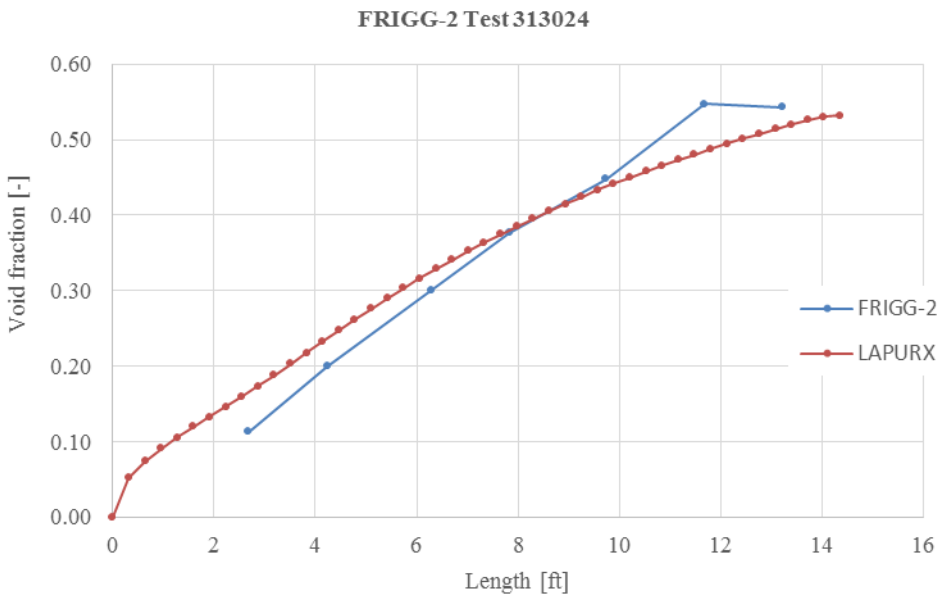


Figure 6.58. Void fraction of FRIGG-2 Test 313024.

6.13.3 Conclusions of Void Fraction Results of LAPUR 6 Compared to FRIGG-2 Data

Void fraction results and FRIGG-2 data were in reasonably good agreement. The highest deviations were similar to those of other models with three equation models and algebraic slip [76]. However, void fractions obtained with LAPUR 6 are practically the same as those of previous version, LAPUR 5.1 release 1. Logically, changes in pressure drop calculation do not affect slip and void fraction calculations because they are independent calculations.

6.14 COMPARISON OF COFRENTES NUCLEAR POWER PLANT MEASURED DECAY RATIOS TO LAPUR 6 RESULTS

6.14.1 Cofrentes Nuclear Power Plant

The Cofrentes NPP is located 2 kilometers from the village of Cofrentes, in the province of Valencia, Spain, on the right bank of the Júcar river, very close to the Embarcaderos reservoir, which serves as a cooling source for the plant.

The plant is equipped with a General Electric BWR/6-type boiling water reactor, with a thermal power level of 3,237 MW and an electrical output of 1,092 MW. Plant cooling is accomplished by means of two natural draught cooling towers, each with a capacity of 50%. The total surface area of the site is 300 Ha.

The construction permit for the Cofrentes NPP was granted in 1975, and the plant was connected to the national grid 9 years later, in October 1984.

6.14.2 Stability Control in Cofrentes Nuclear Power Plant

The Enhanced Option I-A E1A stability solution has been adopted by IBERDROLA as a long-term strategy for stability control of the Cofrentes NPP. Enhanced Option I-A E1A, developed by General Electric Company (GE) and BWR Owners Group, complies with General Design Criterion 12 of 10CFR50.55 Appendix A through the use of licensing features that prevent

reactor instabilities from occurring under operating conditions that can be reasonably anticipated.

A design philosophy of progressive protection is coupled with a conservative approach by means of stability regions boundaries and mandated operator actions.

1. The Exclusion Region is analytically defined to be that area of the licensed core power and flow operating domain where the reactor is susceptible to coupled neutronic/thermal–hydraulic instability. The reactor is automatically prevented from operating in this excluded region by the APRM flow-biased reactor trip function of the Neutron Monitoring System (NMS).
2. The Restricted Region of E1A is defined to be that area of the licensed core power and flow operating domain where the reactor is susceptible to coupled neutronic/thermal–hydraulic instability without regard to core void distributions. Automatic controls such that E1A APRM control-rod block set points, as well as administrative controls (boiling boundary), are implemented to prevent entry into the Restricted Region during scheduled reactor operation. Anticipated transients that originate outside the Restricted Region and terminate inside the Restricted Region are not expected to result in reactor instability. However, continued operation inside the Restricted Region is not permitted without putting in place specified administrative controls.
3. The Monitored Region is defined as that area of the core power and flow operating domain where the reactor may be susceptible to reactor instabilities *under conditions exceeding* the licensing basis of the current reactor system. This defense-in-depth feature is provided to preclude reactor instability even under unanticipated conditions. Continued operation within the Monitored Region boundary requires the presence of an automatic stability detection system. Defense-in-depth features are incorporated into the solution to improve overall reactor safety.

The Cofrentes power flow map including E1A regions is show in the Figure 6.59. The E1A methodology application process is designed such that the E1A stability methodology can be implemented in any GE design BWR

using qualified stability analytical tools. Decay ratio calculations form the framework for the generation and validation of the stability region boundaries.

The qualified stability analytical tool used in the E1A Cofrentes application is LAPUR 6. A methodology for calculating decay ratios using LAPUR 6 has been developed is described in chapter 5. The details can be found in [64] in which a preliminary validation matrix is defined against analytical and plant-measured decay ratios. The methodology application is designed to perform the Generation and Validation evaluations of E1A Regions for Cofrentes based on decay ratio calculations.

Decay Ratio On-line Predictor (DROP) is a research and development project being carried out by IBERDROLA jointly with the Polytechnic University of Valencia. The purpose of the DROP project is to develop a predictor-monitor system for computing the stability margin in BWRs based on LAPUR 6 frequency domain code. One of the tasks for the DROP project has been the validation of LAPUR 6 presented in this document.

6.14.3 Methodology of Calculating Decay Ratios with LAPUR 6

The methodology is based on an automated procedure for generation of LAPUR 6 input and for checking the consistency of LAPUR 6 results. Core channels will be grouped according to the number of LAPUR thermal-hydraulic regions necessary to take into account the core radial power distribution.

The grouping criteria is based on:

- Relative power fraction,
- Different fuel designs mixed in the core, and
- Peripheral or non-peripheral channel. Peripheral channels have a bottom entry orifice (BEO) instead of a side entry orifice (SEO). Peripheral channels are typically collapsed into a single LAPUR-averaged channel for each type.

In order to ensure the quality of the process, the following set of internal validations has been defined:

- Consistency of collapsed LAPUR 6 radial and axial power thermal-hydraulic regions with SIMULATE power radial and axial peaking factors.

- Coherence of LAPUR 6 flow distribution and core pressure drop with SIMULATE output

The following chain of codes is used:

- The SIMULATE [59] computer code is the 3D core simulator used to calculate the core detailed hydraulic and neutronic configuration of the different state points for analysis. The Cofrentes NPP core monitoring system, CAPRICORE, is based on SIMULATE [78] being feasible take configuration data for LAPUR 6 either to predict stability margins on-line or to perform stability licensing calculations off-line.
- PAPU [60] is a post-processor used to obtain Doppler and reactivity density coefficients from the perturbation calculations performed by SIMULATE around the base case.
- LIP pre- and post-processor ([61], [79]) extracts from the SIMULATE summary and output file a database for all core assemblies classified according to type in different output files and generates the complete input data for LAPUR. The process is completely automated and can use LAPUR 6 to either predict stability margins on-line or to perform stability licensing calculations off-line.

6.14.4 Decay Ratio and Frequency Validation: Start-up and End-of-Cycle Coastdowns

The purpose of this validation set was to qualify LAPUR 6 as a stability on-line predictor; therefore, the same automated procedure [71] was followed for all decay ratio calculations.

Average Power Range Monitor (APRM) and Local Power Range Monitor (LPRM) data were collected during the Cofrentes NPP Cycles 16b and 17 coastdown and Cycles 17 and 18 start-up (summer 2007 and November 2009). Cycle 16 is split up in two periods (16a and 16b) due to a fuel failure in mid-cycle, and Cycle 16b corresponds with the Cycle 16 End of Cycle (EOC) after discharging the failed fuel in a mid-cycle outage. The signals were analyzed with noise techniques, and the experimental decay ratios were compared against LAPUR 6 calculations.

The data acquisition system used is the standard of the plant. A sampling rate of 20 Hz for 10 minutes was recorded for each state point in a typical Tabular Trend Report.

Figure 6.59 shows a typical EOC coastdown. The plant is operating in Final Feedwater Temperature reduction operation mode (FFWTR). For the shutdown, the operating crew restores feedwater heaters to increase feedwater temperature. The negative reactivity insertion helps to shut down the reactor. Control rod insertion and core flow decrease allow downshift of the recirculation pumps and uncoupling of the generator, which finally leads the reactor to cold shutdown.

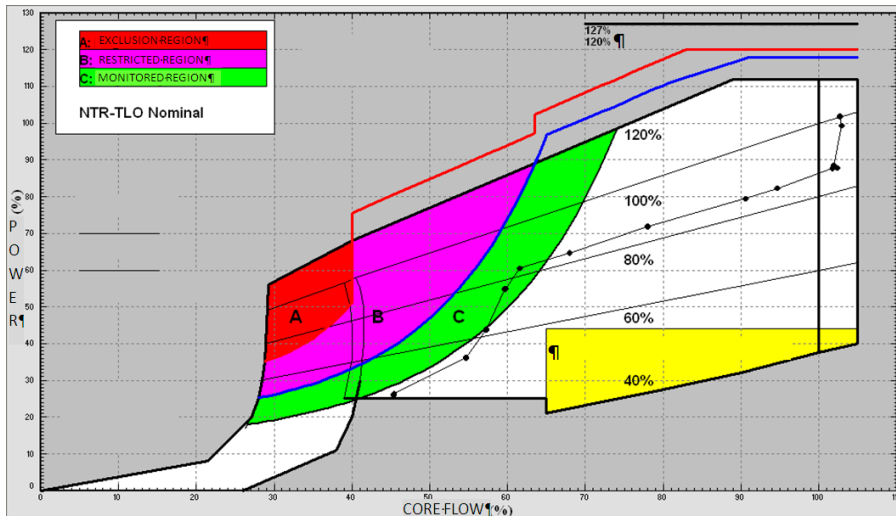


Figure 6.59. Typical path during EOC coastdown (Cycle 16b).

At EOC, the void coefficient reaches the maximum absolute value, and higher decay ratios than at the Beginning of Cycle (BOC) are expected. APRM and LPRM data were taken at power levels close to 90%, 80%, 70%, 50%, and 40% for EOC Cycles 16b and 17. Two additional state points close to 30% and 20% were taken for EOC Cycle 17. During 16b and 17 coastdowns, a total of 12 recordings of 10 minutes were taken.

Figure 6.60 shows the typical path during a start-up. For low-power conditions, a GE-BWR-6 operates with recirculation pumps at low speed and the FCVs close to 50%. When the power is above 25% and before the upshift, entry in Region B is required for a period, and EIA average boiling boundary control above 4 ft (the lowest one-third of the core) using a shallow control rod pattern is mandatory. With a fraction of core boiling boundary (FCBB) greater than 1, that is, a core boiling boundary above 4 ft, Restricted Region FCTR control rod block set points are switched to setup mode to allow entry in this

region (blue arrow number 1 in Figure 6.60). During the maneuver, the FCV position has to be less than 5% to avoid a high peak of neutron flux (blue arrow number 2 in Figure 6.60). From this last state point and power above 25%, the cavitation interlock allows upshift recirculation pumps to operate at high speed (blue arrow number 3 in Figure 6.60). After the upshift, withdrawal of the required control rods in order to reach full power has to be performed out of the Restricted Region because simultaneous boiling boundary control and rod withdrawal is not possible. In order to withdraw enough control rods to reach the target rod pattern, the power ascension is performed inside the Monitoring Region but not too far out of the Restricted Region Boundary.

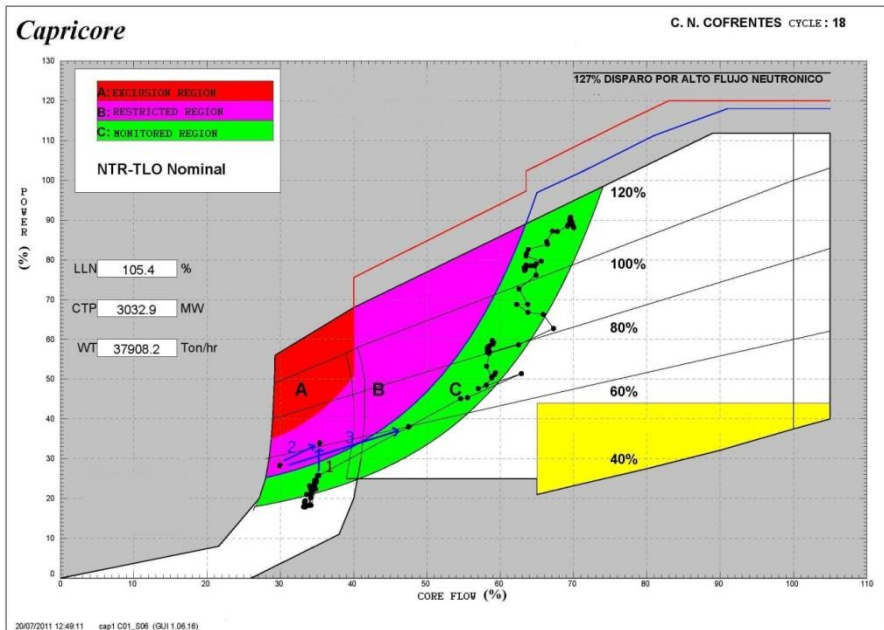


Figure 6.60. Typical start-up path (Cycle 18).

6.14.5 Generation of SIMULATE-3 Core Configuration Data

As described previously, SIMULATE-3 [59] is the nodal simulator used by IBERDROLA for core following and design. It is also the calculation engine for the core monitoring system CAPRICORE [78]. Using real data from the core monitoring system, start-ups and coastdowns are simulated taking into account enough steps to reasonably follow the xenon transient. In figure 6.61, each marked diamond is a step in the Cycle 18 start-up power history. The

black continuous line represents one real state point taken into account in the SIMULATE-3 start-up simulation.

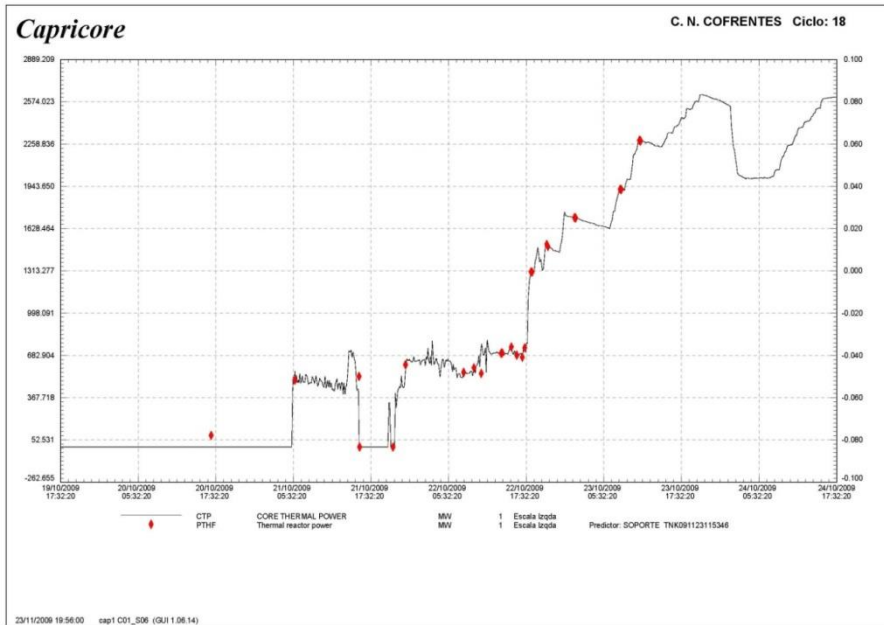


Figure 6.61. Power history used for SIMULATE-3 simulation of C. 18 start-up.

6.14.6 Time Series Analysis of Signal for Decay Ratio Estimation

Different signal time series analysis methods can be used for decay ratio estimation ([92], [2]). After a detailed review of the different time series analysis methods, a method based on the interpolation of an autocorrelation function was selected. The robustness of this method was tested over a full range of decay ratios values using analytical and real signal analysis. A decay ratio monitor called SMART has been developed by the Universidad Politécnic de Valencia (Spain) jointly with IBERDROLA [93]. The SMART stability monitor, which was developed with MATLAB, will be used for autocorrelation-based decay ratio estimation.

6.14.7 Results of Decay Ratio and Oscillation Frequency

According to the procedure described previously, decay ratios from the APRM's autocorrelation function, natural frequency, and the equivalent from LAPUR were estimated.

In figure 6.62, averaged APRM versus LAPUR results are shown. As can be seen, the frequency trend is consistent. The decay ratio values are very low, mainly because at end of the cycle (EOC) the axial power profile is top peaked, which has a stabilizing effect. The state points analyzed appear along the Monitoring Region boundary (green line), which is the locus of a 0.4 decay ratio value. Values obtained were well below Monitoring Region criteria, which indicates the degree of conservatism of the E1A methodology.

Figure 6.63 shows slightly lower values in BOC start-ups when compared with EOC coastdown. Because the reactor power was close to 25% thermal power and 35% core flow for 12 h due to typical tuning problems during the first start-up after the outage, four sets of 10 minute data were taken during this 12 h interval to account for the xenon effect. The values obtained in the four sets of LAPUR calculations are very similar. Decay ratios were obtained at the highest flow rate between 55 and 65%, core flow was around 0.2, and natural frequency was around 0.55–0.63 Hz. Decay ratios were lower in comparison with decay ratio criteria of the Monitoring Region.

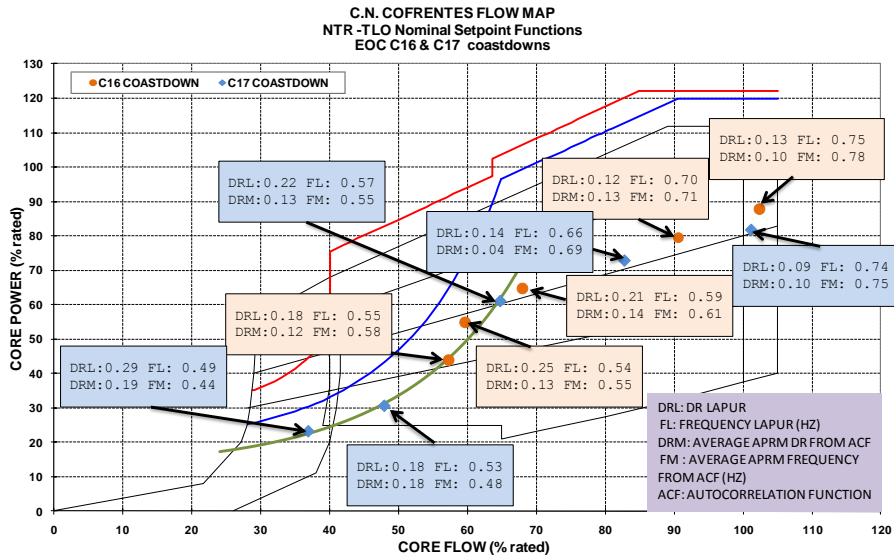


Figure 6.62. Average APRM decay ratio and frequency versus LAPUR results (EOC Cycles 16 and C17 coastdowns).

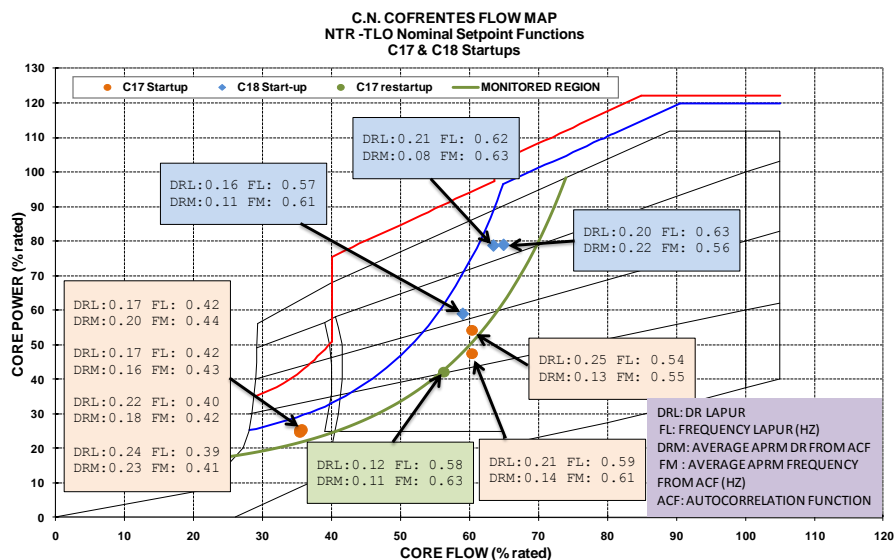


Figure 6.63. Average APRM decay ratio and frequency versus LAPUR results (Cycles 17 and 18 start-ups and coastdowns).

The hottest channel decay ratio for each fuel design was isolated in a LAPUR channel, and exclusive thermal-hydraulic (without neutronic feedback) decay ratio calculations were simultaneously performed for each hot channel. Hot channel decay ratio was close to zero for all of state points.

Obtaining decay ratios from LPRM data was not possible because the signal to noise level was not sufficient to obtain consistent results.

6.14.7.1 Analysis of Data

Estimated decay ratio and natural frequency based on autocorrelation function are in good agreement with LAPUR results.

The results shown in figure 6.64 are in the ± 0.1 band, with noticeably good agreement for the low decay ratios.

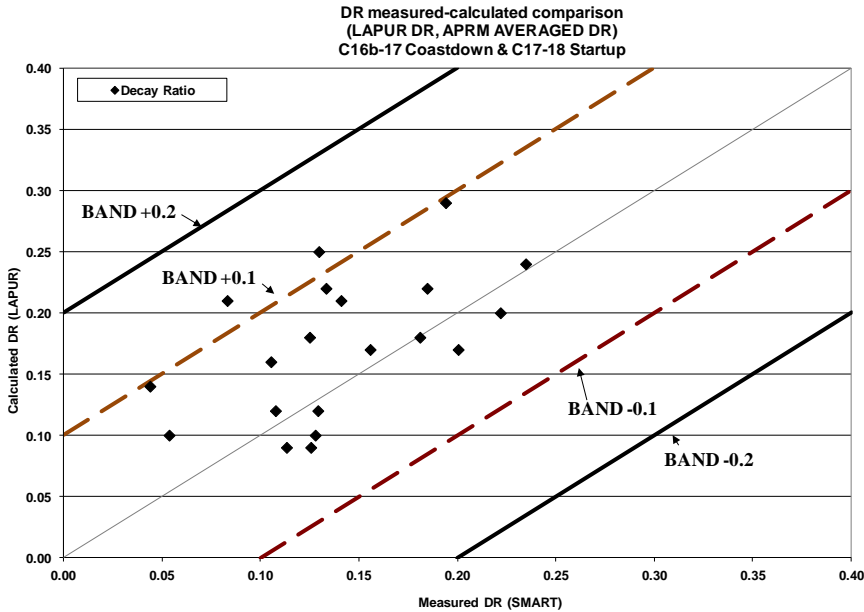


Figure 6.64. Decay ratio based on monitor SMART versus LAPUR.

A bias of 0.3 was obtained by subtracting the SMART decay ratio from the average of LAPUR decay ratio and shows a slightly conservative trend in LAPUR predictions. The sample standard deviation is 0.05, which shows a very reasonable dispersion.

Figure 6.65 shows the natural frequency agreement between LAPUR and SMART. A bias of 0.0 Hz was obtained by subtracting the SMART frequency from the average LAPUR frequency, with a sample standard deviation of 0.04, which shows a very low dispersion of frequency prediction. LAPUR predicts very accurately natural frequency in the 0.40–0.80 Hz.

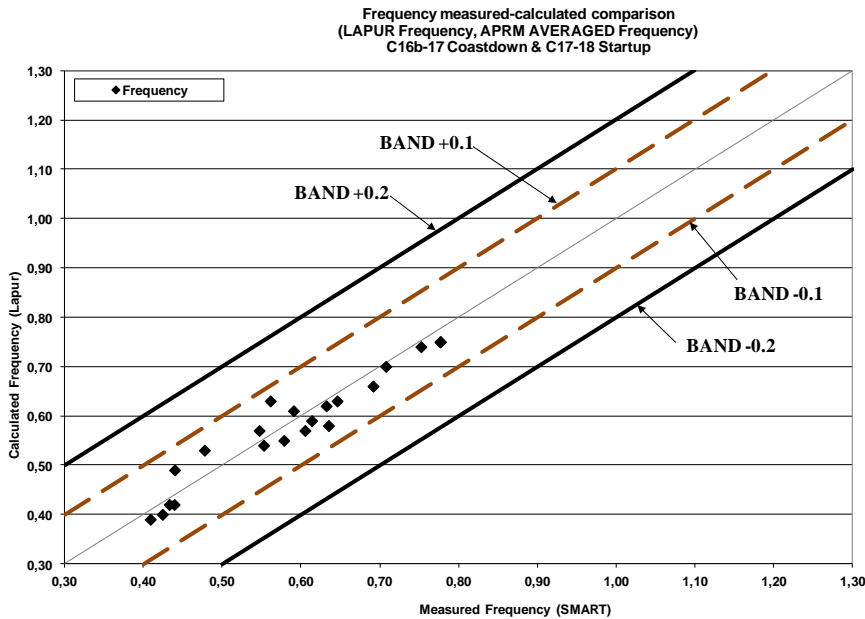


Figure 6.65. Natural frequency based on monitor SMART versus LAPUR.

6.14.7.2 Comparison of SMART Frequency and Power Spectral Density Peaks

In this section, SMART natural frequency based on autocorrelation function is compared with the resonance peaks of a non-parametric spectrum estimation based on Welch’s method and a Hanning window [94], with a segment window length to obtain a resolution of 0.1 Hz. Figure 6.66 compares LAPUR-calculated frequency to the closest frequency peak of Welch’s method spectrum estimation. The periodogram is composed of several peaks. The three highest peaks are extracted, and the closest to autocorrelation-based frequency is plotted against LAPUR-calculated frequency. Due to the low energy of the peaks that is consistently obtained with low decay ratios, a few frequency results are inconsistent, but the majority are reasonably consistent, as shown in the figure.

For the frequency comparison which is out +0.2 band (0.34 PSD, 0.63 LAPUR) when a 0.05 Hz resolution periodogram is obtained, there is a peak close to LAPUR frequency. Figures 6.67 and 6.68 show periodograms with two different resolutions.

Because the decay ratio is very low, the PSD peaks have very low energy, as shown in figures 6.67 and 6.68.

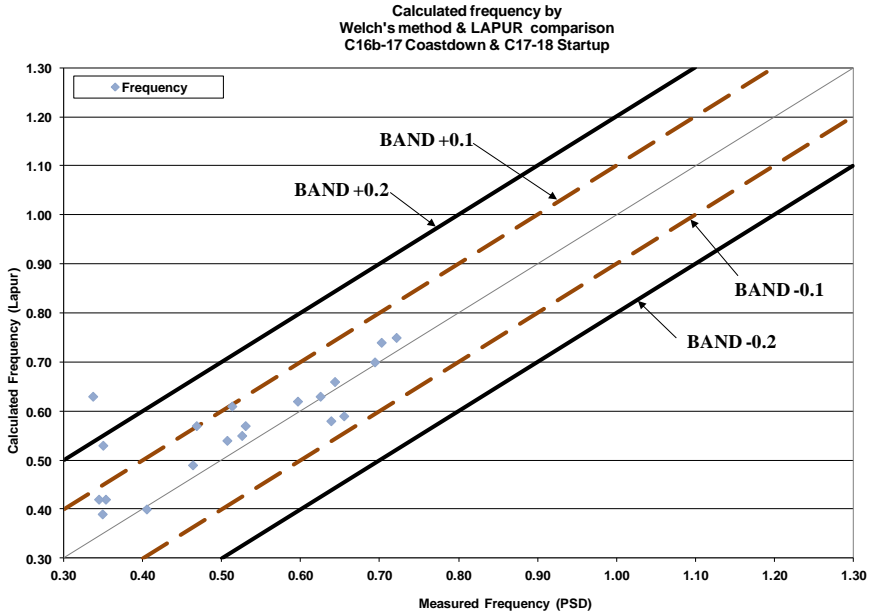


Figure 6.66. Comparison of Welch's method periodogram and LAPUR-calculated frequency.

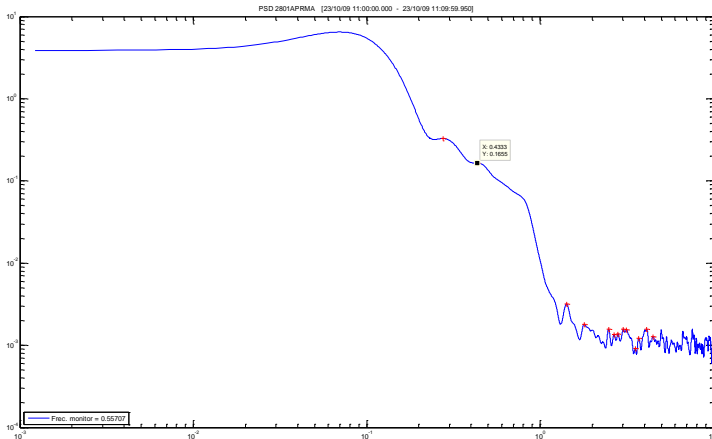


Figure 6.67. Welch's method periodogram at 0.1 Hz resolution.

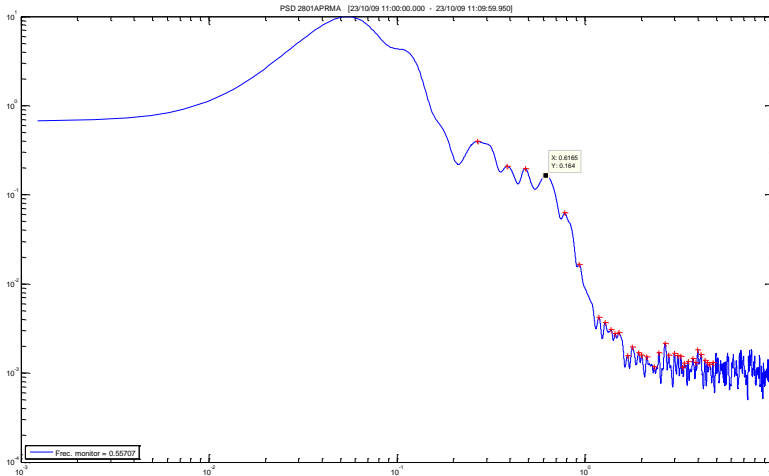


Figure 6.68 .Welch's method periodogram at 0.05 Hz resolution (peak close to LAPUR frequency).

6.15 DECAY RATIO AND FREQUENCY VALIDATION: COFRENTES CYCLE 6 INSTABILITY

6.15.1 Event Description

Shortly after 12 o'clock noon on January 29, 1991, a nuclear thermal-hydraulic instability event occurred during the start-up sequence approximately 30 h after a scram for full power. Conditions at the plant at the time of the event were as follows:

- Middle of cycle at an exposure of 4478 MWD/ST of a planned 9500 MWD/ST cycle.
- Recirculation pumps motors at low speed.
- Flow control valves at minimum position.
- One feedwater train was out of service (6A) and the other (6B) was being placed in service.
- Steam bypass valves closed.
- The operators were withdrawing control rods when oscillations of approximately 10% peak-to-peak of scale were observed.

Event descriptions and stability analysis performed with LAPUR can be also found in [64].

6.15.2 Setup of the Core Configuration

The core configuration was updated using SIMULATE 6.07.15. The first step consisted of identifying the closest SIMULATE restart file to the event, in this case at the beginning of the Cycle 6. This initial restart corresponded to SIMULATE input data from the core following runs. After locating the initial restart file, four SIMULATE runs were conducted to reproduce the core configuration at the beginning of the event.

The first run of SIMULATE updated the core burnup conditions and initialized the xenon transient. For this reason, the reactor was brought to previous scram (01/28/91) conditions. The second run reproduced the scram and considered the reactor shutdown interval until the next startup. Taking into account this time interval was necessary in order to perform the xenon transient calculation. The third run was necessary to enter the time in hours between the shutdown and the start-up beginning xenon transient calculation. The start-up beginning time was unknown, so the interval in hours between the shutdown and the criticality was used as an acceptable approximation. Finally, the fourth run was necessary to calculate the core configuration at the 01/29/91 state point.

6.15.3 LAPUR Input Data

Core channels have been grouped in six regions. In Cycle 6, the core was composed of 8×8 fuel. Two independent LAPURX grouping criteria, one for wide core decay ratio calculation, maintaining a power fraction per the sixth region less than 20%, and a second criteria isolating the hottest channel in one additional region and the other ones with a power fraction less than 20%. Tables 6.5 and 6.6 show the final power distribution obtained.

Table 6.5. Number of channels assigned to LAPUR for channel decay ratio calculations

State point	Channel 1	Channel 2	Channel 3	Channel 4	Channel 5	Channel 6
012991	91	100	108	127	122	76

Power fraction	0.19863	0.19964	0.19833	0.19984	0.15016	0.05342
----------------	---------	---------	---------	---------	---------	---------

Table 6.6. Number of channels assigned to LAPUR for channel decay ratio calculations.

State point	Channel 1	Channel 2	Channel 3	Channel 4	Channel 5	Channel 6	Channel 7
012991	1	91	100	109	127	120	76

Reactor conditions at the beginning of the event are illustrated in table 6.7.

Table 6.7. Number of channels assigned to LAPUR for channel decay ratio calculations.

System pressure	969.1 psia
Core inlet enthalpy	477.97 btu/lb
Core power	1180.7
Core flow rate	25.940E6 lb/h
Bypass flow rate	1.0631E6 lb/h

6.15.4 LAPUR 6 Results

SIMULATE and LAPUR core pressure drops are consistent. A summary of these results is shown in table 6.8.

Table 6.8. SIMULATE-LAPUR pressure drops comparison

State point	SIMULATE core pressure drop (psi)	LAPUR core pressure drop (psi)	Error (%)
012991	5.811	5.841	0.525

Additionally, the consistence between flow distribution from SIMULATE and LAPUR has been verified. Results are shown in Table 6.9.

Table 6.9. Comparison of SIMULATE and LAPUR flow rate channels

State Point 012991	SIMULATE (lb/h)	LAPUR (lb/h)	Error (%)
Channel 1	464754	455640	-1.961
Channel 2	522561	514090	-1.621

Channel 3	574250	567400	-1.193
Channel 4	685725	684480	-0.182
Channel 5	648533	663360	2.286
Channel 6	238338	248790	4.385

6.15.5 Decay Ratio Values Analysis

Execution for wide-core decay ratio—global decay ratio is directly obtained from LAPURW output file.

Execution for channel decay ratio—Channel decay ratio is also obtained from LAPURW output file.

Out of phase decay ratio is calculated. An estimated value of the eigenvalue for the first harmonic flux solution (-1.06\$) has been used.

The core-wide, out of phase, and the highest value of the individual thermal-hydraulic channel decay ratios (the hottest channel) are provided in table 6.10.

Table 6.10. State point 290191 decay ratio values.

Power (MW)	Flow (Mlb/h)	Core decay ratio	Frequency (Hz)	Channel decay ratio (1HC)	Out of phase decay ratio (-1.06\$)
1108.4 (40.8)	25.94 (30.7%)	0.75	0.41	0.69	0.78

The high value of hottest channel decay ratio indicates the high susceptibility of the core to oscillate locally and out of phase.

6.15.6 APRMs Signal Analysis

APRMs signals are available from the event, as shown in figure 6.69. Applying Welch's method with a Hanning window to APRM A, the periodogram in figure 6.70 is obtained. A double peak is clearly identified: the natural frequency and one harmonic, the double of the natural frequency. During BWR unstable oscillations, the fundamental mode of oscillation does not appear alone, but it appears to be always accompanied by at least the first axial oscillation mode. From observations of actual reactor instability tests and

3-D code simulations, it appears that the fundamental mode always excites at least the first axial mode (and probably all higher axial mode harmonics). This fact is an apparent paradox because, in principle, the different harmonic modes are orthogonal to each other, and therefore, one cannot excite the other. In summary, this effect can be explained by the fact that the reactivity feedback is nonlinear, and thus, linear mode orthogonality theorems do not apply [10].

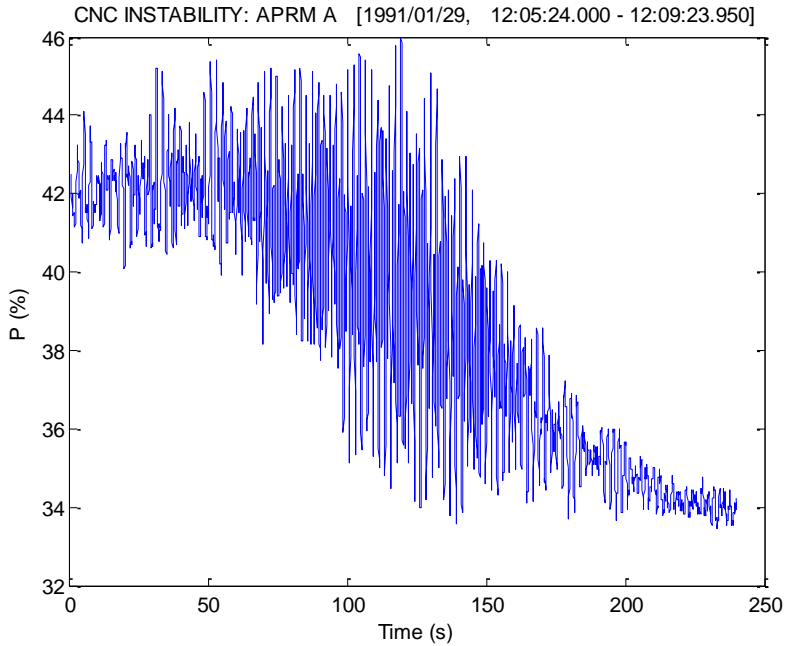


Figure 6.69. APRM A 1991/01/29 Cofrentes instability event.

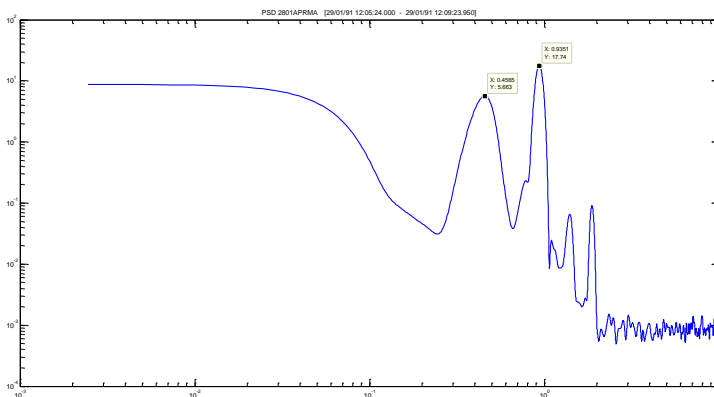


Figure 6.70. PSD based on Welch's method periodogram (290191 Cofrentes instability).

If a standard filter with a pass-band frequencies (0.3–1.3 Hz) is applied, as has been applied for analyses shown previously in this report, the mode with highest DR in the band is obtained which corresponds with the first axial mode (Table 6.11) and cannot be compared with wide-core decay ratios obtained from LAPUR.

In order to obtain autocorrelation-based decay ratios from fundamental mode and from the first axial oscillation mode, two types of notch Butterworth filter (Figure 6.71) have been applied to APRM signals in order to split up fundamental and first axial modes and obtain decay ratio separately. Figure 6.72 shows the effect of filters application in PSD. Results of applying a standard filter, filter type 1 and filter type 2, and filter specifications are shown in table 6.11.

Table 6.11. Filters applied to APRM signal

	Filter 1	Filter 2
Pass-band frequencies	[0.3–0.6] Hz	[0.7–1.3] Hz
Stop-band frequencies	[0.2–4] Hz	[0.6–4] Hz
Pass-band ripple	1 dB	1 dB
Stopband attenuation	20 dB	20 dB

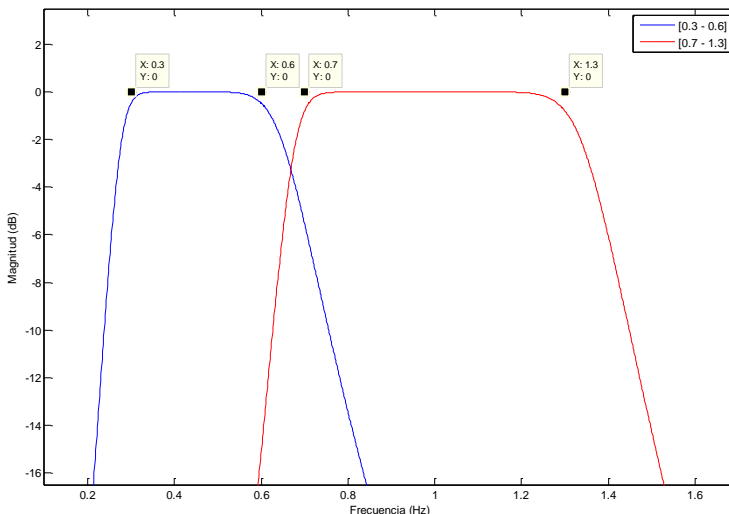


Figure 6.71. Bode diagram of applied Butterworth filters to split up fundamental and first mode.

6.16 LPRM AND APRM DECAY RATIO AND FREQUENCY VALIDATION

Validations above are based on APRM data. Standard data acquisition system of the plant gives high enough sampling rate only for eight selected LPRMs (one from each APRM) selected from the 33×4 levels = 132 LPRMs in the core. However, noise analysis of these LPRMs does not produce consistent noise analysis results. For decay ratio monitoring purposes, the availability of LPRM data with good properties in terms of noise quality is important. Capabilities for local analysis, coherence, and phase are welcome as well.

After searching the market for data acquisition systems with optima sampling rates and high-amplitude resolution in an analog-to-digital converter (16 bits), a RTP2316-M system was selected. The RTP2316-M Data Acquisition System was developed by RTP, a company with broad experience in the field of nuclear engineering. The model is a version of the RTP2300, which has been qualified as 1E Safety Class.

The system consists of the following:

- RTP2300-M chassis with 8 hot-swappable I/O cards with power input options of 115 V AC at 2.1 A, 230 V AC at 1.1 A or 24 V DC at 8 A. The chassis contains a dedicated PLD processor to perform I/O scanning.
- One node processor card, with a Mobile Intel Celeron Processor and 2 PCI-based 100 MHz full-duplex Ethernet controllers for input/output (I/O) communications.
- Two analog input cards: 8436/51 isolated analog input cards with eight input channels for ± 10 V input data. Each of the eight channels is isolated with an anti-aliasing low-pass filter, multiplexed, and amplified before entering to a 16 bits bipolar A/D converter.
- Ethernet output connections to a computer for data collection.

APRM-C and related LPRMs analog volts data were connected to RTP2316-M input cards (Table 6.13).

Table 6.13. RTP2316-M input channels

Signals for each channel from RTP 8436/51 analog input cards		
Card 1	Card 2	Channel
APRM C	14-47A	CH0
22-23B	14-15A	CH1
22-23B → OPTOISOLATOR	46-15A	CH2
38-39B	46-31C	CH3
LOOP A JP FLOW	14-31C	CH4
LOOP B JP FLOW	30-47C	CH5
DOME PRESSURE	30-15C	CH6
38-07B	38-23D	CH7

APRM-C was bypassed in order to guarantee that any spurious signal could progress to any channel of the reactor protection system (RPS) due to was only a temporary connection. LPRM 22-23B was connected through an optoisolator to verify its effect in the noise quality.

6.16.1 New Data Acquisition System Test during Cycle 18 Sequence Exchanges (June 2010, September 2010)

During two consecutive control rod sequence exchanges, June and September 2010, data was taken according to table 6.13 scheme.

The June 2010 control rod sequence exchange, as shown in figure 6.73, includes the verification of power flow map rod lines, specifically the 80% rod line.

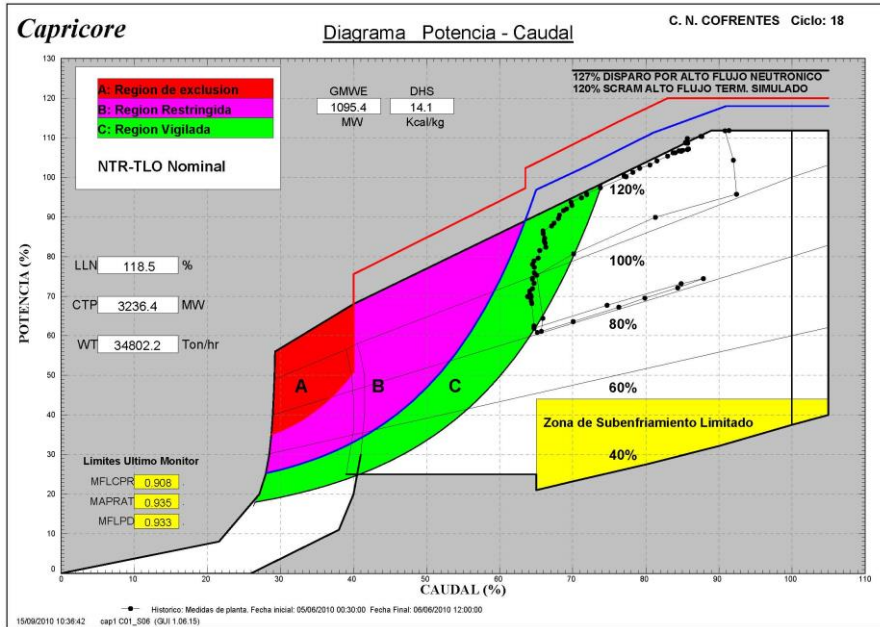


Figure 6.73. June 2010 control sequence exchange roadmap.

Figure 6.74 (September 2010) shows a typical control rod sequence exchange. As can be seen in figures, control rod exchange is carried out between in the region C, E1A monitoring region. Conservatively, the right boundary of this region is considered the locus of power flow map conditions with a wide-core decay ratio of 0.4.

The procedure is clear: recirculation FCV closing to 70% of core flow; control rod insertion to 60–50% of power; sequence exchange at low power to minimize pellet clad interaction (PCI) contact in cladding; withdraw control rod to reach the PCI envelope; and finally increase core flow opening recirculation FCV, maintaining an increase of power around 20 MWe/h (60 MW thermal/h).

6.16.2 Signal Analysis

Signal quality results are summarized in figure 6.75.

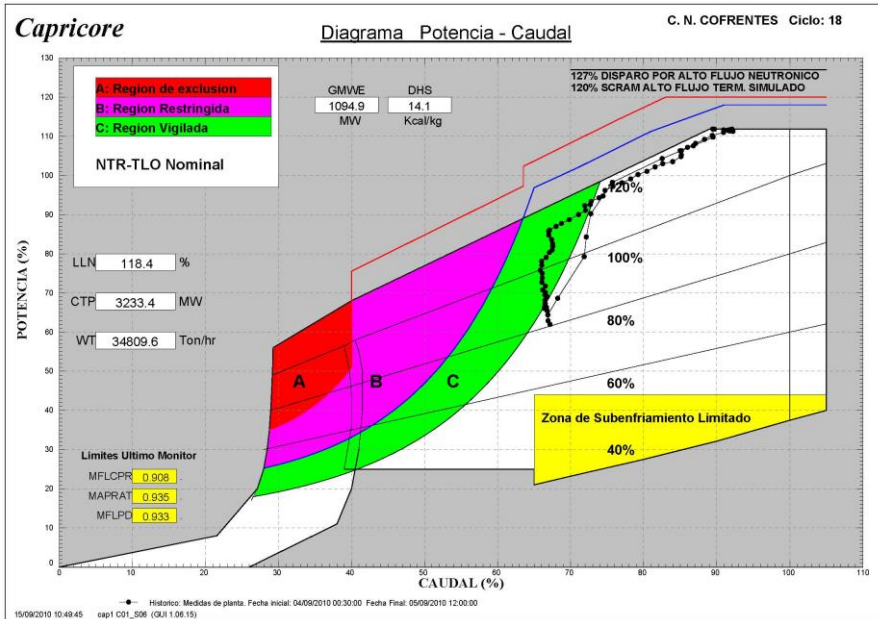


Figure 6.74. September 2010 control sequence exchange roadmap.

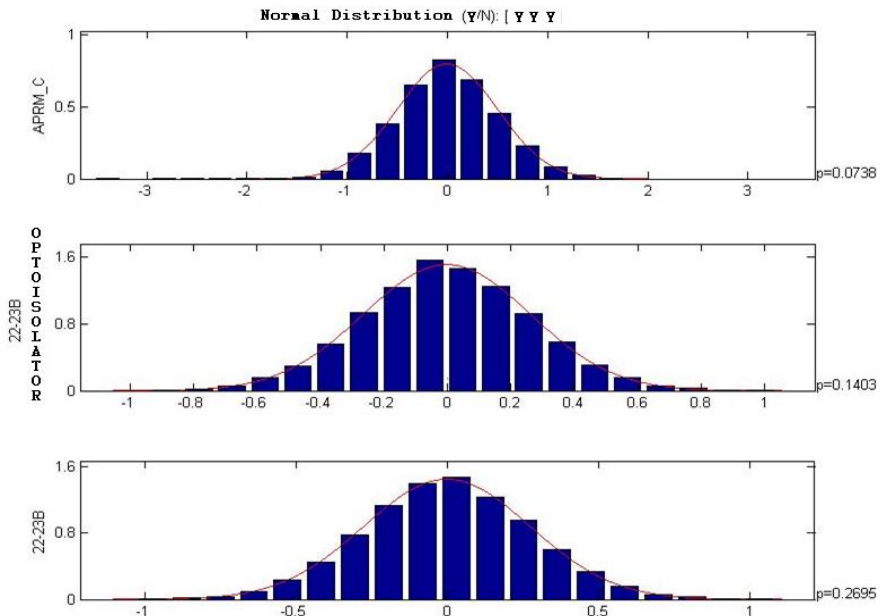


Figure 6.75. Histogram of APRM-C and LPRM 22-23B with and without optoisolator.

Applying the Kolmogorov-Smirnoff normality test to the signal indicates in some cases that noise distribution is normal. The test is not satisfied in all of the cases, but the appearance of the histogram shows a clear normality of signals. Gaussian noise is expected for conditions where the signal is not to be highly autocorrelated (low decay ratio). In case of high decay ratio values, the distribution would look like a sinusoid in Gaussian noise. The distribution of LPRM signal through the optoisolator seems to be unaffected from a statistics standpoint.

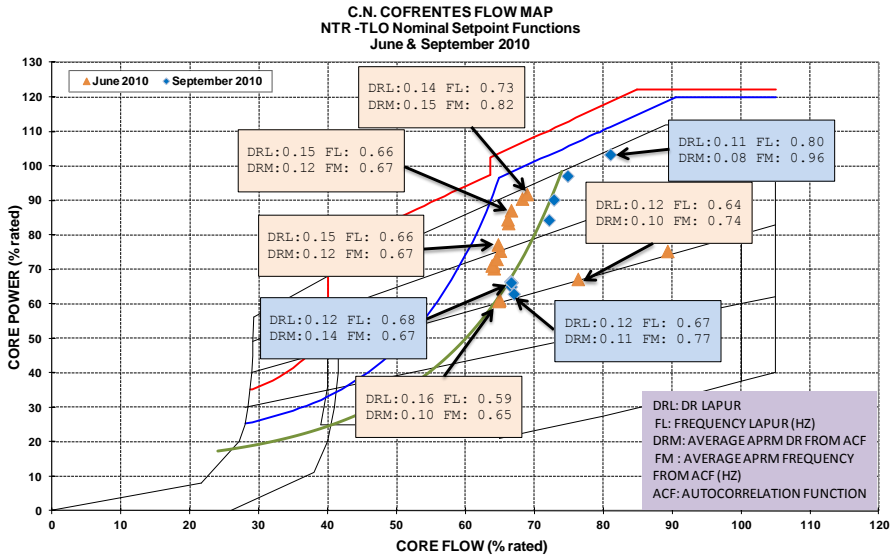
6.16.3 Decay Ratio Results

In figure 6.76 a sample of June and September 2010 decay ratio values is shown. First of all, decay ratio values are lower than 0.2 for all of the state points.

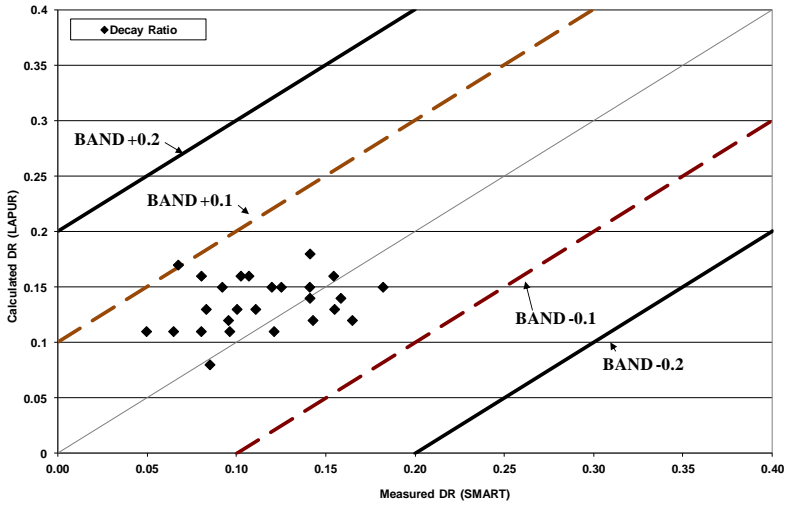
Frequency and decay ratio trends seem to be reasonable. There is a higher inaccuracy in frequency estimation from autocorrelation function, especially for high flow and low decay ratios.

Figures 6.77 and 6.78 show the decay ratio and frequency agreement comparing autocorrelation and LAPUR-based data, respectively.

Decay ratios obtained are smaller than 0.2. Frequencies based on autocorrelation are higher than those predicted by LAPUR, especially for high core flow (higher than 70%). Decay ratio from these state points is very low, and this could cause numerical difficulties in determining the frequency from the autocorrelation function.



DR measured-calculated comparison



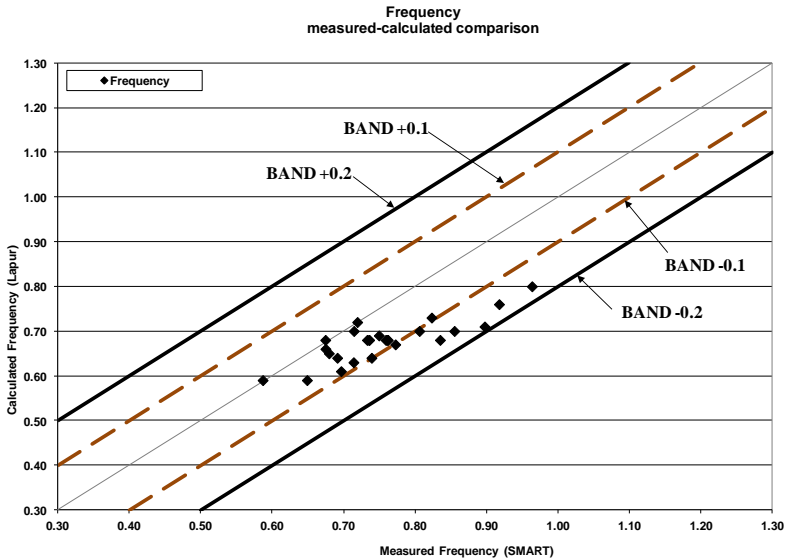


Figure 6.78. June and September 2010 maneuver—frequency comparison.

6.16.4 LPRM Data

Due to better noise resolution capabilities of the RTP system, decay ratios from LPRMs can be obtained.

Figure 6.79 shows reasonable agreement among LPRM, APRM C and LAPUR decay ratios taking into account the increased noncorrelated noise, which LPRM signal usually contains.

Figure 6.80 shows the frequency comparison. The agreement is very good until the frequency is less than 0.8 Hz for signal and 0.7 Hz from LAPUR, for a core flow less than 70%. Decay ratio from these state points is very low, and this could cause numerical difficulties in determining the frequency from the autocorrelation function.

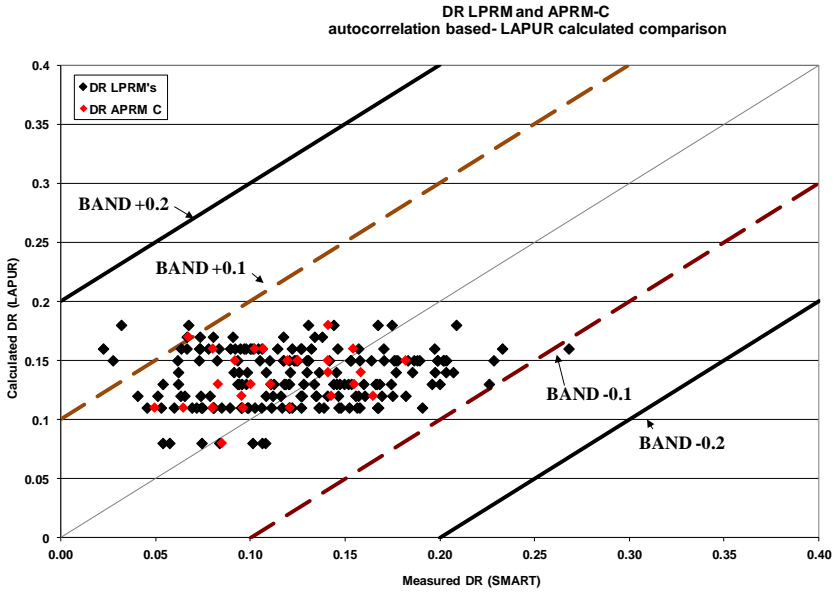


Figure 6.79. LPRM and APRM-C decay ratio from autocorrelation versus LAPUR decay ratio comparison—September and June 2010 sequence exchange.

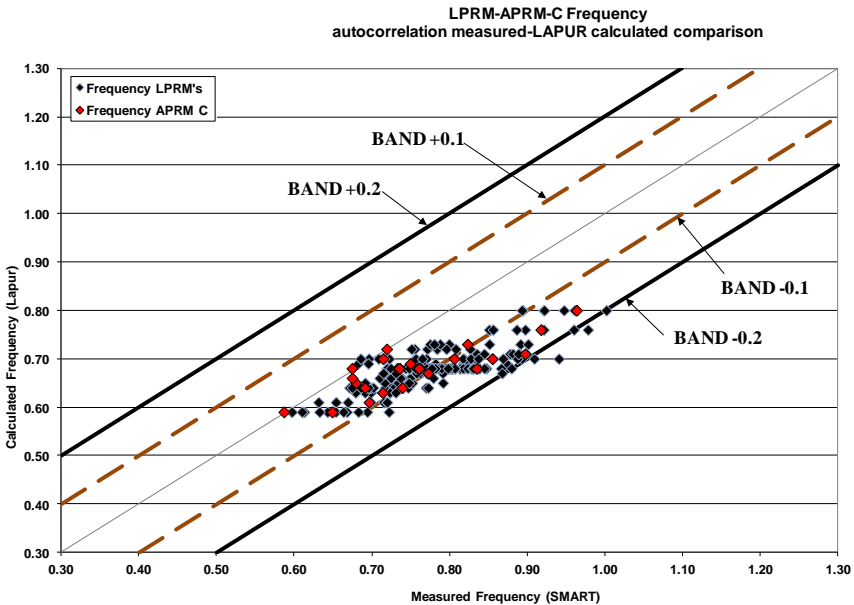


Figure 6.80. LPRM and APRM-C frequency autocorrelation-based versus LAPUR decay ratio comparison—September and June 2010 sequence exchange.

6.17 STABILITY MARGIN SENSITIVITIES DURING CORE DESIGN WITH LAPUR

Once the nuclear bundle design and the number of fresh fuel are defined there exists the possibility of optimizing stability margins for the core design.

The aim of this chapter is to show the sensitivity of the radial power distribution to the wide and hot decay ratio of calculated with LAPUR 6 and how this sensitivity is consistent with the expected results.

In Cofrentes cycle 18, 112 TYPE A and 136 TYPE B will be incorporated as fresh fuel bundles in the core design. Previous experience has indicated that, specifically, stability behavior of TYPE B is slight worse than TYPE A and TYPE C. Wetted perimeter is significant higher for TYPE B than the other coexisting fuel designs, and this feature is not enough compensated for minimizing spacer pressure drop in the two-phase locations of this design. In this context, the power distribution mismatch between fresh fuel designs is important for stability.

If the power contribution per bundle from TYPE B is higher than the power contribution for TYPE A, and TYPE B is operating at higher relative peaking factor than TYPE A, there exists a loss of stability margin. This power per bundle must be similar not only in average but the relative peaking factor distribution must be similar. The loss of stability margin would lead to modify necessarily the E1A related safety setpoints required for stability protection, reducing the stable operating domain with a very important impact in operational flexibility.

The stability margin is established performing a comparison with a previous cycle, cycle 10, which is used as a reference, which shows the degradation of stability margin since cycle 10. Fourteen state points has been run. The E1A methodology [49] establishes that the average plus one standard deviation of the differences, called fbias, determines the size of stability protection regions and the set points of the E1A stability safety systems. There are two fbias: one for wide core decay ratio and a second one for hot channel. For hot channel we have plenty of margin; new design has better performance than previous designs.

However if the wide core fbias was higher than 0.19 we would have to regenerate stability regions and generate new safety set points to reduce the stable domain. This fbias is the base for the actual stability safety system. The mechanism to translate this fbias to safety set points is very complex and is out of the scope of this chapter. In cycle 17 we have obtained a core fbias of 0.18, we have only 0.01 of margin, very small margin.

If it is possible in core design to distribute TYPE A and TYPE B to get similar relative peaking factor per bundle, the stability margin is improved.

We are going to explain the effect with three examples in the next sections.

6.17.1 Example 1 BOC-DF018

This core design corresponds with the design used to determine the bundle design.

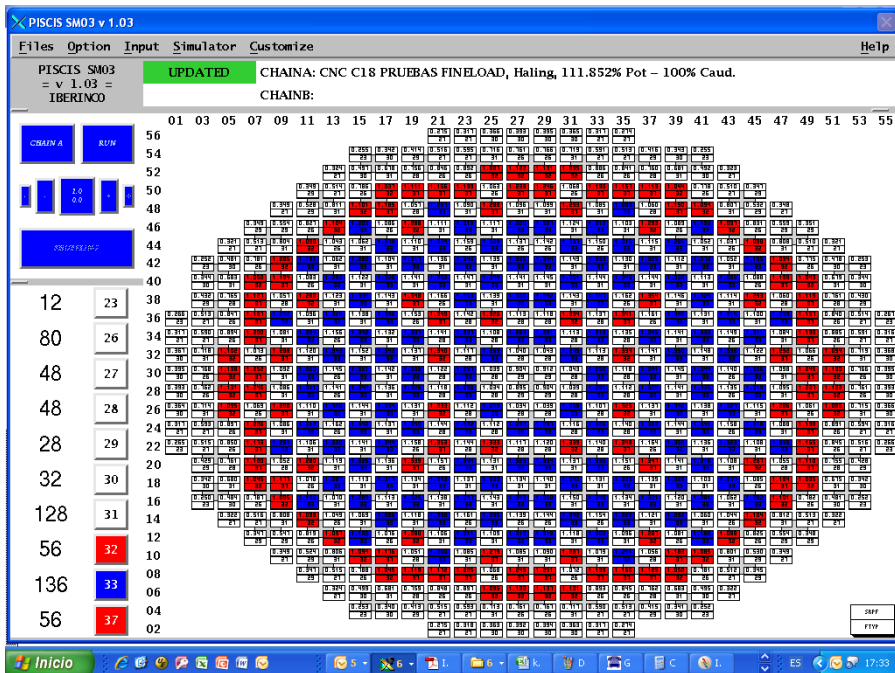


Figure 6.81. BOC-DF018-VARIANTE MAP. Distribution of TYPE B (blue) and TYPE A (red) in this example

In the figure 6.81 the pattern is shown. Sixteen TYPE A are located at an internal square area and the rest of TYPE A are located in an external ring. With this fuel design distribution is reasonable the existence of a mismatch in the power distribution of TYPE B and TYPE A.

The better way to capture the effect in radial peaking factor for each fuel designs is to draw a histogram. The figure 6.82 shows the histogram of relative peaking factor for each design. It can be appreciated that the majority of TYPE B bundles show a relative power peaking higher than TYPE A. TYPE A shows a more flat power distribution covering a wide range of relative peaking factors.

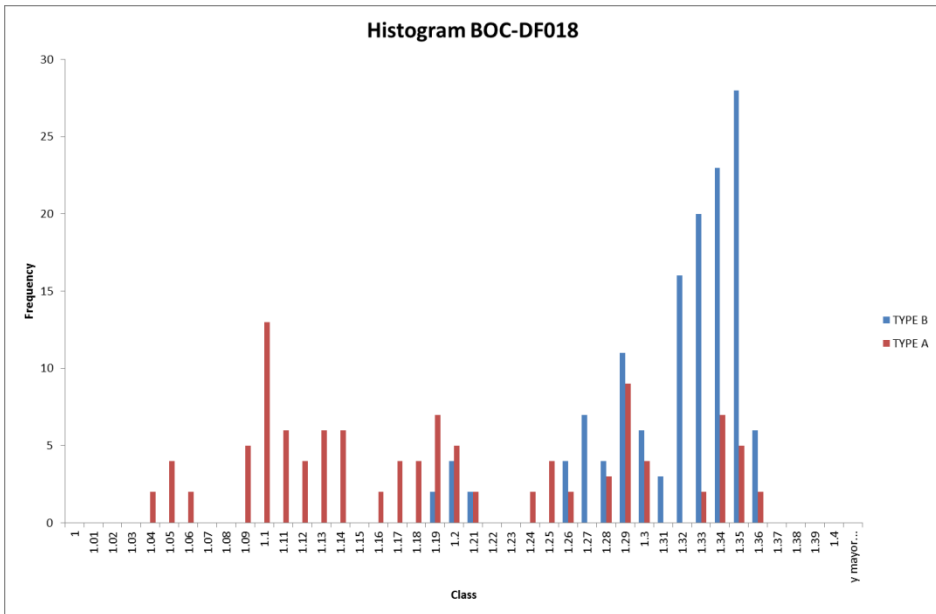


Figure 6.82. Histogram of relative peaking factors for TYPE A and TYPE B

Table 6.14 shows the fbias obtained for this example. The hot channel is for the limiting design, in our case TYPE B. The hot channel fbias is negative, we have plenty of margin. However, if the wide core fbias was higher than 0.19, we would have to regenerate stability regions and generate new safety set points to reduce the stable domain. This fbias is the base for the actual stability safety system. In this case we have only a 0.02 of margin.

Table 6.14. Fbias obtained for the example 1.

Case	Power (MW)	W (%)	DR core C10	DR core C18	DR CHANNEL C10	DR CHANNEL C18
fbias1	1417.8456	30	0.87	0.97	0.34	0.26
fbias2	1466.5536	32	0.79	0.91	0.28	0.19
fbias3	1514.9664	34	0.67	0.81	0.24	0.14
fbias4	1563.084	36	0.58	0.73	0.2	0.1
fbias5	1610.6112	38	0.53	0.69	0.16	0.07
fbias6	1658.1384	40	0.48	0.65	0.12	0.05
fbias7	1705.3704	42	0.44	0.61	0.09	0.03
fbias8	1752.3072	44	0.4	0.56	0.07	0.02
fbias9	1798.9488	46	0.35	0.51	0.05	0.01
fbias10	1845.2952	48	0.31	0.47	0.03	0.01
fbias11	1891.3464	50	0.27	0.42	0.02	0
fbias12	1937.1024	52	0.25	0.4	0.02	0
fbias13	1982.8584	54	0.23	0.37	0.01	0
fbias14	2028.024	56	0.21	0.35	0.01	0
			Core fbias	0.17	Channel fbias	-0.02

6.17.2 Example 2 BOC-DL056-VARIANTE

In the figure 6.83 the core design, named BOC-DL056-VARIANTE, is shown. There is a central ring with TYPE B and there are also two zones where the different designs are located. TYPE A is located in a central cross and TYPE B is located filling available spaces between the ‘blades’ of the TYPE A location. Figure 6.84 shows the histogram of relative peaking factor for each design. It can be appreciate that the majority of TYPE B bundles show a relative power peaking higher than TYPE A. TYPE A is divided basically in two classes: one half with a higher power but the other half with less power than the majority of TYPE B. You have an average power per bundle similar in both designs but the relative power peaking factors are very dissimilar.

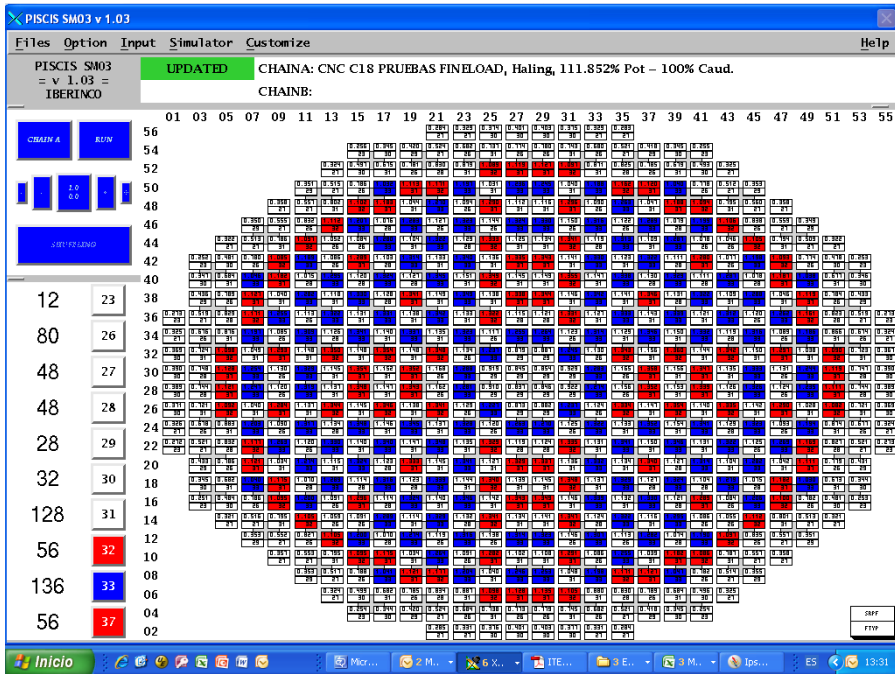


Figure 6.83. BOC-DL056-VARIANTE MAP. Distribution of TYPE B (blue) and TYPE A (red) in this example.

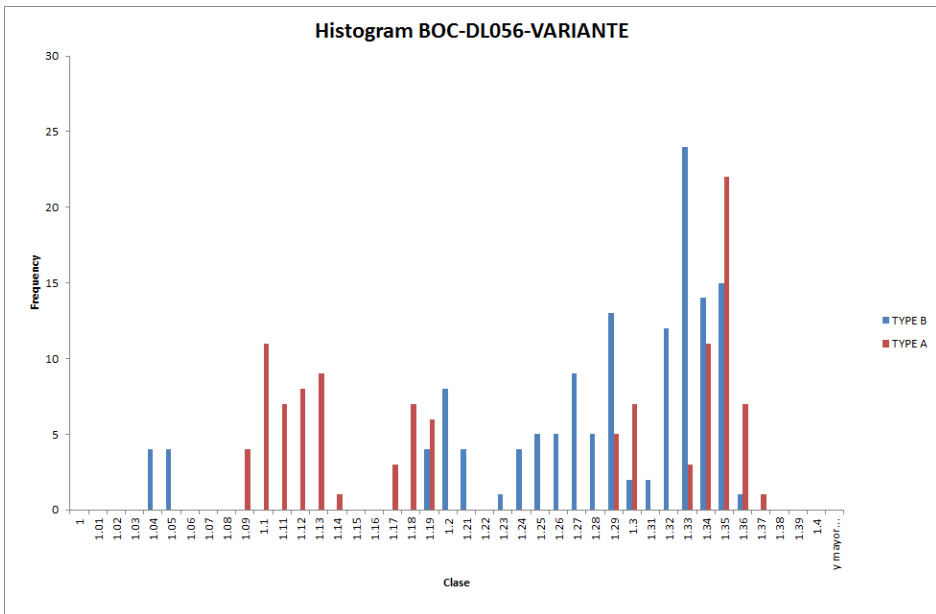


Figure 6.84. Histogram of relative peaking factors for TYPE A and TYPE B.

Table 6.15 shows the fbias obtained for this example. The hot channel is for the limiting design, in our case TYPE B. The hot channel fbias is negative, we have plenty of margin

However, if the wide core fbias was higher than 0.19, we would have to regenerate stability regions and generate new safety set points to reduce the stable domain. This fbias is the base for the actual stability safety system. In this case we have only a 0.02 of margin.

Table 6.15. Fbias obtained for the example 2.

Case	Power (MW)	W (%)	DR core C10	DR core C18	DR CHANNEL C10	DR CHANNEL C18
fbias1	1417.8456	30	0.87	0.97	0.34	0.25
fbias2	1466.5536	32	0.79	0.9	0.28	0.19
fbias3	1514.9664	34	0.67	0.81	0.24	0.14
fbias4	1563.084	36	0.58	0.73	0.2	0.1
fbias5	1610.6112	38	0.53	0.69	0.16	0.07
fbias6	1658.1384	40	0.48	0.65	0.12	0.04
fbias7	1705.3704	42	0.44	0.6	0.09	0.03
fbias8	1752.3072	44	0.4	0.56	0.07	0.02
fbias9	1798.9488	46	0.35	0.51	0.05	0.01
fbias10	1845.2952	48	0.31	0.47	0.03	0.01
fbias11	1891.3464	50	0.27	0.43	0.02	0
fbias12	1937.1024	52	0.25	0.4	0.02	0
fbias13	1982.8584	54	0.23	0.38	0.01	0
fbias14	2028.024	56	0.21	0.35	0.01	0
			Core fbias	0.17	Channel fbias	-0.02

6.17.3 Example 3 BOC-DO079

In figure 6.85 is shown the core design for this example. As can be seen the fresh fuel designs are more mixed in the core.

In this case the relative peaking factor histogram is shown in the figure 6.86. The histogram clearly reflects that the power distribution is more similar between the fresh designs than previous example.

Table 6.16 shows the results of fbias. As can be seen in table 6.16, the stability margin is better than previous examples due to the similarity of radial peaking factors. In this case we have 0.04 of margin in comparison with the fbias limit 0.19.

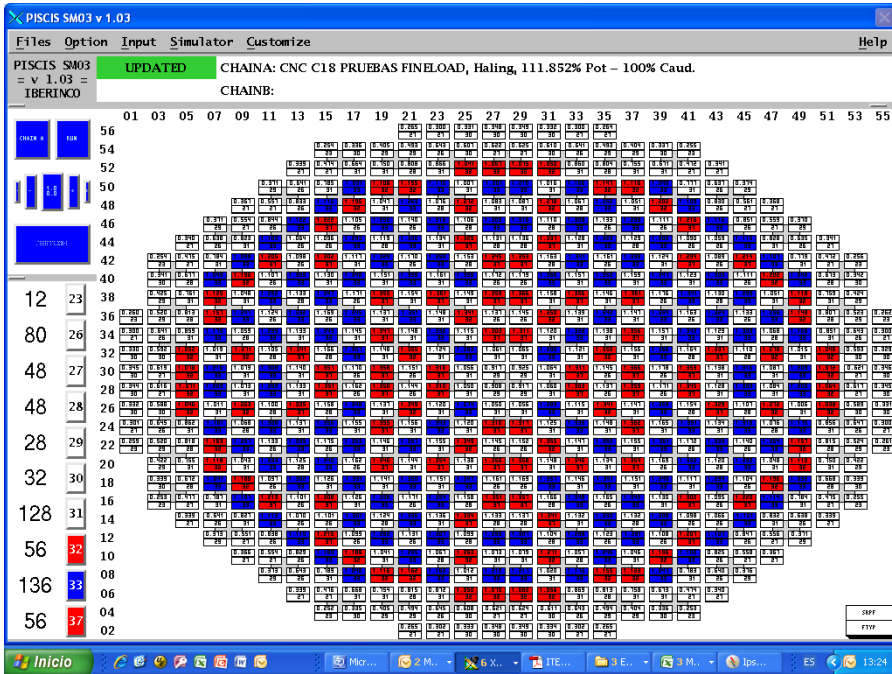


Figure 6.85. BOC-DL0079. Distribution of TYPE B (blue) and TYPE A (red) in this example

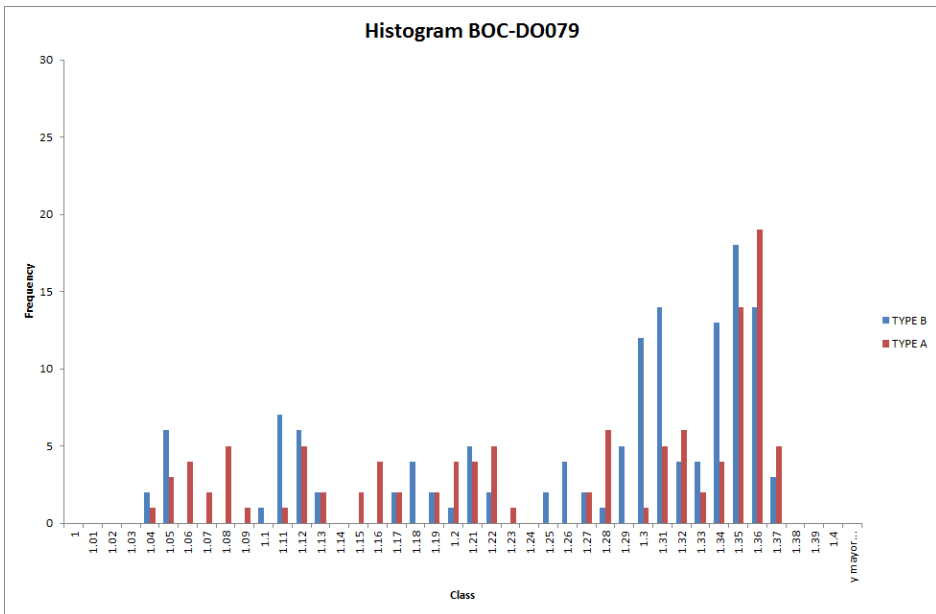


Figure 6.86. Relative peaking factors histogram for this example.

Table 6.16. Fbias obtained for the example 3.

Case	Power (MW)	W (%)	DR core C10	DR core C18	DR CHANNEL C10	DR CHANNEL C18
fbias1	1417.8456	30	0.87	0.95	0.34	0.25
fbias2	1466.5536	32	0.79	0.89	0.28	0.19
fbias3	1514.9664	34	0.67	0.8	0.24	0.14
fbias4	1563.084	36	0.58	0.72	0.2	0.1
fbias5	1610.6112	38	0.53	0.67	0.16	0.07
fbias6	1658.1384	40	0.48	0.63	0.12	0.04
fbias7	1705.3704	42	0.44	0.59	0.09	0.03
fbias8	1752.3072	44	0.4	0.54	0.07	0.02
fbias9	1798.9488	46	0.35	0.49	0.05	0.01
fbias10	1845.2952	48	0.31	0.45	0.03	0.01
fbias11	1891.3464	50	0.27	0.41	0.02	0
fbias12	1937.1024	52	0.25	0.38	0.02	0
fbias13	1982.8584	54	0.23	0.36	0.01	0
fbias14	2028.024	56	0.21	0.34	0.01	0
			Core fbias	0.15	Channel fbias	-0.02

The sensitivity of calculated decay ratio with LAPUR 6 to the radial power distribution of the core and to the fuel design thermal-hydraulic design, highest wetted perimeter and two-phase pressure drop, has been shown by means of three representative examples. The recommendation of a core design with as flatter as possible radial distribution is a powerful mechanism to stabilize the core design is the main learned lesson of this chapter.

6.18 NEW BURNUP-DEPENDENT MODEL FOR URANIA FUEL PELLETT THERMAL CONDUCTIVITY

According to [84]and [85], NRC and Spanish regulatory organism CSN has requested the implementation of a burnup dependent model for urania fuel pellet thermal conductivity in stability codes, in a similar manner as it has been implemented in vendor’s thermal-mechanical fuel codes.

A new version of LAPUR and LIP, called LAPUR 6.1 and LIP 1.2 respectively, [86] have been developed to account for this effect.

6.18.1 LAPUR 6.1 and LIP 1.2 Features

A new option has been added to LAPUR 6.1 through 77-79 input cards of LAPURX module. Card 77 activates the option, card 78 allow us to introduce

burnup in GWd/mT for each fuel type and 79 Gadolinium average concentrations for each fuel type.

Additionally, two minor errors detected in LAPURX have been updated related to coefficients used in the integration of non-recovery pressure losses and derivatives of Jones's two-phase friction correction. The update of these two errors has not any impact neither LAPUR 6.0 nor LAPUR 6.1 results. No modification of LAPURW module is needed.

The correlation for burnup conductivity dependence selected for LAPUR implementation comes from [87]:

$$K = \frac{1}{A + a \cdot \text{gad} + B \cdot T + f(\text{Bu}) + (1 - 0.9 \exp(-0.04\text{Bu}))g(\text{Bu})h(T) + \frac{E}{T^2} \exp(-F/T)}$$

(6.10)

where:

K = thermal conductivity, W/m-K

T = temperature, K

Bu = burnup, GWd/MTU

f(Bu) = 0.00187 · Bu

g(Bu) = 0.038 · Bu^{0.28}

h(T) = 1/(1+396 · e^(-Q/T))

Q = 6380 K

A = 0.0452 m-K/W

B = 2.46E-4 m-K/W/K

C = 5.47E-9 W/m-K³

D = 2.29E14 W/m-K⁵

E = 3.5E9 W-K/m

F = 16361 K

a = 1.1599

gad = weight fraction of gadolinia

As applied in [87] the above model is adjusted for as-fabricated fuel density (in fraction of TD) using the Lucuta recommendation for spherical-shaped pores

$$K_d = 1.0789 \cdot K \cdot \left[\frac{d}{\{1.0+0.5 \cdot (1-d)\}} \right] \quad (6.11)$$

where:

- K= as-given conductivity (reported to apply at 95% TD).
- D= density in fraction of TD.

Note that, according to this correlation the burnup reduces strongly the uranium conductivity. For a third cycle bundle the conductivity degradation is close to a factor of two.

Changes in fuel thermal conductivity affect to fuel transfer function, from which the power generated by the neutronics feeds back the fuel temperature to alter the heat flux from fuel to coolant. A change of fuel thermal conductivity affects the fuel time constant and the conductivity degradation has, in general, a stabilizing effect.

The uncertainty reported in [88] for this correlation goes from a 10% to a 15%. A multiplier of 1.1 has been implemented multiplying the correlation results to cover a 10% of uncertainty on the conservative side.

The implementation of the temperature derivative of the conductivity neperian logarithm has also done for the solution of the fuel dynamic equations.

The implementation of the new model and the miscellaneous updates do not affect to previous LAPUR results when the flag of LAPURX 77 card is deactivated or is not included in the input deck. In table 37 a comparison of results for the fourteen fbias runs for Cofrentes cycle 19, E1A licensing topical results, using the original input deck from [89], are shown. In this table can be seen that results are not impacted for the change of version using the original input deck from LAPUR 6.0.

Table 6.17. Comparison of LAPUR 6.1 and LAPUR 6.0 results with a LAPUR 6.0 input deck.

Case	Power (MW)	W (%)	LAPUR6.1	LAPUR6.0	Diff
fbias1	1417.8456	30	0.89	0.89	0
fbias2	1466.5536	32	0.83	0.83	0
fbias3	1514.9664	34	0.74	0.74	0
fbias4	1563.084	36	0.67	0.67	0
fbias5	1610.6112	38	0.63	0.63	0
fbias6	1658.1384	40	0.58	0.58	0
fbias7	1705.3704	42	0.54	0.54	0
fbias8	1752.3072	44	0.5	0.5	0
fbias9	1798.9488	46	0.46	0.46	0
fbias10	1845.2952	48	0.42	0.42	0
fbias11	1891.3464	50	0.38	0.38	0
fbias12	1937.1024	52	0.36	0.36	0
fbias13	1982.8584	54	0.33	0.33	0
fbias14	2028.024	56	0.31	0.31	0

In a second step the burnup fuel conductivity dependence will also be considered.

Card 77 activates a flag, card 78 allows us to introduce the burnup for each fuel type and card 79 allows us to introduce weight fraction of gadolinia which will be conservatively set to zero.

Table 6.18. Effect of gap conductance increase and burnup fuel conductivity dependence in LAPUR 6.1.

case	Power (MW)	W (%)	LAPUR6.1	LAPUR6.0	Diff
			new conductance burnup dependent conductivity	Original results	
fbias1	1417.8456	30	0.8	0.89	-0.09
fbias2	1466.5536	32	0.75	0.83	-0.08
fbias3	1514.9664	34	0.66	0.74	-0.08
fbias4	1563.084	36	0.6	0.67	-0.07
fbias5	1610.6112	38	0.56	0.63	-0.07
fbias6	1658.1384	40	0.52	0.58	-0.06
fbias7	1705.3704	42	0.48	0.54	-0.06
fbias8	1752.3072	44	0.44	0.5	-0.06
fbias9	1798.9488	46	0.41	0.46	-0.05
fbias10	1845.2952	48	0.37	0.42	-0.05
fbias11	1891.3464	50	0.34	0.38	-0.04
fbias12	1937.1024	52	0.32	0.36	-0.04
fbias13	1982.8584	54	0.3	0.33	-0.03
fbias14	2028.024	56	0.28	0.31	-0.03
				average	-0.05785714

As it can be seen in table 6.18, the introduction of a burnup dependent fuel conductivity has a stabilizing effect (an average of -0.06) and the increase of gap conductance does not compensate for the effect. This stabilizing non-compensated effect has been also observed by the fuel vendors [90][91].

Even though the effect is clear under a physics standpoint and measurement has been taken only in steady state, the stabilizing effect in the fuel time constant is larger than expected.

6.18.2 Update of Methodology for Calculation of Core and Channel Decay Ratios with LAPUR

The interrelation of the physical mechanisms governing the dynamic response of a BWR core is schematically represented in figure 4.1. As depicted in this figure, a disturbance of reactivity can enter the core via either control rod actuation or changes in coolant parameters such as inlet subcooling, flow rate or pressure. Any of these disturbances results in a change in the neutron population that varies the void content in the core which in turn affects the

neutron population. If there were no time delays in the physical processes involved in the system response to a disturbance, the possibility for dynamic instability or oscillations about the new equilibrium value, would not exist. However, the combination of the heat transfer time delay in the fuel (5 to 7 seconds) and the finite sweeping time of void perturbations in the core, can cause self-sustained oscillations of power. The magnitude of the void reactivity coefficients, length of the boiling region in the core, void sweep speed and fuel time constant, are the most important parameters affecting the dynamic stability of the BWR core.

Another mechanism that adds negative reactivity feedback to the core is the Doppler effect. This effect is due to the temperature dependence of the parasitic absorption of neutrons of the U-238 in the fuel. The magnitude of the Doppler reactivity feedback is small compared with the void reactivity, but its immediacy makes it (i) an extremely important factor during large transients, and (ii) a stabilizing agent, even if secondary, for small perturbation transients.

If the fuel time constant accounts for burnup, and a consistent gap conductance is used, point kinetic model and void reactivity coefficient are the main source of uncertainty in the methodology.

Without considering the effect of burnup in conductivity the section 5.3 of chapter 5 is established a correction in void reactivity coefficient. Calculated SIMULATE coefficients in analyzed cases resulted to be higher than LAPURW output coefficient directly evaluated from PAPU reactivity coefficient. For this reason, and since to the least square method error generates an uncertainty in these values (see above), correcting LAPURW output coefficient was considered as a conservative criterion.

There is a multiplier called REAMUL (LAPURW input card 28) that allows us to correct density reactivity coefficients. By means of REAMUL coefficient, the core averaged density reactivity coefficient from LAPURW output file will be corrected up to be equal to the average value obtained from all of the Moderator Temperature Coefficient and Pressure perturbation serie in SIMULATE. This average density coefficient was considered the best estimated value to make consistent with the density coefficient of LAPURW OUTPUT. An error less than 1% is accepted.

Considering the burnup effect in fuel conductivity this correction is clearly underestimated. Applying a 1.1 multiplier to REAMUL results can be seen in table 6.19 This multiplier is justified by the existing scatter in the calculated SIMULATE reactivity coefficient. Now, the average error is close to zero (-0.004). Applying E1A methodology the impact in the regions size is negligible. For cycle 19, Fbias, which includes one standard deviation, applied to LAPUR 6.1 is slightly more conservative than cycle 19 Fbias from LAPUR 6.0 results.

Table 6.19. Effect of gap conductance increase, burnup fuel conductivity dependence in LAPUR 6.1 and a 1.1 multiplier in REAMUL.

case	Power (MW)	W (%)	LAPUR6.1 burnup dependent conductivity and 1.1 x REAMUL	LAPUR6.0 Original results	Diff
fbias1	1417.8456	30	0.86	0.89	-0.03
fbias2	1466.5536	32	0.81	0.83	-0.02
fbias3	1514.9664	34	0.72	0.74	-0.02
fbias4	1563.084	36	0.66	0.67	-0.01
fbias5	1610.6112	38	0.62	0.63	-0.01
fbias6	1658.1384	40	0.58	0.58	0
fbias7	1705.3704	42	0.54	0.54	0
fbias8	1752.3072	44	0.5	0.5	0
fbias9	1798.9488	46	0.46	0.46	0
fbias10	1845.2952	48	0.42	0.42	0
fbias11	1891.3464	50	0.39	0.38	0.01
fbias12	1937.1024	52	0.37	0.36	0.01
fbias13	1982.8584	54	0.34	0.33	0.01
fbias14	2028.024	56	0.32	0.31	0.01
				average	-0.00357143

6.18.3 Changes in LAPUR Methodology Due to the Introduction of a Burnup Dependent Conductivity

According to the results from sensitivity studies in previous sections, the changes in the methodology could be summarized as:

- Incorporation of a burnup dependent fuel conductivity model on the conservative side.

- Incorporation of an extra multiplier of 1.1 through REAMUL card obtained from matching core averaged density reactivity coefficient from LAPURW output to the average value obtained from all of the Moderator Temperature Coefficient and Pressure perturbation series in SIMULATE.

6.19 CHAPTER SUMMARY

Generic validation of the components of pressure drop obtained with the new models implemented in LAPUR 6 r.0 was performed (using default friction models of SIMULATE-3). Comparisons of LAPUR 6 with SIMULATE-3 showed a very good agreement. Components that are dependent on void fractions (elevation and acceleration) showed slight discrepancies due to the void fractions predicted by SIMULATE-3 and LAPUR 6.0 not being equal. However, the relative contribution of these components to the total pressure drop is very low, and the effect can be considered to be negligible.

FRIGG-2 LOOP experimental void fractions data and LAPUR 6 were also compared. Their agreement was similar to those of other codes with three or four equations and dynamic or algebraic slip.

Figures 6.87 and 6.88 show all available Cofrentes plant data from start-up, sequence exchange, and coastdowns.

Reasonable agreement was observed, and the majority of predictions are in the ± 0.1 band. Frequency is reasonably predicted up to 70% of the flow rate (0.7 Hz for LAPUR and 0.8 for autocorrelation-based frequency).

Table 6.20 shows results obtained for Cofrentes instability on January 29, 1991. Agreement for wide-core decay ratio is very good. LAPUR 6 and autocorrelation-based decay ratios and frequency show very consistent results.

Table 6.20. Cofrentes instability results.

State point	Power (MW)	Flow (MLb/h)	Core decay ratio	Frequency (Hz)	Channel decay ratio (IHC)	Out of phase decay ratio (-1.06\$)
012991	1108.4 (40.8)	25.94 (30.7%)	0.75	0.41	0.69	0.78
Autocorrelation-based estimation			0.78	0.47		0.98

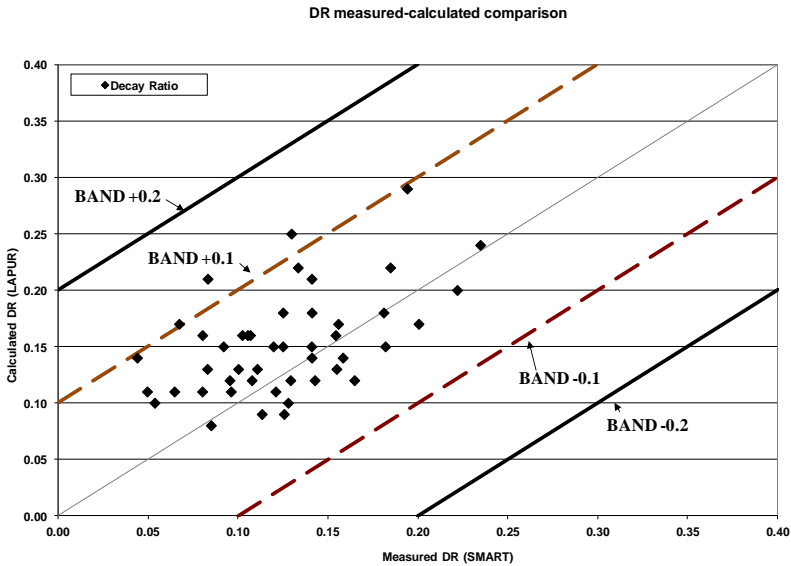


Figure 6.87. Decay ratio autocorrelation based on LAPUR calculation.

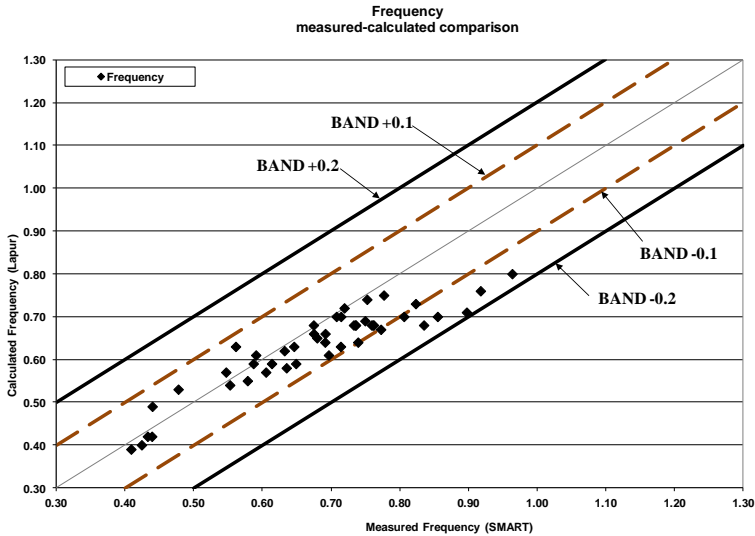


Figure 6.88. Frequency autocorrelation based on LAPUR calculation.

The sensitivity of calculated decay ratios with LAPUR 6 to the radial power distribution of the core and to the thermal-hydraulic applying LAPUR 6 has been shown by means of three representative examples. The recommendation of a core design with as flatter as possible radial distribution is a powerful mechanism to stabilize the core design is the main learned lesson of this chapter.

Finally, a new version of LAPUR and LIP, called LAPUR 6.1 and LIP 1.2 respectively, have been developed to account for the burnup dependence of fuel conductivity. The effect of the implementation of a burnup dependence of fuel conductivity has been separately evaluated.

The evaluation has been performed using data from Cofrentes cycle 19 E1A regions generation and validation topical report. There are not data for fuel types previous to this cycle and used in the qualification to account for this effect. Vendors have only introduced the model in new fuel designs.

According to the results from sensitivity studies in section 6.18, the changes in the methodology required only when burnup dependent fuel conductivity models are available could be summarized as:

- Incorporation of a burnup dependent fuel conductivity model on the conservative side.
- Incorporation of an extra multiplier of 1.1 through REAMUL card obtained from matching core averaged density reactivity coefficient from LAPURW output to the average value obtained from all of the Moderator Temperature Coefficient and Pressure perturbation series in SIMULATE.

Results have shown a similar degree of conservatism when the feedback compensation described above is performed.

7 UNCERTAINTIES OF DECAY RATIO MEASUREMENTS FOR ANALYTICAL CODES QUALIFICATION PURPOSES

One of the main important features in the qualification of analytical methods for decay ratio calculation is the estimation of the uncertainty of the

method used for the estimation of experimental decay ratio through power signal analysis.

The purpose of this chapter is to describe the validation of estimation methods for experimental stability parameters (Decay Ratio and Oscillation Frequency) based on APRM and LPRM signal analysis.

A decay ratio monitor called SMART has been developed by the Universidad Politécnica de Valencia (Spain) jointly with IBERDROLA [93]. The SMART stability monitor, which was developed with MATLAB, will be used for autocorrelation-based decay ratio estimation. The uncertainty of autocorrelation-based decay ratio estimation of SMART will be evaluated in this chapter. This is the only way of determining the real accuracy of LAPUR 6.

7.1 BWR SIGNAL SIMULATOR

There are a lot of BWR models which simulate pretty well the behavior of the reactor, both thermal hydraulics and neutronics. Despite this fact, the signal received through a detector is not clear like a signal from one of these models. Every model simplifies a lot of events to make easier understanding and using it. But if someone wants to simulate a signal just as detectors record it, it is necessary to agree imperfections: noise.

Thie, in a general study on BWR safety [95], proposed that the reactivity $\rho(t)$ could be described by a second order linear differential equation with a Gaussian white noise driving source.

The integration of any BWR reactor model with several independent noise sources must be performed carefully using the modern theory of stochastic differential equations [96], [97]. As pointed Williams [98] there is a great variety of noise sources that can arise in a nuclear plant.

We have chosen the March-Leuba [2] reduced order model which is able to reproduce the phenomenology found in BWR, and has a reactivity model similar to the Thie one. We have added to the model of reactivity of March-Leuba a noise source driving term, as complementary to the temperature feedback term.

On the sections below, it is shown the five equations which rule the model, the transfer function in the frequency domain and the interpretation of a step or a slope on the reactivity.

7.2 REDUCED ORDER MODEL

The equations of the March-Leuba's reduced order model which performs the behavior of a BWR are:

$$\frac{dn}{dt} = \frac{\rho - \beta}{\Lambda} n + \lambda c + \frac{\rho}{\Lambda} \quad (7.1)$$

$$\frac{dc}{dt} = \frac{\beta}{\Lambda} n - \lambda c \quad (7.2)$$

$$\frac{dT}{dt} = An - BT \quad (7.3)$$

$$\frac{d^2 \rho_\alpha}{dt^2} + a_{1c} \frac{d\rho_\alpha}{dt} + a_{1c} \rho_\alpha = kT + b_{d2} dW_2 \quad (7.4)$$

$$\rho = \rho_\alpha + D_F T + b_{d1} dW_1 \quad (7.5)$$

In these equations, we can observe a lot of coefficients: β , λ , Λ , A , B , a_{1c} , a_{2c} , D_f , k , b_{d1} , b_{d2} , which meaning is exposed in the nomenclature. Some of them (β , λ , Λ , A , B , a_{1c} , a_{2c} , D_f) could be obtained from LAPUR, PAPU and SIMULATE's output files. These coefficients will be called parameters of our signal due to the fact that they represent the reactor. The rest of them (k , b_{d1} , b_{d2}) are called user input variables because they are coefficients that define the desired feedback gain or noise intensity and they cannot be obtained using a theoretical model and fitting to it.

7.3 TRANSFER FUNCTION ON FREQUENCY DOMAIN

In order to facilitate the determination of adjust parameters of the model, it will be expressed on the frequency domain in a transfer function.

The system can be represented in two blocks: reactor kinetics ($G(s)$) and Doppler effect and thermal hydraulics feedback mechanisms ($H(s)$).

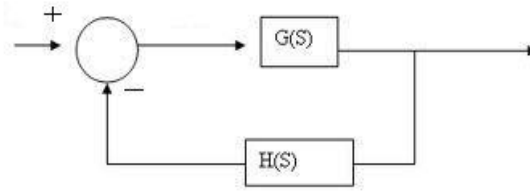


Figure 7.1. Blocks diagram of the system.

$$G(s) = \frac{\partial n(s)}{\partial \rho(s)} = \frac{1}{\Lambda} \frac{(s + \lambda)}{s \left[s + \left(\lambda + \frac{\beta}{\Lambda} \right) \right]} \quad (7.6)$$

$$H(s) = \frac{\partial \rho(s)}{\partial n(s)} = \frac{kA + D_f A (a_{2c} + sa_{1c} + s^2)}{s(a_{2c} + sa_{1c} + s^2)(s + B)} \quad (7.7)$$

It is easy to notice that this is a nonlinear equation system and it has to be linearized to obtain the transfer function of the system. Using the Laplace transformation on the linearized system and operating we obtain the closed loop transfer function:

$$T(s) = \frac{G(s)}{1 + G(s)H(s)} \quad (7.8)$$

$$T(s) = \frac{(s + \lambda)(a_{2c} + sa_{1c} + s^2)(s + B)}{\Lambda s(s + B) \left[s + \left(\lambda + \frac{\beta}{\Lambda} \right) \right] + D_f A (s + \lambda)(a_{2c} + sa_{1c} + s^2) + kA(s + \lambda)} \quad (7.9)$$

The degree of the numerator and the denominator are 4 and 5, respectively. So, it can be assimilated to a transfer function of 4 zeros and 5 poles with a conjugated complex pair of zeros and poles (according to March-Leuba [2])

$$T(s) = \frac{h_1(s)}{h_2(s)} = C \frac{(s - z_1)(s - z_2)(s - z_3)(s - z_3^*)}{(s - p_1)(s - p_2)(s - p_3)(s - p_4)(s - p_4^*)} \quad (7.10)$$

With MATLAB it's easy to find the poles, zeros and the constant C, which represents the transfer function provided by the LAPUR code.

When the user has obtained the coefficients for generating a synthetic signal, it becomes necessary to obtain the corresponding theoretical value for DR and frequency.

7.4 INPUT FILE

7.4.1 Introduction to the Model Parameters

Once the model has been briefly explained it is necessary to identify the parameters which are involved in it and some variables that are necessary for generating the input file. This introduction aims to overview the previous steps which would provide the user the value of the parameters which rule the model.

In order to obtain the transfer function of the behavior of the reactor for a defined setting, the user may have at his disposal the output files of some known codes: PAPU, LAPUR and SIMULATE.

From these codes, it is possible to obtain next coefficients:

D_f : Doppler Coefficient can be obtained using the PAPU code.

β : It is referred to the number of differed neutrons related with the total number of neutrons emitted. There is not only a β coefficient (each differed neutron family has one) but a mean value will be used for the signal generation. It can be also obtained from SIMULATE's output. SIMULATE provides the β for each group and the required mean value (beta-effective).

A : the mean generation time is obtained from the SIMULATE's output (Prompt Lifetime).

A : It is related to the power generated per neutron.

So, attending the five equations model it is only λ , a_{1c} , a_{2c} , B , b_{d1} , b_{d2} and k remaining for determinate.

λ : It is the semidesintegration period of the precursors. It can be obtained using a MATLAB code which has been developed for adjusting the closed loop transfer function values provided by LAPUR to the equation (7.9). This code has been named *zeropole45.m* and it needs *funcobj.m* subroutine in the working directory. It must be run on MATLAB 7.9.0.529 (R2009b).

Zeropole45 must be called introducing 4 arguments: frequencies, and complex value, gain and phase for each frequency. These values are located in

the last lines of LAPURW's output, in a section called CLOSED-LOOP RESPONSE.

Also, it can be also extracted from SIMULATE's output file. Just like has been explained for β , there is not only a value for λ . In this case, the value which will be introduced for the signal generation is the result of the following equation:

$$\lambda = \frac{\sum_i \beta_i}{\sum_i \beta_i / \lambda_i} \quad (7.11)$$

Obtaining λ from two different sources may provide consistence to the coefficients obtained from the fitting.

From this fitting, the user will also obtain:

a_{1c} and a_{2c} : They refer to the parameters for the void reactivity equation.

B : This is a parameter from the heat transfer model related to the heat transferred from the fuel to the coolant.

The zeropole45.m code returns the coefficients ordered like this: λ , B , a_{1c} , a_{2c} . And gain, phase, real response and imaginary response are represented in 4 figures in order to check the fit quality.

Finally, b_{d1} , b_{d2} and k are parameters which cannot be obtained from the fitting. These parameters has to be introduced by trying the values which provide the signal the user is looking for as it will be explained on its respective cards sections.

b_{d1} , b_{d2} : They are parameters related with the intensity of the noise added to the theoretical model. The model contains two types of noise and each of these parameters corresponds to a different type of noise. b_{d1} is referred to the multiplicative one, while b_{d2} refers to the additive one.

k : It is related with the feedback of the model and has a strong influence over DR value. So, the user may try different values of k in order to obtain a signal with desired values of frequency and Decay Ratio.

Finally, in order to observe the response of a monitor to all kind of signal it has been included to the synthetic signal generator the option of generate a BWR response to a slope or a step in the reactivity.

The step signal is conformed introducing the time at which the step will occur and the amplitude of the step. The reactivity (ρ) will remain constant until the step occurs and then it will take the value corresponding to sum the step. The rest of the equations of the model will be conditioned by this one.

The slope signal needs the slope value, the initial time and the final time of itself. It affects to the reactivity just as the step signal and then the effect will be reproduced in the rest of the equations of the system.

7.4.2 Structure

The structure of the input file will be described including some basic rules that has to be taken on account. Afterwards, the coefficients the user has to introduce will be briefly described card by card.

```
*Tipo Calculo. 1=Dr+freq. 2=Dr+freq+Señal sintetica
2
* Tg          beta   lamda
3.66223e-05, 0.0059,0.09
*   A          B
7.0631,0.6031
*   Df
-2.68E-3
* a1c   a2c
4.9537,4.7421
* K
-9.e-2
* y0(i) initial conditions
0.01
0.01
0.1
0.0
0.0
*ttot  timpas
10.,0.05
* bd    bd2
0.6E-6, 0.6E-5
* calculation model pito=1 ito=2
1
* Tipo de Señal: 0=Estacionaria; 1=Escalón; 2=Rampa
0
* Para Escalón Rho-step, tin-step(s); Para Rampa: Rho-slope, tin-slope(s), tfin-slope(s)
5.E-4,10..15.
```

Figure 7.2. Example of input file.

There are some fundamental rules in the construction of the input.

1. The code is programmed for not saving information from the lines starting with a star (*) symbol. That **does not mean that another line with a star will be considered a comment**, but the lines the code will read for information will be the second one, the fourth one, the sixth... and so on.
2. **The code expects all the information in the order it is shown.** I.e. in the second line, the code will read the calculus type; in the fourth line it will read the neutron mean time generation, λ and β ; and so on.
3. If there is more than number in the same line, they will be **separated with a coma (,)**.
4. The entire part will be separated of the decimal one with a point (.
5. The input file has to be named as “**input.dat**”.

7.4.3 Input File Cards

1st CARD

Tipo Calculo

The code can run only to provide theoretical stability parameters of the purposed case or it can generate the signal and calculate these parameters. The user must indicate to the code what results is looking for: a theoretical calculus of DR and frequency (1) or a synthetic signal with the theoretical calculus (2).

2nd CARD

Tg: the mean generation time (λ) is obtained from the SIMULATE's output (Prompt Lifetime).

beta: It is referred to the number of differed neutrons related with the total number of neutrons emitted. There is not only a β coefficient (each differed neutron family has one) but a mean value will be used for the signal generation. It can be also obtained from SIMULATE's output. SIMULATE provides the β for each group and the required mean value (beta-effective).

lamda: It is the semidesintegration period of the precursors (λ). As it has been explained above, it has to be extracted from the fitting of the closed loop transfer function provided by LAPUR to the equation (7.9).

3rd CARD

A: It is related to the power generated per neutron. The equation governed by A comes from this one $\frac{v_f \rho_f c_{pf}}{n_0} \frac{dT}{dt} = Kn - US(T_f - T_c)$, where $v_f \rho_f c_{pf}$ are the fuel volume, density and specific heat capacity, respectively. And $P = Kn_0$ with $K = \frac{30}{\Lambda} 10^{-12}$ given by Lewins [99], so $\frac{dT}{dt} = \frac{P}{v_f \rho_f c_{pf}} n - BT(t)$. Finally,

$$A = \frac{P}{v_f \langle \rho c_p \rangle} \quad (7.12)$$

P is the power of the reactor and the fuel volume can be obtained from the SIMULATE's output. A mean value for the product of fuel density and specific heat capacity has been used $\langle \rho c_p \rangle_f = 3.168 \cdot 10^6 J \cdot K / m^3$.

B: This is a parameter from the heat transfer model related to the heat transferred from the fuel to the coolant. It is obtained from the fitting.

4th CARD

Df: Doppler Coefficient, D_f , can be obtained using the PAPU code. The value that we read on the output of LAPUR or PAPU is a percent value. The user must introduce this value multiplied by 100 in the input file.

5th CARD

a1c and **a2c:** They refer to the parameters for the void reactivity equation a_{1c} and a_{2c} . They are the third and fourth output values from the fitting performed using *zeropole45.m* code.

6th CARD

K: It is related with the feedback of the model and has a strong influence over DR value. The user may try different values of k in order to obtain a signal with desired values of frequency and Decay Ratio. In order to look for the desired value is useful to select the first option in the 1st CARD, so the user

can look for the correct k without waiting to the signal construction. Anyway, it is important to have into account that all the possible values of k have to be negative and that there is a value of this parameter for which DR is equal to 1. From this value, approaching k to zero will reduce de decay ratio.

7th CARD

Initial conditions: These will be the boundary conditions for solving the differential equations system. You may introduce the initial value for each equation in the same order they are defined. It is not possible to define null value for some of the initial conditions but low values are accepted by the code. For example:

1. The first condition is referred to the evolution of the excess of neutrons, so $\delta n(t=0)=0.01$ will be the initial condition: there is not excess of neutrons at the start of the signal.
2. For the precursors population is defined the same initial condition. So, $\delta c(t=0)=0.01$.
3. This is the boundary condition for the heat transfer model. For indicate that there is no heat transfer on $t=0$, $\delta T(t=0)=0.1$.
4. The fourth condition, total reactivity, should be initially $\delta \rho(t=0)=0.0$.
5. And the last one, the void fraction reactivity: $\delta s(0)=-d\rho_v/dt(0)=0$.

In the figure 7.2, these initial conditions have been introduced in the correct form.

8th CARD

The “**GeneradorBWR**” code needs that the user introduces some information that is described in this section for establishing the characteristics of the calculus.

ttot: It means the total time that the code will simulate, the length of the signal. It must be introduced in seconds.

timpas: It refers to the pass of time for next signal point printed. The time pass for solving the integration is established in 1.0E-6 seconds, so this is the

minimum value that can be introduced in this variable. It must be introduced in seconds.

9th CARD

This card includes the parameters related with the desired intensity of noise.

Bd1: It governs the multiplicative noise. This kind of noise produces high peaks that cannot appear in the reactor when a too large value is introduced. In order to determinate a sense value for this parameter, the user may run the signal with $b_{d1}=0$ and increase its value until the produced peaks do not exceed the maximum values with null multiplicative noise in more than 20%. For the Cofrentes' Nuclear Power Plant cases the optimal is usually $b_{d1}=1.0E-6$.

bd2: It governs the additive noise. This one needs a higher order than b_{d1} . The additive noise disturbs the steady state inducing an oscillation in the system. The oscillation may always decay with the same ratio and will provide the DR stability parameter when the monitor evaluates the fluctuations. In order to be coherent with the nuclear power plant, this variable should be adjusted looking for a standard deviation equivalent to that observed on its real signals. In studied cases of Cofrentes, the RMS of the signal is about 1% and the b_{d2} obtained for this level is (for most cases) about $1.0E-4$.

10th CARD

This card is used for indicating the code which method of calculus is expected and for introducing perturbations to the steady state.

Calculation model: there are two integration methods available. If we introduce "1" in this point, the "p order method" will be used. If we introduce "2", the "Taylor strong method" will be used instead.

11th CARD

Signal type: The GeneradorBWR allows the user to generate a steady state signal or to apply a step or a slope in the reactivity in order to obtain different types of signals which can appear in a reactor. This variable is used

or select any of these options. It can take values 0,1 or 2. “0” is for the steady state, “1” for a step incoming signal and “2” for a slope one.

12th CARD

Rho-step/Rho-slope: It is the amplitude of the step or the slope on the reactivity. Do not have any influence for the steady state signal.

tin-step/tin-slope: Here the user indicates the time (expressed in seconds) when the step or slope signal will start to be applied. Do not have any influence for the steady state signal.

tfin-slope: This is only for the slope signal. It refers to the time (expressed in seconds) which ends the slope. Do not have any influence for the steady state signal.

7.5 OUTPUT PROCESSING

The code generates four output files:

1. output.txt General output file with all the coefficients introduced in the code. It can be a checking file for assure the coefficients desired have been read correctly. Furthermore, it contains results for calculus performed by *GeneradorBWR* in order to obtain the final results.
2. DR+Freq.sal Contains the eigenvalues of the jacobian matrix and the calculated value of apparent and asymptotic DR and frequency. Here is indicated the dominating pole.
3. w2joselinois.sal Contains the signal for the five equations in six columns where the first one is the time, followed by each equation solution values.
4. señalmodelobwr.txt Contains only time and neutron excess signal. It is just a copy from the file *w2joselinois.sal* of the signal that would be more useful.

Next, it will be exposed more accurately the outputs containing all the information of the generated signal.

7.5.1 File DR+Freq.sal

This file provides the user the theoretical value of Decay Ratio and frequency for the coefficients of the model that will be used for generate the signal. For obtaining only the DR and frequency, **GeneradorBWR.exe** must be called with a 1 in the second line of the input file.

Once completed an input file, the user runs the executable and obtains an output called '**DR+Freq.sal**'. This file contains in its first lines the eigenvalues of the Jacobian matrix of the system in the equilibrium point defined.

```

Autovalores del Jacobiano

AUTOVALOR PARTE REAL-0.2210449E+03 PARTE IMAGINARIA 0.0000000E+00
AUTOVALOR PARTE REAL-0.1539993E+00 PARTE IMAGINARIA 0.2000120E+01
AUTOVALOR PARTE REAL-0.1539993E+00 PARTE IMAGINARIA-0.2000120E+01
AUTOVALOR PARTE REAL-0.2828132E+01 PARTE IMAGINARIA 0.0000000E+00
AUTOVALOR PARTE REAL-0.8148329E-01 PARTE IMAGINARIA 0.0000000E+00

El polo dominante no es el polo complejo conjugado

Polo dominante          5
Polo conjugado          2

DR_Asintótica= 0.616 Freq= 0.318
DR_Aparente= 0.617 Freq= 0.318

```

Figure 7.3. DR+freq.SAL

Obviously, there are 5 eigenvalues: three of them are real and the other two are a couple of conjugated complex poles. Each of these complex poles can be written as $\lambda_j = \alpha_j \pm i w_j$ (real part and imaginary part), and system's solution must be a linear combination of the poles as it is shown below:

$$y(t) = \sum_j C_j v_j e^{\lambda_j t} \quad (7.13)$$

where C_j are constants and v_j are the eigenvalues of the Jacobian matrix.

In order to obtain a valid value of the Decay ratio of the signal it will be necessary to differentiate between “Apparent Decay Ratio” and “Asymptotic Decay Ratio”. The first one takes on account the more instable real pole and the complex conjugated poles, meanwhile the second one will only include the complex conjugated poles for the calculus.

So, according to the eigenvalues of the Jacobian matrix, the frequency will be fixed by the imaginary part of the complex pole w .

In the other hand, the real part of the dominating complex pole will produce the signal attenuation and the decay ratio (DR) will be defined as it follows:

$$DR = e^{\alpha_j T} \quad \text{with } Re(\lambda_j) \geq \lambda_i \text{ for every real eigenvalue, and } T = 2\pi/w$$

The output advises the user if a real pole is the dominating one and provides the calculated value of DR and w with the method defined above.

The eigenvalues of the jacobian matrix and the DR and w values are provided in a clear format (view figure 7.3). Information about the dominating pole is also available.

On the DR+freq.sal file there is also the apparent DR printed.

7.5.2 Signal Representation Example

At this point, a signal will be represented as an example.

It has been exposed that “**w2joselenois.sal**” contains the results of the calculus. The first column represents the time variable for each point. The other columns correspond to the signals for each of the equations of the system (equations (7.1) to (7.5)). So, the second one contains the values for the generated signal of the neutron excess (figure 7.4).

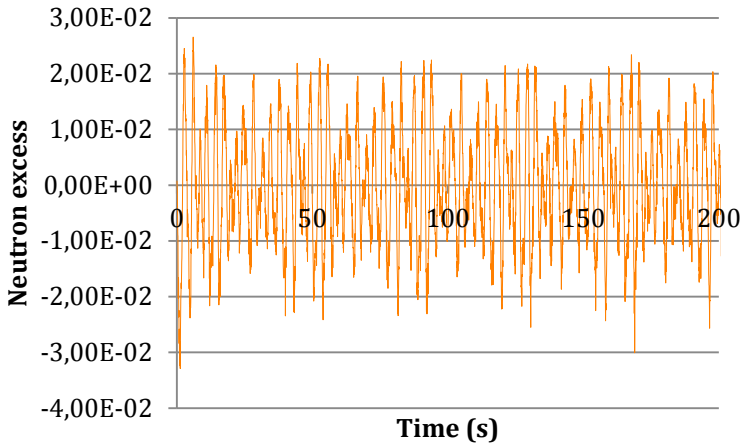


Figure 7.4. Neutron excess.

The third column shows the precursors excess.

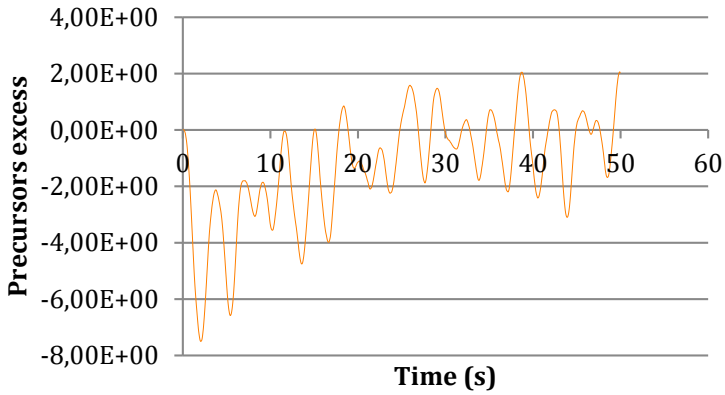


Figure 7.5. Precursors excess.

The fourth one represents the temperature variation.

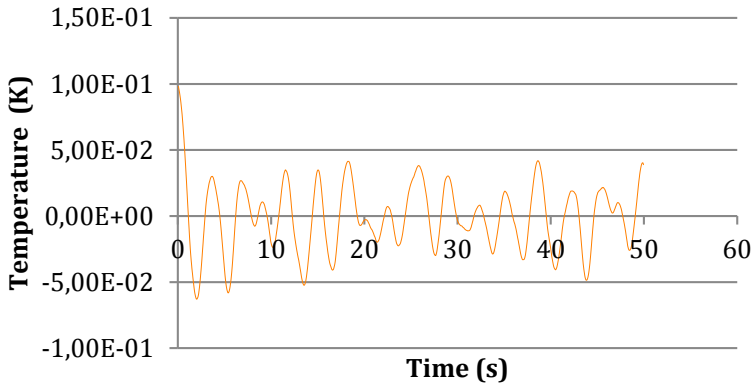


Figure 7.6. Temperature.

The fifth group of numbers matches with the void reactivity.

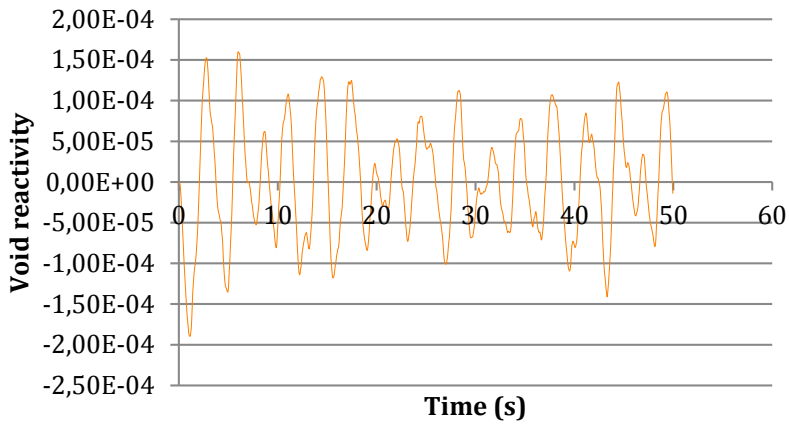


Figure 7.7. Void reactivity.

And the last one contains values for the total reactivity.

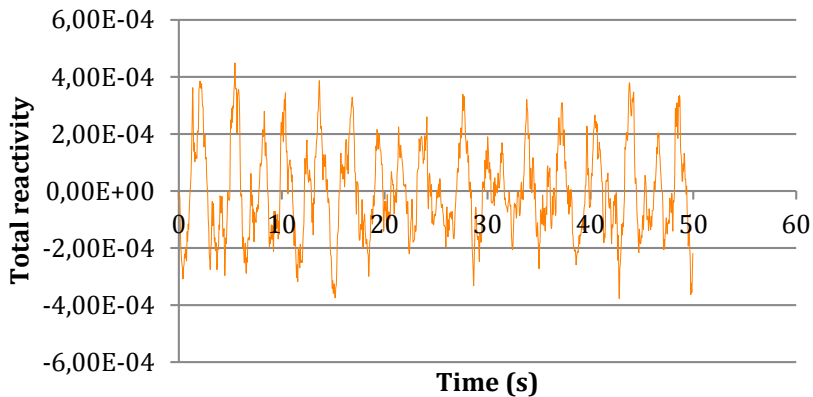


Figure 7.8. Total reactivity.

7.6 VALIDATION WITH A REDUCED ORDER SYNTHETIC SIGNAL GENERATOR

The no linear reduced order model explained above will be used. The objective is to generate a set of 1000 synthetic signals with theoretical values of Decay Ratio and oscillation frequency, and analyze them with a specific technique of noise analysis. The method used is the autocorrelation function based model (ACF). The theoretical and ACF methods results will be compared to probe the validity of the monitor.

The model used is the one developed by March-Leuba [2]. From this point, it will be referred as the “BWR Generator”.

The BWR Generator takes a set of input parameters through an input file, *input.dat*. These parameters are obtained from LAPUR and SIMULATE output files and the variation of feedback and noise level values. To summarize, the input parameters specified in *input.dat* are the following:

Obtained from SIMULATE’s output:

Tg: mean generation time

Beta: referred to the number of differed neutrons related to the total number of neutrons emitted

A: related to the power generated per neutron

Obtained from LAPUR's output

Df: Doppler Coefficient

Obtained from a fitting performed with Matlab using values from LAPUR (script *zeropole45.m*):

B: related to the heat transferred from the fuel to the coolant

Lambda: semi-disintegration period of the precursors

a1c: parameter for the void reactivity equation

a2c: parameter for the void reactivity equation

7.6.1 Preliminary Checking

As a preliminary checking, the dependence of the results of the fitting carried out in *zeropole45.m* on the machine architecture and the version of Matlab used have been checked.

7.6.2 Checking

The BWR Signal Generator have been executed in both 32 bits and 64 bits machines and with different Matlab versions for the generation of input parameters. For each execution, 2 minutes of six different signals (Test Signals) have been created and compared sample to sample (with a sample interval of 50 milliseconds, which yields a total of 2400 samples).

Three different cases of generation of the signals have been compared:

1. Calculation of the input parameters with Matlab R2009b 32 bits and execution of the BWR Generator in Windows 32 bits.
2. Calculation of the input parameters with Matlab R2009b 32 bits and execution of the input parameters in Windows 64 bits.
3. Calculation of the input parameters with Matlab R2011b 64 bits and execution of the generator in Windows 64 bits.

7.6.3 Results

In cases 1 and 2, exactly the same signals are obtained. This demonstrates the independence of the Signal Generator on the system architecture (32 or 64 bits).

In case 3, the input parameters for the generator are slightly different than the ones from cases 1 or 2, as shown in table 7.1 and table 7.2, and that makes the signals to be also slightly different. But the maximum difference between corresponding samples of one and the other signal is of the order of magnitude of 10^{-4} . For this reason, it can be considered that both implementations (Matlab R2009b and Matlab R2011b) are suitable for the validation.

Table 7.1. Input parameters obtained executing zeropole45.m with Matlab R2009b.

	B	lambda	a1c	a2c
Test signal 1	0.3537	0.09	2.8637	4.1845
Test signal 2	0.1826	0.07	5.4297	11.5370
Test signal 3	0.9602	0.09	8.0976	17.7378
Test signal 4	0.1000	0.07	4.5739	9.4466
Test signal 5	0.6031	0.09	4.9537	4.7421
Test signal 6	0.1703	0.07	3.8860	11.8073
Test signal 7	0.2467	0.09	2.4332	3.8211

Table 7.2. Input parameters obtained executing zeropole45.m with Matlab R2011b.

	B	lambda	a1c	a2c
Test signal 1	0.3538	0.09	2.8637	4.1845
Test signal 2	0.1833	0.07	5.4332	11.5227
Test signal 3	0.9599	0.09	8.0968	17.7368
Test signal 4	0.1000	0.07	4.5734	9.441
Test signal 5	0.6396	0.09	4.9701	4.6874
Test signal 6	0.1701	0.07	3.8860	11.8073
Test signal 7	0.2422	0.09	2.4315	3.8217

7.7 INFLUENCE OF THE INPUT PARAMETERS VARIATION

The input file that the generator uses for the generation of signals has multiple input parameters.

Among them, from the specification of the model is known that an increase on the parameter k , related to the feedback of the model, means an increase on the output stability parameters DR and oscillation frequency.

Taking an example CNC case, other input parameters have also been analyzed, observing the influence that a small variation on each one of them has on the generated signal.

As a result, it has been observed that the theoretical Decay Ratio increases with an increase of the following variables:

- A, Tg.

and it decreases when the following variables decrease:

- a1c, a2c, B, beta.

For the case of the oscillation frequency, it increases when the following variables decrease:

- A, a2c, B.

and decrease when the following variables increase:

- a1c, beta, Tg.

7.8 CREATION OF A DATABASE WITH THEORETICAL RESULTS OF DECAY RATIO AND FREQUENCY

To create the set of 1000 signals, the inputs parameters must be chosen in order to obtain a set of signals with uniformly distributed values of Decay Ratio and oscillation frequency.

For this purpose, a total of 11 cases of LAPUR outputs from different situations of Cofrentes NPP are used as input data for the BWR Generator.

These values are used varying the input parameters k , A and B (changing this way feedback, power generated per neutron and heat transferred from the fuel to the coolant). These last three parameters are adjusted to obtain the combination of the different values of DR and oscillation frequency usually observed at the NPP, at which SMART monitor is expected to work: Decay Ratios between 0.1 and 0.9 and frequencies between 0.4 and 0.9 Hz.

After that, 1000 cases have been chosen, using the 8 Cofrentes NPP cases and the selected variations of inputs k , A and B .

7.9 VALIDATION WITH A SET OF 1000 SIGNALS

Once the values of the input parameters are defined, 1000 signals are created, with the following properties:

Sample time: 1ms

Total length: 721 seconds (to discard the first 73 seconds and have 600 seconds to analyze with SMART)

Standard deviation of its amplitude values: between 0.006 and 0.009

Thus, the creation of the set of 1000 signals follows the following steps for each signal:

Checking of the poles of the transfer function.

With the selected input parameters, the theoretical values of Decay Ratio and oscillation frequency are obtained, together with the poles of the transfer function, reading them from one of the outputs of the BWR Generator. These poles of the non linear model are compared with the ones obtained (using Matlab) calculating the transfer function of the linear model [102]. For each of the five poles, the values of linear and non linear models are compared, assuring that the values of the ones of the linear model are nor higher nor lower than a deviation of a 5% of the ones of the linear model.

Search of an input value b_{d2} for the additive noise which gives signals with a noise level similar to the ones observed in Cofrentes and KKL NPP's, that is, with a standard deviation between 0.006 and 0.009, using an approximation algorithm.

Creation of the signal, with a very small sample time (1 millisecond), to simulate analog signals.

Simulation of the Data Acquisition hardware (DAQ). The simulation consists of the following modules:

Takes the BWR Generator output file, `senyalmodelobwr-pito.txt`, and extract the data of time and amplitude of the signal.

Adapts the amplitude level of the signal to the one produced by the APRM's. These are power signals in percentage, with values between 0% and 150% power. Since the BWR Generator creates signals with normalized values, this normalization is undone by choosing a reasonable mean value: 90%. To arrange that, the amplitude values are multiplied by 90, plus an addition of 90.

These values are read by the acquisition system as voltage signals, where 0% corresponds to 0 V and 150% corresponds to 10 V.

The signal is passed through a low pass filter.

Analog-to-digital conversion, simulated by sub-sample from 1ms to 50 ms and by quantifying the amplitude values simulating data acquisition cards with 16 bits.

Conversion in order to show again power percentage values (0 to 150%) from the voltage values is simulated.

The new time and amplitude values are saved in the file `modeloBWR_outDAQ.txt`.

The signals are analyzed with SMART Monitor, using the interpolation method.

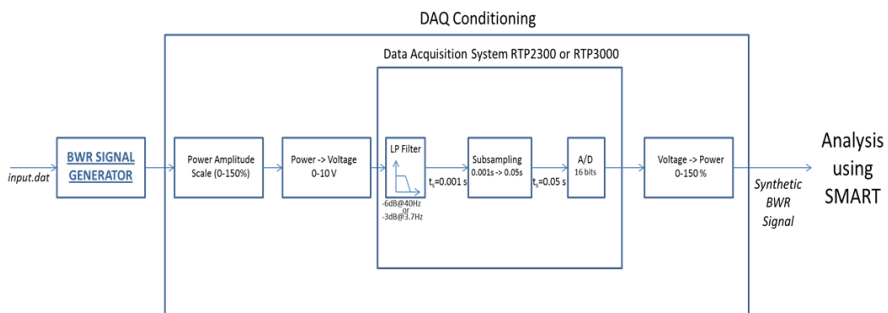


Figure 7.9. Data acquisition hardware

7.10 RESULTS

The results of the simulation with a set of 1000 signals show good accuracy of the stability parameters calculation methods. Figure 7.10 shows that the deviation in calculation of the Decay Ratio is in the band of ± 0.1 , presenting a small bias in the non-conservative direction for high values of DR.

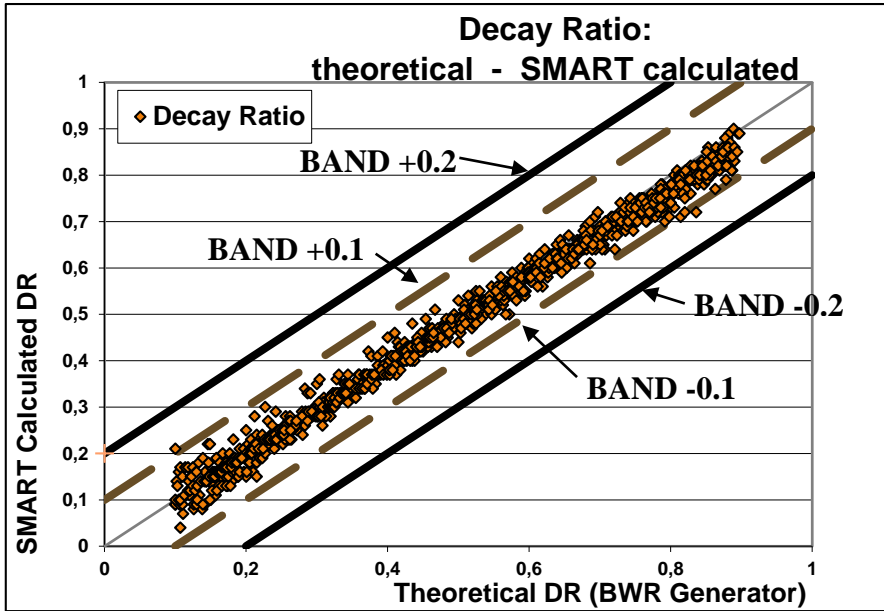


Figure 7.10 Decay Ratio. Analytical vs. Theoretical values

Figure 7.11 shows also a small bias at the calculation of oscillation frequency, having always an error smaller than 0.2, which is higher for high values of frequency.

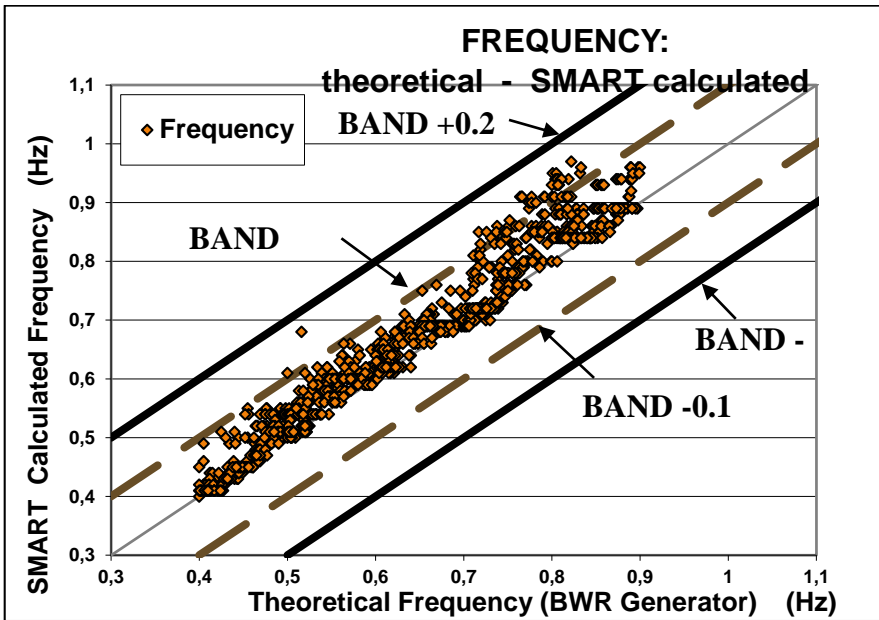


Figure 7.11. Oscillation Frequency. Analytical vs. Theoretical values.

Figure 7.12 shows the dependence of DR calculation versus frequency values: a higher error in DR calculation appears for small frequencies.

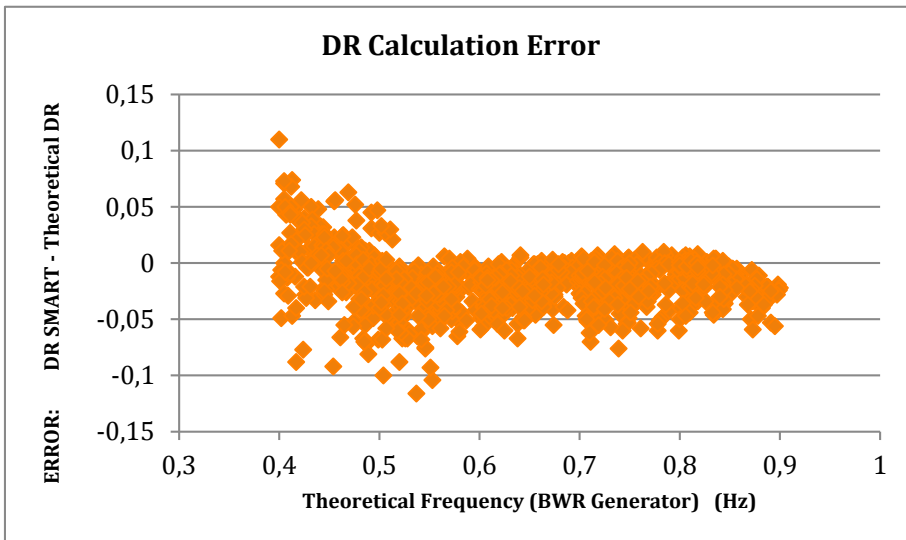


Figure 7.12. DR error vs. Frequency

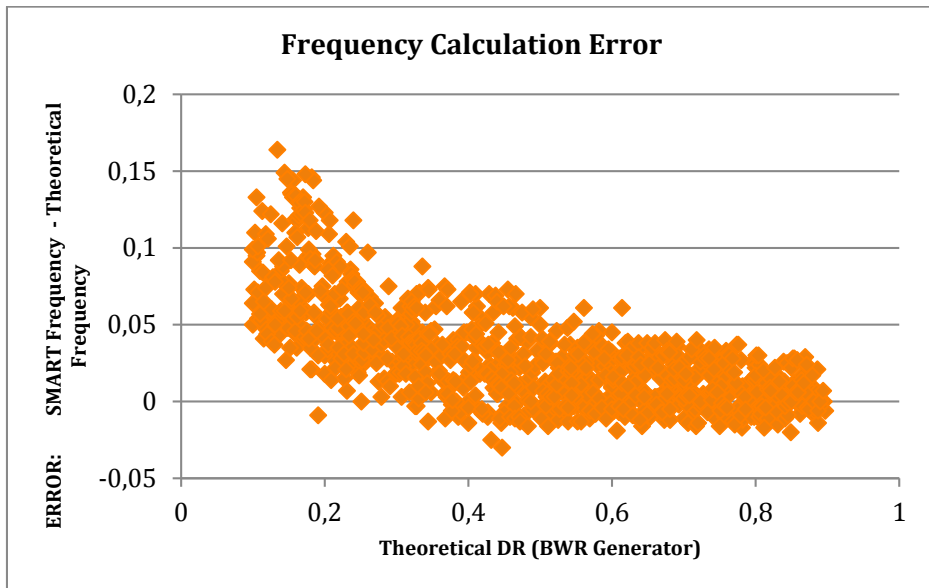


Figure 7.13. Frequency error vs. DR

Figure 7.13 shows the dependence of frequency calculation versus DR values: a higher error in frequency calculation appears for small Decay Ratios.

Using results to estimate the standard deviation of the 1000 signals analyzed, the DR standard deviation is 0.024 and for frequency is 0.032 which allow us to conclude that the accuracy of method used for obtaining decay ratio from autocorrelation function is very good, and the results of LAPUR 6 has a very good agreement.

7.11 CHAPTER SUMMARY

In this chapter by means a BWR noise simulator the uncertainty of the methods used for obtaining experimental decay ratios has been estimated

A decay ratio monitor called SMART has been developed by the Universidad Politécnica de Valencia (Spain) jointly with IBERDROLA [84]. The SMART stability monitor, which was developed with MATLAB, will be used for autocorrelation-based decay ratio estimation. The uncertainty of autocorrelation-based decay ratio estimation of SMART has been evaluated in this chapter. 1000 signals of ten minutes signals have been generated, covering

all the decay ratios ranges and frequencies up to 1 HZ. This is the only way of determining the real accuracy of LAPUR 6.

To create the set of 1000 signals, the inputs parameters has been chosen in order to obtain a set of signals with uniformly distributed values of Decay Ratio and oscillation frequency.

For this purpose, a total of 11 cases of LAPUR outputs from different situations of Cofrentes NPP are used as input data for the BWR Generator. These values are used varying the input parameters k , A and B (changing this way feedback, power generated per neutron and heat transferred from the fuel to the coolant). These last three parameters are adjusted to obtain the combination of the different values of DR and oscillation frequency usually observed at the NPP, at which SMART monitor is expected to work: Decay Ratios between 0.1 and 0.9 and frequencies between 0.4 and 0.9 Hz.

Using results to estimate the standard deviation of the 1000 signals analyzed, the DR standard deviation is 0.024 and for frequency is 0.032 which allow us to conclude that the accuracy of method used for obtaining decay ratio from autocorrelation function is very good, and the results of LAPUR 6 has a very good agreement.

8 CONCLUSIONS AND RECOMMENDATIONS FOR FUTURE WORK

BWR power oscillation is a complex phenomenon caused by a nuclear-coupled density-wave instability. The stability of a BWR depends on many factors such as the reactor power, core flow, pressure, power shape, reactivity feedback coefficients, and the core inlet subcooling. The effects of changing these variables on the system stability may be counter intuitive.

BWR power oscillation events in the past, i.e., the LaSalle-2 and WNP-2 events, call for new approaches to ensure the stability of BWRs. After several years of research, two approaches have been accepted by the NRC. The first approach (Prevention) designates some exclusion regions. Operations inside the exclusion regions are pre-vented by automatic safety systems. The second approach (Detection/Suppression) uses based on LPRM stability algorithms to detect unstable conditions. Automatic safety systems are used to suppress power oscillations once detected. Detect and suppress approaches have been

evolved and reducing conservatism applying order statistic and CSAU approaches to generate set-points for automatic safety systems to suppress power oscillations once detected.

This research is focus on predictive methods for stability margin in decay ratio. In order to avoid instability related scrams reliable predictive methods are very important. Stability margin is complex and in addition of the thermal-hydraulic features of the fuel designs, radial power distribution, cycle length, enrichment, operation with a failed fuel, could produce unexpected stability degradation. The high sensitivity of the stability margin prediction with the accuracy of thermalhydraulic models is critical; bundle pressure drop must be validated component-wise. A good prediction of pressure drop leads to an accurate flow distribution and a good flow distribution allow us to a precise computation of void fraction distribution. In addition, in order to improve shutdown margin and minimize two-phase pressure drop, the new fuel designs introduce partial length rods, that is, fuel design are composed by axial variable area.

For analytical estimation of DR, frequency domain codes are very useful. These types of codes are very fast and their results are very robust in comparison with time domain codes, whose results may be dependent on numeric scheme and nodalization. The only drawback of frequency domain is that you are limited to the linear domain; however, because of regulatory requirements imposed by GDC-12, reactors must remain stable and, thus, reactors always operate in the linear domain.

Several improvements have been performed in the code in order to upgrade it for the new fuel design types. The previous LAPUR 5 release 1 code does not consider channel with variable area and does not distinguish specifically local pressure drop due to spacers in a bundle. The only way to take into account local pressure losses and gains due to spacers and area changes is by means of a friction multiplier given by input. This deficiency leads to adjusting by input friction multiplier in order to account for accurately local and variable area effect on the pressure drop.

The new version is LAPUR 6. This version includes new correlations for computing friction and local losses and capabilities for modelling bundles with variable cross-area. As additional improvements, LAPUR 6 allows to use up to

200 thermalhydraulic channel to represent the core and calculates transfer functions with up to 100 frequency points instead of 25 points for LAPUR 5.1 release 1. The author specified the models to be implemented and participated actively in the development [73], and the author presented in the NURETH meeting the first paper related to LAPUR 6 upgrades [74] .

To check the correct implementation of these changes, the author has performed a two-fold LAPUR 6 validation:

First, the author has validated LAPUR 6 new thermal-hydraulic models comparing each pressure drop component against SIMULATE-3

Second, the author has developed a methodology for calculating Decay Ratios with LAPUR 6 based on an automatic procedure, [64]. This methodology has been approved by CSN and extensively used for E1A application from cycle 12 to 20 and is currently used and present.

The author has presented papers [83] and [80] in ANS and NUTHOS meetings respectively, has published a NUREG CR report, [82], and several licensing topical reports and design record files [81][71], [72], [65], [66], [64], [65], [64], [61] licensed by CSN for E1A Stability Cofrentes application.

Generic validation of the components of pressure drop obtained with the new models implemented in LAPUR 6 r.0 was performed (using default friction models of SIMULATE-3). Comparisons of LAPUR 6 with SIMULATE-3 showed a very good agreement. Components that are dependent on void fractions (elevation and acceleration) showed slight discrepancies due to the void fractions predicted by SIMULATE-3 and LAPUR 6.0 not being equal. However, the relative contribution of these components to the total pressure drop is very low, and the effect can be considered to be negligible.

FRIGG-2 LOOP experimental void fractions data and LAPUR 6 were also compared [82]. Their agreement was similar to those of other codes with three or four equations and dynamic or algebraic slip.

Figures 6.87 and 6.88 show all available Cofrentes plant data, from start-up, sequence exchange, and coastdowns [82].

Reasonable agreement was observed, and the majority of predictions are in the ± 0.1 band. Frequency is reasonably predicted up to 70% of the flow rate (0.7 Hz for LAPUR and 0.8 for autocorrelation-based frequency).

The sensitivity of calculated decay ratios with LAPUR 6 to the radial power distribution of the core and to the thermal-hydraulic applying LAPUR 6 has been shown by means of three representative examples. The recommendation of a core design with as flatter as possible radial distribution is a powerful mechanism to stabilize the core design is the main learned lesson

Finally, the latest version of LAPUR and LIP, called LAPUR 6.1 and LIP 1.2 respectively, have been developed to account for the burnup dependence of fuel conductivity. The author has published a new licensing topical report [86]. The effect of the implementation of a burnup dependence of fuel conductivity has been separately evaluated. The method developed by the author in [86] is used at present for licensing stability in Cofrentes NPP.

The introduction of a burnup dependent fuel conductivity has a stabilizing effect and the increase of gap conductance does not compensate for the effect. This stabilizing non-compensated effect has been also observed by the fuel vendors, which confirms that the author has correctly implemented the models.

For licensing purposes, the author has introduced changes in the methodology in order to maintain previous degree of conservatism:

- Incorporation of a burnup dependent fuel conductivity model on the conservative side.
- Incorporation of an extra multiplier of 1.1 through REAMUL card obtained from matching core averaged density reactivity coefficient from LAPURW output to the average value obtained from all of the Moderator Temperature Coefficient and Pressure perturbation serie in SIMULATE.

Results have shown a similar degree of conservatism when the feedback compensation described above is performed.

A decay ratio monitor called SMART has been developed by the Universidad Politécnica de Valencia (Spain) jointly with the author [93]. The SMART stability monitor, which was developed with MATLAB, will be used

for autocorrelation-based decay ratio estimation. The uncertainty of autocorrelation-based decay ratio estimation of SMART has been evaluated. The author has generated 1000 signals of ten minutes signals, covering all the decay ratios ranges and frequencies up to 1 HZ. This is the only way of determining the real accuracy of LAPUR 6.

To create the set of 1000 signals, the inputs parameters has been chosen in order to obtain a set of signals with uniformly distributed values of Decay Ratio and oscillation frequency.

Using results to estimate the standard deviation of the 1000 signals analyzed, the DR standard deviation is 0.024 and for frequency is 0.032 which allow us to conclude that the accuracy of method used for obtaining decay ratio from autocorrelation function is very good, and the results of LAPUR 6 has a very good agreement.

8.1 RECOMMENDATIONS FOR FUTURE WORK

LAPUR code neutronic feedback is based on point kinetic. The point kinetic model has been not upgrade and a boiling water reactor is axially and radially variable in nature, which leads to axial and radial non symmetrical power distribution. The contribution of the uneven Xenon concentration in the reactor could influence in the stability margin. However the LAPUR frequency reactivity computation is based in point kinetic and a one-dimensional or three dimensional revised formulation should be required. A process of linearization of kinetics equation should be done and this job is out of this dissertation.

Another future work also could be to combine LAPUR 6 code with a time domain code analyzing situations with decay ratios close but less than unity to compare frequency and decay ratio results.

Out of phase model need to be upgraded using more updated data to apply to the LAPUR 6 out of phase model.

Finally a significant stabilizing effect of the degradation of the Urania conductivity with the burnup is noticed. Out of phase oscillations impact and the effect in high burnup fuel should be considered in future work in these topics.

9 REFERENCES

- [1] P.J. Otaduy. "Modeling of the Dynamic Behavior of Large Boiling Water Reactor Cores". Ph.D. dissertation, University of Florida. (1979).
- [2] J. March-Leuba. "Dynamic Behavior of Boiling Water Reactors". Ph.D. dissertation, University of Tennessee, Knoxville. (1984).
- [3] F. D'Auria (Editor). "State of the Art Report on Boiling Water Reactor Stability". OECD NEA/CSNI/R(96)21. (1997).
- [4] J. March-Leuba, J.M. Rey. "Coupled Thermohydraulic-Neutronic Instabilities in Boiling Water Nuclear Reactors: A Review of the State-of-the-Art". *Nuclear Engineering and Design* 145, pp. 97-111. (1993).
- [5] M. Ishii. "Wave Phenomena and Two-Phase Flow Instabilities". In G. Hetsroni, editor, *Handbook of Multiphase Systems*, section 2.4, pp. 2-95 to 2-122. Hemisphere, Washington. (1982).
- [6] J.A. Bouré, A.E. Bergles, L.S. Tong. "Review of Two-Phase Flow Instability". *Nuclear Engineering and Design* 25, pp. 165-192. (1973).
- [7] S. Kakag, T. N. Veziroglu. "A Review of Two-Phase Flow Instabilities". In S. Kakag and M. Ishii, editors, *Advances in Two-Phase Flow and Heat Transfer-Fundamental and Applications*, volume II, pp. 577-667. Martinus Nijhoff Publishers, Boston. (1983).
- [8] A.H. Stenning. "Density-Wave Oscillations". MIT Course 22.36 Class Notes HH-B. (1980).
- [9] M.Z. Podowski. "Instabilities in Two-Phase Systems". In R. T. Lahey, Jr., editor, *Boiling Heat Transfer-Modern Development and Advances*, pp. 271-315. Elsevier Science Publishers, Amsterdam. (1992=).
- [10] J. March-Leuba. "Density-Wave Instabilities in Boiling Water Reactors". NUREG/CR-6003, ORNL/TM-12130. (1992).
- [11] J. E. Meyer, R.P. Rose. "Application of a Momentum Integral Model to the Study of Parallel Channel Boiling Flow Oscillations". *Journal of Heat Transfer, Trans. ASME, Series C* 85(1), pp. 1-9. (1963).
- [12] J. M. Sorensen, A.F.V. Dias, L.D. Eisenhart. "BWR Stability Analysis: A Comparison of Point, One-Dimensional, and Three-Dimensional Neutronic Model Methodologies". In *Proceedings: Sixth International RETRAN Conference*, pp. 21-1-21-19, August. EPRI NP-6949. (1990).
- [13] A. Wysocki, J. March-Leuba, A. Manera, T. Downar. "TRACE/PARCS analysis of out-of-phase power oscillations with a rotating line of symmetry". *Annals of Nuclear Energy* 67, pp. 59-69. (2014).

- [14] J. March-Leuba, E.D. Blakeman. "A Mechanism for Out-of-Phase Power Instabilities in Boiling Water Reactors". *Nuclear Science and Engineering* 107, pp. 173-179. (1991).
- [15] J.L. Munoz-Cobo, M.Z. Podowski, S. Chiva. "Parallel channel instabilities in boiling water reactor systems: boundary conditions for out of phase oscillations". *Annals of Nuclear Energy* 29, pp. 1891-1917. (2002).
- [16] E.D. Blakeman, J. March-Leuba. "A Parametric Analysis of Decay Ratio Calculations in a Boiling Water Reactor Model". Paper published in the Seventh Power Plant Dynamics, Control and Testing Symposium, Knoxville, Tennessee, May. CONF-890555-4. (1989).
- [17] S. Langenbuch, K.D. Schmidt. "A Sensitivity Analysis for the BWR Stability Behaviour". In Proceedings: International Workshop on Boiling Water Reactor Stability, pages 241-256, Holtsville, New York, March 17-19. OECD, NEA. CSNI-R-178. (1990).
- [18] G.C. Park, M.Z. Podowski, M. Becker, R.T. Lahey, S.J. Peng. "The Development of a Closed-Form Analytical Model for the Stability Analysis of Nuclear Coupled Density-Wave Oscillations in Boiling Water Nuclear Reactors". *Nuclear Engineering and Design* 92, pp. 253-281. (1986).
- [19] P. Saha, N. Zuber. "An Analytical Study of the Thermally Induced Two-Phase Flow Instabilities Including the Effect of Thermal Non-Equilibrium". *International Journal of Heat and Mass Transfer* 21, pp. 415-426. (1978).
- [20] O. Yokomizo, I. Sumida, T. Anegawa, Y. Yoshimoto, T. Fukahori. "Examination of Nuclear Thermal Hydraulic Oscillation Modes in BWR Core". In Proceedings of International Workshop on Boiling Water Reactor Stability, pages 175-189, Holtsville, New York, March 17-19. OECD, NEA. CSNI-R-178. (1990).
- [21] A.F. Henry. "Nuclear-Reactor Analysis". The MIT Press, Cambridge, MA. (1975).
- [22] USNRC. "Power Oscillations at Washington Nuclear Power Unit 2". NRC Information Notice 92-74. (1992).
- [23] L.G. Neal, S.M. Zivi. "The Stability of Boiling-Water Reactors and Loops". *Nuclear Science and Engineering* 30, pp. 25-38. (1967).

- [24] J. March-Leuba, C.M. Smith. "Development of an Automated Diagnostic System for Boiling Water Reactor Stability Measurements." *Progress in Nuclear Energy* 15, pp. 27-35. (1985).
- [25] J. Balaram, C.N. Shen, R.T. Lahey, M. Becker. "An Analysis of Boiling Water Nuclear Reactor Stability Margin". NUREG/CR-3291, May 1983.
- [26] L.A. Carmichael, R.O. Niemi. "Transient and Stability Tests at Peach Bottom Atomic Power Station Unit 2 at End of Cycle 2". EPRI NP-564. (1978).
- [27] J. March-Leuba. "LAPUR Benchmark Against In-Phase and Out-of-Phase Stability Tests". NUREG/CR-5605, ORNL/TM-11621. (1990).
- [28] S.W. Jones, M.C. Humphreys. "Stability Monitoring System Demonstration Program at WNP-2". *Transactions of the American Nuclear Society* 60, pp. 483-484. (1989=).
- [29] W. Wulff, H.S. Cheng, A.N. Mallen, U.S. Rohatgi. "BWR Stability Analysis at Brookhaven National Laboratory". In Proceedings of the USNRC Ninth Water Reactor Safety Information Meeting, volume 3, Addition, pages 1-20. NUREG/CP-0119-Vol.3-Add. (1992).
- [30] J. March-Leuba. "Time-space nodalization issues in BWR stability calculations". In NURETH-15, Pisa, Italy. (2013).
- [31] J. H. Mahaffy. "Numerics of codes: stability, diffusion, and convergence". *Nuclear Engineering and Design* 145, pp. 131-145. (1993).
- [32] F. Garzarolli, R. Adamson, P. Rudling, A. Strasser. "BWR Fuel Channel Distortion" ANT International. IZNA11 Special Topic Report. (2011).
- [33] <https://nuclear.gepower.com/fuel-a-plant/products/gnf2-advantage.html>
- [34] GE Hitachi Nuclear Energy. "GEH Simplified Stability Solution (GS3)" NEDO-33766-A, Revision 1. (2015).
- [35] USNRC. "Code of Federal Regulations. Title 10, Part 50, Appendix A: Suppression of Reactor Power Oscillations".
- [36] E. Gialdi, S. Grifoni, C. Parmeggiani, C. Tricoli. "Core Stability in Operating BWR: Operational Experience". *Progress in Nuclear Energy* 15, pp. 447-459. (1985).
- [37] B-G Bergdahl, R. Oguma. "BWR Stability Investigation in Ringhals 1 Measurement Data From October 26, 1989". In Proceedings: International Workshop on Boiling Water Reactor Stability, pp. 142-

- 160, Holtsville, New York, March 17-19. OECD, NEA. CSNI-R-178. (1990).
- [38] P. Mata, P.G. Sedano, J Serra. “Analysis of Cofrentes Abnormal Plant transients with RETRAN-02 and RETRAN-03”. *Nuclear Technology* 100 pp. 203215. (1992).
- [39] T.J. Rausch, H.C. Pfefferlen. “Overview of Current BWR Owners' Group Stability Programs”. In Proceedings: International Workshop on Boiling Water Reactor Stability, pp. 30-44, Holtsville, New York, March 17-19. OECD, NEA. CSNI-R-178. (1990).
- [40] BWR Owners’ Group. “Nine Mile Point 2 Instability Event Briefing”. (2003).
- [41] “Oscillation Power Range Monitor Upscale Reactor Scram during Single Loop Operation”. LER No. 2015-003. (2015)
- [42] H.C. Pfefferlen, G.A. Watford, T.J. Rausch. “BWR Core Thermal-Hydraulic Stability Experience and Safety Significance”. In Proceedings: International Workshop on Boiling Water Reactor Stability, pp. 45-57, Holtsville, New York, March 17-19. OECD, NEA. CSNI-R-178. (1990).
- [43] J. March-Leuba. “Average Power Increase During Limit-Cycle Oscillations”. *Transactions of the American Nuclear Society* 60, pp. 481-482. (1989).
- [44] USNRC. “Power Oscillations in Boiling Water Reactors (BWRs)”. NRC Bulletin No. 88-07, Supplement 1, December 1988.
- [45] NRC Information Notice 92-74, "Power Oscillations at Washington Nuclear Power Unit 2," dated November 10, 1992
- [46] USNRC, “Long-Term Solutions and Upgrade of Interim Operating Recommendations for Thermal-Hydraulic Instabilities in Boiling Water Reactors." NRC Generic Letter 94-02, July 1994.
- [47] GE Nuclear Energy. “BWR Owners' Group Long-Term Stability Solutions Licensing Methodology”. NEDO-31960-A. (1995).
- [48] GE Nuclear Energy. “BWR Owners' Group Long-Term Stability Solutions Licensing Methodology”. NEDO-31960-A, Supplement 1. (1995).
- [49] GE Nuclear Energy. “Reactor Stability Long-Term Solution: Enhanced Option I-A”. NEDO-32339A rev.1. (1998)
- [50] C.M. Mowry, I. Nir, D.W. Newkirk, “Operational Control of Boiling Water Reactor Stability”. *Nuclear Technology* 109, pp 412-428 (1995).

- [51] R.K. Haling. “Operational strategy for maintaining an optimum power distribution throughout life”. Proc. ANS Topical Mtg. Nuclear Performance Power Reactor Cores, TID-7672. (1964).
- [52] EPRI. “Fuel Reliability Guidelines: Pellet-Cladding Interaction”. TR: 1015453. (2008).
- [53] C.D. Williams, M.O. Marlowe, R.B. Adamson, S.B. Wisner, R.A. Rand, J.S. Armijo. “Zircaloy-2 Lined Zirconium Barrier Fuel Cladding”. Zirconium in the Nuclear Industry: Eleventh International Symposium, ASTM STP 1295, pp. 679-694. (1996).
- [54] GE Hitachi Nuclear Energy. “DSS-CD TRACG Application”. NEDE-33147P-A, Revision 4. (2013).
- [55] GE Hitachi Boiling Water Reactor. “Detect and Suppress Solution–Confirmation Density”. NEDC-33075P, Revision 7. (2011).
- [56] GE Nuclear Energy. “BWR Owners' Group Reactor Stability Detect and Suppress Solutions Licensing Basis Methodology for Reload Applications”. NEDO-32465-A. (1996).
- [57] GE Hitachi Nuclear Energy. “Migration to TRACG04/PANAC11 from TRACG02/PANAC10 for Reactor Stability Detect and Suppress Solutions Licensing Basis Methodology for Reload Applications”. NEDO-32465 Supplement 1, Revision 0. (2011).
- [58] GE Nuclear Energy. “Application of Stability Long-Term Solution Option II to Oyster Creek”. NEDC-33065P, Revision 0 (2002).
- [59] Studsvik Scandpower. “SIMULATE-3 User’s Manual” SSP-01/414 Rev 3. (2003).
- [60] A. Escrivá, J.L. Muñoz-Cobo, G. Verdú, M.J. Palomo. “Aplicación de LAPUR para el cálculo del margen de estabilidad en reactores BWR” DIQN-98/003 Universidad Politécnica de Valencia. (1998).
- [61] J. Melara. “Descripción del programa LIP”. IT-COSNU-260. (2006).
- [62] GE Hitachi Nuclear Energy. “ODYSY Application for Stability Licensing Calculations Including Option I-D and II Long Term Solutions,” NEDE-33213P-A. (2009).
- [63] GE Nuclear Energy. “Cofrentes Cycle 10 Reactor Stability Long Term Solution: Enhanced option I-A Stability Region Boundary. Generation and Validation”. GENE-A13-00367-49, rev.2. (1998).
- [64] J. Melara. “Methodology and Procedure for Calculation of Core and Channel Decay Ratios with LAPUR”. IT-CONUC-028, rev. 4. (2006).

- [65] J. Melara. "Validation of Variable Area and New Friction Models Implemented in LAPUR6 code". IT-COSNU-259. (2006)
- [66] J. Melara "Validación de los nuevos modelos t/h de LAPUR6". CC-COSNU-415. (2006).
- [67] P.J. Otaduy, J. March Leuba J. "LAPUR User's Guide". NUREG/CR-5421. (1990).
- [68] A. Escrivá, J.L. Muñoz-Cobo. "Improvements made in LAPUR 5 to obtain LAPUR 6.0 r.0". GTIN-06/03. Universidad Politécnica de Valencia. (2006).
- [69] A. Escrivá, J.L. Muñoz-Cobo. "Actualización del Código LAPUR 5". DIQN/LAP001. Universidad Politécnica de Valencia. (2000)
- [70] J.M Dey "Benchmark de C.N. Cofrentes mediante el sistema de gestión de núcleos de Studsvik. Ciclo 1-15b". IT-COSNU-251. (2006).
- [71] J. Melara. "Cualificación de LAPUR 6.0 para su aplicación en C.N Cofrentes". CC-COSNU-414 rev. 0. (2006).
- [72] J. Melara. "Verificación del Modelo Termohidráulico de SIMULATE-3 para CN Cofrentes". IT_CONUC-075 rev. 6. (2011).
- [73] A. Escrivá, J. L. Muñoz Cobo, J. Melara, M. Albendea, J. March-Leuba. "LAPUR 6.0 Users Manual". NUREG/CR-6958. (2008).
- [74] A. Escrivá, J.L. Muñoz-Cobo, J. Melara "Upgrade of the Thermalhydraulic Capabilities of the Stability Code LAPUR 5, for the New Fuel Type Designs". NURETH-11. (2005).
- [75] "FIBWR: A Steady-state Core Flow Distribution Code for Boiling Water Reactors Computer Code User's Manual". EPRI NP-1924-CCM. (1981).
- [76] "RETRAN-3D—A Program for Transient and Thermal-Hydraulic Analysis for Complex Fluid Systems". Vol. 4 Assessment manual. NP-7450(A) Rev. 1. (2006)
- [77] D. Chisholm. "Pressure Gradients Due to Friction During the Flow of Evaporating Two-phase Mixtures in Smooth Tubes and Channels" *Journal Heat Mass Transfer* Vol. 16, pp. 347–358. (1973)
- [78] M. Albendea, A. Crespo. "CAPRICORE: A New on-line Monitoring System," EPHISOR 2000 ANS International Topical Meeting on Advances in Reactor Physics and Mathematics and Computation into the Next Millennium. (2000)-

- [79] Y. Tofiño. “Predictor de estabilidad para la vigilancia continua de un reactor tipo BWR,” Proyecto Fin de Carrera. ETSI de Minas. Premio Mejor Proyecto Fin de Carrera SNE. (2004)
- [80] J. Melara, A. Escriva, J.L Muñoz-Cobo, M.E.Montesinos, J.A. March-Leuba, M. Albendea. “Validation of LAPUR 6 for Stability Prediction. Application to Cofrentes NPP”. American Nuclear Society. 2008 Annual Meeting, June 8-12. Anaheim, California. (2008)
- [81] J. Melara. “Validación de los nuevos modelos t/h de LAPUR6”. CC-COSNU-415. (2006).
- [82] J. Melara, C. Lora A. Escriva, J.L Muñoz-Cobo, M. Albendea. “Validation of LAPUR 6.0 Code”. NUREG/CR-7124 (2012).
- [83] J. Melara, C. Lora, A. Escriva, J.L Muñoz-Cobo, M. Albendea. “Stability Control Methods in Cofrentes NPP”. The 9th International Topical Meeting on Nuclear Thermal-Hydraulics, Operation and Safety (NUTHOS-9) N9P0192 Kaohsiung, Taiwan, September 9-13, 2012
- [84] NRC. “Nuclear fuel thermal conductivity degradation”. NRC Information Notice 2009-23. (2009)
- [85] Resolución del Ministerio de Industria, Turismo y Comercio del 27 de Julio 2011. 001 N°201100034041
- [86] J. Melara “Incorporación de la dependencia de la conductividad de la Urania con el quemado en la metodología de estabilidad”. CC-CONUC-618 (2012).
- [87] K.J. Geelhood, W.G. Luscher, C.E. Beyer. “FRAPCON-3.4: A Computer Code for the Calculation of Steady-State Thermal-Mechanical Behavior of Oxide Fuel Rods for High Burnup”. NUREG/CR-7022 Vol. 1. (2011).
- [88] D.D. Lanning, C.E. Beyer, K.J. Geelhood. “FRAPCON-3 Updates, Including Mixed-Oxide Fuel Properties”. NUREG/CR-6534 Vol.4. (2005).
- [89] J. Melara. “C.N. Cofrentes ciclo 19. Generación y validación de regiones E1A”. IT-CONUC-343. (2011).
- [90] NRC. “Staff assessment of AREVA codes and methods with regards to thermal conductivity degradation experimental data” ML120740363. (2012).

- [91] GNF. “The PRIME Model for Analysis of Fuel Rod Thermal–Mechanical Performance: Part 1–Technical Bases”. NEDC-33256P-A, Revision 1. (2010).
- [92] G. Verdu, D. Ginestar, J.L. Muñoz-Cobo, J. Navarro, M.J. Palomo, P. Lansaker, J.M. Conde, E. Sartori. “Forsmark 1 & 2 Boiling Water Reactor Stability Benchmark: Time Series Analysis Methods for Oscillation during BWR Operation”. NEA/NSC/DOC (2001) 2, OECD. (2001).
- [93] M.E. Montesinos, J.L. Muñoz-Cobo, C. González, A. Escrivá, C. Lora, J. Melara, M. Albendea. “Utilización del monitor SMART V2.1, para el cálculo de estabilidad de un reactor de agua en ebullición,” 36 Reunión Anual de la Sociedad Nuclear Española, Santiago de Compostela. (2010)
- [94] J.G. Proakis, D.G. Manolakis. “Tratamiento Digital de Señales”. Madrid: Prentice Hall. (1998).
- [95] J.A. Thie. “Boiling Water Reactor Stability”. *Nucleonics* 16(3), pp. 102-110. (1958).
- [96] P.E. Kloeden, E. Platen. “Numerical Solution of Stochastic Differential Equations”. Springer. (1992).
- [97] K. Burrage. “High strong order explicit Runge-Kutta methods for stochastic ordinary differential equations”. *Applied numerical mathematics*, Volume 22 Issue 1-3. (1996).
- [98] M.M.R. Williams. “Random processes in nuclear reactors”. Editorial Pergamon Press, Oxford. (1974).
- [99] J. Lewins. “Nuclear Reactor Kinetics and Control”. Pergamon Press. (1978).
- [100] J.L. Muñoz-Cobo, R. Merino. “Synthetic BWR Signal Generation”. GTIN-11/01. Universidad Politécnica de Valencia. (2011)
- [101] J.L. Muñoz-Cobo, M.E. Montesinos, J. Peña, A. Escrivá, C. González, J. Melara, “Validation of reactor noise linear stability methods by means of advanced stochastic differential equation models”. *Annals of Nuclear Energy* 38, pp. 1473–1488. (2011)
- [102] A. Escrivá. “Nuevas Aportaciones al Estudio de la Estabilidad de Reactores de Agua en Ebullición: Desarrollo de un Modelo Fenomenológico No Lineal para el Estudio de la Dinámica”. Tesis Doctoral. Universidad Politécnica de Valencia. (1998).

- [103] A. Escrivá, J.L. Muñoz-Cobo. “PAPU. Models, Correlations and User’s Manual”. GTIN-02/001. Universidad Politécnica de Valencia. (2002).

APPENDIX A. PROCEDURE FOR USING PAPU POSTPROCESSOR

This Appendix consists of five parts:

Part A.1 specifies the input files and input parameter values used when calculating reactivity coefficients for LAPUR (to be used jointly with Ref. [103], section 5).

Part A.2 specifies the input data that may be changed in every particular calculation.

Part A.3 indicates how to extract from PAPU output files the reactivity coefficients required by LAPURW.

Part A.4 is an example of an LAPURX input file.

Part A.5 is an example of an LAPURW input file.

A.1 INPUT FILES DESCRIPTION

PAPU requires the following input files

infile:

This is the KINETIC FILE from a SIMULATE perturbation run renamed as infile.

ajustfile:

This file contains initial values of adjust parameters. This parameter file is maintained for all calculations. Characters in bold does not constitute input data

card1

K NAMK UK WK A B

1 1 0. 1.e-6 0.0.

card2

K NAMK UK WK A B

2 2 0. 1.e-6 0.0.

card3

K NAMK UK WK A B

3 3 0. 1.e-6 0.0.

card4

K NAMK UK WK A B

4 4 0. 1.e-6 0.0.

card5

0, 0, UK WK A B

0 0 0. 1.e-6 0.0.

card6

CWORD CWORD2 WORD7

TAUR 5000. 1.E-06

card6

EXIT

where:

- K:** adjust parameter order number. If K=0 there is not more parameters
- NAMK** adjust parameter order number. If NAMK=0 there is not more parameters
- UK** adjust parameter initial value
- WK** error associated to adjust parameter
- A** minimum value associated to adjust parameter. If A=0, the value is not limited.
- B** maximum value associated to adjust parameter. If B=0, the value is not limited

CWORD TAUR

CWORD2 ITERATION NUMBER

WORD7ERROR

entrada:

entrada is the other input file. Input cards will be described next. Characters in bold does not constitute input data

card1

.true. **input data print option**

card2

.false.,.false. **KINETIC data print option, KINETIC data print option**

card3

1 Calculation of liquid temperature option

card4

25,15.24,15.24 **number of core nodes, core node size (cm) reflector thickness (cm)**

card5

1 Print option for cross sections of lower and upper reflector

card6

0 file "tthfile" (not used)

card7

'CASO DE ','PRUEBA ','DOPPLER ' **title**

card8

0,1,1,1,1,1,1,1,1,1,1,1,1,1 **different print options (see Ref. [103])**

card9

.true. **print option of subroutine AJUSTED output data**

card10

1, 1, 0 **number of lower core nodes excluded, number of upper core nodes excluded, option of least squares (Doppler coefficient calculation)**

card11

'CASO DE ','PRUEBA ','ALFA ' **title**

card12

0,1,1,1,1,1,1,1,1,1,1,1,1,1 **different print options (see Ref. [103])**

card13

.false. **print option of subroutine AJUSTEA output data**

card14

6, 2, 0 **number of lower core nodes excluded (to be specified each calculation see section A2), number of upper core nodes excluded, option of least squares (Void coefficient calculation)**

card15

.false. **print option of subroutine AJUSTEDE output**

card16

6, 2, 0 **number of lower core nodes excluded (to be specified each calculation see section A2) , number of upper core nodes excluded, option of least squares (Density coefficient calculation)**

card17

3.83507e-07,-2.39473e-07 **boron coefficients (not used)**

card18

12.4511e-06,-6.85041e-06 **boron coefficients (not used)**

card19

4 **boron coefficients (not used)**

card20

0. **boron coefficients (not used)**

card21

500. **boron coefficients (not used)**

card22

1000. **boron coefficients (not used)**

card23

1500. **boron coefficients (not used)**

card24

'CASO DE ','PRUEBA ','BORO ' **title for boron coefficient calculation (not used)**

card25

0,1,1,1,1,1,1,1,1,1,1,1,1,1,1,1 **print option (not used)**

card26

.false. **print option subroutine ajusteb (not used)**

card27

0, 0, 0 **number of lower core nodes excluded, number of upper core nodes excluded, option of least squares ((not used))**

A.2 PAPU INPUT FILE MODIFICATIONS

Papu postprocessor requires **two input files**:

ajustfile. Which is a parameter file. This file will be fixed for all calculations

entrada. In this last file the modification of the same parameter in two card is performed for each calculation. This parameter determines the number of lower core nodes to be excluded of density reactivity calculation. Core nodes with no net voids generation will be not considered.

The number of core nodes without net generation of voids (negative values) can be seen in the core void profile located in the SIMULATE OUTPUT file (OUTPUT SUMMARY). The unique values modified in **entrada** file can be seen in the table A.2.1.

Table A.2.1. Modified values in entrada input file for PAPU reactivity coefficient calculation

card14

6,2, 0 **lower core node excluded, upper core node excluded, option of least squares**

^----**modified value for each calculation**

card16

6, 2, 0 **lower core node excluded, upper core node excluded, option of least squares**

^----**modified value for each calculation**

entrada file parameters could have also been given interactively but, in order to keep input and output data used in calculations, standard input is redirected to **entrada** and standard output is redirected to **salida** file. Then, PAPU execution procedure will be:

```
papu_executable_file < entrada > salida
```

A.3 PAPU OUTPUT FILES

PAPU postprocessor results can be seen in **two output files**

salida, redirected from standard output, which contains least squares approximation errors. This file will be keep for all calculations.

papusal, which contain the Doppler and density reactivity coefficients.

Only one value of Doppler coefficient appears and this is directly used as LAPURW input data. input

Two different sets of density coefficient values appear in two columns. The left column labelled as REACTA, comes from an adjust from voids and reactivity values. The right column, labelled as REACTDE, comes from an adjust from density and reactivity values. These last values, with the REACTDE label, will be used as LAPURW input data for all calculations.

Predictive Methods for Stability Margin in BWR

15.24, 15.24, 15.24, 15.24, 15.24, 35.9700
 33.290, 15.24, 15.24, 15.24, 15.24, 15.24, 15.24,
 15.24, 15.24, 15.24, 15.24, 15.24, 15.24, 15.24,
 15.24, 15.24, 15.24, 15.24, 15.24, 15.24, 15.24,
 15.24, 15.24, 15.24, 15.24, 15.24, 35.9700

5

0.00000 ,0.28909 ,1.08704 ,1.37849 ,1.53344 ,1.59653 ,1.57869 ,
 1.53434 ,1.48987 ,1.44569 ,1.39945 ,1.32995 ,1.24085 ,1.14935 ,
 1.07134 ,0.90366 ,0.84968 ,0.82002 ,0.77482 ,0.74063 ,0.69747 ,
 0.64852 ,0.58486 ,0.49880 ,0.22092 ,0.12979 ,0.00000 ,
 0.00000 ,0.28862 ,1.17042 ,1.52402 ,1.70295 ,1.75100 ,1.70311 ,
 1.62973 ,1.56010 ,1.48341 ,1.40522 ,1.32280 ,1.22376 ,1.12135 ,
 1.03010 ,0.84783 ,0.77985 ,0.75103 ,0.70233 ,0.66456 ,0.61531 ,
 0.55513 ,0.48062 ,0.38272 ,0.21453 ,0.08879 ,0.00000 ,
 0.00000 ,0.28323 ,1.05429 ,1.35972 ,1.51163 ,1.58331 ,1.60944 ,
 1.60295 ,1.57120 ,1.51676 ,1.45368 ,1.37527 ,1.28040 ,1.18114 ,
 1.08347 ,0.88723 ,0.82149 ,0.79900 ,0.75121 ,0.71464 ,0.66805 ,
 0.61257 ,0.53798 ,0.43267 ,0.20491 ,0.10346 ,0.00000 ,
 0.00000 ,0.30954 ,0.91432 ,1.09409 ,1.19129 ,1.28536 ,1.37511 ,
 1.44453 ,1.48454 ,1.49416 ,1.48095 ,1.42882 ,1.36239 ,1.28887 ,
 1.18991 ,0.98142 ,0.92677 ,0.89116 ,0.85159 ,0.82086 ,0.78772 ,
 0.75738 ,0.69070 ,0.58029 ,0.25101 ,0.11435 ,0.00000 ,
 0.00000 ,0.29389 ,0.95125 ,1.15266 ,1.26236 ,1.35437 ,1.43769 ,
 1.49490 ,1.52013 ,1.48952 ,1.43076 ,1.37399 ,1.30618 ,1.22771 ,
 1.12452 ,1.02342 ,0.94944 ,0.86870 ,0.79570 ,0.77581 ,0.74078 ,
 0.70257 ,0.64354 ,0.54473 ,0.40314 ,0.13090 ,0.00000 ,
 0.00000 ,0.27887 ,0.91543 ,1.10826 ,1.20718 ,1.29434 ,1.37977 ,
 1.44896 ,1.48803 ,1.47011 ,1.42380 ,1.37632 ,1.31390 ,1.24508 ,
 1.15091 ,1.05699 ,0.98588 ,0.90250 ,0.82749 ,0.80835 ,0.77304 ,
 0.73428 ,0.67526 ,0.57425 ,0.42403 ,0.13698 ,0.00000 ,
 0.00000 ,0.30736 ,0.92979 ,1.09158 ,1.17429 ,1.25851 ,1.34372 ,
 1.41467 ,1.46022 ,1.44251 ,1.40254 ,1.35693 ,1.29976 ,1.23374 ,
 1.14504 ,1.06068 ,0.99363 ,0.91634 ,0.84740 ,0.83046 ,0.80059 ,
 0.77179 ,0.71420 ,0.60805 ,0.44902 ,0.14190 ,0.00000 ,
 0.00000 ,0.29726 ,1.23832 ,1.58515 ,1.72473 ,1.75458 ,1.70342 ,
 1.61758 ,1.54833 ,1.47451 ,1.39330 ,1.31119 ,1.21865 ,1.11231 ,
 0.96185 ,0.88123 ,0.80387 ,0.74710 ,0.70458 ,0.66121 ,0.60807 ,
 0.53959 ,0.45358 ,0.34199 ,0.23576 ,0.08933 ,0.00000 ,
 0.00000 ,0.27941 ,1.15586 ,1.50586 ,1.65667 ,1.70423 ,1.67765 ,
 1.61163 ,1.55625 ,1.48990 ,1.41311 ,1.33217 ,1.23850 ,1.13223 ,
 0.98187 ,0.90442 ,0.82666 ,0.76643 ,0.72238 ,0.67735 ,0.62413 ,
 0.55795 ,0.47315 ,0.36185 ,0.25261 ,0.10037 ,0.00000 ,
 0.00000 ,0.30054 ,1.10582 ,1.39247 ,1.53439 ,1.57611 ,1.54707 ,
 1.49962 ,1.45659 ,1.39208 ,1.33407 ,1.26424 ,1.18304 ,1.11256 ,
 1.03946 ,0.96766 ,0.91407 ,0.84758 ,0.78116 ,0.75609 ,0.71147 ,
 0.65602 ,0.58903 ,0.49810 ,0.38503 ,0.14995 ,0.00000 ,
 0.00000 ,0.28240 ,1.07465 ,1.37720 ,1.53192 ,1.57462 ,1.53613 ,
 1.48246 ,1.43646 ,1.38087 ,1.32876 ,1.26056 ,1.17793 ,1.10705 ,
 1.03653 ,0.96648 ,0.91651 ,0.85899 ,0.79919 ,0.77792 ,0.73356 ,
 0.67517 ,0.60755 ,0.51280 ,0.41609 ,0.14858 ,0.00000 ,
 0.00000 ,0.27104 ,1.05729 ,1.39154 ,1.57654 ,1.64028 ,1.60646 ,
 1.54703 ,1.49106 ,1.43258 ,1.37289 ,1.29762 ,1.20368 ,1.11900 ,
 1.03380 ,0.94817 ,0.88660 ,0.82705 ,0.76580 ,0.73970 ,0.68949 ,
 0.62225 ,0.54580 ,0.44551 ,0.37070 ,0.11910 ,0.00000 ,
 0.00000 ,0.25975 ,0.98919 ,1.32750 ,1.51468 ,1.59896 ,1.60171 ,
 1.56780 ,1.52243 ,1.46406 ,1.40239 ,1.32262 ,1.22746 ,1.14031 ,
 1.05074 ,0.96138 ,0.89602 ,0.83141 ,0.76666 ,0.74304 ,0.69193 ,
 0.62461 ,0.54722 ,0.44603 ,0.36224 ,0.13936 ,0.00000 ,

7

Appendix A. Procedure for using PAPU Postprocessor

```

13,      1,      2,      3,      4,      5,      6,      7,
      8,      9,     10,     11,     12,     13,
9
13, 0.00209, 0.19912, 0.12269, 0.01528, 0.00096, 0.01738, 0.03388,
      0.00201, 0.05369, 0.00224, 0.19982, 0.19879, 0.15204,
10
13, 41.28, 46.58, 44.90, 192.76, 37.40, 37.97, 177.24,
      30.69, 35.46, 35.44, 40.67, 40.56, 40.18,
11
13, -0.378, -0.378, -0.378, -0.378, -0.409, -0.409, -0.409,
      -0.337, -0.337, -0.409, -0.409, -0.409, -0.409,
13
13, 0., 0., 0., 0., 0., 0., 0.,
      0., 0., 0., 0., 0., 0.,
14
13, 1, 107, 100, 24, 1, 19, 52,
      1, 31, 1, 92, 99, 96,
15
13, 92, 92, 92, 92, 96, 96, 96,
      91, 91, 96, 96, 96, 96,
16
13, 1, 1, 1, 1, 2, 2, 2,
      3, 3, 4, 4, 4, 4,
17
4, 450.260, 450.260, 450.260, 450.260
18
4, 296.590, 296.770, 293.930, 296.770
19
4, 98.970, 94.960, 90.960, 94.960
20
4, 98.970, 94.960, 90.960, 94.960
21
4, 1.107, 0.952, 1.013, 0.952
22
4, 0.100, 0.100, 0.100, 0.100
23
4, 0.100, 0.100, 0.100, 0.100
24
4, 1.300, 1.300, 1.300, 1.300
25
4, 0.125, 0.125, 0.125, 0.125
26
13, 1, 1, 1, 1, 2, 2, 2,
      3, 3, 4, 4, 4, 4,
27
4, 10.504, 10.506, 10.461, 10.506
28
4, 0.876, 0.848, 0.887, 0.848
29
4, 0.5125, 0.5125, 0.5125, 0.5125
30
4, 0.0393, 0.0393, 0.0393, 0.0393
31
4, 0.06600, 0.06050, 0.06200, 0.06050
32
4, 0.3407, 0.4436, 0.3662, 0.2840
33
4, 0.00900, 0.00750, 0.00850, 0.00750
34

```

Predictive Methods for Stability Margin in BWR

13,	1,	1,	1,	1,	2,	2,	2,	
	3,	3,	4,	4,	4,	4,		
35								
36	4,	1,	1,	1,	1,	1,		
		450.260,						
		450.260,						
		450.260,						
		450.260,						
37								
		1.000,						
		1.000,						
		1.000,						
		1.000,						
53								
	.1E-2	.5E-3	.5E-3	.2E-4	.5E-3	.1E-8	.5E-3	.5E-7
58								
13,	1,	1,	1,	1,	2,	2,	2,	
	3,	3,	4,	4,	4,	4,		
59								
	4,	4,	3,	3,	3,	3,		
60								
		64.460	274.340	399.050	450.260			
		174.440	307.340	450.260				
		242.440	414.290	450.260				
		174.440	307.340	450.260				
61								
		98.97,	92.78,	104.36,	110.55			
		94.96,	98.00,	104.08				
		90.96,	99.26,	108.30				
		94.96,	98.00,	104.08				
62								
		1.107,	1.020,	1.310,	1.415			
		0.952,	1.013,	1.150				
		1.013,	1.214,	1.355				
		0.952,	1.013,	1.150				
63								
13,	1,	1,	1,	1,	2,	2,	2,	
	3,	3,	4,	4,	4,	4,		
64								
	4,	9,	9,	8,	9,	9,		
65								
		78.005,	124.705,	171.405,	218.205,	264.905,	302.105,	339.405,
		376.605,	443.390					
		79.530,	123.830,	168.130,	212.430,	256.730,	301.030,	345.330,
		389.630,	442.440					
		81.440,	132.640,	183.840,	235.040,	286.240,	337.440,	388.640,
		443.080						
		79.530,	123.830,	168.130,	212.430,	256.730,	301.030,	345.330,
		389.630,	442.440					
66								
		0.957,	0.951,	0.951,	0.951,	0.995,	0.576,	0.576,
		0.576,	0.718,					
		0.809,	0.809,	0.809,	0.758,	0.758,	0.758,	0.677,
		0.677,	0.344,					
		0.755,	0.755,	0.755,	0.755,	0.639,	0.639,	0.497,
		0.497,						
		0.809,	0.809,	0.809,	0.758,	0.758,	0.758,	0.677,
		0.677,	0.344,					

67	4,	2,	2,	2,	2
68	4,	0.1002,	0.2380,	0.0950,	0.2380
69	4,	1.000,	1.000,	1.000,	1.000
70	4,	1.000,	1.000,	1.000,	1.000
71	4,	0.1246,	0.2000,	0.1240,	0.2000
72	4,	-1.000,	-1.000,	-1.000,	-1.000
73	4,	2,	2,	2,	2
74	4,	1.000,	1.000,	1.000,	1.000
75	4,	1.000,	1.000,	1.000,	1.000
76	4,	1.000,	1.000,	1.000,	1.000
0					

A.5 LAPURW INPUT EXAMPLE

26_08_07_18_18_04

```

1
13 1 1
2
      1      107      100      24      1      19      52
      1      31      1      92      99      96
3
      450.2600
4
      0.28      -0.26
5
1 6
6
      1
7
6 0.204E-03 0.127E-02 0.115E-02 0.248E-02 0.907E-03 0.219E-03
8
6 0.012776 0.031650 0.121512 0.322343 1.404112 3.876157
9
      1
10
1 0.0
11
      1
12
1 0.2788E-04
17
      -0.277E-02
18
1 7
19
      1      1      1      1      1      1      1
      1      1      1      1      1      1
20
0.0      0.2      0.4      0.6      0.8      1.0      1.2
21
33.4884 24.2756 17.6394 13.5799 12.0970 13.1908 16.8613
22
100 0.010 0.100 0.120 0.140 0.160 0.180 0.200
      0.210 0.220 0.230 0.240 0.250 0.260 0.270
      0.280 0.290 0.300 0.310 0.320 0.330 0.340
      0.350 0.360 0.370 0.380 0.390 0.400 0.410
      0.420 0.430 0.440 0.450 0.460 0.470 0.480
      0.490 0.500 0.510 0.520 0.530 0.540 0.550
      0.560 0.570 0.580 0.590 0.600 0.610 0.620
      0.630 0.640 0.650 0.660 0.670 0.680 0.690
      0.700 0.710 0.720 0.730 0.740 0.750 0.760
      0.770 0.780 0.790 0.800 0.810 0.820 0.830
      0.840 0.850 0.860 0.870 0.880 0.890 0.900
      1.000 1.100 1.200 1.300 1.400 1.500 1.600
      1.700 1.800 1.900 2.000 3.000 4.000 5.000
      6.000 7.000 8.000 9.000 10.000 20.000 50.000
      100.000 200.000
23
0 1 1 1 1 1 0 0 0 0 0 0 0 0
0 0 0 0 0 0 0 0

```


Appendix A. Procedure for using PAPU Postprocessor

```
24
1  1  1  1  1  1  1  1  1  1  1  1  1
28
1.15
29
6  0.000  -0.500  -1.060  -1.089  -1.500  -2.000
30
4
0
```